STUDIES ON THERMOPHYSICAL PROPERTIES OF NANOFLUIDS AND THEIR APPLICATION IN GROUND SOURCE HEAT PUMP

By

Jagannadha Reddy Satti

RECOMMENDED:

Dr. Chuen-Sen Lin

Dr. Jifeng Peng

Dr. Sun Woo Kim

Dr. Debendra K. Das
Advisory Committee Chair

Dr. Rorik A. Peterson
Chair, Department of Mechanical Engineering

APPROVED:

Dr. Douglas J. Goering
Dean, College of Engineering and Mines

Dr. John C. Eichelberger
Dean of the Graduate School

7 December 2015
Date

STUDIES ON THERMOPHYSICAL PROPERTIES OF NANOFLUIDS AND THEIR APPLICATION IN GROUND SOURCE HEAT PUMP

A

DISSERTATION

Presented to the Faculty

of the University of Alaska Fairbanks

in Partial Fulfillment of the Requirements

for the Degree of

DOCTOR OF PHILOSOPHY

By

Jagannadha Reddy Satti, M.S.

Fairbanks, Alaska

December 2015

Abstract

The goals of this dissertation were to measure the thermal conductivity, specific heat, and density of different propylene glycol nanofluids; compare the results with existing correlations; and develop new correlations with the obtained data. A numerical study has been performed to study the benefits of nanofluids in cold climate ground source heat pumps. Nanofluids are dispersions of nanoparticles with average sizes of less than 100 nm in heat transfer fluids such as water, oil, ethylene glycol, and propylene glycol. In cold regions, the common heat transfer fluids used are ethylene glycol (EG) and propylene glycol (PG). In the present research, a propylene glycol (PG) and 40% water (W) by mass fluid mixture was used as a base fluid, which has a freezing point of -51.1 ^{0}C.

Experiments were conducted to measure the density of several nanofluids containing nanoscale particles of aluminum oxide (Al_2O_3), zinc oxide (ZnO), copper oxide (CuO), titanium oxide (TiO_2), and silicon dioxide (SiO_2). These particles were individually dispersed in a base fluid of 60:40 propylene glycol and water (PG/W) by mass. Additionally, Carbon Nanotubes (CNT) dispersed in deionized water (DI) were also tested. Initially, a benchmark test was performed on the density of the base fluid in the temperature range of 0°C to 90°C. The measurements were performed with different particle volumetric concentrations from 0 to 6% and nanoparticle sizes ranging from 10 to 76 nm. The temperature range of the measurements was from 0° to 90°C. These results were compared with the values predicted by a currently acceptable theoretical equation for nanofluids. The experimental results showed good agreement with the theoretical equation, with a maximum deviation of -3.8% for copper oxide nanofluid and an average deviation of -0.1% for all the nanofluids tested.

An experimental study has been carried out to determine the thermal conductivity of five different nanofluids, containing aluminum oxide, copper oxide, zinc oxide, silicon dioxide, and titanium dioxide nanoparticles, dispersed in a base fluid of 60:40 (by mass) propylene glycol and water. The effect of particle volumetric concentrations up to 6% was studied with temperatures ranging from 243K to 363K. The thermal conductivity of nanofluids showed a direct relationship with particle volumetric concentration, particle size, properties, and temperature. Several existing theoretical models for thermal conductivity of nanofluids were compared with the experimental

data, but they all showed some disagreement. Therefore, the most agreeable model was selected and refined for propylene glycol nanofluids. This model considered the thermal conductivity of nanofluids as a function of Brownian motion, Biot number, fluid temperature, particle volumetric concentration, and the properties of the nanoparticles and base fluid. This model provided good agreement with 600 experimental data points of five nanofluids, with an average absolute deviation of 1.79 percent.

Specific heat was measured for five different nanofluids containing aluminum oxide (Al_2O_3), zinc oxide (ZnO), copper oxide (CuO), titanium oxide (TiO_2), and silicon dioxide (SiO_2) nanoparticles dispersed in a base fluid of 60% propylene glycol and 40% water by mass (60:40 PG/W). The measurements were carried out over a temperature range of -30°C to 90°C, for nanoparticle volumetric concentrations of 0.5% to 6%, and for average particle sizes ranging from 10 nm to 45 nm to evaluate their effects on the specific heat. From comparison, it was found that the existing specific heat correlations were not able to predict the measured experimental values, therefore, a new correlation was developed to predict the specific heat of various 60:40 PG/W based nanofluids. This new correlation is in good agreement with 610 experimental data points of the five nanofluids, with a maximum deviation of -5% exhibited by the Al_2O_3 nanofluid and an average deviation of -0.094% for all five nanofluids.

The COP of a GSHP in cold climates is limited by the circulation of heat transfer fluid in a ground heat exchanger loop at very low temperatures. This requires a greater tube length in the ground heat exchanger to absorb an adequate amount of heat. One way to increase the COP of a GSHP is by replacing the heat transfer fluid with more efficient fluid, such as a nanofluid. In this paper, a GSHP operating in central Alaska is analyzed. Analytical and numerical studies were performed on the ground heat exchanger of the GSHP. Results calculated from modeling showed good agreement with experimental data for a conventional heat transfer fluid, a methanol and water mixture, validating the models. Next, the analysis were performed using Al_2O_3 and CuO nanofluids with three different particle volumetric concentrations, 0.5, 1, and 2%. The results showed nanofluids absorbed more heat than the basefluid. The ground temperature was varied from 273 to 288K and the fluid velocity from 1 m/s to 5 m/s. The best heat absorption rate of 12% over the basefluid was observed for an Al_2O_3 nanofluid of 2% concentration at a ground temperature of 273K.

Table of Contents

Page

List of Figures

Page

List of Tables

Page

List of Appendices

Page

Acknowledgements

My most sincere thanks go to my principal advisor, Dr. Debendra K. Das, for his constant supervision, support, encouragement, and invaluable guidance during my doctoral studies. I also greatly thank my advisory committee members Dr. Chuen-Sen Lin, Dr. Jifeng Peng, and Dr. Sun Woo Kim for their valuable suggestions and commitment to this dissertation.

Financial support from National Aeronautics and Space Administration, Experimental Program to Stimulate Competitive Research and the University of Alaska Fairbanks Mechanical Engineering Department is gratefully acknowledged.

I would like to express a special word of thanks for my friends in the nanofluids group at UAF, especially Dr. Ravikanth S. Vajjha and Dustin R. Ray for their reviews on my work, which helped me finish this dissertation on time.

I express my deepest gratitude to my parents, Mr. Surya Prabhakara Reddy Satti and Mrs. Parvathi Satti, and my sister, Mrs. Raja Rajeswari Kovvuri, for their encouragement and support to pursue doctoral study.

Chapter 1 Introduction

1.1 Description of nanofluids

Nanofluids are new heat transfer fluids, which contain very small quantities of nanoparticles that are uniformly and stably suspended in a fluid. Suspension of these tiny particles dramatically changes the properties of the fluid. The average sizes of the particles that are suspended in the fluid are less than 100 nm. Choi [1] coined the term "nanofluids" for this new type of heat transfer fluids. With increasing thermal loads from engines, optical devices (lasers), and microelectronics (CPU), cooling is crucial to maintain optimal performance and reliability of devices. The conventional methods to increase heat transfer are providing extra surface area by using fins or microchannel heat exchangers. However, the high-pressure drop in microchannels caused problems in their application. Modern manufacturing methods provided the opportunity to process and produce different nanoscale materials. The thermal, mechanical, optical, magnetic and electrical properties of nanomaterials are superior to those of conventional materials. This caught the attention of material scientists and engineers: a major advance would be suspending these nanoparticles into fluids and enhancing their heat transfer. Argonne National Laboratory has pioneered high thermal conductivity fluids, called nanofluids, by suspending nanoparticles in conventional coolants [1]. Most heat transfer fluids have a low thermal conductivity compared to metals. A coolant, propylene glycol, and water (PG/W) mixture with proportional mass of 60:40 has a thermal conductivity of 0.334 W/mK at 20°C, whereas aluminum oxide has a thermal conductivity 100 times greater at 36.0 W/m K. However, the specific heat of metals is much lower than that of liquids. This is illustrated in Figure 1.1 with other thermophysical properties.

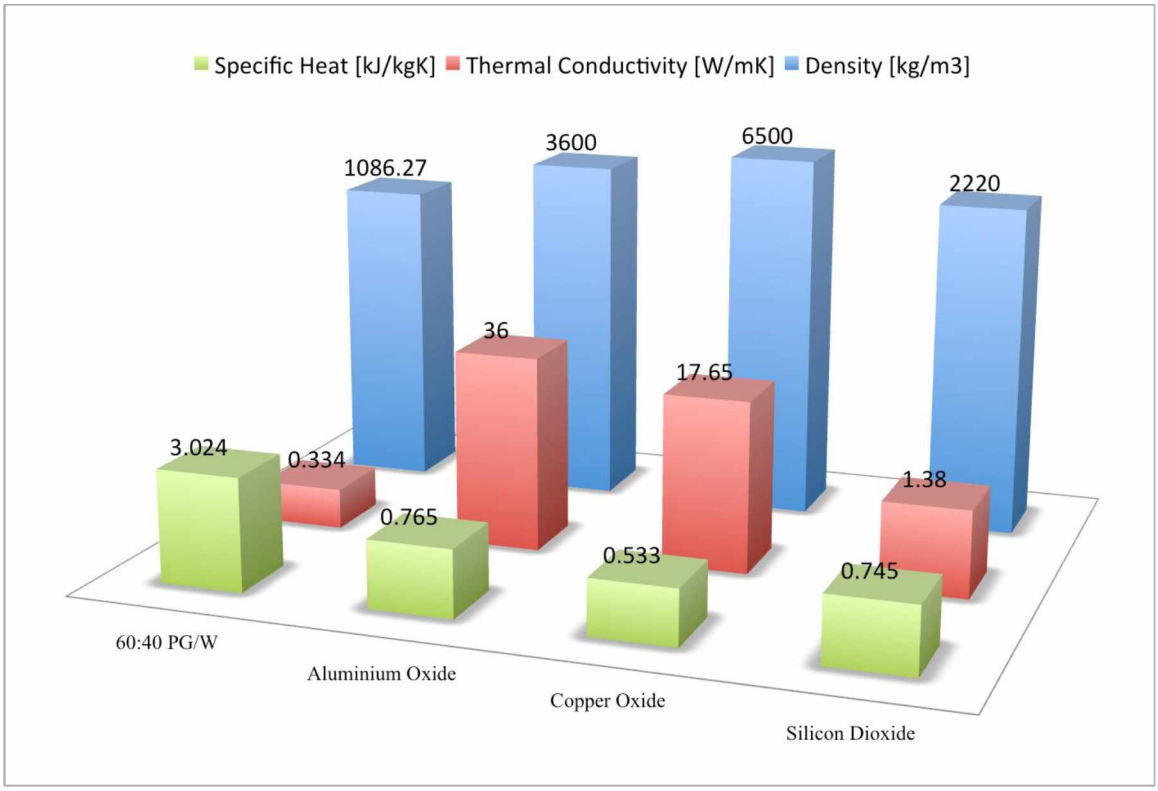

Figure 1.1 Properties comparison between PG/W, Al_2O_3, CuO and SiO_2

Thus, mixing metals and fluids can bridge the gap between fluids and solids. In recent years, researchers have shown that dispersing a small volume of nanoparticles in conventional heat transfer fluids can significantly enhance their thermal conductivity and convective heat transfer coefficient [2–6], by as much as 45% for a constant Reynolds number with Al_2O_3 at a concentration of 1.34% dispersed in distilled water. These results have motivated both the industrial and scientific communities to explore the thermophysical properties of nanofluids, which strongly influence fluid dynamics and heat transfer characteristics. Some of the potential benefits of nanoparticles over microparticles are mentioned by several researchers [6–8]:

- **Improved heat transfer and stability**: Nanoparticles suspended in conventional fluids increase the surface area for heat exchange, resulting in better heat transfer. Since the nanoparticles are nanometer-scale, this keeps them afloat in fluid for a longer time, which increases stability.

- **Microchannel cooling:** Microchannel heat exchangers are used in places where high heat transfer rates are required. Using nanofluids in these heat exchangers can increase the heat transfer rate dramatically [7].
- **Minimal clogging:** Micrometer-sized particles cause clogging problems when used in systems. This problem can be eradicated using nanoparticles. Due to their size, nanoparticles can pass through narrow passages without clogging, thus enhancing heat transfer.
- **Miniaturization:** Nanofluids can help in miniaturizing electronic devices. Nanofluids can extract more heat than conventional fluids, which helps in designing small components.
- **Cost and energy savings:** Nanofluids are more efficient than conventional fluids, which leads to cost and energy savings in heat transfer by coolants.
- **Pumping power:** To improve heat transfer by two times, we have to increase the pumping power by nearly 10 times. Nanofluids increase the heat transfer for the same operating conditions. So, in order to get the required heat transfer, nanofluids do not require as much pumping power as conventional coolants.

Comprehensive studies summarized by Das et al. [6] and Minkowycz et al. [8] have described many aspects of a large number of nanofluids, focusing on thermophysical properties and convective heat transfer. It is now well established that their thermophysical properties make nanofluids beneficial in heat transfer applications. Many papers have been published in the last decade by researchers studying nanofluids. A few examples are: thermophysical properties [9–13]; heat transfer coefficient and friction factor characteristics [2, 14, 15]; and applications in different types of heat exchangers, such as, air coils [16, 17] , radiators [18], and plate heat exchangers [19].

1.2 Making of Nanofluids

Nanofluids are prepared using two-step and one step methods [7, 20]. In the single step method, the nanoparticles are evaporated directly into the base fluid, while in the two step method, nanoparticles are produced, then dispersed in the base fluid. The two step method works well for oxide nanoparticles, but is not effective for metal nanoparticles. The single step method is preferable for high conductivity pure metal nanoparticles.

1.2.1 Two-step method

The two-step method is the most widely used method to prepare nanofluids. In this method, nanoparticles are prepared as dry powders using inert gas condensation. Chemical vapor deposition has been used to produce nanoparticles for making nanofluids. The nano-sized powder is then dispersed into the fluid in the second step. Methods like magnetic force agitation, ultrasonic agitation, high shear mixing, among others, are employed to stabilize the nanofluids. Surfactants are added to enhance the stability of nanofluids. The volume of the surfactants added is very small compared to the volume of the nanoparticles. Figure 1.2 explains the two-step method used for nanofluid preparation. The two-step method is the most economical method for producing nanofluids at a large scale, because nanopowder synthesis techniques have already been scaled up to industrial production. The problem faced by this method is nanoparticle agglomeration, even after hours of ultrasonication of nanofluids. Due to difficulty in preparing stable nanofluids by the two-step method, several advanced techniques, like the one step method, have been developed.

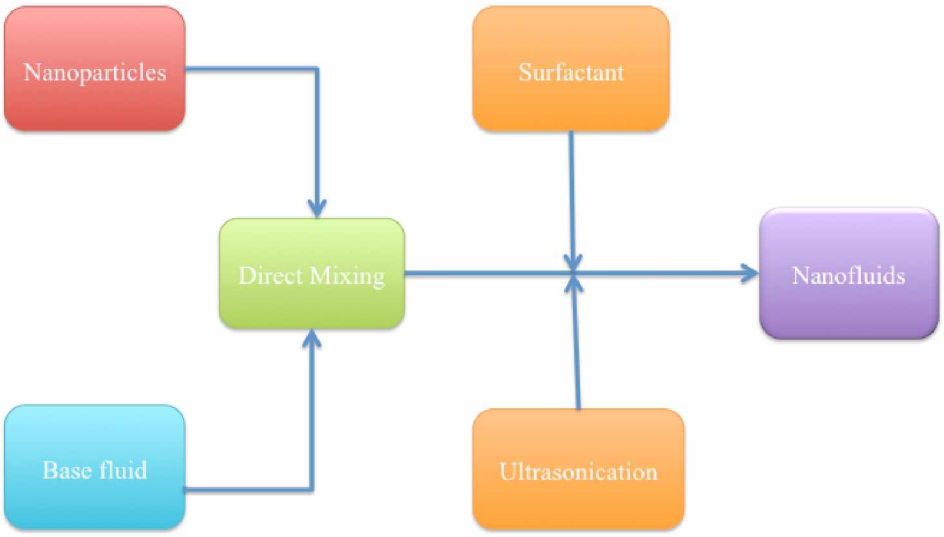

Figure 1.2 Two-step method for nanofluid preparation

1.2.2 One-step method

To reduce the agglomeration of nanoparticles, the physical vapor condensation method is used to prepare copper ethylene glycol nanofluids. The one step process consists of continuously making nanoparticles and dispersing them in the base fluid simultaneously. Figure 1.3 shows the instrument used to prepare nanofluids through the one step method. This process avoids drying, storage, transportation, and dispersion of nanoparticles, decreasing their chances of agglomeration. This method also increases the stability of nanofluids. However, preparation of nanofluids using the one step method is difficult because of factors like incomplete reaction and the vapor pressure of fluid, which play a very important role in this method. This method is only favorable for fluids with a low vapor pressure.

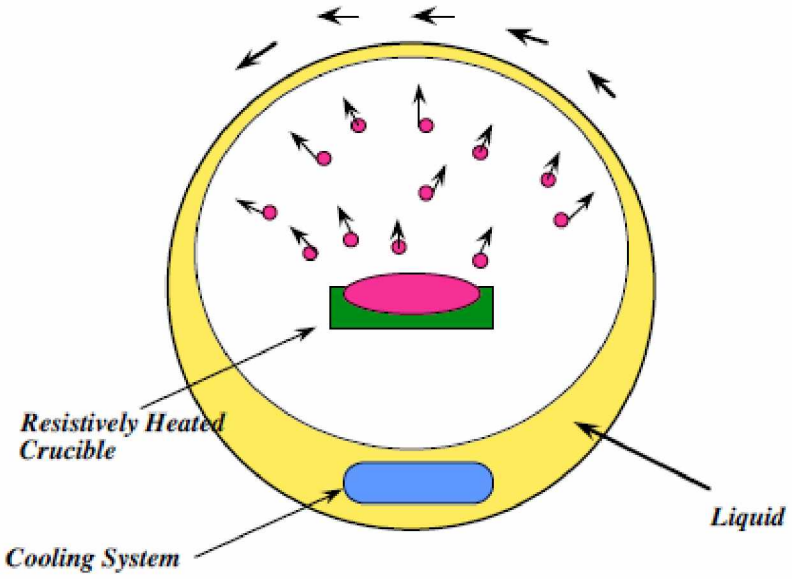

Figure 1.3. Nanofluid production by the one step method. (Source: Eastman et al. [21])

1.3 Benefits of nanofluids in cold climates

In cold climate regions like Alaska, Canada, Northern Europe, and Russia, the ambient temperatures may reach -40°C. In such regions, Ethylene Glycol (EG) and Propylene Glycol (PG) are commonly used as heat transfer fluids. Pure EG or PG will freeze around -40°C, but when they are mixed with pure water, their freezing point is depressed below -40°C. Therefore, it is common practice to use a mixture of water and EG or PG as the heat transfer fluid in building heating systems, automobiles, and heat exchangers of industrial plants that are exposed to low temperatures. The mixture of 60% of propylene glycol and 40% water (60:40 PG/W) by volume has the lowest freezing temperature, -51.1°C ASHRAE [22].

Vajjha and others [2] conducted measurements on different nanofluids with 60:40 EG/W base fluids. EG is toxic in nature and takes a longer time to degrade in the environment, while PG is non-toxic in nature and easily decomposes in the environment. Therefore, it is safer to use PG/W in human interaction applications. For heating residential buildings in cold regions, PG/W is the recommended heat transfer fluid due to the possibility of mixing with potable water in the household plumbing systems. For this reason, 60:40 PG/W has been selected as the base fluid for our experiments. Determining the thermophysical properties of the nanofluid is essential for

determining the convective heat transfer coefficient and the pumping power, because the Reynolds and Prandtl numbers depend on viscosity, specific heat, density, and thermal conductivity. Until now, very few experimental studies have been done to measure the density, thermal conductivity, and specific heat of PG/W nanofluids. Therefore, these properties have been measured and correlations have been developed in this dissertation.

1.4 Application of nanofluids

Nanofluids have four important characteristic features, which are required by energy systems (fluid and thermal systems) [8, 23]:

- Increased thermal conductivity
- Strong temperature-dependent thermal conductivity
- Nonlinear increase in thermal conductivity with nanoparticle concentration
- Increase in boiling critical heat flux.

These features enhance the application of nanofluids to improve heat transfer and energy efficiency in industrial and engineering areas like industrial coolants, smart fluids, nuclear reactor coolants, geothermal power extraction, nanofluids in automobile fuels, brake fluids, car radiator coolant, and microelectronics cooling. Nanofluids finds applications where heat transfer fluids are being used to exchange heat. Industry coolants are used in public utilities, the oil and gas industry, the food and beverage processing industry, solar energy, and heating, ventilation, and air conditioning (HVAC), among other areas. The following sections provide brief descriptions of the application of nanofluids in different areas.

1.4.1 Automotive

The research on using nanofluids as coolants in automobiles is being carried. The nanofluid group at the University of Alaska Fairbanks performed research on the potential use of nanofluid coolants in automobiles. Vajjha et al. and Ray and Das [18, 24] studied the application of nanofluids in automobile radiators. Vajjha performed a numerical study using Al_2O_3 and CuO in EG/W nanofluids. They found a heat transfer coefficient enhancement of 94% for a 10% volume

concentration of Al_2O_3 nanofluids. Ray and Das performed analytical and numerical studies on the application of Al_2O_3, CuO, and SiO_2 nanofluids in automobile radiators. They found that at optimal radiator operating conditions, the pumping power decreased by 35.3%, reduce the surface area by 7.4% by using 1% Al_2O_3 nanofluids.

1.4.2 Electronics cooling

Recent advancements in electronics and microchips have proportionately increased the heat dissipated from them. In order to maintain their performance, the produced heat should be removed efficiently. Nanofluids are used for cooling microchips in computers as well as in other electronic applications. The nanofluids group at the University of Alaska Fairbanks has performed research on the application of nanofluids in electronics cooling. Namburu et al. [25] studied the application of CuO and water nanofluids in heat sinks of electronics. They found that nanofluids increase the heat transfer coefficient nearly 2 times. This proved that nanofluids could efficiently transfer the heat from heat sinks. Researchers have performed both analytical and numerical studies on nanofluid application in heat sinks and found significant improvement in thermal performance.

1.4.3 Building Heating

Heat exchangers are used to exchange heat in building heating and cooling systems. These heat exchangers use nanofluids with thermophysical properties superior to those of the traditional fluid. The use of nanofluids in HVAC systems could result in reducing the volumetric flow rate and the required pumping power. Kulkarni et al. [17] studied the application of nanofluids for cold climate housing. They performed an analytical analysis using CuO, Al_2O_3, and SiO_2 nanoparticles dispersed in 60:40 EG/W nanofluids in conventional finned–tube heat exchangers used in heating systems of cold buildings. The results showed that a maximum 37% reduction in flow rate was attained for a 6% volumetric concentration of Al_2O_3. For a 6% volumetric concentration of CuO at constant Reynolds number, a reduction of 20.37% surface area was observed. Strandberg and Das [16] performed a theoretical analysis on the application of CuO nanofluids in hydronic building heating systems. They found an enhancement of 87% in Nusselt number relative to the base fluid at a constant Reynolds number of 14,000. These studies proved that nanofluids can be applied for building heating and cooling systems.

1.4.4 Biomedical applications

Nanofluids are being used in many biomedical applications, including nano-drug delivery, cancer therapeutics, cryopreservation, nanocryosurgery, and sensing and imaging [8]. In conventional drug delivery systems, the drug concentration in the blood will increase and then drop as the drug is metabolized. This cycle is repeated as the required outcome is achieved. By contrast, in nano-drug delivery systems, a controlled drug delivery takes place by well-timed release of drug. This helps in drug delivery for extended periods of time in the required region. Researchers are working on a way to perfect this system. Magnetic nanofluids are being used in biomedical applications to recognize and treat tumors. More research still needs to be done to produce stable nanofluids that are compatible with tissue cells. In cryosurgery, nanoparticles are introduced near the tumor cells. They can kill the tumor cells by regulating the temperature of the nanoparticles from outside.

1.4.5 Nanofluids under zero gravity

Nanofluids can become an excellent heat transfer agent for spacecrafts. The serious weakness of nanofluids is particle settling, which does not occur in the zero gravity environment. Therefore, nanofluids will be valuable candidates for heat transfer in the International Space Station and spacecrafts being designed for deep space, such as those of the Mars mission.

1.5 Summary of chapters

This dissertation has been written in manuscript format. Chapter 1 gives a brief introduction to nanofluids and their engineering applications. Chapters 2, 3, and 4 describe the experimental study on thermophysical properties of 60:40 PG/W. Chapter 5 studies the application of nanofluids in ground source heat pumps. Chapters 2, 3, 4 and 5 were under review by different journals. Chapter 6 summarizes the conclusions drawn from the present research.

Chapter 2 describes density measurements performed on several nanofluids containing nanoscale particles of aluminum oxide (Al_2O_3), zinc oxide (ZnO), copper oxide (CuO), titanium oxide (TiO_2), and silicon dioxide (SiO_2). These particles were individually dispersed in a base fluid of 60:40 propylene glycol and water (PG/W) by mass. Additionally, Carbon Nanotubes (CNT) dispersed in deionized water (DI) were also tested. Initially, a benchmark test was performed on

the density of the base fluid in the temperature range of 0°C to 90°C. The measured data agreed with the values presented in the handbook of American Society of Heating, Refrigerating, and Air Conditioning Engineers (ASHRAE) within a maximum error of 1.6%. After this validation run, density measurements of various nanofluids with particle volumetric concentrations from 0 to 6% and nanoparticle sizes ranging from 10 to 76 nm were performed. The temperature range of the measurements was from 0 to 90°C. These results were compared with the values predicted by a currently acceptable theoretical equation for nanofluids. The experimental results showed good agreement with the theoretical equation with a maximum deviation of -3.8% for copper oxide nanofluid and an average deviation of -0.1% for all the nanofluids tested.

In Chapter 3, an experimental study was carried out to determine the thermal conductivity of five different nanofluids containing aluminum oxide (Al_2O_3), zinc oxide (ZnO), copper oxide (CuO), titanium oxide (TiO_2), and silicon dioxide (SiO_2). Dispersed in a base fluid of 60:40 (by mass) propylene glycol and water. The effect of particle volumetric concentrations up to 6% was studied, with temperature ranging from 243K to 363K. The thermal conductivity of nanofluids showed a direct relationship with particle volumetric concentration, particle size, properties, and temperature. Several existing theoretical models for thermal conductivity of nanofluids were compared with the experimental data, but they all showed some disagreement. Therefore, the most agreeable model was selected and refined for propylene glycol nanofluids, utilizing the framework presented in earlier research. This model considered the thermal conductivity of nanofluids as a function of Brownian motion, Biot number, fluid temperature, particle volumetric concentration, and the properties of the nanoparticles and base fluid. This model provided good agreement, with 600 experimental data points of five nanofluids having an average absolute deviation of 1.79 percent.

Chapter 4 describes the specific heat measurements of five different nanofluids containing aluminum oxide (Al_2O_3), zinc oxide (ZnO), copper oxide (CuO), titanium oxide (TiO_2), and silicon dioxide (SiO_2) nanoparticles dispersed in a base fluid of 60% propylene glycol and 40% water by mass (60:40 PG/W). The measurements were carried out over a temperature range of -30°C to 90°C, for nanoparticle volumetric concentrations of 0.5% to 6%, and for average particle sizes ranging from 10 nm to 45 nm to evaluate their effects on the specific heat. From comparison, it was found that the existing specific heat correlations were not able to predict the measured

experimental values, therefore, a new correlation was developed to predict the specific heat of various 60:40 PG/W based nanofluids. This new correlation is in good agreement with 610 experimental data points of the five nanofluids, with a maximum deviation of -5% exhibited by the Al_2O_3 nanofluid and an average deviation of -0.094% considering all five nanofluids.

Chapter 5 describes the applications of nanofluids in ground source heat pumps (GSHP). GSHP is the most energy efficient heating system for buildings available. The coefficient of performance (COP) of cold climate ground source heat pumps (GSHP) is lower, around 2.0, compared to that of tropical climate GSHP, about 4.0. The COP of a GSHP in cold climates is limited by the circulation of heat transfer fluid in a ground heat exchanger loop at very low temperatures. This requires a greater tube length in the ground heat exchanger to absorb an adequate amount of heat. One way to increase the COP of a GSHP is by replacing the heat transfer fluid with more efficient fluid, such as a nanofluid. In this paper, a GSHP operating in central Alaska is analyzed. Analytical and numerical studies were performed on the ground heat exchanger of the GSHP. Results calculated from modeling showed good agreement with experimental data for a conventional heat transfer fluid, a methanol and water mixture, validating the models. Next, the analysis were performed using Al_2O_3 and CuO nanofluids with three different particle volumetric concentrations, 0.5, 1, and 2%. The results showed nanofluids absorbed more heat than the basefluid. The ground temperature was varied from 273 to 288K and the fluid velocity from 1 m/s to 5 m/s. The best heat absorption rate of 12% over the basefluid was observed for an Al_2O_3 nanofluid of 2% concentration at a ground temperature of 273K.

Chapter 6 summarizes the overall conclusions drawn from the present studies. This chapter also lists some recommendations derived from the present study, which researchers can follow to carry forward the advancement of nanofluids.

1.6 References

[1] Choi, S., 1995, "Enhancing thermal conductivity of fluids with nanoparticles," ASME Dev. Appl. Non-Newtonian Flows, **66**, pp. 99–105.

[2] Vajjha, R. S., and Das, D. K., 2012, "A review and analysis on influence of temperature and concentration of nanofluids on thermophysical properties, heat transfer and pumping power," Int. J. Heat Mass Transf., **55**(15-16), pp. 4063–4078.

[3] Kakaç, S., and Pramuanjaroenkij, A., 2009, "Review of convective heat transfer enhancement with nanofluids," Int. J. Heat Mass Transf., **52**(13-14), pp. 3187–3196.

[4] Fan, J., and Wang, L., 2011, "Review of Heat Conduction in Nanofluids," ASME J. Heat Transf., **133**(4), pp. 040801,1–14.

[5] Saidur, R., Leong, K. Y., and Mohammad, H. A., 2011, "A review on applications and challenges of nanofluids," Renew. Sustain. Energy Rev., **15**(3), pp. 1646–1668.

[6] Das, S. K., Choi, S. U. S., and Patel, H. E., 2006, "Heat Transfer in Nanofluids—A Review," Heat Transf. Eng., **27**(10), pp. 3–19.

[7] Choi, S. U. S., Zhang, Z. G., and Keblinski, P., 2004, "Nanofluids," Encyclopedia of Nanoscience and Nanotechnology, Journal of Nanoscience and Nanotechnology, p. 727.

[8] Minkowycz, W., Sparrow, E., and Abraham, J., 2012, Nanoparticle Heat Transfer and Fluid Flow, CRC Press, 3rd edition, Boca Raton.

[9] Namburu, P. K., Kulkarni, D. P., Misra, D., and Das, D. K., 2007, "Viscosity of copper oxide nanoparticles dispersed in ethylene glycol and water mixture," Exp. Therm. Fluid Sci., **32**(2), pp. 397–402.

[10] Sahoo, B. C., Das, D. K., Vajjha, R. S., and Satti, J. R., 2013, "Measurement of the Thermal Conductivity of Silicon Dioxide Nanofluid and Development of Correlations," ASME J. Nanotechnol. Eng. Med., **3**(4), p. 041006.

[11] Vajjha, R. S., and Das, D. K., 2009, "Experimental determination of thermal conductivity of three nanofluids and development of new correlations," Int. J. Heat Mass Transf., **52**(21-22), pp. 4675–4682.

[12] Vajjha, R. S., Das, D. K., and Mahagaonkar, B. M., 2009, "Density measurement of different nanofluids and their comparision with theory," Pet. Sci. Technol., **27**, pp. 612–624.

[13] Vajjha, R. S., and Das, D. K., 2010, Measurements of Nanofluids Properties and Heat Transfer Computation, LAP Lambert Academic Publishing.

[14] Yang, Y., Zhang, Z. G., Grulke, E. A., Anderson, W. B., and Wu, G., 2005, "Heat transfer properties of nanoparticle-in-fluid dispersions (nanofluids) in laminar flow," Int. J. Heat Mass Transf., **48**(6), pp. 1107–1116.

[15] Sarkar, J., 2011, "A critical review on convective heat transfer correlations of nanofluids," Renew. Sustain. Energy Rev., **15**(6), pp. 3271–3277.

[16] Strandberg, R., and Das, D. K., 2009, "Hydronic Coil Performance Evaluation With Nanofluids and Conventional Heat Transfer Fluids," ASME J. Therm. Sci. Eng. Appl., **1**(1), p. 011001.

[17] Kulkarni, D. P., Das, D. K., and Vajjha, R. S., 2009, "Application of nanofluids in heating buildings and reducing pollution," Appl. Energy, **86**(12), pp. 2566–2573.

[18] Ray, D. R., and Das, D. K., 2014, "Superior Performance of Nanofluids in an Automotive Radiator," ASME J. Therm. Sci. Eng. Appl., **6**(4), p. 041002.

[19] Ray, D. R., Das, D. K., and Vajjha, R. S., 2014, "Experimental and numerical investigations of nanofluids performance in a compact minichannel plate heat exchanger," Int. J. Heat Mass Transf., **71**, pp. 732–746.

[20] Das, S. K., Choi, S. U. S., Yu, W., and Pradeep, T., 2008, Nanofluids: Science and Technology, John Wiely & Sons, Inc., New Jersey.

[21] Parker, J. C., and Wollenberger, J., 1996, Nanophase and Nanocomposite Materials IH, Materials Research Society, Pittsburgh, Pennsylvania.

[22] ASHRAE, 2009, "Physical properties of secondary coolants (Brines)," ASHRAE Handbook, American Society of Heating Refrigerator and Air Conditioning Engineers, Inc, Atlanta.

[23] Das, S. K., Choi, S. U. S., Yu, W., and Pradeep, T., 2008, Nanofluids: Science and Technology, John Wiley & Sons, Inc., USA.

[24] Vajjha, R. S., Das, D. K., and Kulkarni, D. P., 2010, "Development of new correlations for convective heat transfer and friction factor in turbulent regime for nanofluids," Int. J. Heat Mass Transf., **53**(21-22), pp. 4607–4618.

[25] Namburu, P. K., Das, K. D., and Vajjha, S. R., 2012, "Comparison of the Performance of Copper Oxide Nanofluid with Water in Electronic Cooling," J. ASTM Int., **9**(5), pp. 104342, 1–15.

Chapter 2 Thermal Conductivity Measurements of Propylene Glycol Nanofluids and Comparison with Correlations[1]

2.1 Abstract

This paper presents the specific heat measurements of three nanofluids containing aluminum oxide, zinc oxide, and silicon dioxide nanoparticles. The first two are dispersed in a base fluid of 60:40 by mass of ethylene glycol and water (60:40 EG/W) and the last one in deionized water. Measurements were conducted over a temperature range of 315–363 K, which is the normal range of operation of automobile coolants and building heating fluids in cold regions. The nanoparticle volumetric concentrations tested were up to 10%. The measured values were compared with existing equations for the specific heat of nanofluids. A close agreement with the experimental data was not observed. Therefore, a new general correlation was developed for the specific heat as functions of particle volumetric concentration, temperature, and the specific heat of both the particle and the base fluid from the present set of measurements. The correlation predicts the specific heat values of each nanofluid within an average error of about 2.7%.

2.2 Introduction

Heat exchangers are used in a wide range of applications from food processing to residential heating and cooling. While heat exchangers have been steadily improved through better materials and increased surface area, the heat transfer fluid remains unchanged. Fluids have inherently low thermal conductivity compared to that of a solid. The thermal conductivity of a fluid can be increased by dispersing solid particles in a liquid. This concept of dispersing solid particles in fluid has existed for years. Researchers first tried to use micro- and millimeter particles suspended in fluids, but encountered problems such as sedimentation, clogging, erosion and high pumping power. With nanoparticles, several of the problems were resolved. Thus, a new class of heat transfer fluids was created called nanofluids, Nanofluids are defined as suspensions of solid

---

[1] Satti, J. R, Das, D. K. and Ray, D, "Thermal Conductivity Measurements of Propylene Glycol Nanofluids and Comparison with Correlations," under review by ASME Journal of Heat and Mass Transfer.

nanoparticles (less than 100nm) in fluid. Nanofluids can consist of a variety of nanoparticles, such as metals (Al, Cu, Ag, Au), metal oxides (Al_2O_3, ZnO, CuO, TiO_2) and carbon-based materials (nanotubes, graphite, nanodiamonds). The nanoparticles are traditionally dispersed in base fluids (b_f) such as water, ethylene glycol (EG), propylene glycol (PG) and oils. As recommended in ASHRAE [1], in cold regions, it is a common practice to use a mixture of glycol and water for heating and cooling applications. The addition of ethylene or propylene glycol depresses the freezing point of mixture but decreases its thermal conductivity. Due to ethylene glycol's toxicity, it is substituted by propylene glycol, even though propylene glycol has lower thermal conductivity than ethylene glycol. This can be overcome by suspending nanoparticles in PG/W to increase the thermal conductivity of the fluid. There has been a lack of studies conducted on the thermal conductivity of PG/W based nanofluids. Thus, we have conducted measurements of the thermal conductivity of various nanoparticles (Al_2O_3, ZnO, CuO, SiO_2 and TiO_2) suspended in 60:40 PG/W with concentrations and temperature ranging from 1% to 6% and 243K to 363K, respectively. A brief discussion about the past research and different models is provided in the following sections. Different theoretical models for predicting thermal conductivity of nanofluids have been developed in recent years. A comparison has been conducted between experimental data and previous models. This comparison shows that the model of Parsher et al. [2] matches our experimental data better than other models. The Prasher et al. model is refined by deriving a new value of a correlation constant from our experimental data of PG/W based nanofluids, which further improves the accuracy of the model.

2.3 Previous work

2.3.1 Experimental

In the 19th century, Maxwell [3] developed a theoretical model to predict thermal conductivity of solid particles in liquids. Maxwell's model worked for micro- and millimeter particles, but under-predicted the thermal conductivity of nanofluids. Thermal conductivity measurements started with Masuda et al. [4] in the year 1993. By dispersing nanoparticles in water, they observed changes in its thermal conductivity. They dispersed Al_2O_3, TiO_2 and SiO_2 nanoparticles in water. They observed thermal conductivity increases with increasing particle concentration for Al_2O_3 and TiO_2. They did not observe any change in thermal conductivity for SiO_2 nanoparticles.

Lee et al. [5] measured thermal conductivity of Al_2O_3 and CuO nanoparticles suspended in ethylene glycol and water (EG/W) using a transient hot wire method. They found that a 4% volume concentration of CuO nanoparticles improved the thermal conductivity by 20%. They determined that thermal conductivity increases linearly with volume concentration. Eastman et al. [6] reported higher thermal conductivity with Cu/EG nanofluids compared to that of pure EG and CuO/EG mixtures. A volumetric concentration of 0.3% Cu in EG improved the thermal conductivity by 40% compared to the base fluid. Choi et al. [7] dispersed multiwall carbon nanotubes (MWCNT) in oil and reported 160% enhancement of the thermal conductivity for a volume concentration of 1% . They observed a nonlinear relationship between the thermal conductivity enhancements and the nanotube concentration. This phenomenon was also found with oxide and metallic nanoparticles.

The thermal conductivity of SiC particles dispersed in EG/W measured by Xie et al. [8] and showed at a 22.9% enhancement at a 4% volumetric concentration.. Das et al. [9] studied the effects of temperature (21℃ – 51℃) on thermal conductivity of nanofluids with volumetric concentrations varying from 1% to 4% . Their choice of nanofluids consisted of Al_2O_3 and CuO dispersed in water. They found that for a 1% concentration of CuO, the thermal conductivity of the nanofluid (k_{nf}) was enhanced from 6.5% at 21 ℃ to 29% at 51℃. Wang et al. [10] described a model considering the surface adsorption between nanoparticles and fluid. They compared their model with experimental data of 50 nm CuO/Water with a volume concentration less than 0.5%. Murshed et al. [11] measured thermal conductivity of TiO_2/Water nanofluids. They found that their experimental data did not match with existing theoretical models. Putnam et al. [12] measured the thermal conductivity of C-60 and C-70 suspended in toluene with volume concentration less than 1%. Similarly, they measured Au particles suspended in ethanol. They found no significant increase in k_{nf} with concentrations less than 1%. They said that effective medium theory couldn't predict the thermal conductivity of nanofluids with volume concentrations less than 1%. Liu et al. [13] presented a chemical reaction method that produces CuO nanoparticles. Utilizing their nanoparticles, they found that k_{nf} was enhanced by 23.8% for 0.1% volume concentration for CuO/water nanofluid. Li et al. [14] performed experiments on an Al_2O_3/water nanofluid with volume concentration up to 6% using transient and steady state methods. They did not find any

difference in measured values between the two methods. They concluded that the thermal conductivity of nanofluids is independent of measurement technique.

2.4 Role of parameters

Detailed research has been carried out to study the effect of different parameters on the thermal conductivity of nanofluids. The parameters that affect the thermal conductivity of nanofluids are volume concentration, particle size, temperature, and pH, among others. The effect of each of these parameters varies with different nanofluids. For oxide and metallic nanofluids, all early experiments showed a linear increase in thermal conductivity with volume concentration. It is the most common parameter studied in measuring the thermal conductivity of nanofluids. Vajjha et al. [15] measured the thermal conductivity of three different (Al_2O_3, ZnO, CuO) ethylene glycol nanofluids. They found that thermal conductivity of nanofluids increases with volume concentration. There is an exception to this trend: Murshed et al. [11] performed experiments with both rod-shaped (10nm diameter X 40nm length) and spherical (15nm diameter) TiO_2 nanoparticles in water. They found that K_{nf} enhancement is not linear with volume concentration in both cases. This non-linearity was also observed for Al_2O_3/Water nanofluids.

Temperature is one of the important factors to study. The thermal conductivity of a fluid changes with temperature. A similar effect was also observed with nanofluids. The study on the effect of temperature on nanofluids was done by Das and others [9]. They performed experiments on Al_2O_3 and CuO/Water nanofluids over a temperature range from 20 ℃ to 50 ℃. The motion of nanoparticles was suggested to be responsible for the observed strong sensitivity to temperature. Vajjha et al. [15] measured the thermal conductivity of three different (Al_2O_3, ZnO, CuO) 60:40 EG/W nanofluids. They studied the effect of temperature on the thermal conductivity of nanofluids. They found that thermal conductivity increases with temperature. There are exceptions to this trend: Duangthongusk et al. [16] observed decreasing thermal conductivity with increasing temperature for TiO_2/Water nanofluids with particle volume fractions from 0.2% to 2%. Wang et al. [17] performed experiments on $CePO_4$/water nanofluids and found that K_{nf} did not increase linearly with temperature. Wei et al. [18] performed experiments on Cu_2O/water nanofluids and also found that K_{nf} did not increase linearly with temperature.

Nanoparticle size is another parameter that has attracted the attention of researchers. Chon et al. [19] performed experiments with Al_2O_3/Water nanofluids with different particle sizes of 150nm, 47nm and 11nm at a volume fraction of 1%. Due to Brownian motion the smaller particles travel faster and result in better thermal conductivity. Other researchers observed a similar trend. Vajjha et al. [15] studied the effect of particle size on the thermal conductivity of 60:40 EG/W nanofluids. They found smaller particle size nanoparticles showed higher thermal conductivity. However, the opposite phenomenon is also observed. Shima et al. [20] performed experiments with Fe_2O_3 nanofluids and found that k_{nf} increases as particle size increases. Beck et al. [21] performed experiments on Al_2O_3 nanofluids and found that K_{nf} increase was not linear with particle size. Fang et al. [22] performed molecular dynamics simulation on nanoparticles and proposed that, due to an increase of phonon mean free path in the small sized particles, nanoparticle thermal conductivity decreases as particle size decreases.

The pH of nanofluids also plays a role in the measurement of thermal conductivity. Li et al. [23], through experiments on copper/water nanofluids, showed that thermal conductivity varied widely as a function of pH. The thermal conductivity of the nanofluid increased as the pH increased from a value of 2, reached a peak around pH = 9, and then decreased until pH 12 was reached. Therefore, there is an optimum value of pH that ensures the highest thermal conductivity. Zhu et al. [24] studied the dispersion behavior and thermal conductivity of Al_2O_3/water nanofluids. Their experiments were conducted within the pH range of 2 to 12. They also confirmed that the dispersion stability and the thermal conductivity of this nanofluid were highly dependent on its pH. They achieved different pH values of nanofluids by adding different proportions of HCl and NaOH solutions. They found maximum thermal enhancement was observed at pH 8. Lee et al. [25] dispersed 25 nm mean diameter copper oxide nanoparticles in deionized water. They did not use any surfactant or dispersant in the preparation of their nanofluids. Their particle size measurements showed the size range of agglomerated particles from 160 to 280 nm within a pH range of 3 to 11. Their thermal conductivity measurements showed a maximum enhancement of 12% over that of the base fluid at the lower pH of 3, while at a pH of 8, the enhancement was negligible. However, at a pH of 11 the thermal conductivity value again increased by about 11%. They concluded that the surface charge states of nanoparticles were a basic parameter that enhanced the thermal conductivity of nanofluids. Konakanchi et al. [26] measured the pH of three

different (Al_2O_3, ZnO, SiO_2) 60:40 PG/W nanofluids. They found that pH is a function of temperature, volumetric concentration and particle diameter. They found that pH increases with temperature and particle size.

2.5 Theoretical models

Maxwell [3] provided a theoretical Eq. (2.1) to predict the effective thermal conductivity of solid and liquid mixtures. This equation is used for predicting thermal conductivity of micro and millimeter sized solid particles suspended in liquids:

$$k_{nf} = \frac{k_p + 2k_{bf} + 2(k_p - k_{bf})\phi}{k_p + 2k_{bf} - (k_p - k_{bf})\phi} k_{bf} \tag{2.1}$$

where k_{nf} is the thermal conductivity of the solid- liquid mixture.

Hamilton and Crosser [27] further extended Maxwell's model by including a particle shape factor, as shown in Eq. (2.2):

$$k_{nf} = \frac{k_p + (n-1)k_{bf} - (n-1)\phi(k_{bf} - k_p)}{k_p + (n-1)k_{bf} + \phi(k_{bf} - k_p)} k_{bf} \tag{2.2}$$

where n is the empirical shape factor given by $\frac{3}{\psi}$ and ψ is the particle sphericity, defined as surface area of a sphere. For spherical particles, n=3. These preliminary models were used to determine the thermal conductivity of micro- and millimeter-sized particle suspensions.

Yu and Choi [28] proposed a modified Maxwell model by including the effect of fluid layer around nanoparticles. They developed a correlation as shown in Eq. (2.3):

$$k_{pe} = \frac{(2(1-\gamma) + (1+\chi)^3(1+2\gamma))\gamma}{-(1-\gamma) + (1+\chi)^3(1+2\gamma)} k_p \tag{2.3}$$

where $\gamma = \frac{k_{layer}}{k_p}$ is the ratio of nanolayer thermal conductivity to particle thermal conductivity and $\chi = \frac{h}{r}$ *is* the ratio of nanolayer thickness to particle radius. Finally, thermal conductivity of the nanofluid can be calculated using Eq. (2.4):

$$k_{nf} = \frac{k_{pe} + 2k_{bf} + 2(k_p - k_{bf})(1+\chi)^3\phi}{k_{pe} + 2k_{bf} - (k_p - k_{bf})(1+\chi)^3\phi} k_{bf} \tag{2.4}$$

Xuan et al. [29] proposed a model considering the Brownian motion of nanoparticles and their aggregation. They added apparent thermal conductivity of nanofluid to Maxwell's model, as shown in Eq. (2.5):

$$k_{nf} = \frac{k_p + 2k_{bf} - 2(k_{bf} - k_p)\phi}{k_p + 2k_{bf} + (k_{bf} - k_p)\phi} k_{bf} + \frac{\rho\phi C_{p_p}}{2}\sqrt{\left(\frac{KT}{3\pi\mu_{bf} r_c}\right)} \tag{2.5}$$

where r_c is the mean radius of gyration of the cluster, μ_{bf} is the viscosity of basefluid, and K is the Boltzmann constant.

The model of Koo and Klienstreuer [30, 31], as shown in Eq. (2.6), takes into consideration particle size, volume fraction, temperature and properties of base fluid. It also considers the Brownian motion of nanoparticles:

$$k_{nf} = \frac{k_p + 2k_{bf} - 2(k_{bf} - k_p)\phi}{k_p + 2k_{bf} + (k_{bf} - k_p)\phi} k_{bf} + 5\times 10^4 \beta\phi\rho_{bf} C_{p_{bf}} \times \sqrt{\frac{KT}{\rho_p d_p}} f(T, \phi, etc) \tag{2.6}$$

where β is a fraction of liquid which changes with different particles and $f\ (T, \phi)$ is a function of temperature and volume concentration, which changes from liquid to liquid.

Xue and Xu [32] developed an implicit relation, Eq. (2.7), for the effective thermal conductivity of CuO/water and CuO/EG nanofluids based on a model that accounts for interfacial shells between the nanoparticles and the liquid.

$$\left(1 - \frac{\phi}{\omega}\right) \times \frac{k_{nf} - k_{bf}}{2k_{nf} + k_{bf}} + \frac{\phi}{\omega} \frac{\left((k_{nf} - k_2)(2k_2 + k_p) - \omega(k_p - k_2)(2k_2 + k_{nf})\right)}{(2k_{nf} + k_2)(2k_2 + k_p) + 2\omega(k_p - k_2)(k_2 - k_{nf})} = 0 \tag{2.7a}$$

$$\omega = \left[\frac{r_p}{r_p + t}\right]^3 \tag{2.7b}$$

Here, k_2 is the thermal conductivity of the interfacial shell and t is the thickness of the shell.

Prasher et al. [2] proposed a conduction-convection model Eq. (2.8). They considered convection as due to Brownian motion of the nanoparticles and added it to the Maxwell-Garnett conduction model:

$$\frac{k_{nf}}{k_{bf}} = (1 + A\,Re^{m}\,Pr^{0.333}\,\phi)\left[\frac{(k_p(1+2\alpha)+2k_m)+2\phi(k_p(1-\alpha)-k_m)}{(k_p(1+2\alpha)+2k_m)-\phi(k_p(1-\alpha)-k_m)}\right] \quad (2.8a)$$

where the coefficient A = 4×10^4; m=2.5 $\pm$ 15% for water-based nanofluids, m=2.6 $\pm$ 15% for ethylene glycol based nanofluids and m=2.05 $\pm$ 15% for oil-based nanofluids and $\propto$ is the reciprocal of nanoparticle Biot number. The thermal boundary resistance is R_b. The k_m, $\propto$, R_b and Re can be calculated by Eq. (2.8b)

$$k_m = k_{bf}\left[1+\left(\frac{1}{4}RePr\right)\right], \propto = \frac{2R_b k_m}{d_p}, R_b(bf) = \frac{\rho_w c_{p_w}}{\rho_{bf} c_{p_{bf}}} * R_b(w) and$$

$$Re = \frac{1}{\nu}\sqrt{\frac{18KT}{\pi\rho_p d_p}} \quad (2.8b)$$

where R_b (w) is 0.77×10^{-8} Km^2W^{-1}.

Jang and Choi [33] proposed a theoretical model Eq. (2.9) by considering the energy transfer due to the collision between particles and base fluid molecules. This results in enhanced thermal conductivity of the fluid.

$$k_{nf} = k_{bf}(1-\phi) + \beta_1 k_p \phi + \frac{C_1 d_{bf}}{\rho_p} k_{bf} Re_{dp}^2 Pr\phi \quad (2.9)$$

Vajjha and Das [15] provided a new correlation to find the thermal conductivity of ethylene glycol nanofluids. They improved the Koo and Klienstreuer model by finding the new function of temperature and particle size and β values for ethylene glycol nanofluids.

$$k_{nf} = \frac{k_p + 2k_{bf} - 2(k_{bf}-k_p)\phi}{k_p + 2k_{bf} + (k_{bf}-k_p)\phi} k_{bf} + 5 \times 10^4 \beta\phi\rho_{bf} C_{p_{bf}} \times \sqrt{\frac{KT}{\rho_p d_p}} f(T,\phi,etc) \quad (2.10a)$$

$$f(T,\phi) = (2.8217 \times 10^{-2}\phi - 3.91123 \times 10^{-3})\left(\frac{T}{T_0}\right) + (-3.0669 \times 10^{-2}\phi - 3.91123 \times 10^{-3}) \quad (2.10b)$$

2.6 Preparation and characterization of nanofluids

2.6.1 Nanofluids samples

The nanofluids were procured from two different manufacturers (Alfa Aesar [34] and Nanostructured and Amorphous Materials, Inc. [35]). These manufacturers have developed

effective surfactants/dispersants for several nanofluid suspensions. Different nanofluids purchased from them have shown stable suspensions and no significant settling was observed in the bottles. We were unable to determine the different surfactants or dispersants the manufacturer employed as additives to stabilize the nanofluids, because this is proprietary information. In the study below, five types of nanofluids, namely Al_2O_3, ZnO, CuO, SiO_2 and TiO_2 nanoparticles, were dispersed in PG/W. Pure laboratory grade propylene glycol was mixed with deionized water in the proportion of 60 to 40 by mass using an electronic mass balance apparatus. The characteristics of materials procured for our experiments are shown in Table 2.1.

2.7 Ultrasonication of nanofluids

The sonication of nanofluids was carried out in two stages. First, the bottle containing aqueous concentrated mother nanofluid as supplied by the vendor was sonicated, then subjected to ultrasonication in a Branson model 5510 Sonicator [36] under a frequency of 40 kHz with a power of 185 W. We subjected the mother nanofluid (the original fluid from the manufacturer) to ultrasonication for three 2-hour sessions. The purpose of the first stage of ultrasonication was to break down the particles that had agglomerated due to long-term storage. The number of sonication sessions depended on the degree of sedimentation. Sonication was performed until careful visual examination showed a uniform dispersion of nanoparticles in the liquid. In the second stage, measured volume of samples from this concentrated mother fluid were pipetted into to a calculated mass of pure laboratory grade PG and de-ionized water in a test tube placed on a precise electronic mass balance in necessary proportions to prepare 0.5, 1, 2, 3, 4, and 6 % volumetric concentrations of nanofluids in the 60:40 PG/W solution.

2.8 Particle size measurement

Just before measuring the thermal conductivity of a sample of each concentration, the test tube containing the fluid was sonicated by immersion in the bath for two hours to ensure a uniform dispersion of nanoparticles in the suspension. In order to verify whether agglomerated particles were present in the sample prior to the thermal conductivity measurement, the sample was examined for particle size distribution under a transmission electron microscope (TEM). Figure 2.1 shows a TEM image of one of the Al_2O_3 nanofluid samples of 0.5% volumetric concentration.

The particle size result for this nanofluid is consistent with the data provided by the vendor. Alfa Aesar's Al_2O_3 nanofluid came with a specification of APS 45 nm. We noticed from the TEM image that a majority of nanoparticles fell near this average size, with a few smaller and a few larger particles, which should yield an overall average particle size of 45 nm.

From similar TEM images of the other four nanofluids containing Al_2O_3, ZnO, CuO, SiO_2 and TiO_2 nanoparticles, no agglomeration was observed. This was due to: (a) the nanofluid manufacturers have developed successful surfactants or dispersants that are already present in these purchased nanofluids, making them stably suspended and free from agglomeration or coagulation; (b) the sonication of the mother fluid before sample preparation followed by the second sonication of the dilute sample ensured breaking off of agglomerated particles, if any.

2.9 Principle of measurement

Different methods have been established to measure the thermal conductivity of nanofluids. The techniques that are commonly used to measure thermal conductivity are the transient hot wire technique, the thermal constants analyzer technique, the steady state parallel plate method, and the 3ω method. Das et al. [37], Williams and Buongiorno et al. [14] and Paul et al. [38] explained the techniques and their use in measurement of nanofluid thermal conductivity in detail. Our measurement technique is similar to the transient plane technique. The advantages of this method are low sample volume, no direct contact with samples, and prevention of convection in samples. The C-Therm thermal conductivity apparatus [39] has been used to measure the thermal conductivity of nanofluids. It works using the following principle. The heat equation with a constant supply of heat per sec per volume G' is given below

$$\rho C_p \frac{\partial T}{\partial t} = \lambda \frac{\partial^2 T}{\partial x^2} + G' \tag{2.11}$$

With the assumption of two semi-infinite media in contact, heat generated at the interface at a constant rate per unit area per unit time. A further assumption is that the effusivity sensor represents one medium and the other medium is the tested material. They are both at the same temperature and in equilibrium. The solutions for Eq. (2.11) are provided by equations (2.12) and (2.13):

$$\Delta T_1(x,t) = \frac{2G\sqrt{t}}{e_1 + e_2} ierfc \frac{|x|}{2\sqrt{a_1 t}}, for\ x < 0, t > 0 \quad (2.12)$$

$$\Delta T_1(x,t) = \frac{2G\sqrt{t}}{e_1 + e_2} ierfc \frac{|x|}{2\sqrt{a_2 t}}, for\ x \geq 0, t > 0 \quad (2.13)$$

where ΔT is the change in sensor surface temperature, G is the heat flux supplied to the sensor (W/m^2), t is the time measured from start of process, e_1 and e_2 are the equivalent effusivity of the sensor and material, respectively, $(\frac{W\sqrt{s}}{m^2 K})$, a_1 and a_2 are the equivalent diffusivity of the sensor and material, $(\frac{m^2}{s})$, λ_1 and λ_2 are the thermal conductivity of the sensor and material, respectively $(\frac{W}{mK})$, ρ_1 and ρ_2 are the equivalent density of the sensor and material $(\frac{Kg}{m^3})$, and Cp1 and Cp2 are the specific heats of the sensor and material $(\frac{J}{Kg*K})$, respectively.

Using the above solution, the instrument measures the increase in temperature of the sample for a fixed amount of heat flux at the interface plane. Using the measured values of temperature increase and heat flux given to testing sample, instrument measures the thermal conductivity of the sample. This process of measurement is further explained by C-Therm Technologies [39].

2.10 Procedure

A schematic diagram of the thermal conductivity measurement setup is shown in Figure 2.2. The figure shows a thermal conductivity sensor, which is used to measure the thermal conductivity of nanofluid samples. The sensor is placed in a thermal chamber in which the temperature of the nanofluid is varied. The sensor is connected to a data acquisition system, which corresponds with it in recording temperature and measuring thermal conductivity of nanofluid samples. The data acquisition system is connected to a computer. The data acquired from measurements is stored in the computer. Using this experimental setup, we are able to measure thermal conductivity of propylene glycol nanofluids in a temperature range between 243K (-30 ℃) to 363K (90 ℃). This helped us study the behavior of nanofluids at low temperatures, which has not been studied previously.

The experiment starts with sonicating the sample for 2 hours before starting the experiments placed in the volume cell of the sensor. This cell holds a small volume of nanofluid

right on top of the sensor. The volume cell has a lid that covers the volume cell and prevents outside air from entering the volume cell. The sensor is placed inside a thermal chamber where the ambient temperature is varied. The thermal chamber is set to reach a temperature of 243K (-30 ℃) in 1 hour. The sensor is kept at 243K for half an hour to reach temperature stability before the measurement was started. An average of 7 readings were taken for every measurement. For the next temperature measurement point, the chamber is made to reach a temperature difference of 10℃ in half an hour. The measurement process is then repeated again. Measurements were taken at temperature increments of 10 ℃. The measurements were taken between 243K (-30 ℃) and 363K (90 ℃). The experiments were performed on five different nanoparticles, Al_2O_3, ZnO, CuO, SiO_2 and TiO_2 with volume concentrations varying from 0.5% to 6%. With these experiments, we studied the effect of different material nanoparticles, temperature, volume concentration, and particle size on thermal conductivity of 60:40 PG/W.

2.11 Results and discussion

2.11.1 Benchmark test case

Before using the apparatus for measuring the thermal conductivity of nanofluids, a benchmark test was performed with water and 60:40 PG/W, whose thermal conductivities are accurately known. Figure 2.3 compares the measured thermal conductivity and the values from Bejan [40] and ASHRAE [1] for water and 60:40 PG/W, respectively. The measured values showed a maximum deviation of 2.1% at 284 K for water and a maximum deviation of 3.6% at 242 K for 60:40 PG/W compared to the data from Bejan and ASHRAE, respectively. The base fluid thermal conductivity (k_{bf}) equation derived for 60:40 PG/W using ASHRAE data has been used in all subsequent calculations.

2.11.2 Al_2O_3 nanofluid

Thermal conductivity measurements were taken for three different diameters (15nm, 20nm, 45nm) of Al2O3 nanoparticles dispersed in 60:40 PG/W with a temperature range of 242K (-30℃) to 363K (90℃). The volumetric concentration varied for each diameter (15nm, 20nm, 45nm) from 0.5% to 2%, 0.5% to 4%, and 0.5% to 6%, respectively. Figures 2.4-2.6 show the thermal conductivity of these nanofluids as a function of temperature.

Figure 2.4 shows the thermal conductivity values of a 15nm Al_2O_3 nanofluid. At lower temperatures (242K), a 0.5% volume concentration showed 2% enhancement, and at 363K it showed 3.3% enhancement with 60:40 PG/W. The 2% volume concentration nanofluid at 242K showed 8% enhancement, and at 363K it showed 10.5% enhancement.

Figure 2.5 shows the thermal conductivity values of 20nm Al_2O_3 nanofluid. The higher volume concentration showed better thermal conductivity enhancement. At lower temperatures 242K, the 0.5% volume concentration showed 2% enhancement, and at 363K it showed 4.3% enhancement with 60:40 PG/W. The 4% volume concentration nanofluid at 242K showed 4.4% enhancement, and at 363K it showed 7.3% enhancement.

Figure 2.6 shows the thermal conductivity values of 45nm Al_2O_3 nanofluid. The higher volume concentration showed greater thermal conductivity enhancement. At lower temperatures 242K, the 0.5% volume concentration showed 3.6% enhancement, and at 363K it showed 4.8% enhancement with 60:40 PG/W. The 6% volume concentration nanofluid showed 8.3% enhancement at 242K and 12.2% enhancement at 363K. From the figures shown above, the thermal conductivity is strongly affected by temperature, concentration and particle size. We see that the thermal conductivity of Al_2O_3 is directly related to temperature and concentration. These results prove that the thermal conductivity of 60:40 PG/W Al_2O_3 nanofluids increases with temperature and volume concentration.

2.11.3 ZnO nanofluid

Thermal conductivity measurements were taken for three different diameters (36nm, 50nm, 76nm) of ZnO nanoparticles dispersed in 60:40 PG/W with a temperature range of 242K (-30 ℃) to 363K (90 ℃). The volumetric concentration varied for each diameter (36nm, 50nm, 76nm) from 0.5% to 2%, 0.5% to 4%, and 0.5% to 6%, respectively. Figures 2.7-2.9 show the thermal conductivity of these nanofluids as a function of temperature.

Figure 2.7 shows the thermal conductivity values of the 36nm ZnO nanofluid with volume concentrations from 0.5% to 4%. The measured temperature range is between 242K (-30 ℃) and 363K (90℃). The higher volume concentrations showed greater thermal conductivity enhancement. At lower temperatures 242K, 0.5% volume concentration showed 1.6%

enhancement, and at 363K it showed 2.34% enhancement with 60:40 PG/W. The 4% volume concentration nanofluid showed 9.6% enhancement at 242K and 10.57% enhancement at 363K.

Figure 2.8 shows the thermal conductivity values of the 50nm ZnO nanofluid with volume concentrations from 0.5% to 6%. The measured temperature range is between 242K (-30 ℃) and 363K (90 ℃). The higher volume concentrations showed greater thermal conductivity enhancement. At lower temperatures 242K, 0.5% volume concentration showed 2.3% enhancement, and at 363K it showed 3.7% enhancement with 60:40 PG/W. The 6% volume concentration nanofluid showed 15.86% enhancement at 242K and 17.19% enhancement at 363K.

Figure 2.9 shows the thermal conductivity values of 76nm ZnO nanofluid with volume concentrations from 0.5% to 6%. The measured temperature range is between 242K (-30℃) and 363K (90℃). The higher volume concentration showed greater thermal conductivity enhancement. At lower temperatures 242K, the 0.5% volume concentration showed 4.3% enhancement, and at 363K it showed 6% enhancement with 60:40 PG/W. The 6% volume concentration nanofluid showed 17.3% enhancement at 242K and 21.36% enhancement at 363K. From the figures shown above, the thermal conductivity is strongly affected by temperature, concentration and particle size. We see that the thermal conductivity of ZnO is directly related to temperature and concentration. These results prove that thermal conductivity of 60:40 PG/W ZnO nanofluids increases with temperature and volume concentration.

2.11.4 CuO nanofluid

Figure 2.10 shows the thermal conductivity measurements of CuO nanofluid with temperature. This figure explains the effect of volume concentration and temperature on the thermal conductivity of CuO nanofluids. After observing these results, it was found that the thermal conductivity increases with temperature and volume concentration.

Figure 2.10 shows the thermal conductivity values of CuO nanofluid with volume concentrations from 0.5% to 6%. The measured temperature range is between 242K (-30 ℃) and 363K (90 ℃). The higher volume concentration showed greater thermal conductivity enhancement. The 0.5% volume concentration showed 2.3% enhancement at 242K and 4.4%

enhancement at 363K with 60:40 PG/W. The 6% volume concentration nanofluid showed 12.5% enhancement at 242K and 15.6% enhancement at 363K.

2.11.5 SiO_2 nanofluid

Figure 2.11 shows the thermal conductivity measurements of SiO_2 nanofluid with temperature. This figure explains the effect of volume concentration and temperature on the thermal conductivity of SiO_2 nanofluids. After observing these results it was found that the thermal conductivity increases with temperature and volume concentration. Figure 2.11 shows the thermal conductivity values of SiO_2 nanofluid with volume concentrations from 0.5% to 5%. The measured temperature range is between 242K (-30°C) and 363K (90°C). The higher volume concentrations showed greater thermal conductivity enhancement. The 0.5% volume concentration showed no enhancement with temperature. The 6% volume concentration nanofluid showed 4.7% enhancement at 242K and 7.2% enhancement at 363K.

2.11.6 TiO_2 nanofluid

Figure 2.12 shows the thermal conductivity measurements of TiO_2 nanofluids with temperature. This figure explains the effect of volume concentration and temperature on thermal conductivity of TiO_2 nanofluids. After observing these results it was found that the thermal conductivity increases with temperature and volume concentration.

Figure 2.12 shows the thermal conductivity values of TiO_2 nanofluids with volume concentrations from 0.5% to 1.5%. The measured temperature range is between 242K (-30°C) and 363K (90°C). The higher volume concentrations showed greater thermal conductivity enhancement. The 0.5% volume concentration showed 1% enhancement at 242K and 3.56% enhancement at 363K with 60:40 PG/W. The 1.5% volume concentration nanofluid showed 4.7% enhancement at 242K and 7.3% enhancement at 363K.

2.11.7 Particle size effect

The effect of particle size on thermal conductivity enhancement has been studied for Al_2O_3 and ZnO nanofluids. Three different particle sizes have been studied for both nanofluids. The

enhancement seems to be better with increasing particle size. The same trend was observed by Shima et al. [20] and Fang et al. [22] for other nanofluids.

Figure 2.13 shows the variation of thermal conductivity of Al_2O_3 nanofluids with different particle sizes for the same volume concentration and varying temperatures. The results show that Al_2O_3 nanofluid thermal conductivity enhancement increases with increasing particle size. For the same volume concentration, the higher particle sizes yielded greater thermal conductivity enhancement than the lower particle sizes.

Figure 2.14 shows the thermal conductivity enhancement of ZnO nanofluids of different particle sizes with varying temperatures. The observed results were similar to those of Al_2O_3 nanofluids. In ZnO nanofluids, the higher particle sizes showed greater enhancement than smaller ones for the same volume concentration.

2.11.8 Thermal conductivity correlation

After experimentally determining the thermal conductivities of five nanofluids, it was attempted to select a correlation, which will be suitable for all of them. As described in the introduction, there are a number of models available to predict the thermal conductivity of nanofluids. The drawback of these models is that they are not general enough to be valid for several nanofluids. Researchers are still trying to find a single correlation that works for all nanofluids, but it does not seem possible at present. We compared our experimental data with the existing models to find out, if any of them satisfy our experimental data of PG/W nanofluids. Figure 2.15 compares the thermal conductivity of 6% Al_2O_3 (45nm) nanofluid experimental values with several existing models. The Hamilton-Crosser model, Eq. (2.2), and Xuan et al. model, Eq. (2.5), predict almost similar values, because the second term of Eq. (2.5) is very small. Except the model of Prasher et al. [2], other theories fail to match our experimental results. Prasher et al. had proposed m=2.5 $\pm$ 15% for water-based nanofluids, m=1.6 $\pm$ 15% for ethylene glycol-based and m=1.05 $\pm$ 15% for oil-based nanofluids. No m value for propylene glycol-based nanofluids was available. Therefore we attempted with a value of m=2.5 as shown in Figure 2.15, and found the model matches the data well at 363K but not at 243K. Therefore, the m value can be optimized by statistical analysis of 600 data points to get a better agreement. We performed statistical analysis using Minitab [41] to arrive at an

optimum value of m which will yield better best agreement for propylene glycol nanofluids. Some positive aspects of Prasher et al. model are: it contains the particle Reynolds number due to the Brownian velocity, Prandtl number, Biot number and Maxwell type mixture property. Therefore, we believe this model has the necessary physics built into it. Our statistical analysis focused on determining the optimum value of the constant m in Eq. (2.8a) for five different propylene glycol based nanofluids. The results of these analyses are summarized in Table 2.2.

Our experimental results comprised of 600 data points derived from five different nanoparticles with various particle sizes, volumetric concentrations and PG/W base fluid. The parameter m changes with different types of nanofluids. Our objective was to derive a common m value that predicts thermal conductivity of all five propylene glycol nanofluids. The Minitab statistical software gave a value (m = 2.698) that works for all propylene glycol nanofluids tested in our experiments within the deviation summarized in Table 2.2. Figure 2.16 shows the comparison between our experimental results and model predictions with m = 2.698. The plot shows good agreement between the experimental data and model prediction within the bounds summarized in Table 2.2. The correlation is valid in the range: 15 nm < d_p < 76 nm, 0.005 < Ø < 0.06, and 243 K < T < 363 K.

2.12 Conclusions

From a set of carefully conducted experiments, the thermal conductivities of five propylene glycol water based nanofluids were measured over a temperature range of 243K–363K for various nanoparticles and volumetric concentrations. The results showed an increase in thermal conductivity of nanofluids with increasing concentration and temperature. As the nanoparticles diameter increased, the thermal conductivity increased. It was noticed that several correlations did not capture the thermal conductivity variations with temperature and concentration properly. The reason for this is that models are usually developed without considering large experimental data sets. The model presented by Prasher et al. [2] proved effective. This model was refined using a broader set of experimental data, which provided a new correlation constant m for 60:40 PG/W based nanofluids. With this new value of m = 2.698, Eq. (2.8a) gives accurate predictions of thermal conductivity of different PG/W nanofluids over a wide range of concentration, temperature and particle sizes. Since the nanofluids exhibit enhanced thermal conductivity with increasing

temperature, it is concluded that their application in higher temperature environments will be more beneficial.

2.13 Acknowledgement

Financial support from the National Aeronautics and Space Administration, Experimental Program to Stimulate Competitive Research grant # AK-NNX11AM16A is gratefully acknowledged.

2.14 Nomenclature

d_p	Nanoparticle diameter (m)
c_p	Specific heat (J kg^{-1} K^{-1})
k	Thermal conductivity (W m^{-1} K^{-1})
m	Empirical constant for different nanofluids
Pr	Prandtl number
R_b	Thermal boundary resistance ($m^{-2}KW^{-1}$)
Re	Brownian Reynolds number
T	Temperature (K)
T_0	Reference temperature (273 K)
PG/W	Propylene glycol and water mixture

Greek symbols

α	Reciprocal of particle Biot number
K	Boltzmann constant 1.381 x 10^{-23} (J K^{-1})
μ	Viscosity (kg $m^{-1}s^{-1}$)
ν	Kinematic viscosity (m^2 s^{-1})
ρ	Density (kg m^{-3})
ϕ	Particle volumetric concentration %

Subscripts

bf	Base fluid
nf	Nanofluid
p	Nanoparticle
w	Water

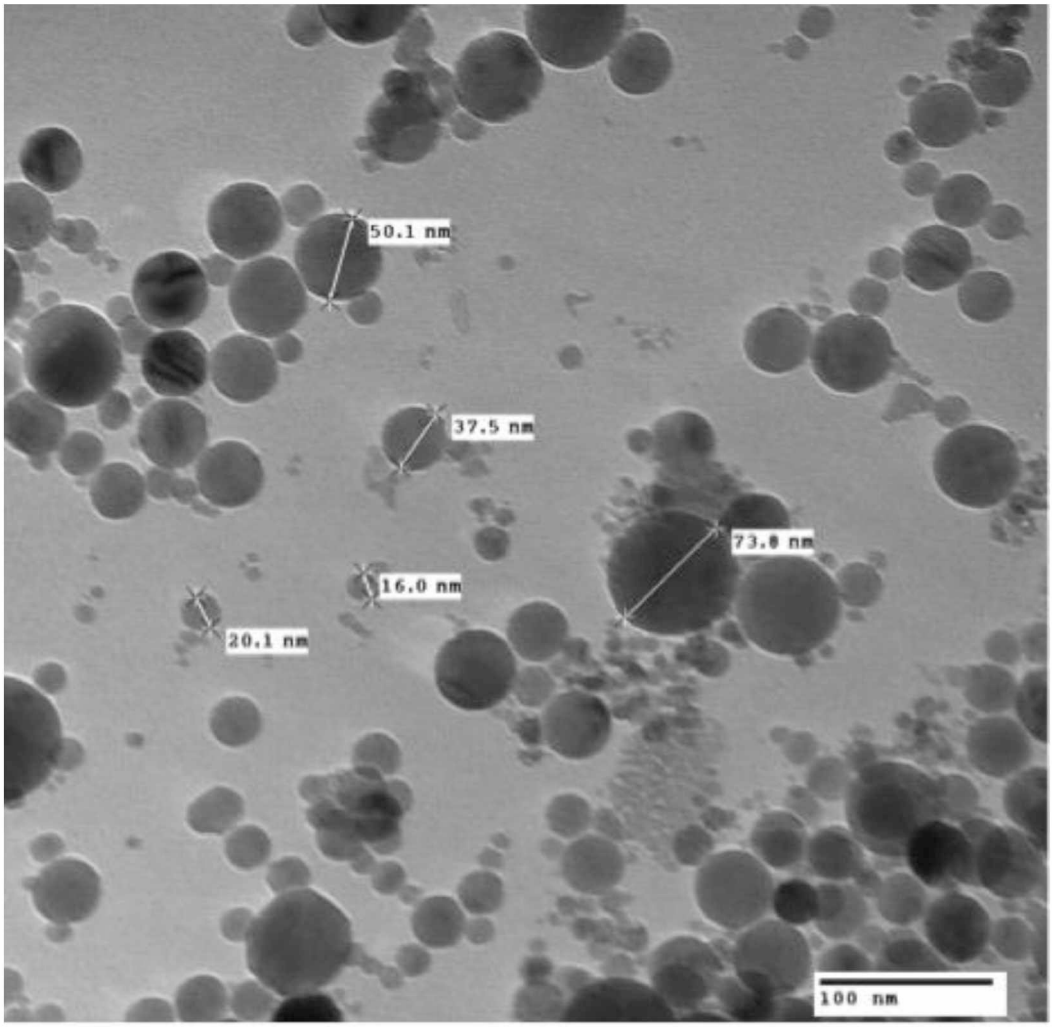

Figure 2.1. TEM image of Al_2O_3 45nm nanoparticles

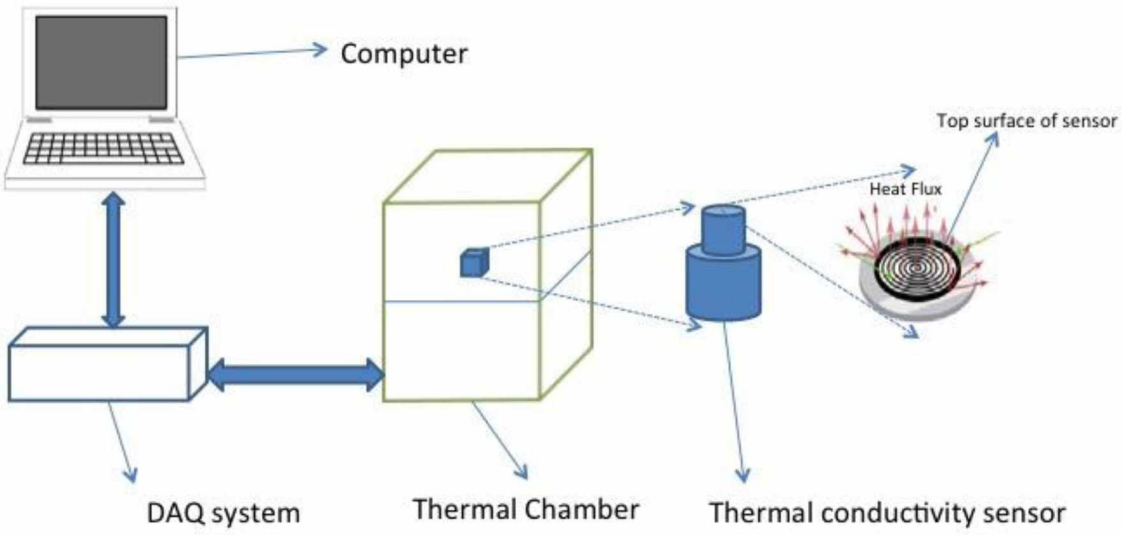

Figure 2.2. Schematic diagram of experimental setup of thermal conductivity measurement.

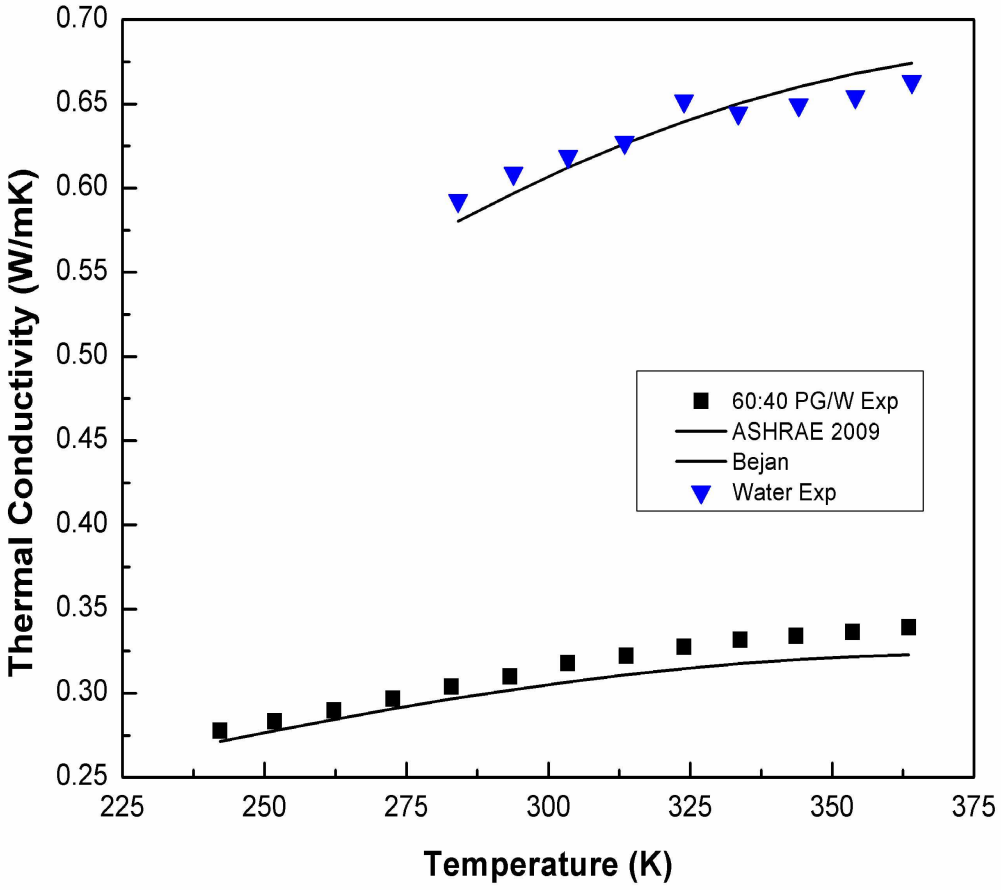

Figure 2.3. Benchmark test results of reference fluids.

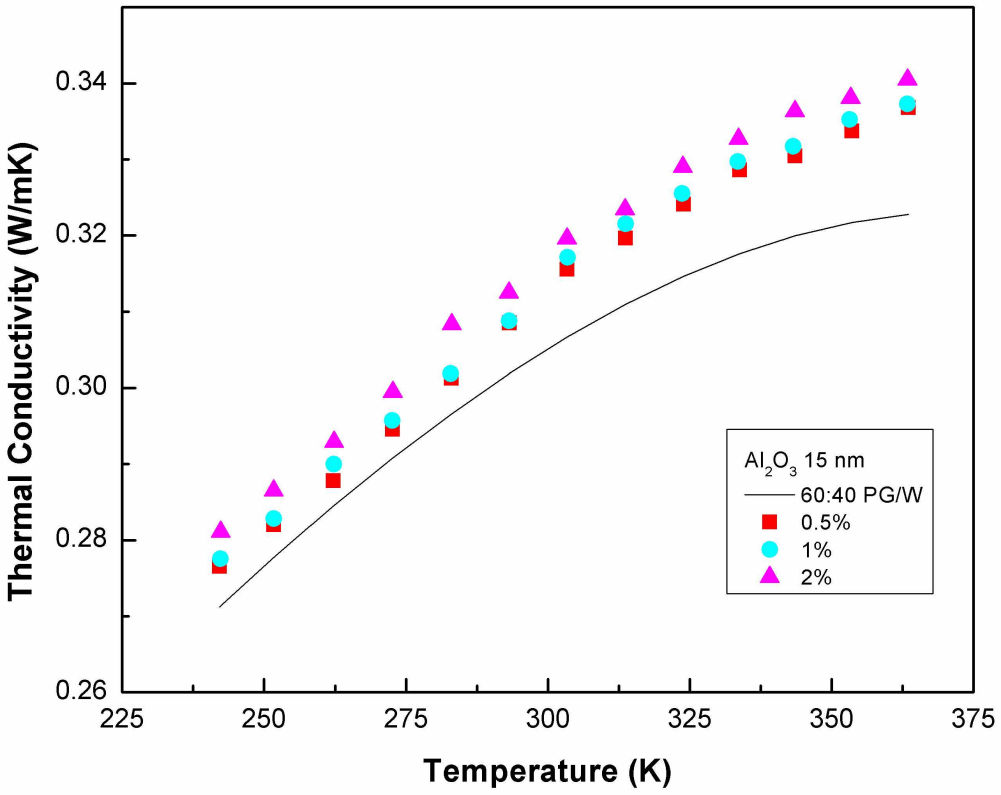

Figure 2.4. Measured thermal conductivity of 15nm Al_2O_3 nanofluids with varying temperature and concentration.

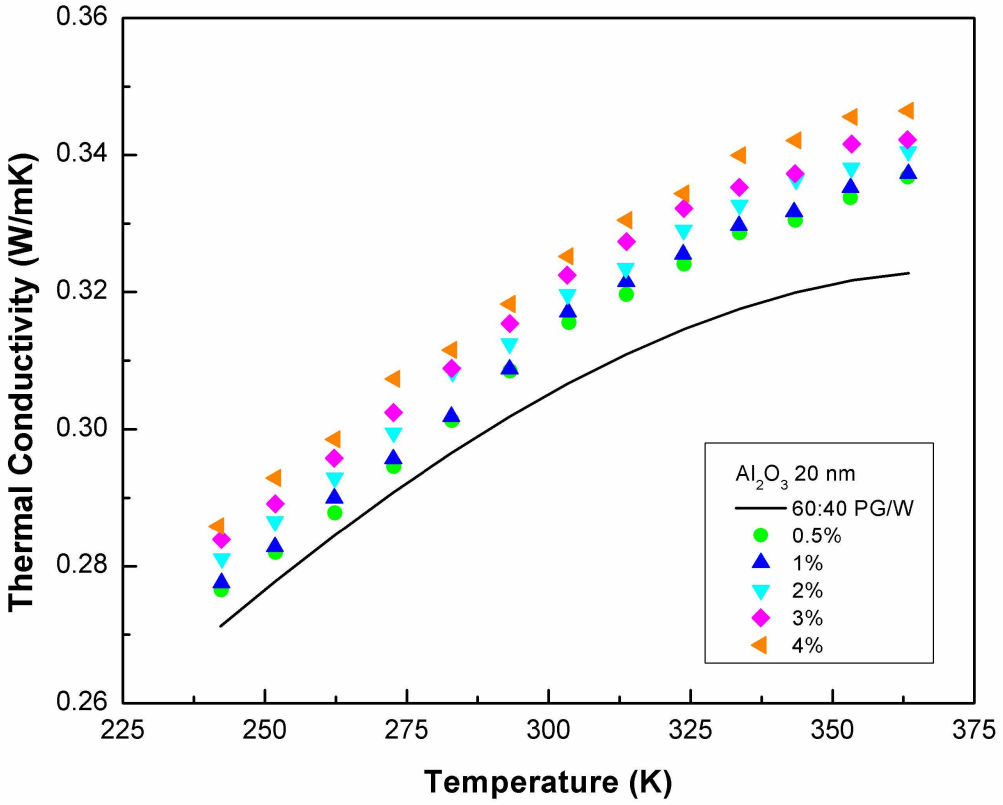

Figure 2.5. Thermal conductivity measurement of 20nm Al_2O_3 nanofluid with varying temperature and concentration.

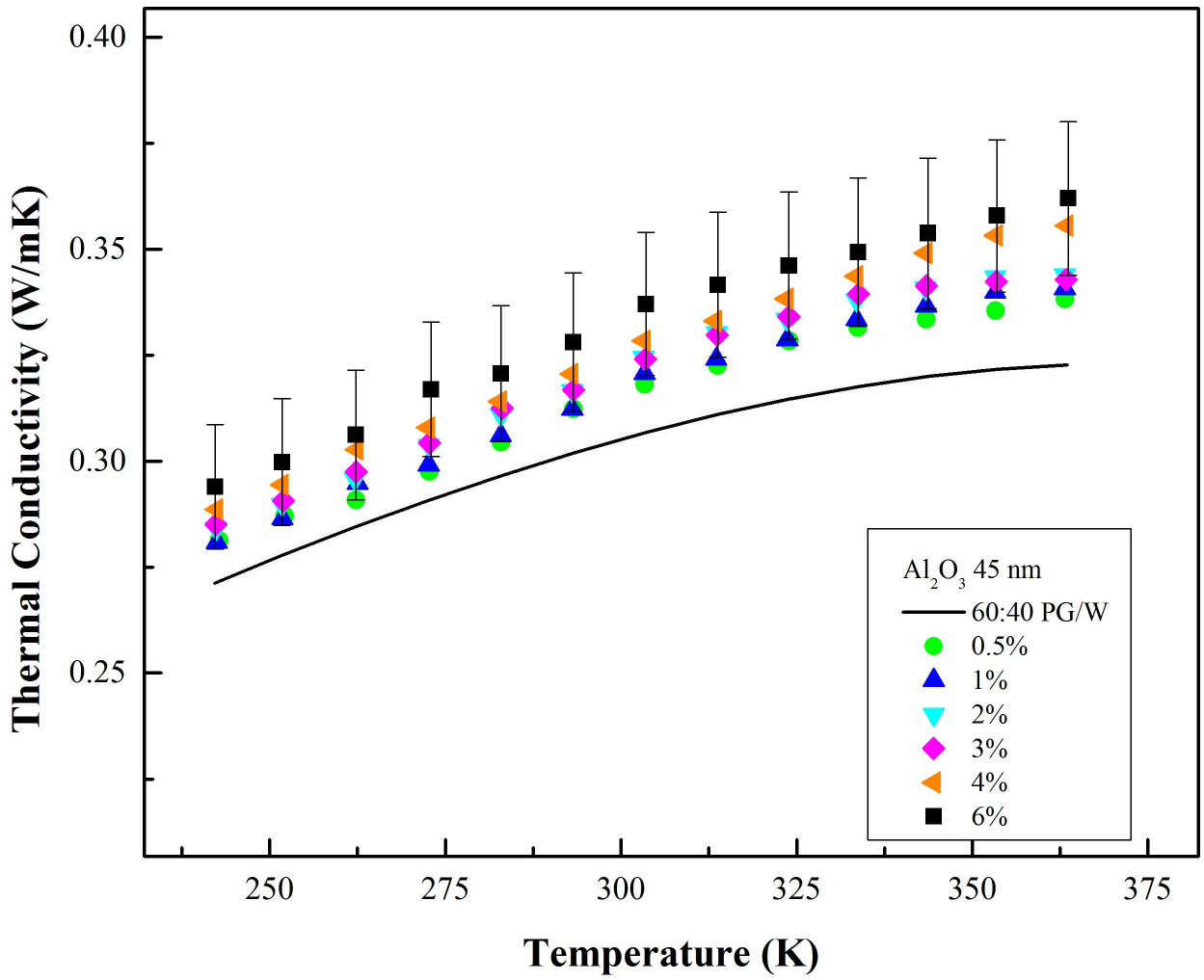

Figure 2.6. Measured thermal conductivity of 45nm Al_2O_3 nanofluid with varying temperature and concentration.

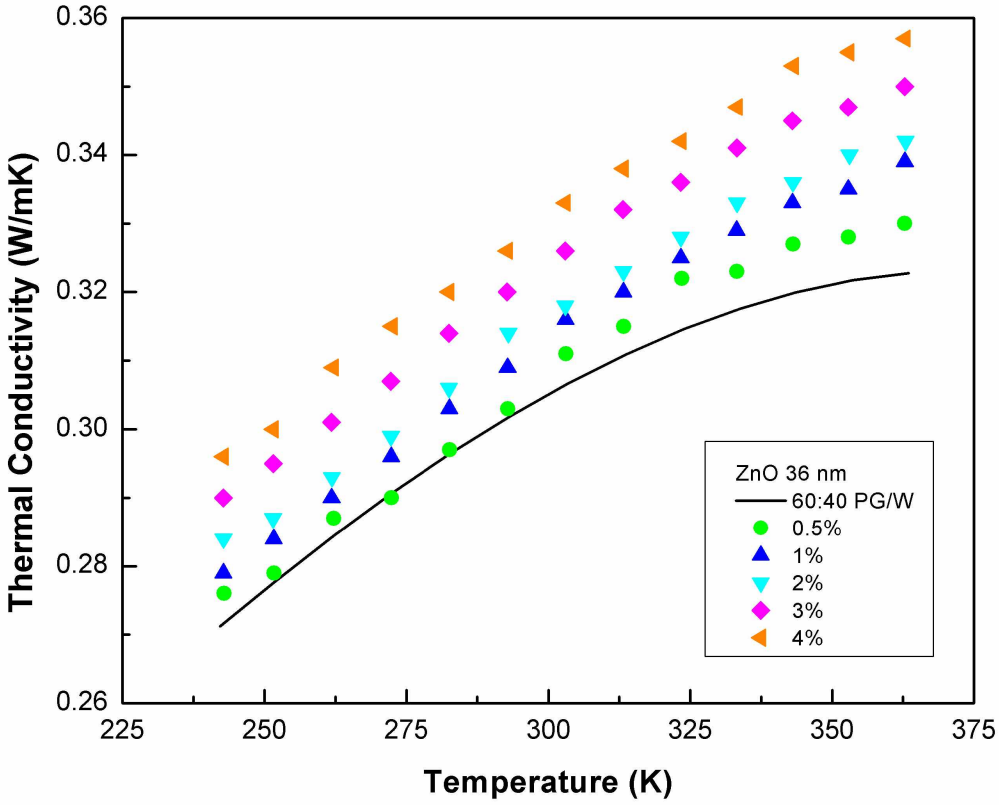

Figure 2.7. Measured thermal conductivity of 36nm ZnO nanofluids with varying temperature and concentration.

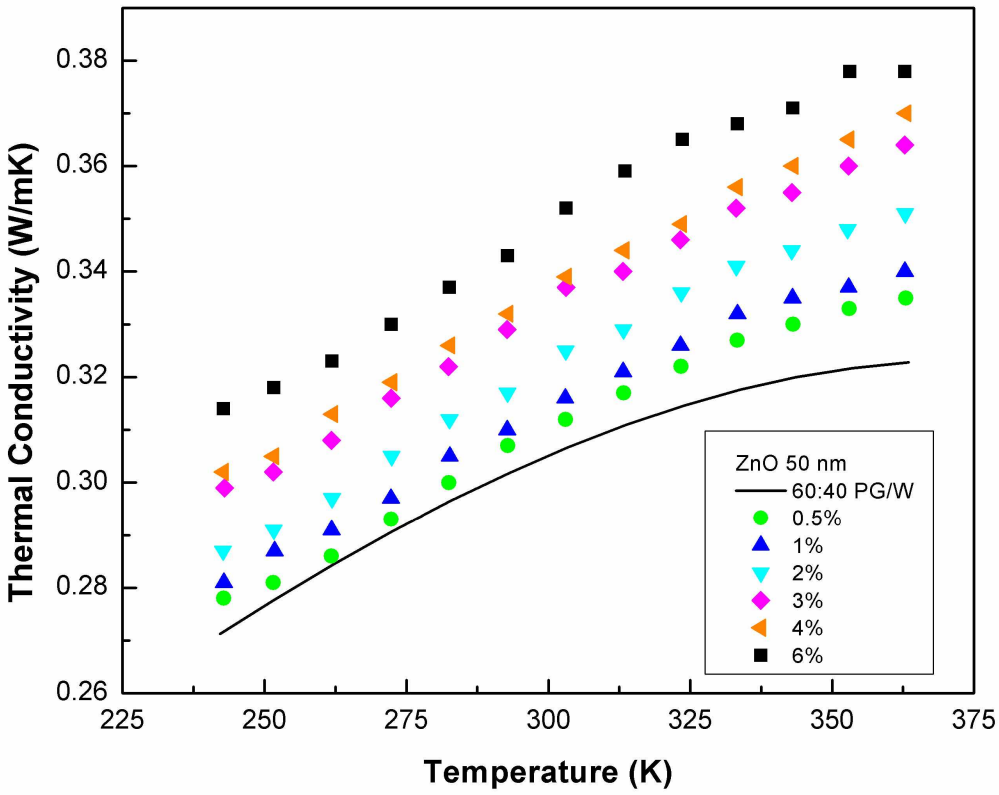

Figure 2.8. Measured thermal conductivity of 50nm ZnO Nanofluids with varying temperature and concentration.

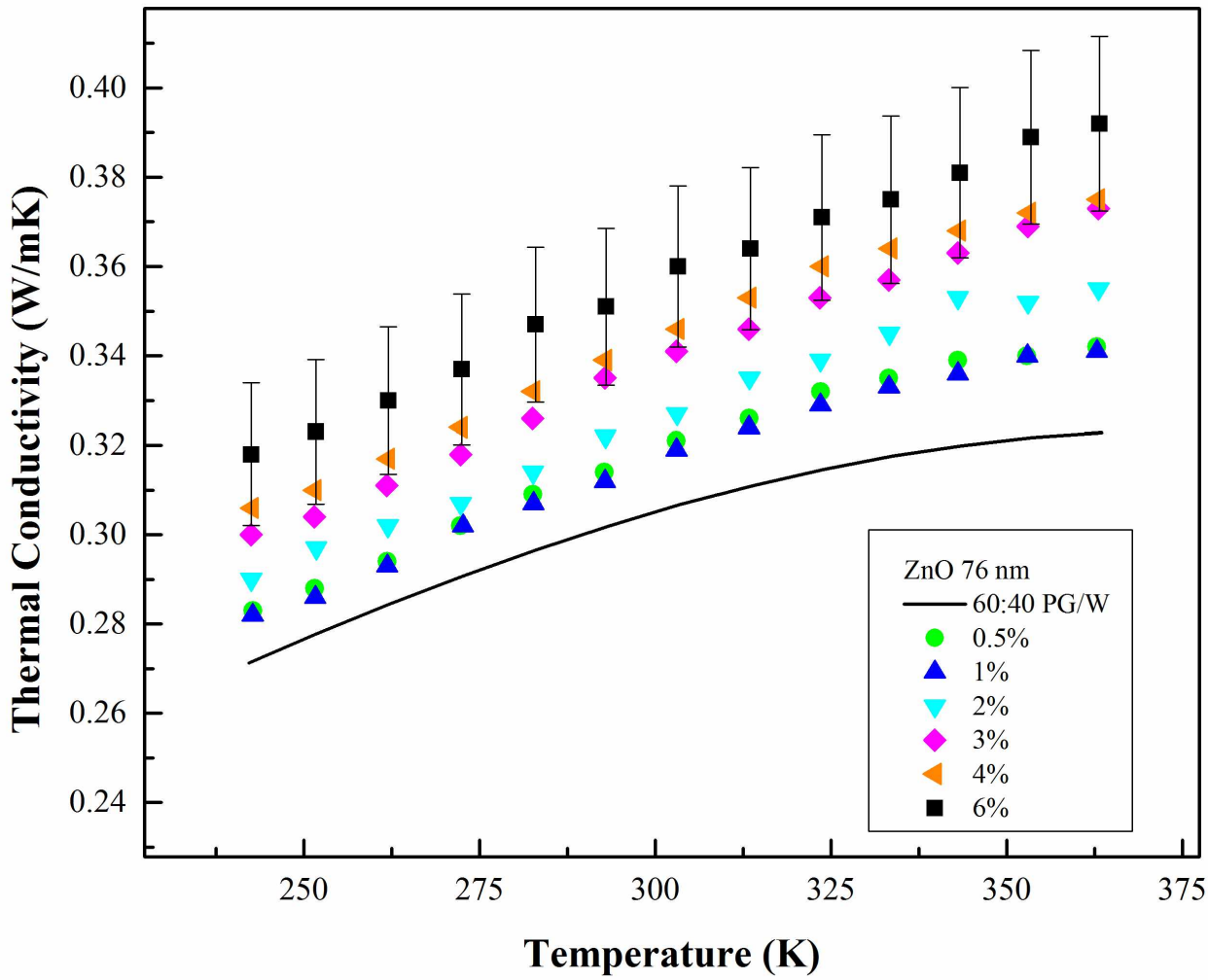

Figure 2.9. Measured thermal conductivity of 76nm ZnO nanofluids with varying temperature and concentration.

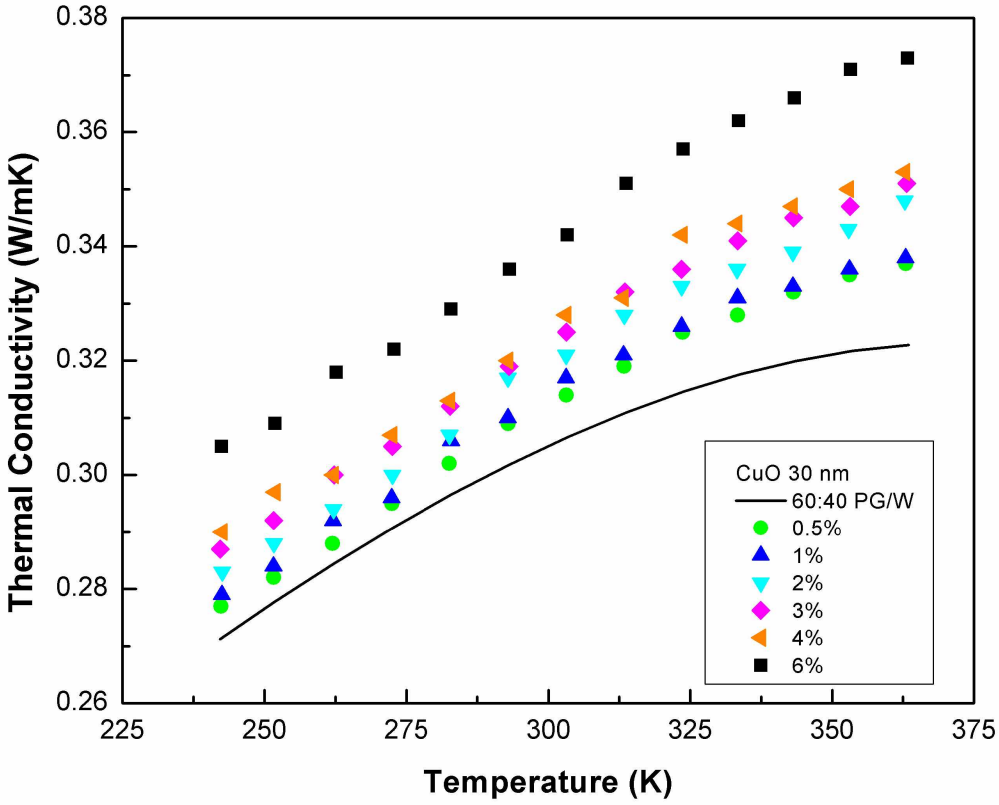

Figure 2.10. Measured thermal conductivity of 30nm CuO nanofluids varying with varying temperature and concentration.

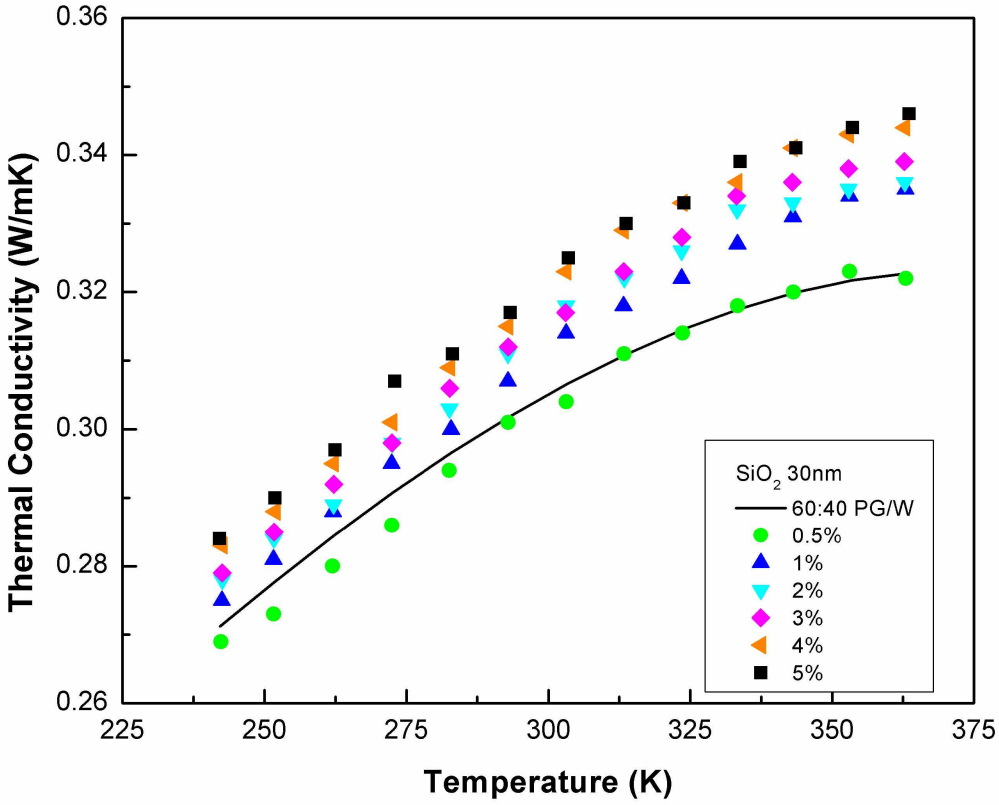

Figure 2.11. Measured thermal conductivity of 30 nm SiO_2 nanofluids with varying temperature and concentration.

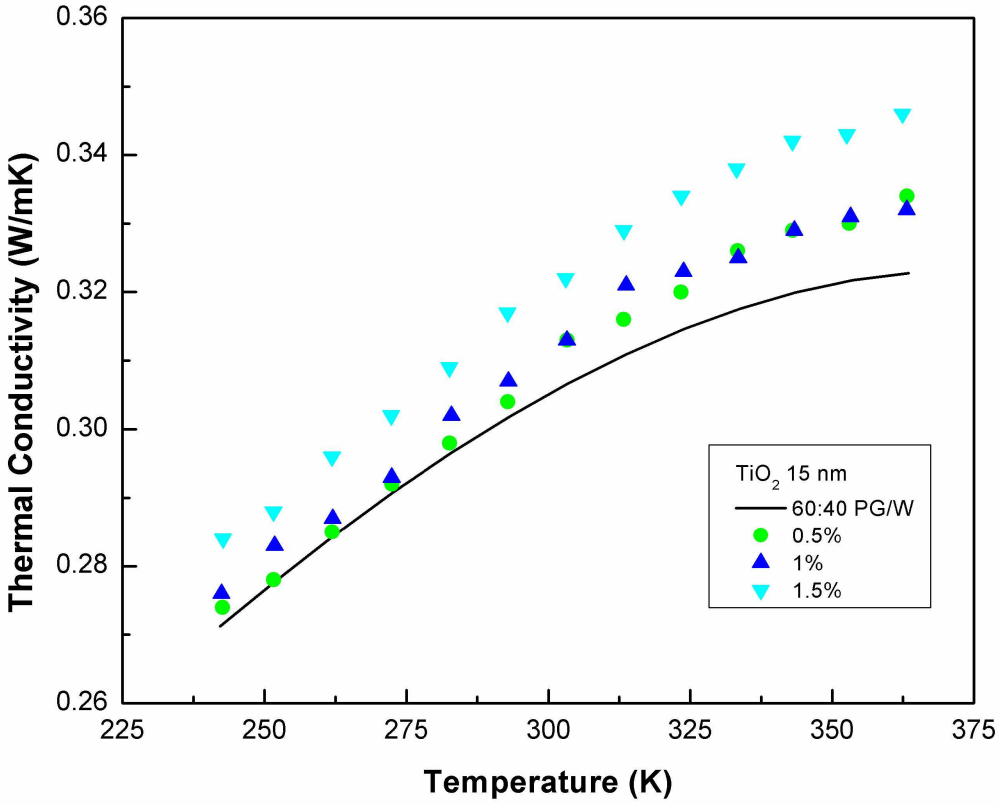

Figure 2.12. Measured thermal conductivity of 15 nm TiO_2 nanofluids with varying temperature and concentration.

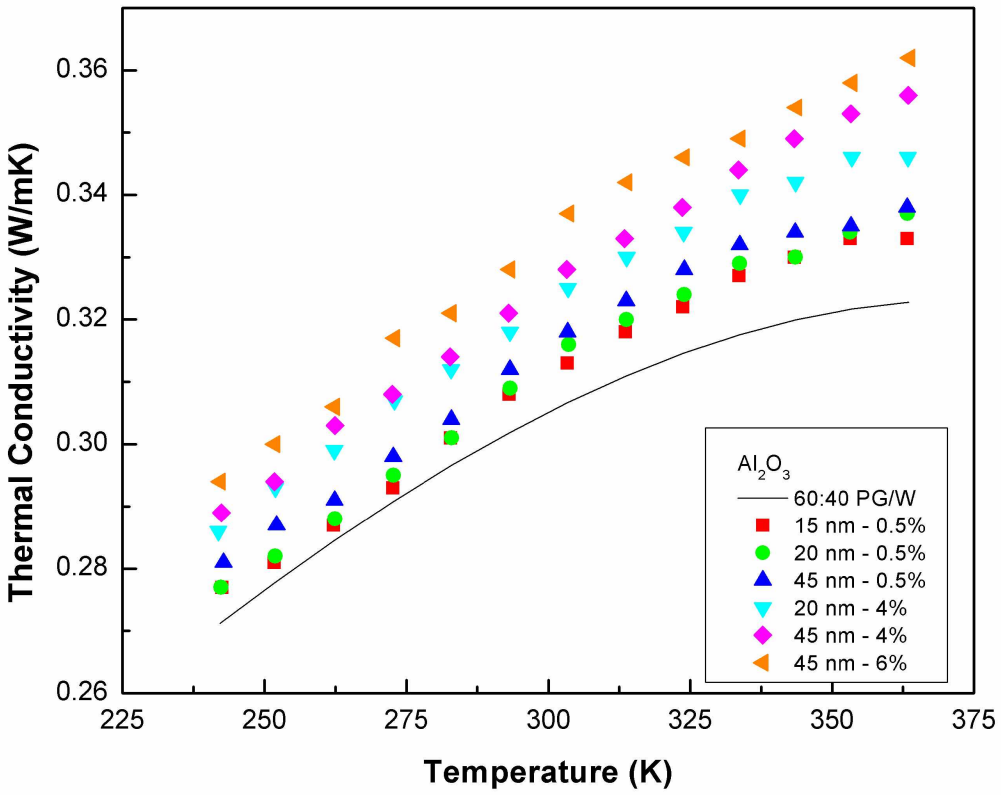

Figure 2.13. Effect of particle size on thermal conductivity of Al_2O_3 nanofluids.

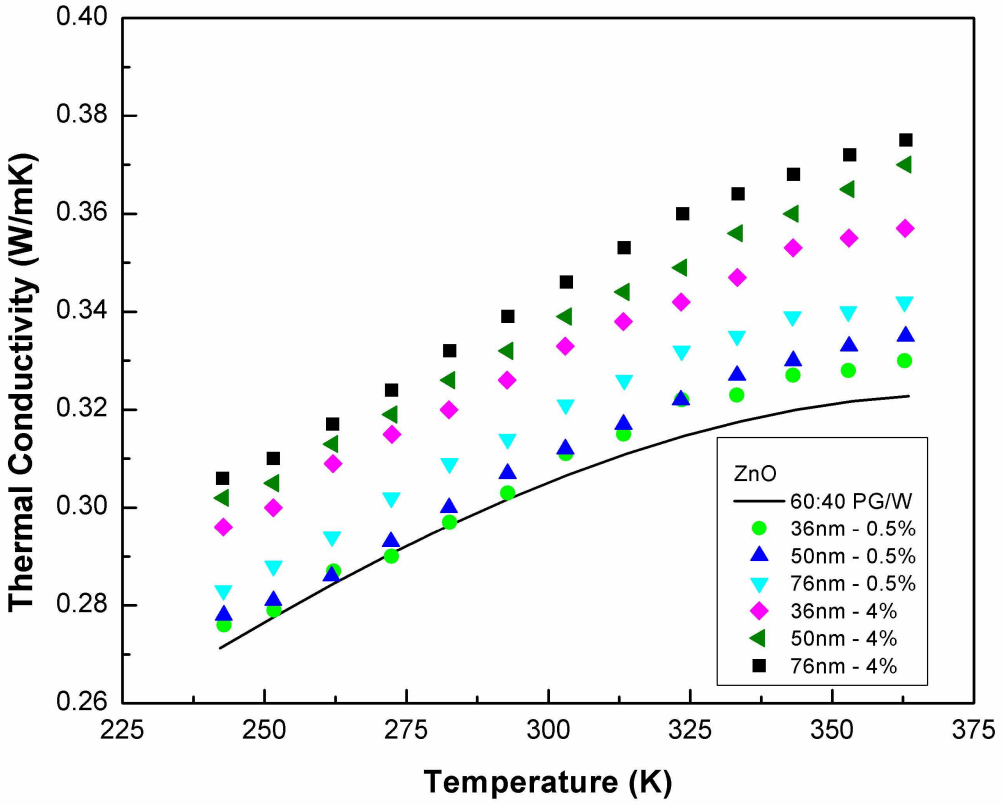

Figure 2.14. Effect of particle size on thermal conductivity of ZnO nanofluids.

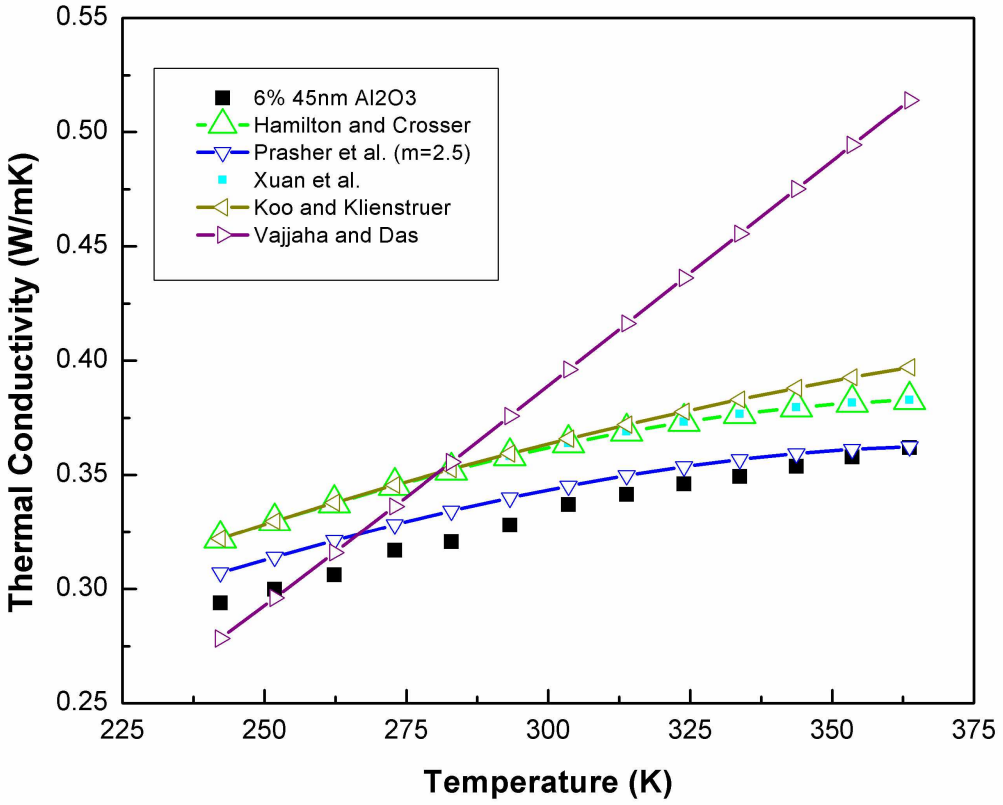

Figure 2.15. Comparison of experimental data with existing models.

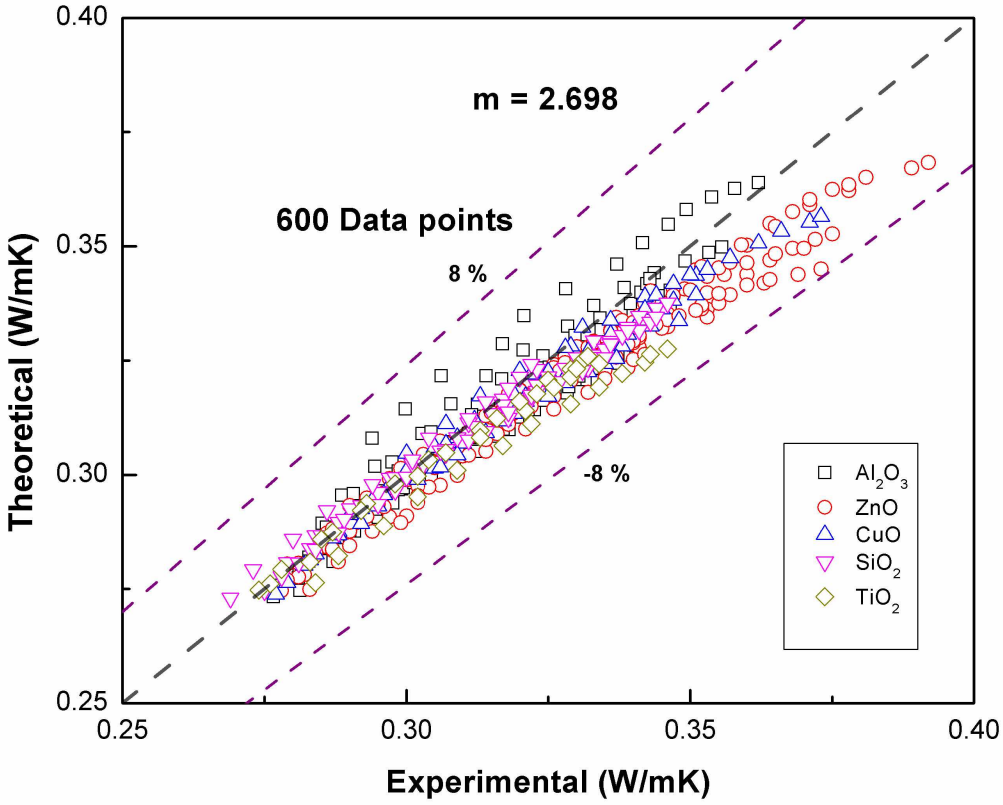

Figure 2.16. Comparison of experimental values with theoretical model with m = 2.698

Table 2.1. Material characteristics of nanofluids used in the present experiments

Manufacturer	Material	Particle size (nm)	Particle Density (g/cc)	Parent nanofluid concentration wt % in H_2O
Alfa Aesar	Al_2O_3	20	3.6	30
Alfa Aesar	Al_2O_3	45	3.6	50
Nanostructured and Amorphous Materials, Inc.	Al_2O_3	15	3.6	15
Nanostructured and Amorphous Materials, Inc.	SiO_2	30	2.41	25
Alfa Aesar	ZnO	36	5.6	40
Alfa Aesar	ZnO	50	5.6	50
Alfa Aesar	ZnO	76	5.6	50
Alfa Aesar	CuO	30	6.31	50
Nanostructured and Amorphous Materials, Inc.	TiO_2	15	4.23	15

Table 2.2. Statistical results of the analysis with optimum value of m=2.698.

Nanoparticles	Max Deviation $\frac{Exp-Theory}{Exp} * 100$ (+) (%)	Max Deviation $\frac{Exp-Theory}{Exp} * 100$ (-) (%)	Avg. Abs. Deviation $\frac{1}{N}\sum\left(\left\|\frac{Exp-Theory}{Exp}\right\|\right) * 100$ (%)	R^2
Al_2O_3	4.808	0.018	4.388	0.923
ZnO	1.144	8.103	2.208	0.971
CuO	4.622	0.018	1.152	0.978
SiO_2	2.893	0.042	0.929	0.982
TiO_2	5.632	0.010	2.768	0.959
Summary for all data points (N=600)	5.632	-8.103	1.79	0.925

2.15 References

[1] ASHRAE, 2009, "Physical Properties of Secondary Coolants (Brines)," ASHRAE Handbook, American society of Heating Refrigerator and Air Conditioning Engineers, Inc, Atlanta.

[2] Prasher R., Bhattacharya P., and Phelan P. E., 2006, "Brownian-Motion-Based Convective-Conductive Model for the Effective Thermal Conductivity of Nanofluids," ASME J. Heat Transf., **128**(6), p. 588.

[3] Maxwell J. C., 1891, A Treatise on Electricity & Magnetism, Dover Books on Physics, New York.

[4] Masuda H., Ebata A., Teramae K., and Hishinuma N., 1993, "Alteration of Thermal Conductivity and viscosity of Liquid by dispersing Ultra-Fine Particles (Dispersions of Al2O3, SiO2 and TiO2 Ultra-FIne Particles)," Netsu Bussei, **4**(4), pp. 227–233.

[5] Lee S., Choi S. U.-S., Li S., and Eastman J. A., 1999, "Measuring Thermal Conductivity of Fluids Containing Oxide Nanoparticles," ASME J. Heat Transf., **121**(2), p. 280.

[6] Eastman J. A., Choi S. U. S., Li S., Yu W., and Thompson L. J., 2001, "Anomalously increased effective thermal conductivities of ethylene glycol-based nanofluids containing copper nanoparticles," Appl. Phys. Lett., **78**(6), p. 718.

[7] Choi S. U. S., Zhang Z. G., Yu W., Lockwood F. E., and Grulke E. A., 2001, "Anomalous thermal conductivity enhancement in nanotube suspensions," Appl. Phys. Lett., **79**(14), p. 2252.

[8] Xie H., Wang J., Xi T., and Liu Y., 2002, "Thermal Conductivity of Suspensions Containing Nanosized SiC Particles," Int. J. Thermophys., **23**(2), pp. 571–580.

[9] Das S. K., Putra N., Thiesen P., and Roetzel W., 2003, "Temperature Dependence of Thermal Conductivity Enhancement for Nanofluids," ASME J. Heat Transf., **125**, p. 567.

[10] Wang B.-X., Zhou L.-P., and Peng X.-F., 2003, "A fractal model for predicting the effective thermal conductivity of liquid with suspension of nanoparticles," Int. J. Heat Mass Transf., **46**(14), pp. 2665–2672.

[11] Murshed S. M. S., Leong K. C., and Yang C., 2005, "Enhanced thermal conductivity of TiO2—water based nanofluids," Int. J. Therm. Sci., **44**(4), pp. 367–373.

[12] Putnam S. A., Cahill D. G., Braun P. V., Ge Z., and Shimmin R. G., 2006, "Thermal conductivity of nanoparticle suspensions," J. Appl. Phys., **99**(8), p. 084308.

[13] Liu M.-S., Lin M. C.-C., Tsai C. Y., and Wang C.-C., 2006, "Enhancement of thermal conductivity with Cu for nanofluids using chemical reduction method," Int. J. Heat Mass Transf., **49**(17-18), pp. 3028–3033.

[14] Li C. H., Williams W., Buongiorno J., Hu L.-W., and Peterson G. P., 2008, "Transient and Steady-State Experimental Comparison Study of Effective Thermal Conductivity of Al2O3/Water Nanofluids," ASME J. Heat Transf., **130**(4), p. 042407.

[15] Vajjha R. S., and Das D. K., 2009, "Experimental determination of thermal conductivity of three nanofluids and development of new correlations," Int. J. Heat Mass Transf., **52**(21-22), pp. 4675–4682.

[16] Duangthongsuk W., and Wongwises S., 2009, "Measurement of temperature-dependent thermal conductivity and viscosity of TiO2-water nanofluids," Exp. Therm. Fluid Sci., **33**(4), pp. 706–714.

[17] Wang L., and Wei X., 2009, "Nanofluids: Synthesis, Heat Conduction, and Extension," ASME J. Heat Transf., **131**(3), p. 033102.

[18] Wei X., Zhu H., Kong T., and Wang L., 2009, "Synthesis and thermal conductivity of Cu2O nanofluids," Int. J. Heat Mass Transf., **52**(19-20), pp. 4371–4374.

[19] Chon C. H., Kihm K. D., Lee S. P., and Choi S. U. S., 2005, "Empirical correlation finding the role of temperature and particle size for nanofluid (Al[sub 2]O[sub 3]) thermal conductivity enhancement," Appl. Phys. Lett., **87**(15), p. 153107.

[20] Shima P. D., Philip J., and Raj B., 2009, "Role of microconvection induced by Brownian motion of nanoparticles in the enhanced thermal conductivity of stable nanofluids," Appl. Phys. Lett., **94**(22), p. 223101.

[21] Beck M. P., Yuan Y. H., Warrier P., and Teja A. S., 2009, "The effect of particle size on the thermal conductivity of alumina nanofluids," J. Nanoparticle Res., **11**(5), pp. 1129–1136.

[22] Fang K.-C., Weng C.-I., and Ju S.-P., 2006, "An investigation into the structural features and thermal conductivity of silicon nanoparticles using molecular dynamics simulations," Nanotechnology, **17**(15), pp. 3909–3914.

[23] Li X. F., Zhu D. S., Wang X. J., Wang N., Gao J. W., and Li H., 2008, "Thermal conductivity enhancement dependent pH and chemical surfactant for Cu-H2O nanofluids," Thermochim. Acta, **469**(1-2), pp. 98–103.

[24] Zhu D., Li X., Wang N., Wang X., Gao J., and Li H., 2009, "Dispersion behavior and thermal conductivity characteristics of Al2O3–H2O nanofluids," Curr. Appl. Phys., **9**(1), pp. 131–139.

[25] Lee D., Kim J.-W., and Kim B. G., 2006, "A new parameter to control heat transport in nanofluids: surface charge state of the particle in suspension.," J. Phys. Chem. B, **110**(9), pp. 4323–4328.

[26] Konakanchi H., Vajjha R. S., Chukwu G. A., and Das D. K., 2014, "Measurements of pH of Three Nanofluids and Development of New Correlations," Heat Transf. Eng., **36**(1), pp. 81–90.

[27] Hamilton R. . L., and Crosser O. K., 1962, "Thermal Conductivity of Hetrogenous Two-Component Systems," I EC Fundam., **1**(3), pp. 187–191.

[28] Yu W., and Choi S. U. S., 2003, "The Role of Interfacial Layers in the Enhanced Thermal Conductivity of Nanofluids: A Renovated Maxwell Model," J. Nanoparticle Res., **5**, pp. 167–171.

[29] Xuan Y., Li Q., and Hu W., 2003, "Aggregation structure and thermal conductivity of nanofluids," AIChE J., **49**(4), pp. 1038–1043.

[30] Koo J., and Kleinstreuer C., 2004, "A new thermal conductivity model for nanofluids," J. Nanoparticle Res., **6**(6), pp. 577–588.

[31] Koo J., and Kleinstreuer C., 2005, "Laminar nanofluid flow in microheat-sinks," Int. J. Heat Mass Transf., **48**(13), pp. 2652–2661.

[32] Xue Q., and Xu W.-M., 2005, "A model of thermal conductivity of nanofluids with interfacial shells," Mater. Chem. Phys., **90**(2-3), pp. 298–301.

[33] Pil Jang S., and Choi S. U. S., 2007, "Effects of Various Parameters on Nanofluid Thermal Conductivity," ASME J. Heat Transf., **129**(5), p. 617.

[34] Alfa Aesar (2014), www.alfaaesar.com.

[35] Nanostructured & Amorphous Materials (2014), http://www.nanoamor.com/home.

[36] Bransonic Tabletop Ultrasonic Cleaners (2010), Bransonic Ultrasonic Corporation, Danbury, CT.

[37] Das S. K., Choi S. U. S., Yu W., and Pradeep T., 2008, Nanofluids: Science and Technology, A John Wiley & Sons, Inc., USA.

[38] Paul G., Chopkar M., Manna I., and Das P. K., 2010, "Techniques for measuring the thermal conductivity of nanofluids: A review," Renew. Sustain. Energy Rev., **14**(7), pp. 1913–1924.

[39] Wooden N., 2008, Operating Procedure for the TCi: Small Volume Test Kit for Thermal Conductivity Testing, C-Therm technologies, Amherst, Nova Scotia, Canada, B4H 4S8.

[40] Bejan A., 1993, Heat Transfer, John Wiely & Sons, Inc.

[41] Minitab 16 Statistical Software (2013). [Computer Software], Minitab, Inc. (www.minitab.com), State College, PA.

Chapter 3 Specific Heat Measurements of Five Different Propylene Glycol Based Nanofluids and Development of a New Correlation[1]

3.1 Abstract

This paper presents the specific heat measurements of five different nanofluids containing aluminum oxide (Al_2O_3), zinc oxide (ZnO), copper oxide (CuO), titanium oxide (TiO_2), and silicon dioxide (SiO_2) nanoparticles dispersed in a base fluid of 60% propylene glycol and 40% water by mass (60:40 PG/W). The measurements were carried out over a temperature range of -30 to 90 °C, for nanoparticle volumetric concentrations of 0.5 to 6%, and for average particle sizes ranging from 15 to 76 nm to evaluate their effects on the specific heat. From comparison, it was found that the existing specific heat correlations were not able to predict the measured experimental values. Therefore, a new correlation was developed to predict the specific heat of measured nanofluids. This new correlation is in good agreement with 610 experimental data points of the five nanofluids with a maximum deviation of -5% exhibited by the Al_2O_3 nanofluid and an average deviation of -0.094% for all five nanofluids.

3.2 Introduction

Nanofluids have become a topic of interest for improving heat transfer performance related to energy savings. Therefore, researchers have been investigating the various thermophysical properties of nanofluids. Most of the researchers gave attention to the thermal conductivity and viscosity properties. However, specific heat (*Cp*) is also a vital characteristic of nanofluids, but currently very limited literature is available on the specific heat of nanofluids. Even less is available for propylene glycol based nanofluids, which prompted our study. Mixtures of glycol and water are commonly used in cold regions for heating and cooling applications. The addition of ethylene or propylene glycol to water depresses the freezing point of the mixture but also decreases its thermal conductivity. Due to ethylene glycol's toxicity, it is not used in residential

---

[1] Satti, J. R, Das, D. K. and Ray, D, "Specific Heat Measurements of Five Different Propylene Glycol Based Nanofluids and Development of a New Correlation ," accepted by International Journal of Heat and Mass Transfer..

facilities, where there is a chance of the mixing of this fluid with potable water. Therefore, the non-toxic, propylene glycol is preferred. A mixture of 60% propylene glycol and 40% water (60:40 PG/W) by mass is most commonly used in subarctic climate, which has the lowest freezing temperature (-51.1 ^{0}C) [1] among glycol and water mixtures. One of the drawbacks with using PG/W is its low thermal conductivity when compared to pure water. This can be overcome by dispersing high thermal conductivity nanoparticles in PG/W to increase the thermal conductivity of the fluid. The addition of particles changes the specific heat, so we have conducted specific heat measurements of 60:40 PG/W based nanofluids with various nanoparticles, e.g., Al_2O_3, ZnO, CuO, SiO_2 and TiO_2. The particle volumetric concentrations were varied from 0.5 to 6% and the temperature ranged from 243K (-30˚C) to 363K (90˚C). The objective of this study was to measure the specific heats of PG/W based nanofluids and analyze the data for dependence on various parameters. Next, then compare the measured data with available theory. If the agreement was not good, then develop a correlation to calculate specific heat of PG/W based nanofluids, as a function of temperature, volumetric concentration, particle size, density and specific heat and the base fluid density and specific heat.

3.3 Importance of accurate specific heat measurement

Basic heat transfer equations presented by Bejan [2] show that an accurate value of the specific heat is essential for determining total heat transfer rate $\dot{q}$, heat exchanger effectiveness ε, Nusselt number Nu and the thermal diffusivity α. These equations Eq. (3.1-3.4) summarized below show that they all depend on the specific heat.

$$\dot{q} = \dot{m} \cdot Cp \cdot \Delta T = \varepsilon \cdot C_{min} \cdot (T_{hot\ inlet} - T_{cold\ inlet}) \tag{3.1}$$

$$\varepsilon = \frac{1 - exp(-NTU \cdot (1 - C^*))}{1 - C^* exp(N - TU(1 - C^*))} \tag{3.2}$$

$$where\ C^* = \frac{C_{min}}{C_{max}}, C = \dot{m}c_p, C_{min}\ is\ the\ smaller\ of\ C, and\ NTU = UA/C_{min}$$

$$Nu = 0.023 * Re^{0.8} * Pr^{0.4} \quad (turbulent\ flow) \tag{3.3}$$

$$where\ Pr = \frac{Cp\mu}{k}$$

$$Diffusivity\ \alpha = \frac{k}{\rho C_p} \tag{3.3}$$

An analysis was performed examining the influence of specific heat on the thermal and fluid dynamic performance of the fluid in a counter flow concentric tube heat exchanger. Using the ε-NTU method outlined by Kays and London [3] and the Eq. (3.1-3.3), an analysis was performed with varying specific heat of the cooler fluid to can examine how it affects the Prandtl number, Nusselt number, heat transfer coefficient, overall heat transfer coefficient, heat transfer rate, NTU, effectiveness, and temperature difference. The parameters used in this analysis are outlined in Table . The values of the parameters taken where mirrored after a small heat exchanger manufactured by P.A. Hilton [4]. The enhancement of the various parameters is calculated using Eq. 3.3

$$\text{Parameter } \% = \frac{\text{Enhanced} - \text{Normal}}{\text{Normal}} \tag{3.3}$$

The 'Normal' variable refers to the parameter calculated with water, while the 'Enhanced" variable refers to the calculated parameter with some increase in specific heat. The effects of specific heat on various parameters are shown in table 3.1. First, note the Prandtl number, Nusselt number, heat transfer coefficient and heat transfer rate parameters uses the left axis, while the NTU, effectiveness, and temperature difference of cooler fluid parameters uses the right axis. From the figure, we can see most of the parameters show a fairly linear relationship. The Prandtl number shows a one to one relationship with specific heat. Nusselt number and heat transfer coefficient show a less dependent relationship with specific heat. This is due to the Prandtl number being raised to 0.4. As shown in the figure we can see if specific heat could be increased by 29%, then Nusselt number and heat transfer coefficient would both increase by 10.7%. Overall heat transfer coefficient showed least dependence of specific heat than any of the other parameters as seen when specific heat increases by 29% the overall heat transfer coefficient only increases by 7.5%. This could be due to overall heat transfer coefficient enhancement is also dependent on the heat transfer area and heat transfer coefficients on both sides of the heat exchanger. The NTU parameter shows to decrease with increasing specific heat this is due to the C_{min} (which is usually the cooler fluid) increases equally to increasing specific heat. The decrease of NTU effects effectiveness and temperature difference of the cooler fluid. Even though the temperature difference of the cooler fluid decreases the heat transfer rate increases as seen when specific heat increases by 29% the heat transfer rate increases by 8.4%. However, there is a void in the knowledge regarding the specific heat of PG/W based nanofluids in the present literature

discussion about the previous theoretical and experimental research was provided in the following sections.

3.4 Previous work

3.4.1 Theoretical studies

Pak and Cho [5] were one of the first to propose a correlation, Eq. (3.6), for the specific heat of nanofluid in 1998, based on a mixture of liquid and particle.

$$Cp_{nf} = (1-\phi)Cp_{bf} + \phi Cp_{np} \tag{3.3}$$

where Cp is the specific heat, ϕ is the volumetric concentration of nanoparticles, the subscripts *bf* represents base fluid, *np* the nanoparticles, and *nf* the nanofluid. This equation does not satisfy the conservation of energy principle. Therefore, Xuan and Roetzel [6] modified Eq. (3.6) based on conservation of energy of both particles and fluid, assuming thermal equilibrium between two phases.

$$m_{nf}Cp_{nf}(\Delta T) = m_{bf}Cp_{bf}(\Delta T) + m_{np}Cp_{np}(\Delta T) \tag{3.4}$$

which can be simplified to

$$\rho_{nf}Cp_{nf} = (1-\phi)\rho_{bf}Cp_{bf} + \phi\rho_{np}Cp_{np} \tag{3.5}$$

where the nanofluid density is given by the mixture theory:

$$\rho_{nf} = (1-\phi)\rho_{bf} + \phi\rho_{np} \tag{3.6}$$

3.4.2 Experimental studies

O'Hanley et al. [7] measured specific heat of water and ethylene glycol based nanofluids with Si, Al, and Cu nanoparticles using digital scanning calorimeter (DSC). Their results were compared with Pak and Cho's correlation Eq. (3.6) and Xuan and Roetzel's correlation (3.7b). They found the deviation of data to be significantly greater with Eq. (3.6) than Eq. (3.7b). The maximum deviation of 7% was reported using Eq. (3.6). Vajjha and Das [8] measured the specific heat of Al_2O_3 and ZnO nanoparticles suspended in 60:40 EG/W and SiO_2 in water. They found the measured data was not in good agreement with the existing correlations Eq. (3.6) and Eq. (3.7b).

Therefore, they developed a new correlation Eq. (3.9) for the specific heat of nanofluids as a function of temperature, volumetric concentration and the specific heat of the base fluid. This correlation predicted the specific heat values of each nanofluid within an error of 2.7%.

$$\frac{C_{p_{nf}}}{C_{p_{bf}}} = \frac{\left[(A * T) + B * \left(\frac{Cp_{np}}{Cp_{bf}}\right)\right]}{C + \phi} \tag{3.7}$$

Here, A, B, C were curve-fit coefficients given in Ref. [8]. This correlation was valid for a volume concentration up to 10% and temperature range of 315 – 363 K for the nanofluids they tested. Vajjha and Das [9] updated the previous correlation, Eq. (3.9) by adding the data of CuO, 60:40 EG/W nanofluids and nondimensionalized the temperature term with a reference temperature T_0 = 273K to make the correlation dimensionally homogenous and expressed it as Eq. (3.10).

$$\frac{Cp_{nf}}{Cp_{bf}} = \frac{\left[\left(A_1 * \frac{T}{T_0}\right) + B_1 * \left(\frac{Cp_{np}}{Cp_{bf}}\right)\right]}{C_1 + \phi} \tag{3.8}$$

where A_1, B_1, and C_1 are 0.243, 0.517, and 0.425 for Al_2O_3 nanofluid; 0.482, 1.193, and 0.802 for SiO_2 nanofluid; and 0.125, 0.985, and 0.299 for ZnO nanofluid, respectively. The measurements made by Vajjha and Das [8, 9] was with a laboratory-made apparatus, which was limited to measurements only in the positive temperature range, usually above 315K (42°C). It was not capable of the property measurement in the negative (below 0°C) range of temperature.

3.4.3 Volumetric concentration effect

The volumetric concentration was found to play a vital role in predicting thermophysical properties of the nanofluids. Research showed specific heat of nanofluid decreased with an increase in volume concentration of nanofluid. This is as expected since the specific heat of a metal or oxidized metal has a lower specific heat than a liquid. Kulkarni et al. [10] observed that specific heat of Al_2O_3 nanofluid decreased from 4.84% to 16.14% for a volume concentration between 2 to 6% of nanoparticle concentration. Namburu et al. [11] measured the specific heat of silicon dioxide nanoparticles suspended in 60:40 EG/W with varying concentrations between 2 to 10% for different particle sizes. It was only at one temperature of 50°C. They found the specific heat of

SiO_2 nanofluid decreased with an increase in volumetric concentration. For a 10% volumetric concentration, they found 12% decrease in specific heat of nanofluid in comparison with the base fluid. Bergman [12] measured the specific heat of Al_2O_3 – water and Al_2O_3 – HFE 7100 nanofluids and found specific heat decreased with an increase in volume concentration. Pantzali et al. [13] also measured the specific heat of Al_2O_3 – water nanofluids with varying volumetric concentration between 2 to 8%. They found a 20% decrease in specific heat with 8% volume concentration compared with the base fluid. Sonawane et al. [14] performed experiments by dispersing the Al_2O_3 nanoparticles in aviation turbine fuel to measure the thermophysical properties of the colloid and evaluate the heat transfer capability of the nanofluid. They measured specific heat using an in-house apparatus at low volume concentrations between 0 to 1%. They found that there was no significant difference in measured specific heat with volume concentration. Shin and Benerjee [15] measured specific heat of eutectic salt nanofluids. They dispersed Al_2O_3 nanoparticles in eutectic salt. The measurements were performed by using a DSC. They reported for a 1% mass concentration of mixture yielded a 32% enhancement in base fluid specific heat, at 495 ^{0}C.

3.4.4 Temperature effect

Along with volumetric concentration, the temperature also influences the specific heat of nanofluids. Only a few researchers have performed experiments at higher temperatures, most conducted the measurements at room temperature. Robertis et al. [16] measured the effect of temperature on specific heat of nanofluids using modulated DSC. They found that as the temperature increased the specific heat of Cu-EG nanofluid decreased. Ho and Pan [17] performed experiments to find the optimum volume concentration of Al_2O_3 nanoparticles which gave maximum enhancement of specific heat of molten hitec salt. They studied the effect of temperature in the range of 200-350℃ on the specific heat of hitec salt nanofluid. They found for a weight concentration of 0.016% the nanofluid yielded 20% enhancement in specific heat. They also found the specific heat of nanofluid was decreasing with increase in particle concentration. They reported a 2% concentration yielded 4% decrease in specific heat. Shin and Benerjee [18] found a specific heat enhancement of 14% for 1% silica concentration suspended in alkali metal chloride salt eutectic solution at 500 ^{0}C. They also found that the specific heat of nanofluid also decreased with an increase in temperature. Vajjha and Das [9] performed experiments with Al_2O_3 and ZnO nanoparticles suspended in 60:40 EG/W and SiO_2 nanoparticles suspended in deionized water to

measure specific heat in a temperature range of 315 to 360 K. They found the specific heat of nanofluid decreased with an increase in volumetric concentration and it increased with an increase in temperature, but the value of specific heat of nanofluid was still below the base fluid value.

Therefore from the previous research, we can conclude that specific heat of nanofluid is a function of the volumetric concentration, temperature, and properties of nanoparticle and base fluid. Specific heat of nanofluids generally decreases with an increase in volume concentration and increases with an increase in temperature. Therefore, our present goal was to study the effect of above-mentioned parameters on specific heat of 60:40 PG/W nanofluids, especially in the negative temperature range for cold weather applications. Then compare the data with available correlations and if the comparisons show inadequate agreement, then develop a new correlation.

3.5 Preparation and characterization of nanofluids

3.5.1 Nanofluids samples preparation

The nanofluids were procured from two different manufacturers. They are Alfa Aesar [19] and Nanostructured Amorphous Materials [20]. These manufacturers have developed effective surfactants/dispersants for several nanofluid suspensions. Different nanofluids purchased from them have shown stable suspensions and no significant settling was observed during a short-term storage. The different surfactants or dispersants employed by the manufacturers to stabilize the nanofluids were proprietary information. In the study, five types of nanoparticles Al_2O_3, SiO_2, ZnO, CuO and TiO_2, dispersed in 60:40 PG/W were used. Pure laboratory grade propylene glycol was mixed with deionized water in the proportion of 60 to 40 by mass using an electronic mass balance scale. The characteristics of nanoparticles procured for our experiments are tabulated in Table 3.2.

3.5.2 Ultrasonication of nanofluids

The sonication of nanofluids was carried out in two stages. First, the glass bottle containing aqueous concentrated mother nanofluid as supplied by the vendor was sonicated. It was subjected to ultrasonication in a Branson model 5510 Sonicator [22] under a frequency of 40 kHz with a

power of 185 W. The ultrasonication bath was filled with water up to the designated operating level. Then the water was degassed for 5 min for removal of dissolved gases following the recommendation of the manufacturer. The mother nanofluid was contained in a glass bottle (plastic bottle deformed), with a gasketed screwed cap to prevent escapement of water vapor, so that the concentration remained constant. We subjected the mother nanofluid to ultrasonication for at least three sessions, each of 2-hour duration followed by a brief cooling period to prevent overheating. The purpose of the first stage ultrasonication was to break down the particles that have agglomerated due to long-term storage. The number of sonication sessions may depend on the degree of sedimentation. Sonication must continue until the liquid volume show a uniform dispersion of nanoparticles by careful visual examination. In the next step, a measured sample from this concentrated mother fluid was taken by a pipette and added to calculated mass of pure laboratory grade PG and de-ionized water of necessary proportions in a test tube placed on a precise electronic mass balance to prepare 0.5, 1, 2, 3, 4, and 6 %volumetric concentrations of nanofluids in the 60:40 PG/W solution. Just before measuring the specific heat of a sample of each concentration, the test tube containing the sample nanofluid was sonicated by immersing it in the bath for two hours to ensure a uniform dispersion of nanoparticles in the suspension.

3.6 Particle size measurement

In order to verify whether agglomerated particles were present in the sample prior to the specific heat measurement, the sample was examined for particle size distribution under transmission electron microscope (TEM). Figure shows the TEM image of one of the ZnO nanofluid samples of 0.5% volumetric concentration. The particle size result for this nanofluid is consistent with the data provided by the vendor. Alfa Aesar's ZnO nanofluid came with a specification of APS 50 nm. We noticed from the TEM image that majority of nanoparticles fell near this average size (36 and 65nm), with some smaller in size. From the distribution it appeared that the combination of larger and smaller particles should yield an overall average particle size of 50 nm. The ZnO nanoparticles show rod-like shape, whereas Al_2O_3 and TiO_2 nanoparticles showed spherical shape.

From similar TEM images of other four nanofluids, containing Al_2O_3, CuO, TiO_2 and SiO_2 nanoparticles, no agglomeration was observed. It is due to two effects: (a) the nanofluid manufacturers have developed successful surfactant or dispersant that is already present in these

nanofluids, making them stably suspended and free from agglomeration or coagulation. (b) Secondly, the sonication of the parent concentrated nanofluids before sample preparation followed by the second stage sonication of the dilute sample prior to the specific heat measurements, ensured breaking off of agglomerated particles, if any.

3.6.1 Principle of specific heat measurement

In the present study, a C-Therm TCi thermal property analyzer [23] apparatus was used to measure the specific heat of nanofluids. The principle used in this apparatus is based on the transient plane source method. The C-Therm system has a sensor, control electronics and computer software. The spiral sensor element applies a momentary, constant heat source to the nanofluid sample. The temperature rise induces a change in the voltage drop of the sensor element. The thermophysical properties of nanofluid are inversely proportional to the sensor voltage. The TCi system measures both thermal conductivity k and effusivity e directly. Using these two values the specific heat Cp of nanofluid is obtained from Eq. (3.11) by the system's computer when a user –inputted density ρ is provided from the measurements of Anton Paar density meter.

$$C_p = \frac{e^2}{k.\rho} \tag{3.9}$$

where C_p is the specific heat of the fluid and ρ is the density of the fluid, calculated using Eq. (3.7).

3.6.2 Experimental setup

A schematic diagram of the experimental setup is shown in Figure . The C-Therm sensor is placed in the Thermotron [24] thermal chamber. The temperature of the fluid sample can be precisely maintained at desired levels using this chamber. The chamber has the capability to maintain temperature from -73°C to 177°C. The measurements were taken holding the fluid sample at a constant temperature for at least 20min. The C-Therm apparatus measures the temperature, thermal conductivity, effusivity and specific heat through data acquisition system (DAQ). The DAQ takes 10 measurements off all parameter at 5-second interval to insure accurate results. A standard deviation (SD) of the data is taken to verify if the test run is acceptable. The data, which has a SD of less than 0.1, is then passed to the computer for further processing. Ten measurements are then averaged to determine the specific heat of the sample at the recorded temperature. Using this

experimental setup and procedure, the specific heat measurements of five different nanofluids were conducted over a temperature range from 243K (-30 °C) to 363K (90 °C). These measurements allowed us to study the behavior of nanofluids at low temperatures, which had not been explored yet.

3.7 Results and discussion

3.7.1 Benchmark test case

Before measuring the specific heat of nanofluids, a benchmark test was performed with DI water in a temperature range of 5 ^{0}C to 90 ^{0}C and 60:40 PG/W in a temperature range of -30 ^{0}C to 90 ^{0}C. The specific heat values of water and PG/W are accurately known from Bejan [2] and ASHRAE [1] respectively. Figure 3.4 shows the comparison between measured specific heats and the values taken from Bejan and ASHRAE. A maximum deviation of 3.6% at 284 K for water and a maximum deviation of 2.12% at 243 K for 60:40 PG/W were observed in Figure 3.4 when compared between measured values and the data from Bejan and ASHRAE, respectively. Curve-fit expressions for the base fluid specific heat and density were derived using ASHRAE data. These two correlations are summarized in Table 3.3. These two correlations are used in subsequent calculations.

3.7.2 Al_2O_3 nanofluid

Figures 3.5-3.7 show the specific heat measurements of Al_2O_3 nanofluids consisting of three different average particle sizes (APS), 15nm, 20nm and 45nm, respectively with temperature ranging from 243K to 363K. These figures show the effect of nanoparticle volumetric concentration and temperature on the specific heat of Al_2O_3 nanofluids. It is observed from these the specific heat increased with an increase in temperature and it decreased with an increase in nanoparticle volumetric concentration.

Figure 3.5 shows the specific heat values of Al_2O_3 nanofluid of APS 15nm with volumetric concentration from 0.5 to 2%, which was limited by the mother fluid concentration. From the figure, one could see the specific heat wasn't a strong function of volumetric concentration except for the initial addition of nanoparticles. This could be due to the small concentration range that

was tested. However, the data shows $Cp_{2\%} < Cp_{1\%} < Cp_{0.5\%}$, although the differences are small. The specific heat of the nanofluid was reduced by about 27% at 243K and by about 19% at 363K when compared to that of the base fluid. The marginal loss in specific heat when the concentration increases from 0.5% to 2%, is a great benefit while considering the enhancement in thermal conductivity. Because, many researchers have shown that a small increase in concentration can enhance conductivity quite a bit, making the fluid very successful for heat transfer.

Figure 3.6 shows the specific heat values of 20nm APS Al_2O_3 nanofluid with volumetric concentration from 0.5% to 4%. The measurements showed, as the particle volumetric concentration of nanofluids increased the specific heat of nanofluids decreased. The trend is $Cp_{4\%} < Cp_{3\%} < Cp_{2\%} < Cp_{1\%} < Cp_{0.5\%}$ at equal temperatures. For example, a 0.5% particle volumetric concentration showed 27% decrease at 243K in specific heat values and similarly a 4% volumetric concentration showed 32% decrease at 243K compared to base fluid values. At 363 K the 0.5% concentration showed 20% decrease and 4% concentration showed 26% decrease in specific heat value compared to the base fluid. Therefore, decreases more as the temperature increases. This characteristic proves that nanofluids should be used at as high temperature as possible to get better beneficial effect.

Figure 3.7 shows the specific heat values of a 45nm APS Al_2O_3 nanofluid with volume concentrations from 0.5% to 6%. The measurements showed similar trends as those in the previous Figures 3.5 and 3.6. At 363 K, the 0.5% concentration showed a 19.5% decrease and 6% showed a 26.02% decrease in the specific heat value.

3.7.3 ZnO nanofluid

Figures 3.8 through 3.10 show the specific heat measurements of ZnO nanofluids of 36, 50, and 76nm APS, respectively, with varying temperatures and concentrations. These figures exhibit similar effects as explained for the Al_2O_3 nanofluids.

Figure 3.8 shows the specific heat values of a ZnO nanofluid of APS 36nm with particle volumetric concentrations from 0.5% to 4%. At 243K the 0.5% volume concentration showed a 28% decrease in specific heat and the 4% particle volume concentration showed a 32% decrease. At 363 K the 0.5% concentration showed a 21.7% decrease in specific heat and the 4%

concentration showed a 28.5% decrease. These trends are similar to those observed for Al_2O_3 nanofluids.

Figure 3.9 shows the specific heat values of a 50 nm APS ZnO nanofluid with volume concentrations from 0.5% to 6%. At 243 K, the 0.5% volume concentration showed a 27% decrease in specific heat and the 6% concentration showed a 35.4% decrease compared to 60:40 PG/W. At 363 K, the 0.5% concentration showed a 20.9% decrease in specific heat and the 6% concentration showed a 30.9% decrease. Another observation was that for the base fluid, there is 17% increase in specific heat in the measured temperature range. In the same temperature range, the 0.5% volumetric concentration had a specific heat increase of 29% and the 6% volumetric concentration, 25% . This proves that the specific heat increase of nanofluids with temperature is greater than that of the base fluid.

Figure 3.10 displays the specific heat values of a 76 nm APS ZnO nanofluid with volume concentrations from 0.5% to 6%. At 243K, decreases in specific heat by 24% and 34% were observed for 0.5% and 6% volume concentrations, respectively. At 363 K, the 0.5% concentration showed a 19.66% decrease and the 6% concentration showed a 29.33% decrease in specific heat values. A consistent decrease in the specific heat values ($Cp_{6\%} < Cp_{4\%} < Cp_{3\%} < Cp_{2\%} < Cp_{1\%} < Cp_{0.5\%}$) at a fixed temperature is observed from the experimental data in Figs 3.8 and 3.9.

3.7.4 CuO nanofluid

Figure 3.11 shows the specific heat values of a CuO nanofluid with volume concentrations from 0.5% to 6% with an APS of 30 nm. At 243K, the 0.5% volume concentration nanofluid showed a 28% decrease in specific heat compared with the 60:40 PG/W. At the same temperature, the 6% volume concentration nanofluid showed a 38% decrease in specific heat. At 363 K, the 0.5% concentration showed a 20.8% decrease and the 4% concentration showed a 33.8% decrease in specific heat. Figure 3.11 shows a clear and consistent decrease in specific heat at constant temperatures from 0.5 to 6% volume concentrations. In other words, for the same temperature, the specific heat of a nanofluid diminishes consistently as the volume concentration increases. Notice that the CuO nanofluid has the greatest spread of data for different concentrations because it has the highest density of all the nanofluids (Table 3.2).

3.7.5 SiO_2 Nanofluid

Figure 3.12 shows the specific heat values of a SiO_2 nanofluid of APS 30nm with volume concentrations from 0.5% to 5%. The specific heat of SiO_2 nanoparticles is lower than that of the previously discussed Al_2O_3, ZnO, and CuO nanoparticles, as observed in Table 3.2. Therefore, it appears that variation in volumetric concentration only affects the specific heat values of the SiO_2 nanofluid by a small margin. The data points nearly overlap. This may be due to measurement inaccuracies of the apparatus. A careful examination of Figure 3.12 shows that the specific heats of the 5% volumetric concentration nanofluids are consistently below those of 1% concentration, which is the same trend found for Al_2O_3, ZnO, and CuO nanofluids.

3.8.6 TiO_2 Nanofluid

Figure 3.13 shows the specific heat values of a TiO_2 nanofluid of APS 15 nm. The concentrations tested were at the low levels of 0.5%, 1%, and 1.5%. This experiment is similar to the one conducted on the Al_2O_3 nanofluid of 15 nm at low concentrations shown earlier in Figure 3.5. Similar results are also observed in Figure 5.13. Due to the low volume concentration range of 0.5% to 1.5%, the changes in specific heat values are very small. The data points overlap within the accuracy of the measuring apparatus.

3.7.7 Particle size effect

The nanoparticle size affects the thermophysical properties of nanofluids, for example, their thermal conductivity, as demonstrated by Vajjha and Das [7]. Therefore, an objective of our investigation was to study this aspect for the specific heat of nanofluids. In our experiments we had selected two nanofluids, Al_2O_3 and ZnO, with multiple particle sizes. The Al_2O_3 nanofluid had three particle sizes: 15, 20, and 45 nm. The ZnO nanofluid also had three particles sizes: 36, 50, and 76 nm.

Figure 3.14 compares the specific heats of Al_2O_3 nanofluids with different particle sizes (15, 20, and 45 nm) for two particle volumetric concentrations, 0.5% and 4%, over the experimental temperature range of 243 to 363 K. From the figure, it is clear that the specific heat values of the 0.5% concentration overlap for all three particle sizes. For the 4% concentration, the

specific heat data are nearly the same for 20 and 45 nm, with small deviations appearing at the higher temperatures. These small deviations may be due to the experimental error plus the error associated with the density equation (Eq. 3.8), which is used to arrive at the specific heat values. Therefore, it can be said that the specific heat of nanofluids is not dependent on particle size.

Figure 3.15 compares the specific heat of ZnO nanofluids of three different particle sizes (36, 50, and 76 nm) for two volumetric concentrations (0.5% and 4%) as a function of temperature. For the 0.5% concentration, the specific heat data overlap for all three particle sizes. A similar observation can also be made for the 4% concentration, where the specific heat deviations among the three particle sizes are marginal. These results are similar to those observed for the Al_2O_3 nanofluid in Figure 3.14. Therefore, the measured data show that the specific heat of nanofluids is not dependent on the particle size within the concentration and temperature ranges of our experiments.

3.7.8 Comparison between the theories and experiments

As described in the Introduction section, there are two theoretical equations available in the literature to predict the specific heat of nanofluids: one by Pak and Cho [5] and a second by Xuan and Roetzel [6]. We compared the measured values of specific heat with the predictions of these two theoretical equations. This comparison is displayed in Figure. 3.16, displays this comparison for an Al_2O_3 nanofluid with a 6% volumetric concentration of 45 nm particles. From this figure it is evident that neither equation matches the experimental data. Pak and Cho's equation is off by nearly 40% and Xuan and Roetzel's is off by about 30% from the measured data. All the other nanofluids exhibited similar degrees of disagreement among the measured specific heat values and the theoretically predicted specific heat values. Pak and Cho's equation always showed a higher degree of disagreement form the experimental data than Xuan and Roetzel's.

3.8 Development of a new correlation

Since the two existing specific heat models could not predict the measured specific heat data correctly, we proceeded to develop a new correlation that could predict the specific heat of all the nanofluids tested.

3.9 Guidance from the measured data and theory

From the measured data it was observed that the specific heat of a nanofluid, Cp_{nf}, increased as temperature increased. Specific heat is also a function of the volumetric concentration (ϕ), the density of the nanofluid(ρ_{nf}), and the properties of the base fluid (ρ_{bf},Cp_{bf}) and the nanoparticles (ρ_p and Cp_p). The characteristics of some of these properties had been analyzed previously by Vajjha and Das [48]. They had analyzed the variation of Cp_{nf} and ρ_{nf} and their product,$Cp_{nf}\rho_{nf} = Cv_{nf}$ the volumetric heat capacity with the volume concentrationϕ. Figure. 3.17 presents this variation of different parameters for Al_2O_3 and ZnO nanofluids at a temperature of 293 K. The density increases and the specific heat decreases with an increase in the volume concentration ϕ. Their product, the volume heat capacity Cv_{nf}, also increases with an increase in ϕ, as observed in Figure 3.17. The data shows a nearly linear increment of volumetric specific heat Cv_{nf} with concentration ϕ. Therefore, the pertinent parameters to develop a correlation Cp_{nf} are: $\phi, T, \rho_{nf}, \rho_{bf}, Cp_{bf}, \rho_{np}$ and Cp_{np}. With a total of 610 measured values of specific heat at hand, we employed the statistical software package Minitab [41] to derive a general correlation that can predict the specific heat for five different nanoparticles suspended in a 60:40 PG/W base fluid. This new correlation is presented as Eq. (3.12). In order to make this equation dimensionally homogeneous, both sides have been nondimensionalized by reference density and specific heat of the base fluid at the reference temperature of T_0 = 273 K.

$$\frac{\rho_{nf}Cp_{nf}}{\rho_{bf_0}Cp_{bf0}} = 0.371641 + 1.00713\phi + 0.345370\left(\frac{T}{T_0}\right) + 0.039107\left(\frac{Cp_{np}\rho_{np}}{Cp_{bf}\rho_{bf}}\right) \quad (3.10)$$

This equation is valid for 243K<T<363K and 0<ϕ<0.06 for the five 60:40 PG/W nanofluids tested, but can be extended to other nanofluids in the future by additional experiments.

The accuracy of the empirical model Eq. (3.12) in predicting the specific heats of nanofluids is shown in Figure 3.18, derived from 610 data points of five different nanofluids. This correlation has a maximum deviation of -5% and an average deviation of -0.09% from the measured specific heat values.

3.10 Conclusions

From a set of carefully conducted experiments, the specific heat of five different nanofluids (Al_2O_3, CuO, SiO_2, TiO_2, and ZnO nanoparticles) dispersed in 60:40 PG/W base fluid was measured. From these data the effects of temperature (243-363 K), particle volumetric concentration (0.5-6%) and particle size (15-76 nm) on the specific heat were studied. The results showed a decrease in the specific heat with increasing concentration and an increase in the specific heat with increasing temperature, which were in agreement with previously published results. At low concentrations, between 0.5% and 1.5%, the reduction in specific heat was small, indicating that nanofluids can be beneficial at dilute concentrations by increasing thermal conductivity and keeping the viscosity increase to a smaller value. The experimental results show that particle size has no significant effect on the specific heat of nanofluids. The measured existing specific heat correlations from the literature failed to predict the measured specific heat values with good agreement. Therefore, a new specific heat correlation was developed for five different nanoparticles dispersed in 60:40 PG/W, which predicted the specific heat of the tested nanofluids with an average deviation of -0.094%. With additional testing in the future, this correlation can be refined to be applicable to many other nanofluids.

3.11 Acknowledgement

Financial support from the National Aeronautics and Space Administration, Experimental Program to Stimulate Competitive Research grant # AK-NNX11AM16A is gratefully acknowledged.

3.12 Nomenclature

Cp	Specific heat ($Jkg^{-1}K^{-1}$)
Cv	Volumetric specific heat ($Jm^{-3}K^{-1}$)
d	Diameter of particle (nm)
e	Effusivity ($W\sqrt{s}\,m^{-2}K^{-1}$)
k	Thermal Conductivity ($Wm^{-1}K^{-1}$)
Nu	Nusselt Number
PG/W	Propylene Glycol and Water
Pr	Prandtl number

T_0	Reference temperature (273 K)
Re	Reynolds number
T	Temperature (K)

Greek symbols

ρ	Density (kgm^{-3})
ϕ	Particle volumetric concentration %

Subscripts

bf	Base fluid
nf	Nanofluid
o	At reference temperature T_0
np	Nanoparticle

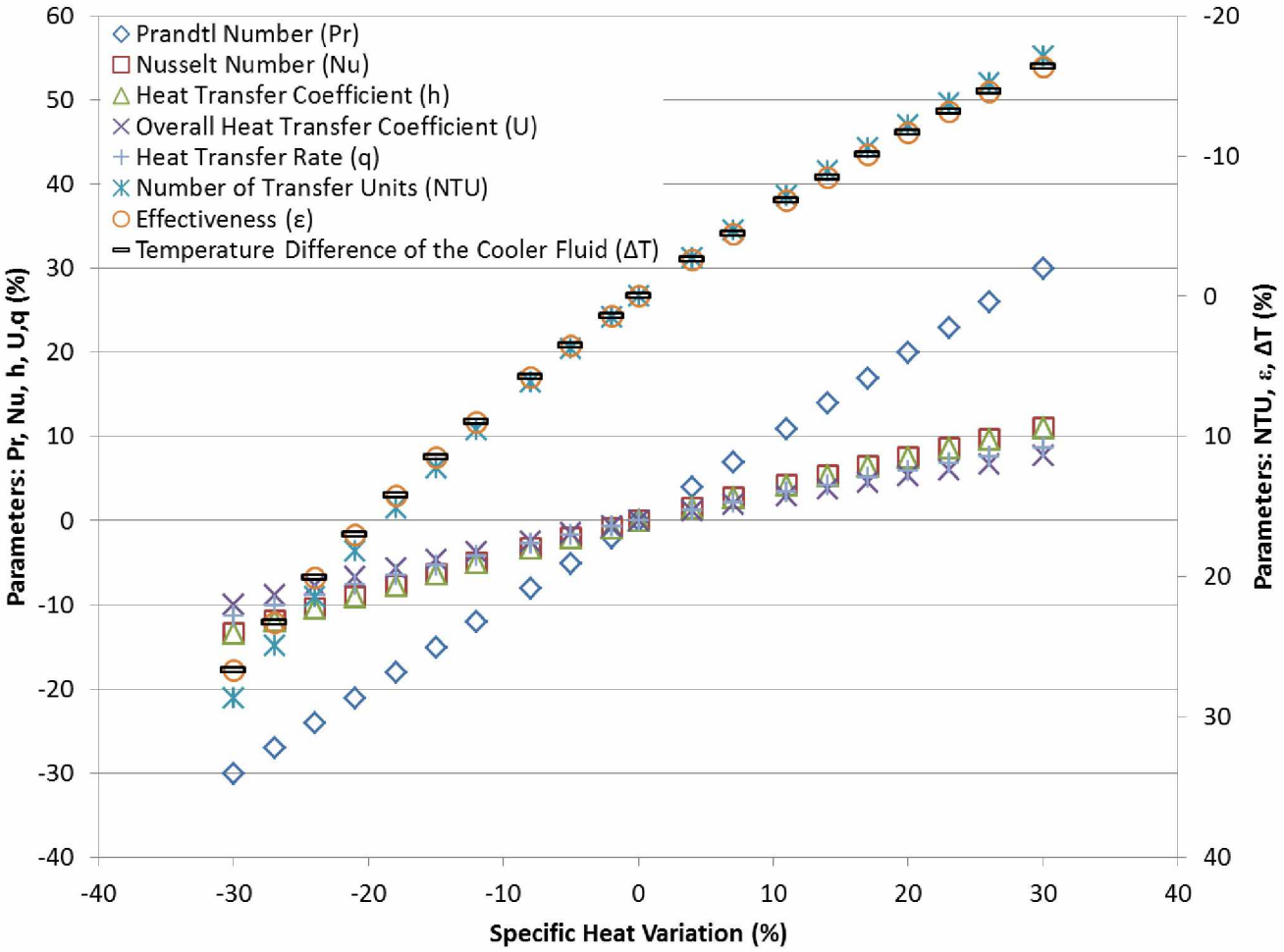

Figure 3.1. Effects of specific heat on performance parameters

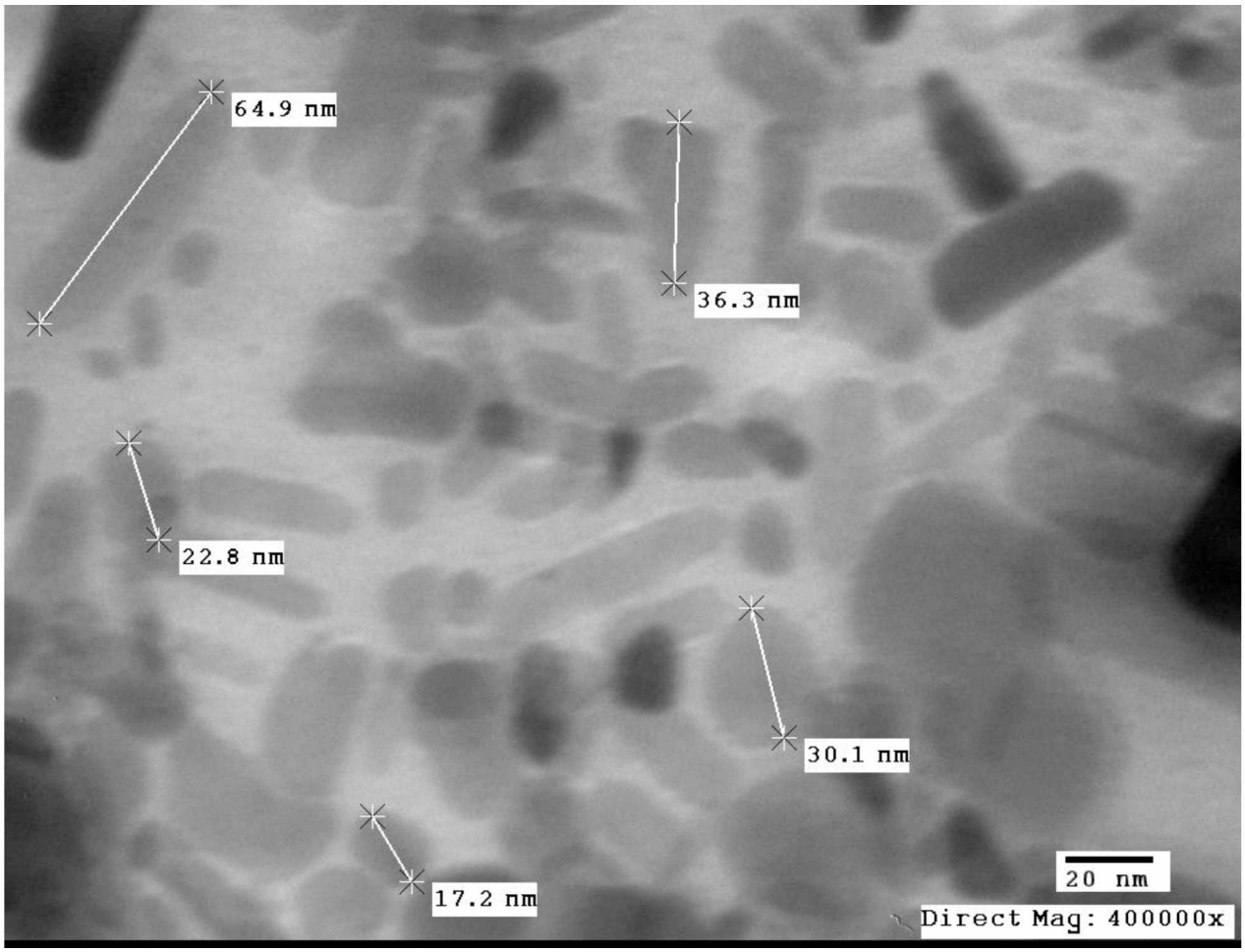

Figure 3.2. The TEM image of ZnO 50nm nanoparticles

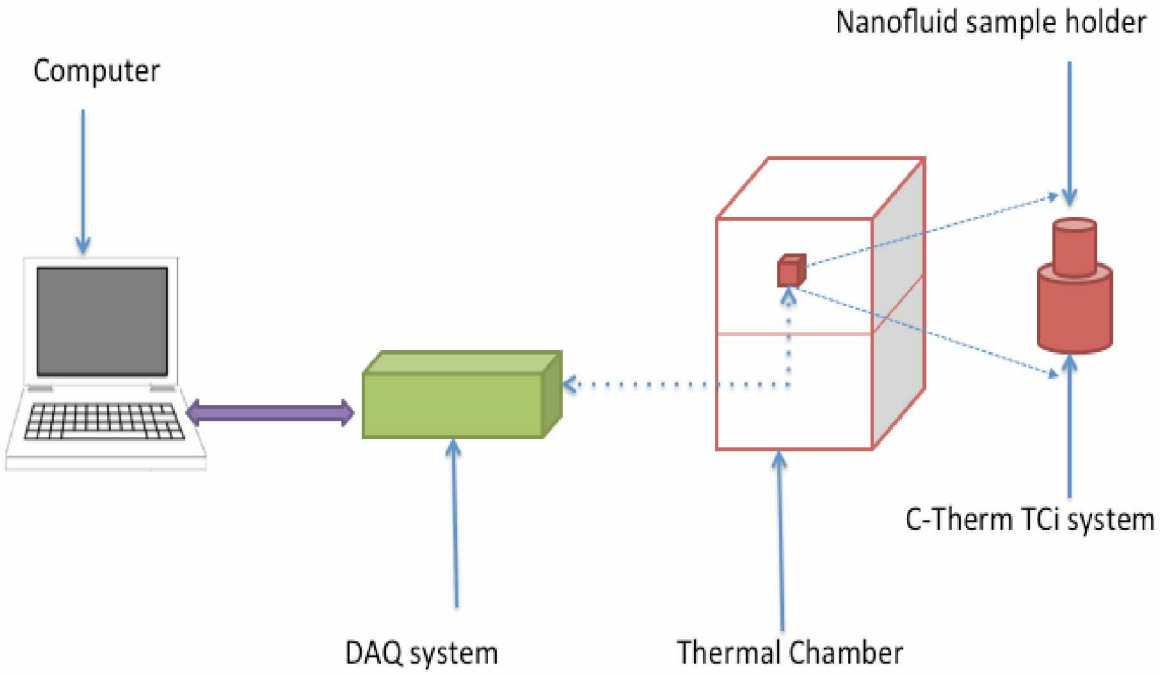

Figure 3.3. Schematic diagram of the experimental setup for the specific heat measurement

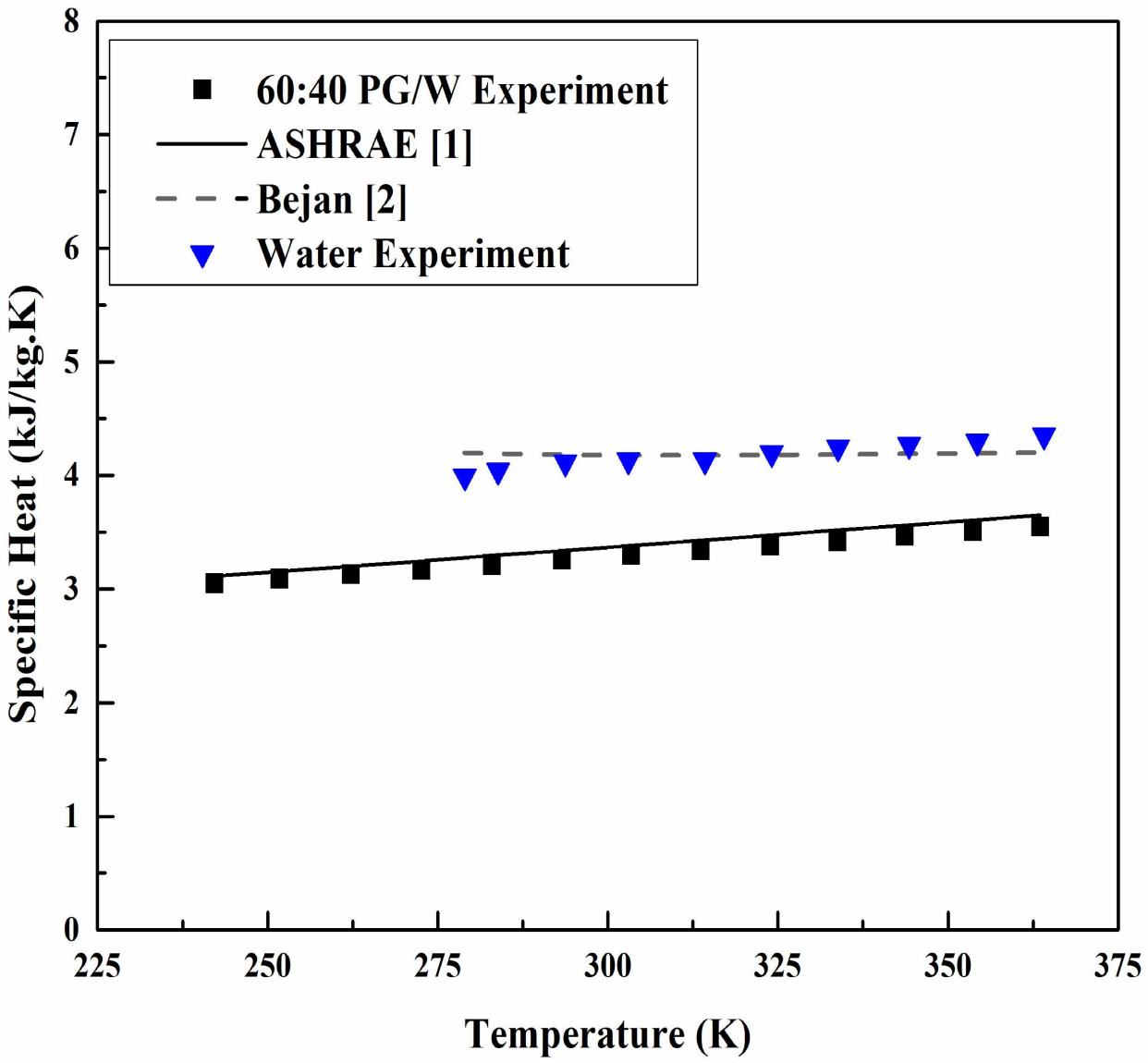

Figure 3.4. Benchmark test results for the specific heats of water and PG/W.

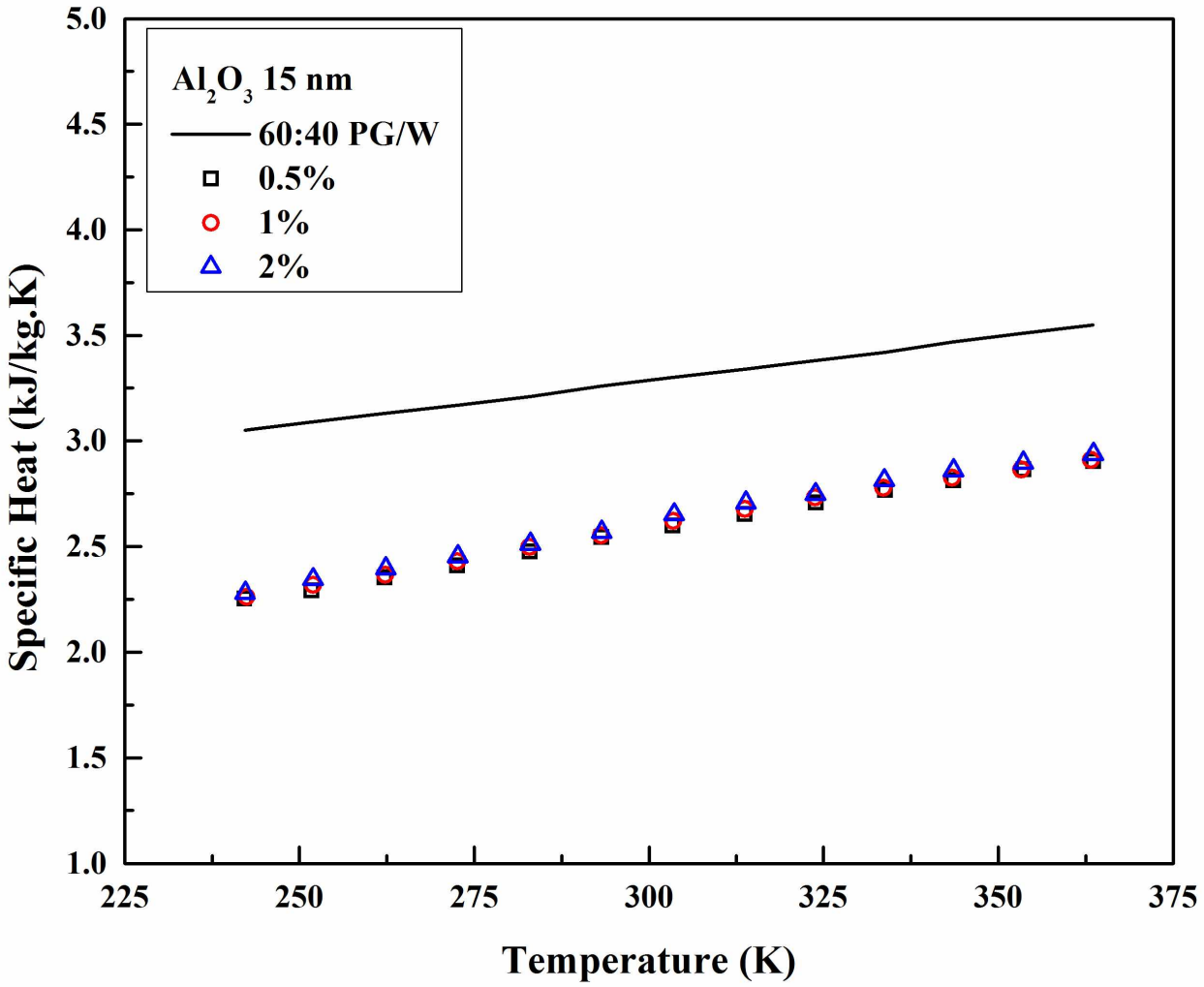

Figure 3.5. Specific heat measurement of 15nm APS Al_2O_3 nanofluids with varying temperatures and volumetric concentrations.

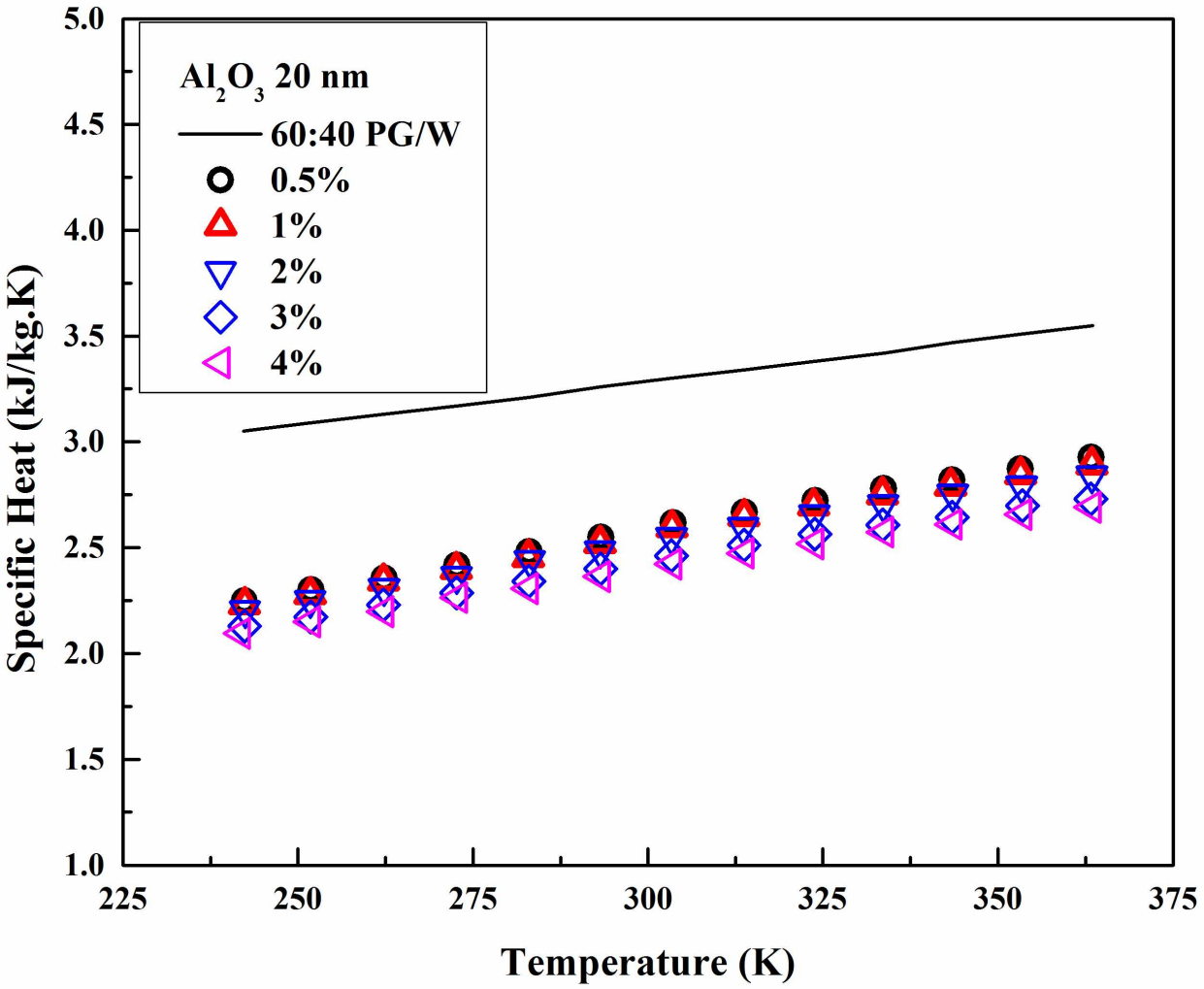

Figure 3.6. Specific heat variation of 20nm APS Al_2O_3 nanofluid with varying temperatures and volume concentrations.

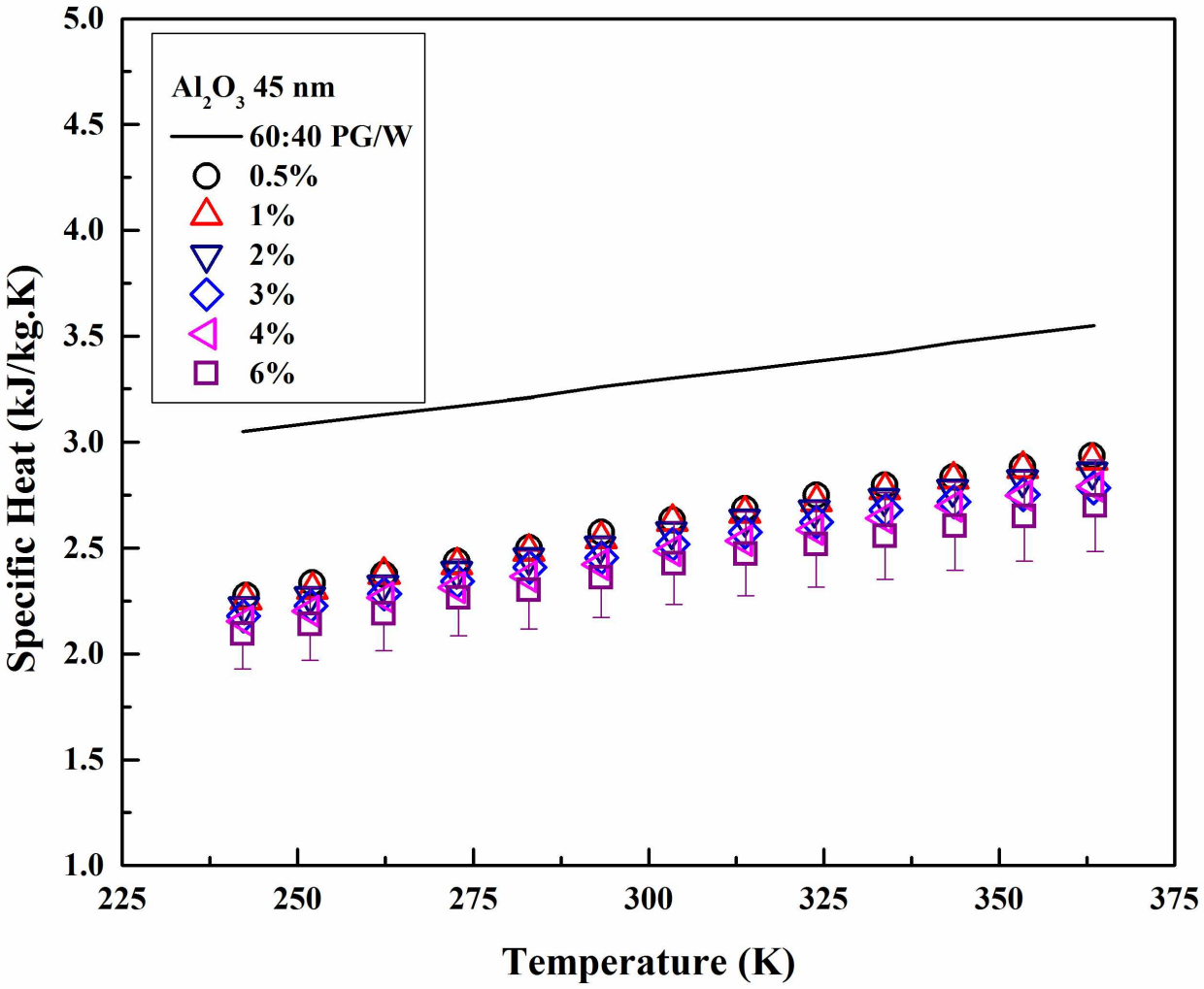

Figure 3.7. Specific heat variation of 45nm APS Al_2O_3 nanofluid with varying temperatures and volume concentrations

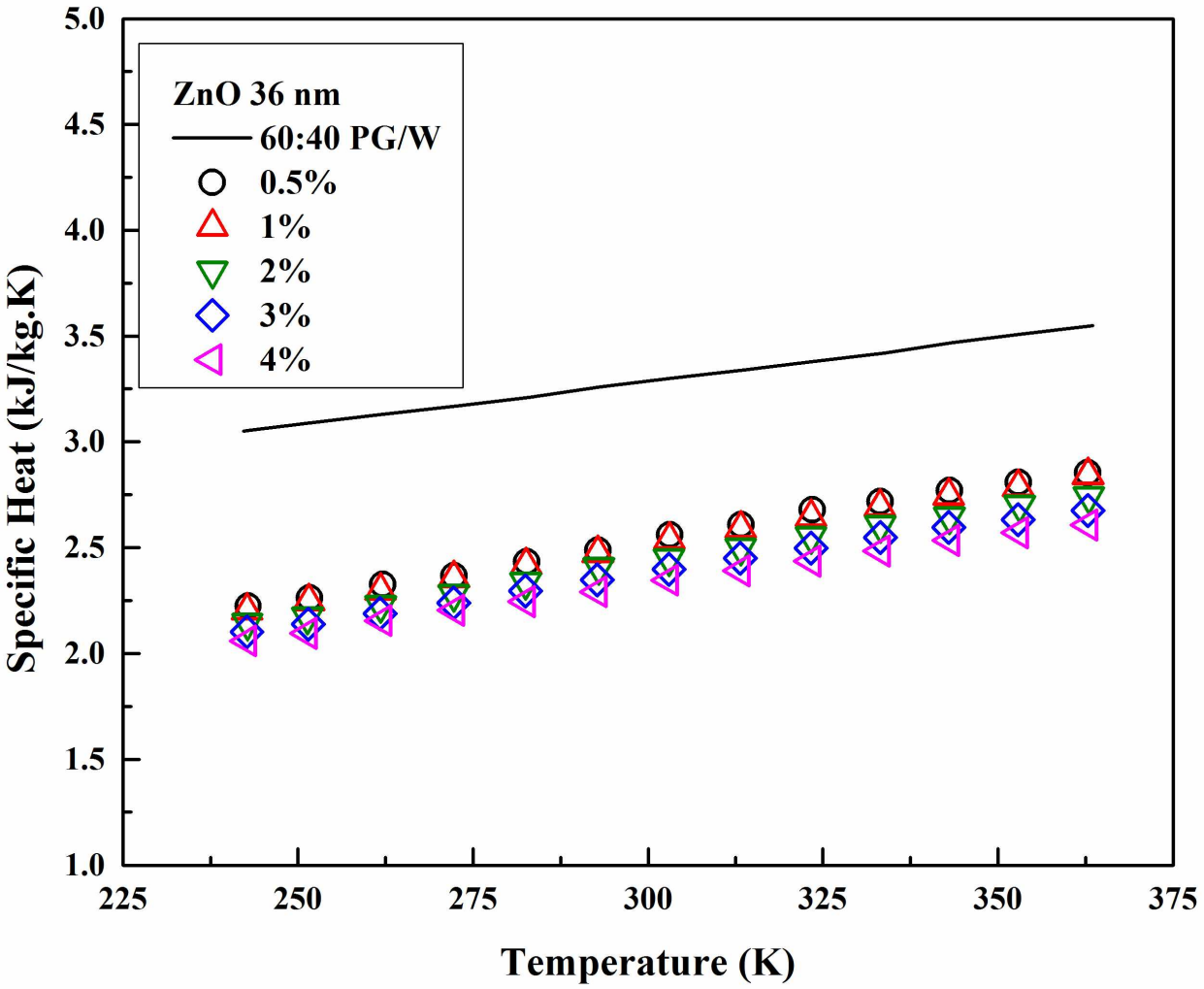

Figure 3.8. Specific heat variation of 36nm ZnO nanofluids with varying temperatures and volumetric concentrations

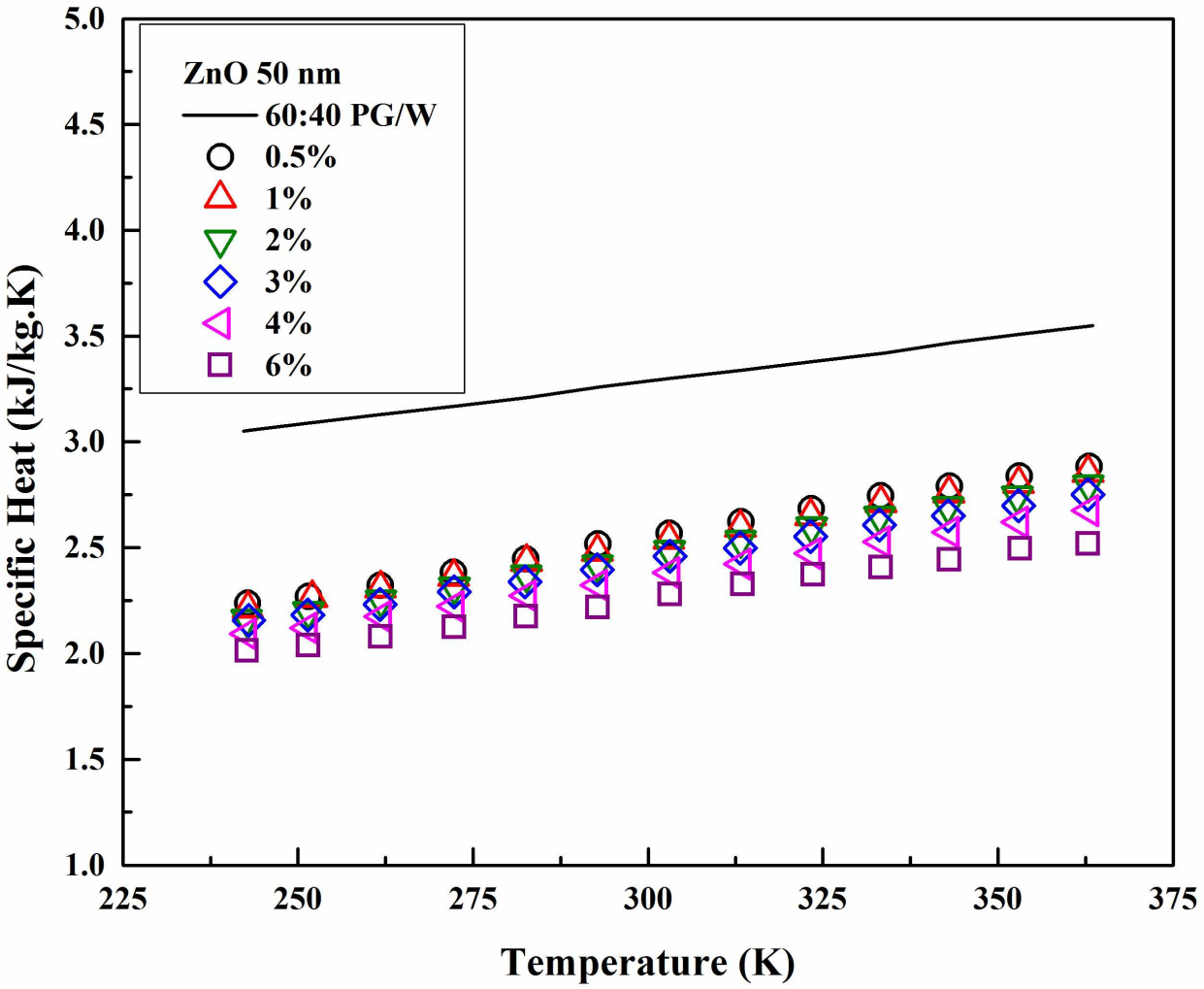

Figure 3.9. Specific heat variation of 50nm APS ZnO nanofluids with varying temperatures and volumetric concentrations

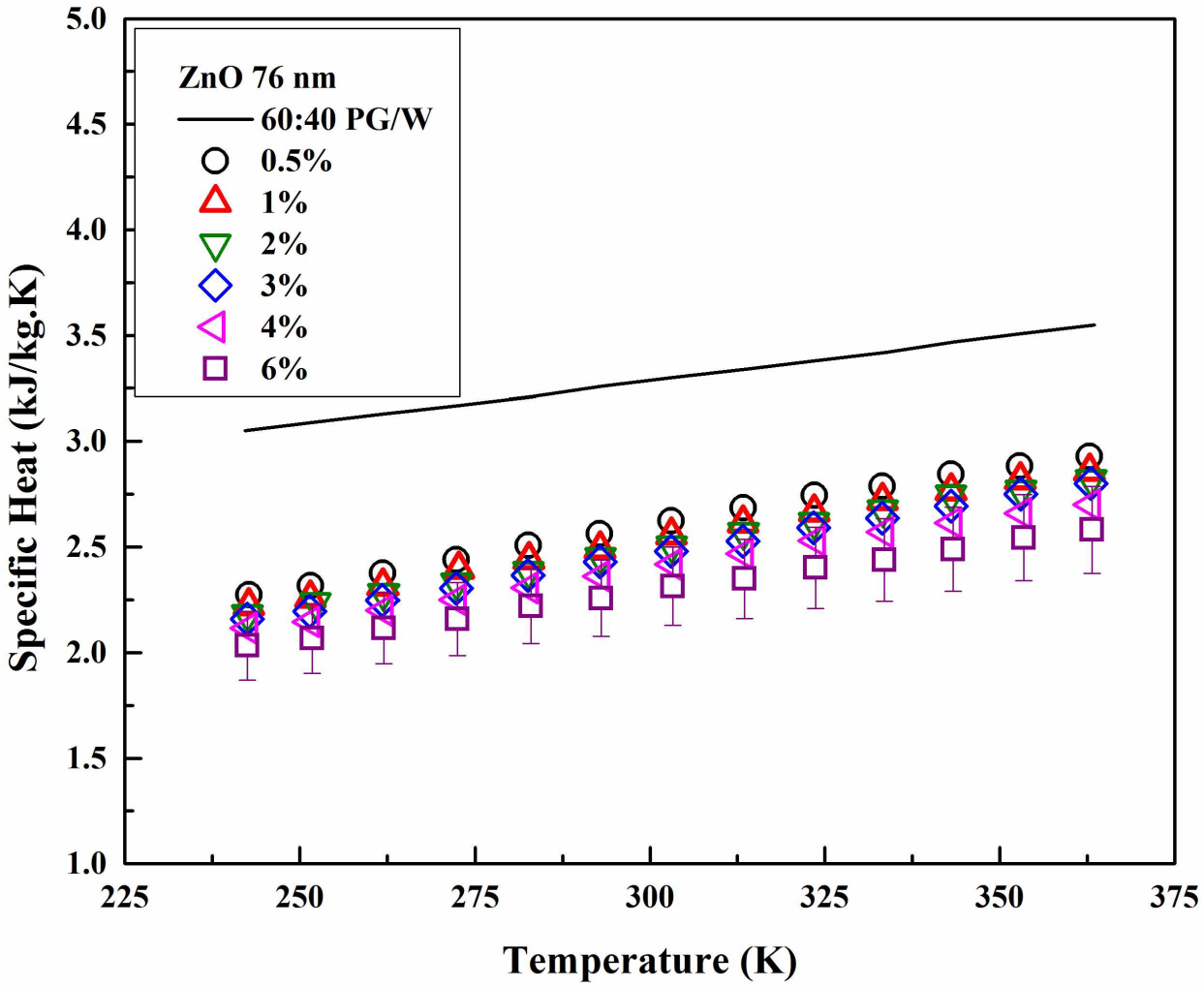

Figure 3.10. Specific heat variation of 76nm APS ZnO nanofluids with varying temperatures and volumetric concentrations

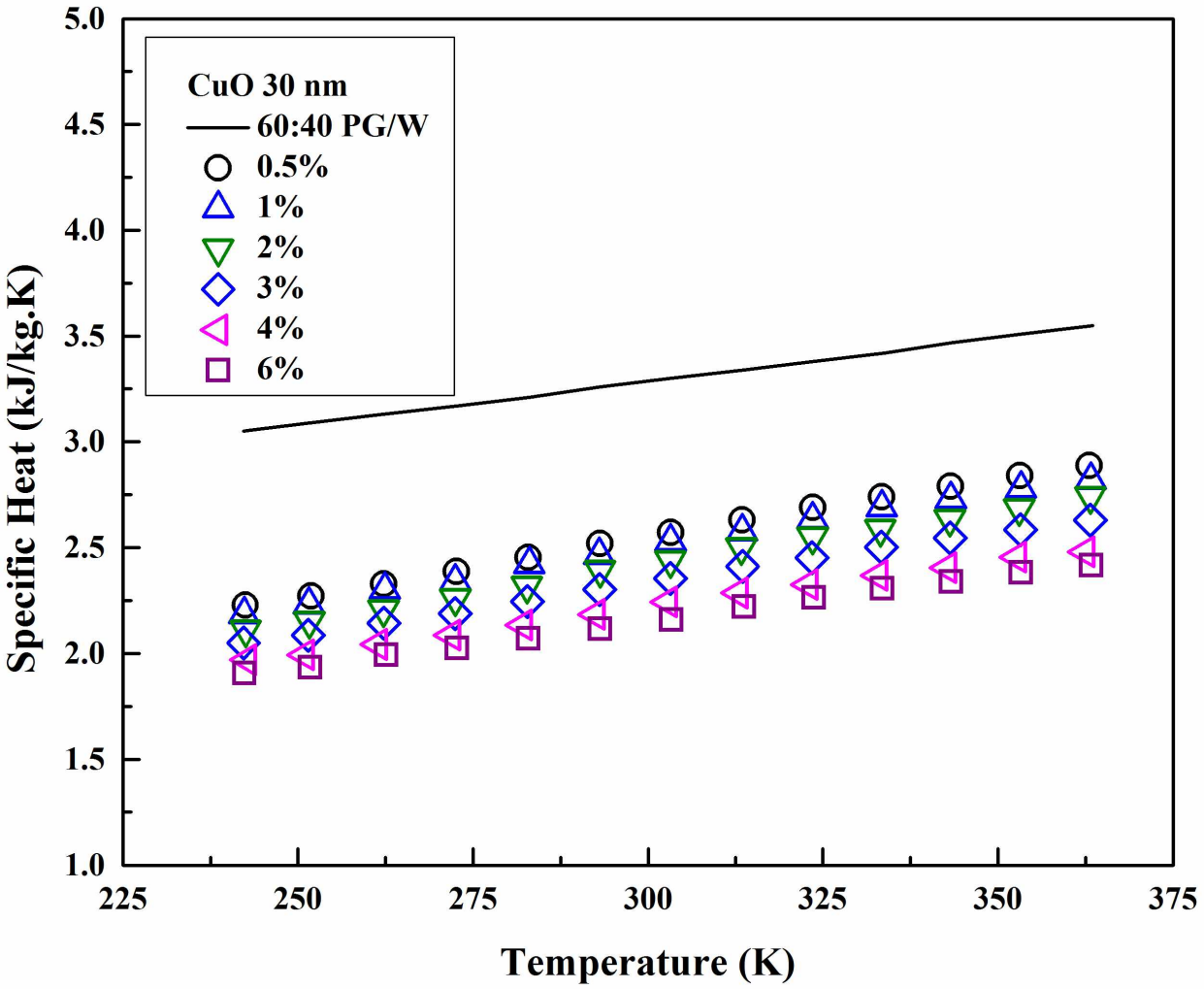

Figure 3.11. Specific heat variation of CuO nanofluids varying with varying temperatures and volumetric concentrations

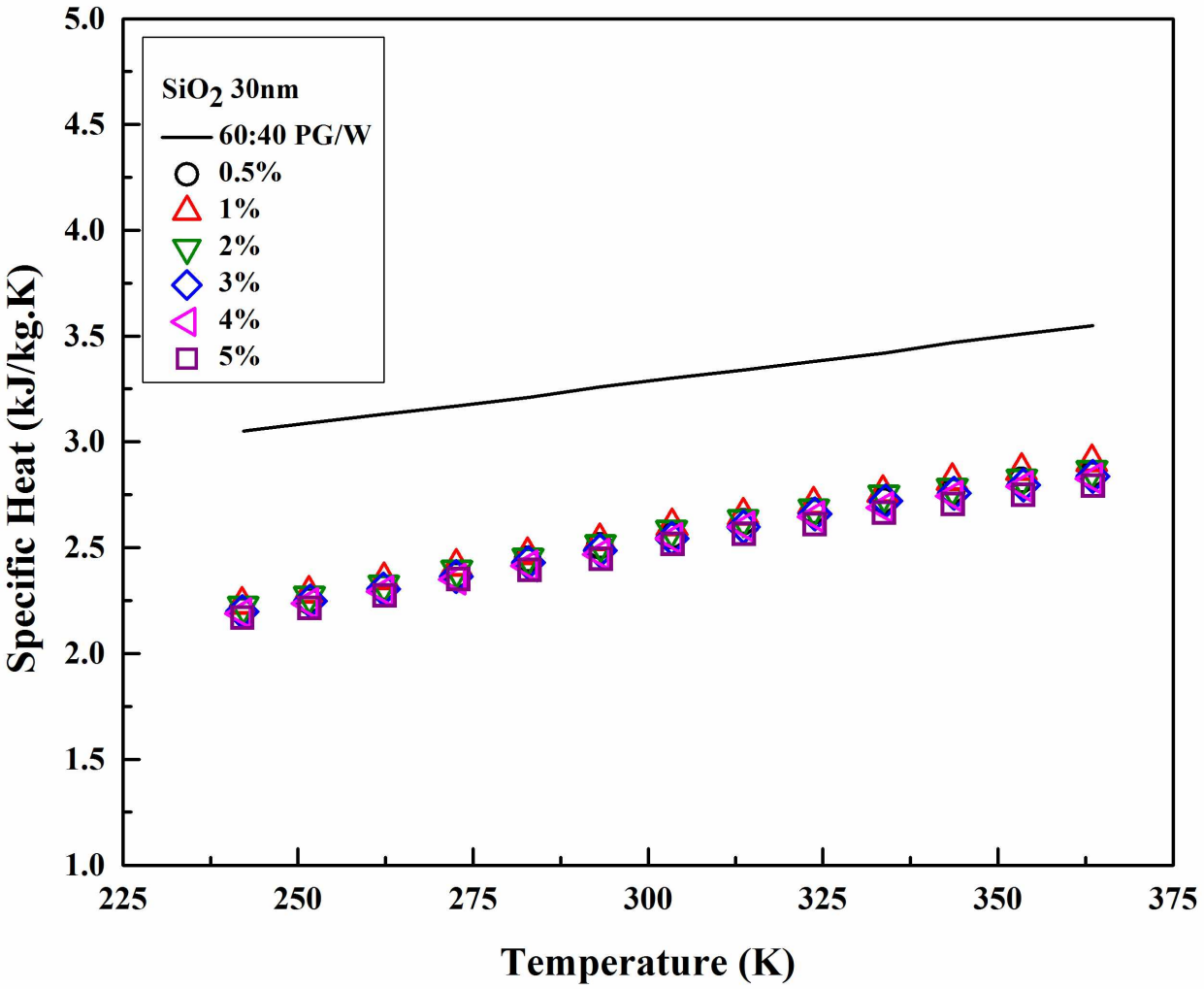

Figure 3.12. Specific heat variation of SiO_2 nanofluids of APS 30nm with varying temperatures and volumetric concentrations

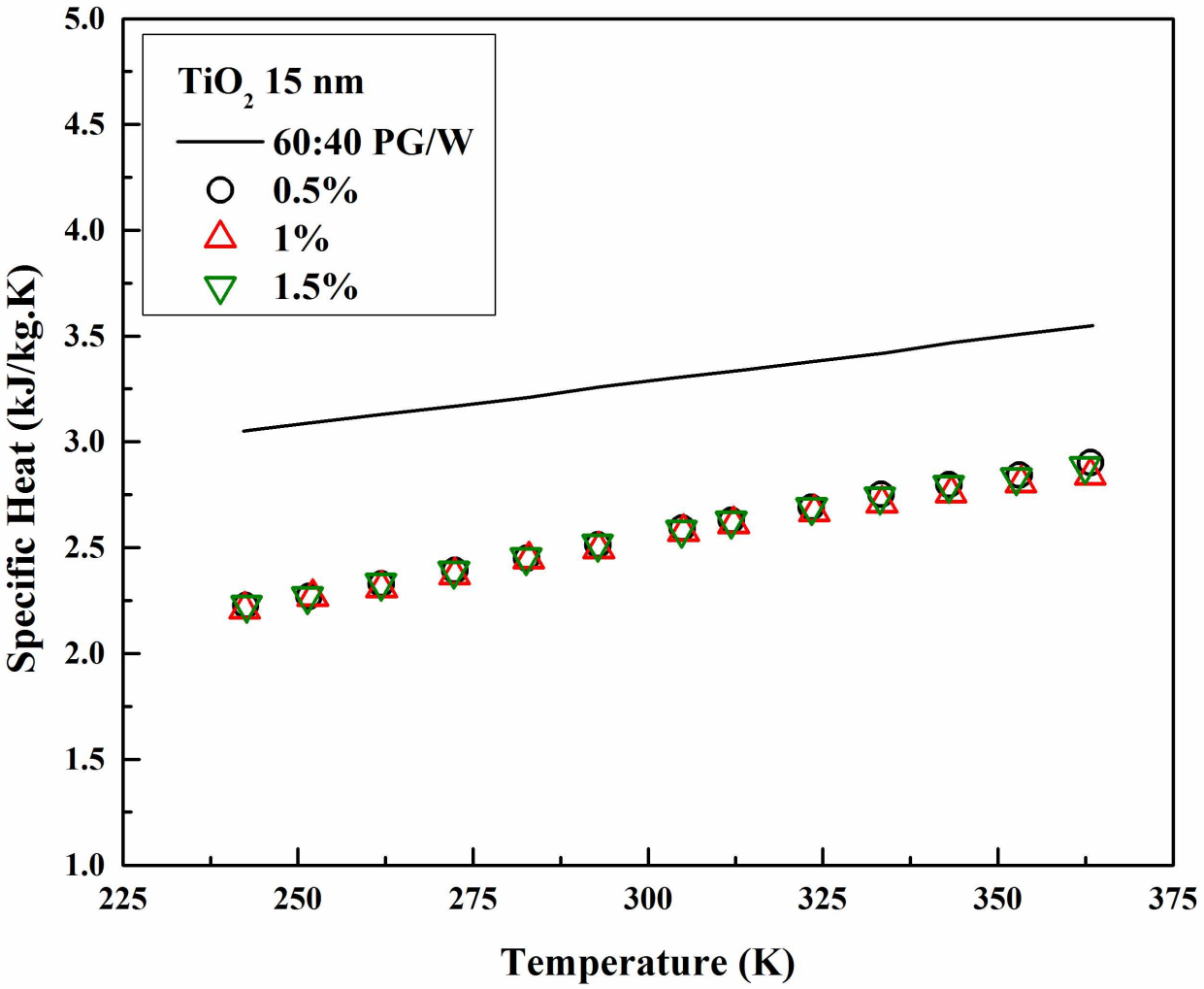

Figure 3.13. Specific heat measurements of TiO_2 nanofluids of APS 15nm with varying temperature and concentration

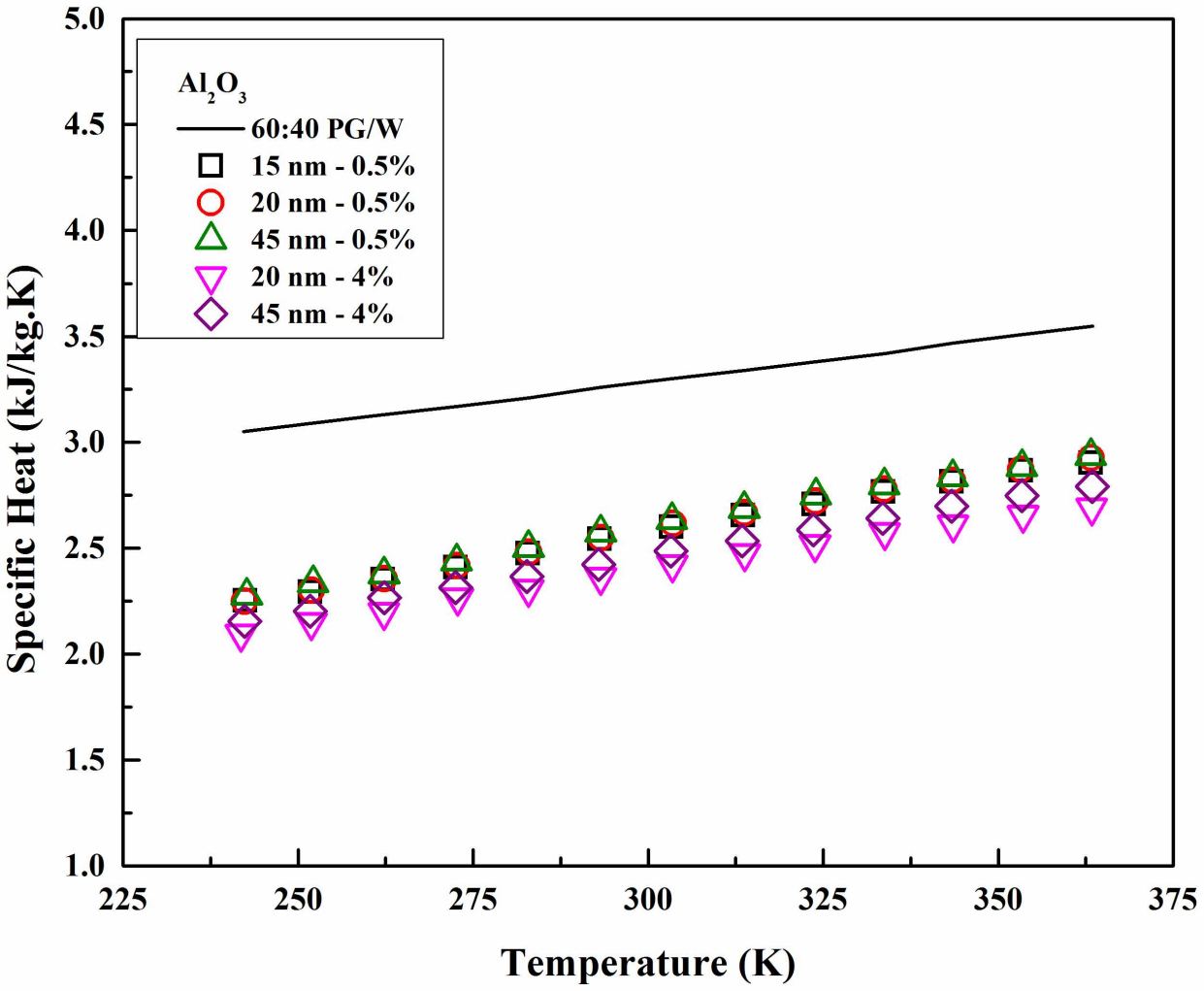

Figure 3.14. Particle size effect on the specific heat of Al_2O_3 nanofluids at equal volumetric concentrations and temperatures

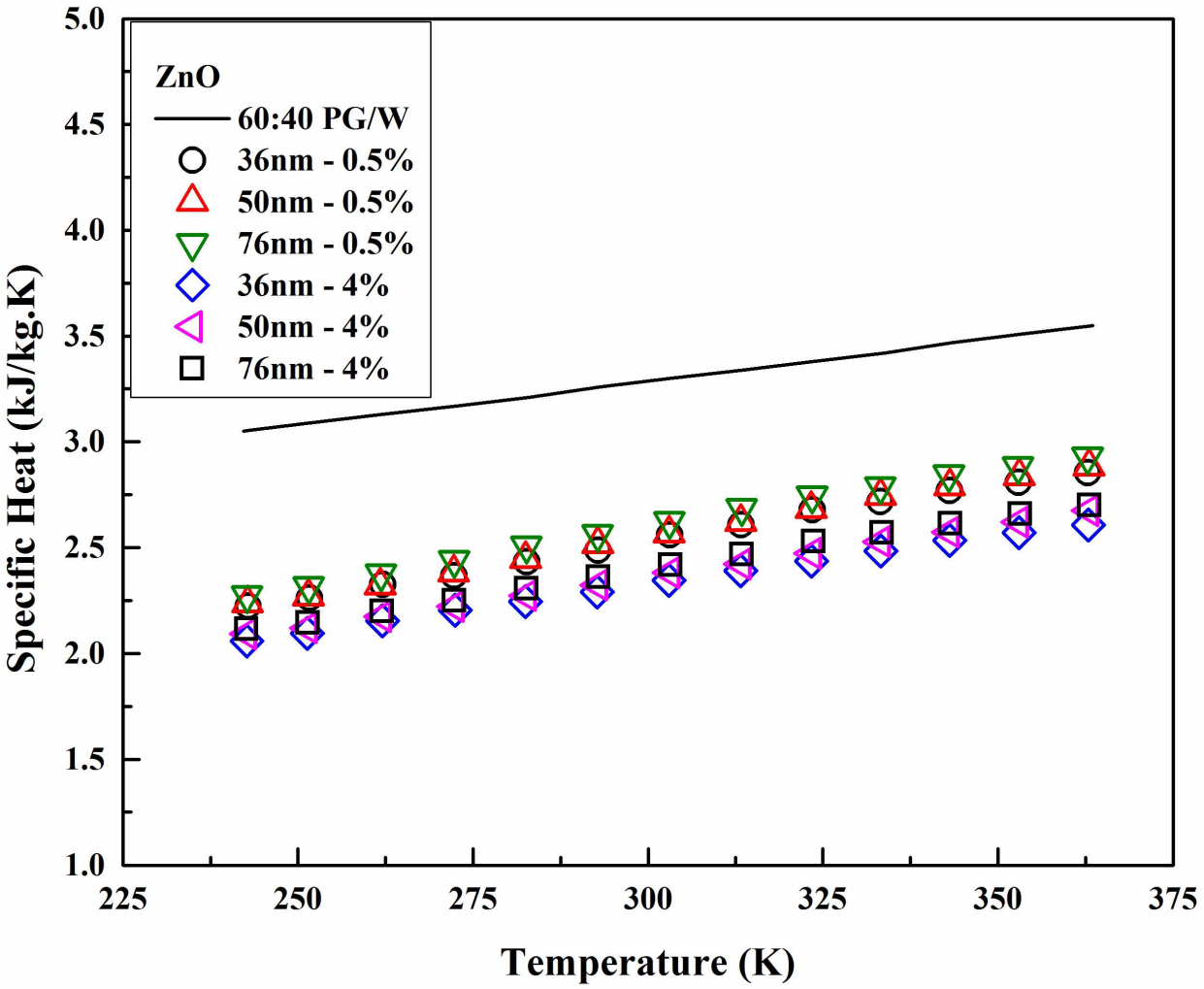

Figure 3.15. Particle size effect on the specific heat of ZnO nanofluids at equal volume concentrations and temperatures

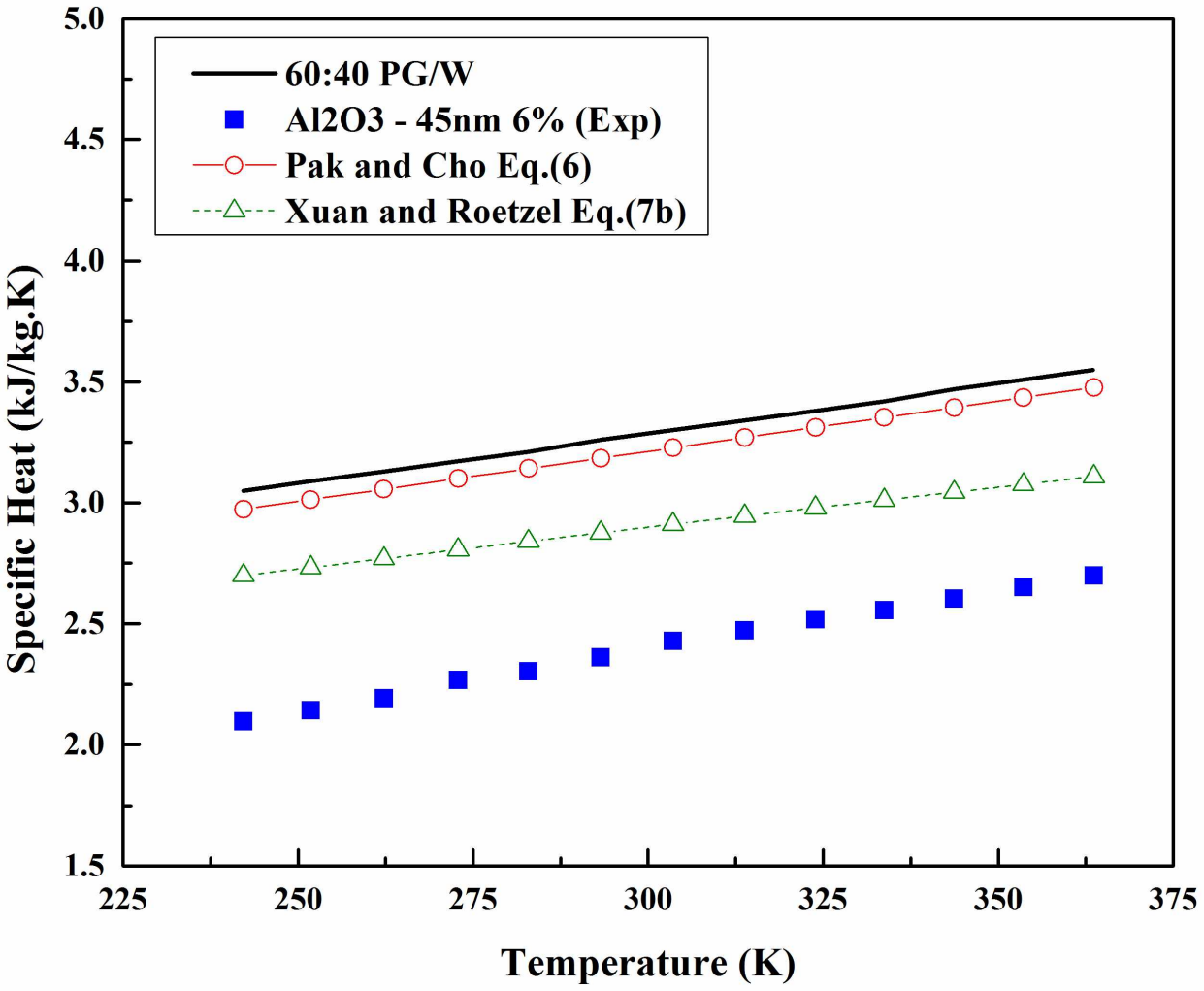

Figure 3.16. Experimental data comparison with two existing equations for the specific heat of a nanofluid

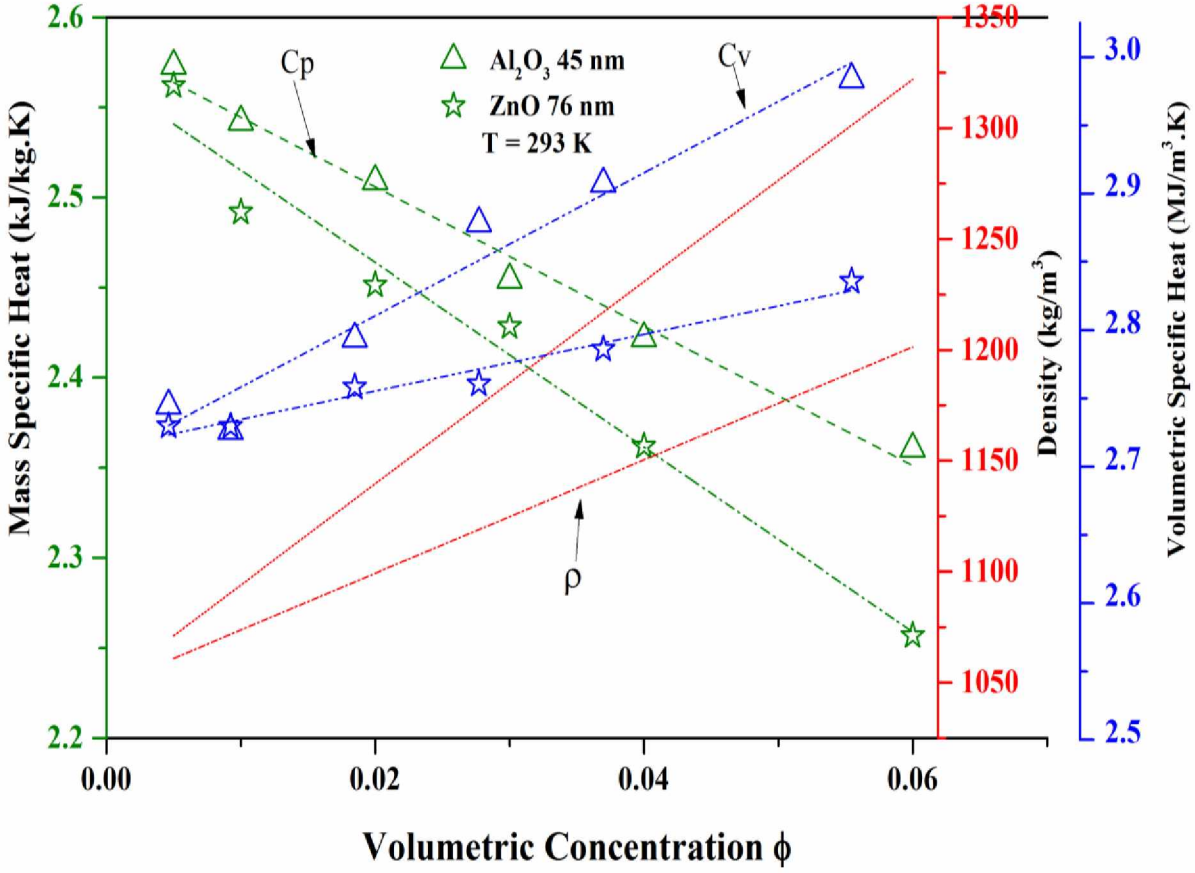

Figure 3.17. Variation of the density, mass specific heat and volumetric specific heat of the nanofluids with volume concentration at 293K

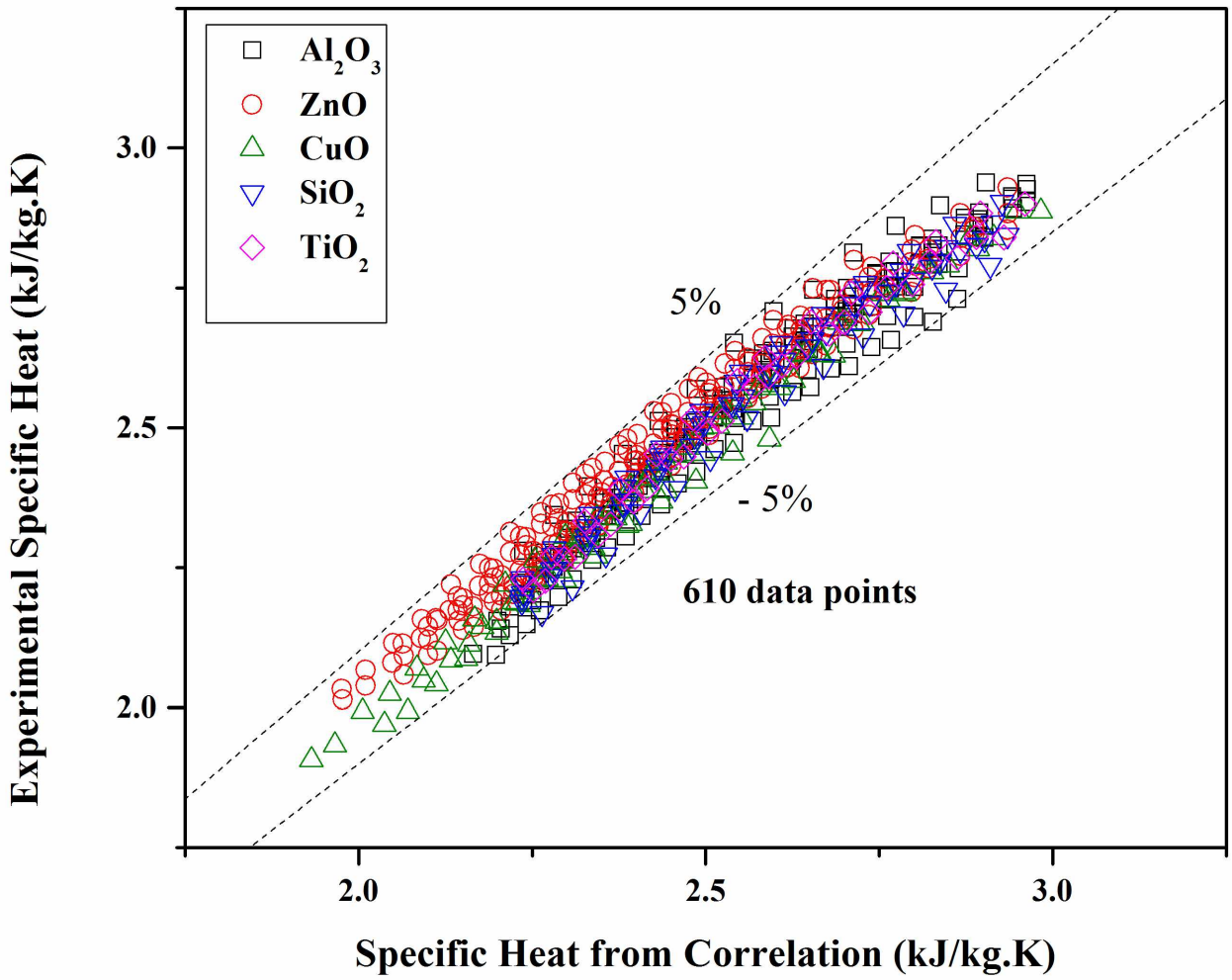

Figure 3.18. Comparison between the specific heat values from experiments and those predicted by Eq. (3.12)

Table 3.1. Parameters for study of specific heat effects on thermal and fluid dynamic performance

Parameters	**Value**
Hot Inlet (K)	363
Cold Inlet (K)	310
Hot Fluid Velocity (m/s)	0.25
Cold Fluid Velocity (m/s)	0.25
Fluid	Water
Heat Exchanger [43]	Concentric Tube in counter flow
Outer Diameter (m)	0.022
Inner Diameter (m)	0.012

Table 3.2. Some characteristics of nanofluids used in the present experiments.

Manufacturer	Material	Particle size (nm)	Particle Density (g/cc)	Specific Heat (J/kg.K)	Parent nanofluid concentration wt % in H_2O
Alfa Aesar [19]	Al_2O_3	20	3.6 [34]	765 [21]	30
Alfa Aesar	Al_2O_3	45	3.6	765	50
Nanostructured and Amorphous Materials, Inc. [20]	Al_2O_3	15	3.6 [35]	765	15
Nanostructured and Amorphous Materials, Inc.	SiO_2	30	2.2	745 [21]	25
Alfa Aesar	CuO	30	6.5	535.6 [21]	50
Alfa Aesar	ZnO	36	5.6	514 [21]	40
Alfa Aesar	ZnO	50	5.6	514	50
Alfa Aesar	ZnO	76	5.6	514	50
Nanostructured and Amorphous Materials, Inc.	TiO_2	15	4.2	683 [21]	15

Table 3.3. PG/W 60:40 correlations for the specific heat and density for 238 K ≤ T ≤ 398 K (-35 C ≤ T ≤ 125 C)

Property	Correlation	Constants	R^2	Error
Density	$\frac{\rho}{\rho_0} = A + B\left(\frac{T}{T_0}\right) + C\left(\frac{T}{T_0}\right)^2$	$\rho_0 = 1059\frac{kg}{m^3}$ $A = 0.9468;\ B = 0.2319;$ $C = -0.1787$	1	1.94E-3%
Specific Heat	$\frac{Cp}{Cp_0} = A + B\left[\frac{T}{T_0}\right]$	$Cp_0 = 3250\frac{J}{kg\cdot K}$ $A = 0.6294;\ B = 0.3707$	1	0.017%

The subscript "0" refers to the fluid property at the standard reference temperature of 273K (T_0).

3.13 References

[1] ASHRAE, 2009, "Physical properties of secondary coolants (Brines)," ASHRAE Handbook, American Society of Heating Refrigerator and Air Conditioning Engineers, Inc, Atlanta.

[2] Bejan, A., 1993, Heat Transfer, John Wiely & Sons, Inc., New York.

[3] Kays, W. M., and London, A. L., 1998, Compact Heat Echangers, 3rd edition, KRIEGER PUBLISHING COMPANY, MALABAR, FLORIDA.

[4] 2015, "P. A. Hilton (2015)" [Online]. Available: http://www.p-a-hilton.co.uk/index.php.

[5] Pak, B. C., and Cho, Y. I., 1998, "Hydrodynamic and heat transfer study of dispersed fluids with submicron metalic oxide particles.," Exp. Heat Transf., **11**, pp. 151–170.

[6] Xuan, Y., and Roetzel, W., 2000, "Conceptions for heat transfer correlation of nanofluids," Int. J. Heat Mass Transf., **43**(19), pp. 3701–3707.

[7] O'Hanley, H., Buongiorno, J., McKrell, T., and Hu, L., 2012, "Measurement and Model Validation of Nanofluid Specific Heat Capacity with Differential Scanning Calorimetry," Adv. Mech. Eng., **2012**, pp. 1–6.

[8] Vajjha, R. S., and Das, D. K., 2009, "Specific Heat Measurement of Three Nanofluids and Development of New Correlations," ASME J. Heat Transf., **131**(7), p. 071601.

[9] Vajjha, R. S., and Das, D. K., 2012, "A review and analysis on influence of temperature and concentration of nanofluids on thermophysical properties, heat transfer and pumping power," Int. J. Heat Mass Transf., **55**(15-16), pp. 4063–4078.

[10] Kulkarni, D. P., Vajjha, R. S., Das, D. K., and Oliva, D., 2008, "Application of aluminum oxide nanofluids in diesel electric generator as jacket water coolant," Appl. Therm. Eng., **28**(14-15), pp. 1774–1781.

[11] Namburu, P. K., Kulkarni, D. P., Dandekar, A., and Das, D. K., 2007, "Experimental investigation of viscosity and specific heat of silicon dioxide nanofluids," Micro Nano Lett., **2**(3), p. 67.

[12] Bergman, T. L., 2009, "Effect of reduced specific heats of nanofluids on single phase, laminar internal forced convection," Int. J. Heat Mass Transf., **52**(5-6), pp. 1240–1244.

[13] Pantzali, M. N., Kanaris, A. G., Antoniadis, K. D., Mouza, A. A., and Paras, S. V., 2009, "Effect of nanofluids on the performance of a miniature plate heat exchanger with modulated surface," Int. J. Heat Fluid Flow, **30**(4), pp. 691–699.

[14] Sonawane, S., Patankar, K., Fogla, A., Puranik, B., Bhandarkar, U., and Sunil Kumar, S., 2011, "An experimental investigation of thermo-physical properties and heat transfer performance of Al2O3-Aviation Turbine Fuel nanofluids," Appl. Therm. Eng., **31**(14-15), pp. 2841–2849.

[15] Shin, D., and Banerjee, D., 2014, "Specific heat of nanofluids synthesized by dispersing alumina nanoparticles in alkali salt eutectic," Int. J. Heat Mass Transf., **74**, pp. 210–214.

[16] De Robertis, E., Cosme, E. H. H., Neves, R. S., Kuznetsov, A. Y., Campos, A. P. C., Landi, S. M., and Achete, C. A., 2012, "Application of the modulated temperature differential scanning calorimetry technique for the determination of the specific heat of copper nanofluids," Appl. Therm. Eng., **41**, pp. 10–17.

[17] Ho, M. X., and Pan, C., 2014, "Optimal concentration of alumina nanoparticles in molten hitec salt to maximize its specific heat capacity," Int. J. Heat Mass Transf., **70**, pp. 174–184.

[18] Shin, D., and Banerjee, D., 2011, "Enhancement of specific heat capacity of high-temperature silica-nanofluids synthesized in alkali chloride salt eutectics for solar thermal-energy storage applications," Int. J. Heat Mass Transf., **54**(5-6), pp. 1064–1070.

[19] Alfa Aesar (2014), www.alfaaesar.com.

[20] Nanostructured & Amorphous Materials (2014), http://www.nanoamor.com/home.

[21] Lide, D., 1995, CRC Handbook of chemistry and physics, 84th edition, CRC Press, USA.

[22] "Bransonic Tabletop Ultrasonic Cleaners (2010)" [Online]. Available: http://www.sonicsonline.com/b8510.html.

[23] Wooden, N., 2008, Operating Procedure for the TCi: Small Volume Test Kit for Thermal Conductivity Testing, C-Therm technologies, Amherst, Nova Scotia, Canada, B4H 4S8.

[24] Thermatron, 2004, "Environmental Test Chamber Instruction Manual."

[25] Paar, A., Anton Paar Digital Density Meter for Liquids and Gases DMA 4500, Graz, Austria.

[26] Minitab 16 Statistical Software (2013). [Computer Software], Minitab, Inc. (www.minitab.com), State College, PA.

Chapter 4 Measurements of Densities of Propylene Glycol Based Nanofluids and Comparison with Theory [1]

4.1 Abstract

Density measurements were performed on several nanofluids containing nanoscale particles of aluminum oxide (Al_2O_3), zinc oxide (ZnO), copper oxide (CuO), titanium oxide (TiO_2), and silicon dioxide (SiO_2). These particles were individually dispersed in a base fluid of 60:40 propylene glycol and water (PG/W) by mass. Additionally, Carbon Nanotubes (CNT) dispersed in deionized water (DI) were also tested. Initially, a benchmark test was performed on the density of the base fluid in the temperature range of 0°C to 90°C. The measured data agreed within a maximum error of 1.6% with the values presented in the handbook of American Society of Heating, Refrigerating, and Air Conditioning Engineers (ASHRAE). After this validation run the density measurements of various nanofluids with particle volumetric concentrations from 0 to 6% and nanoparticle sizes ranging from 10 to 76 nm were performed. The temperature range of the measurements was from 0° to 90°C. These results were compared with the values predicted by a currently acceptable theoretical equation for nanofluids. The experimental results showed good agreement with those of the theoretical equation with a maximum deviation of -3.8% for copper oxide nanofluid and an average deviation of -0.1% for all the nanofluids tested.

4.2 Introduction

Heat transfer fluids (water, ethylene glycol, propylene glycol, mineral oil, etc.) are widely used in power generation, heating and cooling systems, chemical-processing plants and in electronic cooling. The effectiveness of any heat transfer process depends on the thermophysical properties of heat transfer fluids. Researchers are constantly experimenting with new types of heat transfer fluids to improve their heat transfer capability. Nanofluids are one such new class of heat transfer fluids widely believed to be promising. Choi [1] proposed the concept of nanofluids by observing

---

[1] Satti, J. R, Das, D. K. and Ray, D., "Measurements of Densities of Propylene Glycol Based Nanofluids and Comparison with Theory," accepted by ASME Journal of Thermal Science and Engineering Applications.

the previous work on ultra-fine particles dispersed in liquid. Nanofluids are suspensions of solid particles of size less than 100 nm in a fluid. Addition of these solid nanoparticles enhances the thermal conductivity of the fluid-solid mixture. Therefore nanofluids possess better thermal conductivity than the normal heat transfer fluids. When the nano sized solid particles are added to base fluids, the thermophysical properties of the fluid are changed. Over the past decade, researchers conducted experiments on different nanofluids focusing on thermal conductivity and proved enhancement of this property after addition of solid nanoparticles. Eastman et al. [2] and Vajjha et al. [3, 4], conducted experiments on different ethylene glycol based nanofluids and proved the enhancement of thermal conductivity of ethylene glycol after the addition of solid nanoparticles. As the research on nanofluids is growing, the requirement for accurate measurements of thermophysical properties of nanofluids is becoming increasingly important. The most needed thermophysical properties of nanofluids are thermal conductivity, viscosity, density and specific heat. Numerous papers have been published on thermal conductivity and viscosity of different nanofluids. However the literature is very limited on the density variation of nanofluids with temperature, volumetric concentration and nanoparticle size. Therefore, the objective of our research is to do such measurements and compare the experimental results with the available theory.

4.3 Cold region heat transfer fluids

In cold climate regions like Alaska, Canada, Northern Europe, Russia etc., the ambient temperatures may reach around - 40^0 C. In such regions, Ethylene Glycol (EG) and Propylene Glycol (PG) are commonly used as heat transfer fluids. However, even pure EG or PG will freeze around - 40^0 C, but when they are mixed with pure water, their freezing point is depressed below - 40^0 C. Therefore, it is common practice to use a mixture of water and EG or PG as the heat transfer fluid in building heating systems, automobiles, heat exchangers of industrial plants that are exposed to low temperatures. The mixture of 60% of propylene glycol and 40% water (60:40 PG/W) by volume has the lowest freezing temperature of -51.1 ^{0}C ASHRAE [5]. Vajjha et al. [3, 4] conducted measurements on different nanofluids with 60:40 EG/W as base fluid. However EG is toxic in nature and it takes longer time to degrade in the environment. On the other hand, PG is non-toxic in nature and easily decomposes in the environment. Therefore it is safer to use PG/W in human interaction applications. For heating residential buildings in cold regions, PG/W is the

recommended heat transfer fluid due to the possibility of mixing of this with the potable water in the household plumbing systems. For this reason 60:40 PG/W has been selected as base fluid for our experiments.

4.3.1 Objective

After adding nanoparticles to base fluid, the thermophysical properties of base fluid will change. The change would depend on the nanoparticle, volume concentration and nanoparticle size. It is well known from text books [6, 7] that the properties of liquids change with temperature. The goal of the present experiments is to study the density variation of different nanofluids with varying volume concentration, nanoparticle size and temperature. The densities of several different nanofluids containing Al_2O_3, ZnO, TiO_2, CuO, SiO_2, and CNT nanoparticles dispersed in PG/W were measured and the experimental results were compared with available theory. The densities measured for different nanoparticle sizes and volumetric concentrations up to 6% in a temperature range of 0 ℃ to 90 ℃.

Different nanofluids come with their respective surfactants or dispersants to make these suspensions stable. Often the information about these additives is not revealed by the nanofluid vendor, because it is proprietary. These additives may affect the density and other thermophysical properties of nanofluids. Therefore, another important objective of the present research is to determine, how much these additives affect the measured values and can the available theory still predict a results close to the measurements.

4.4 Importance of accurate density measurement

4.4.1 Heat transfer consideration

For low concentration nanofluids, Pak and Cho [8] showed that the heat transfer characteristics can be quantified by Eq. (4.1), which is similar to the well-known Dittus - Bolter correlation [9]. Although this equation was originally developed for single-phase fluids, researchers [8] have shown this equation to hold for low concentration nanofluids as well.

$$Nu_{nf} = C.Re_{nf}^{a}.Pr_{nf}^{b} \tag{4.1}$$

In the above equation, the Nusselt Number ($Nu_{nf} = hd/k_{nf}$) contains the heat transfer coefficient h in a tube of diameter d for a nanofluid of thermal conductivity k_{nf}. The Reynolds number $(Re_{nf} = Vd\rho_{nf}/\mu_{nf})$ for the nanofluid flowing with average velocity V is a function of density ρ_{nf} and viscosity μ_{nf}. Prandtl number ($Pr_{nf} = Cp_{nf}\mu_{nf}/k_{nf}$) is dependent on nanofluid properties, specific heat Cp_{nf}, viscosity μ_{nf}, and thermal conductivity k_{nf}. For single-phase fluid in case of heating $a = 0.8$ *and* $b = 0.4$ and $C = 0.023$. Pak and Cho [8], performed experiments on Al_2O_3 and TiO_2 nanofluids and derived constant values of Eq. (4.1) as $C = 0.021$, $a = 0.8$ *and* $b = 0.5$; subsequently other researchers [10–12] have performed experiments on different nanofluids to find heat transfer coefficient of nanofluids. From Eq. (4.1) it is evident that heat transfer coefficient is a function of Reynolds number (*Re*). Reynolds number is a function of density of fluid. Therefore, the heat transfer coefficient is dependent on the density of a fluid. A small variation in density results in change of heat transfer coefficient of fluid. In order to calculate the total heat transfer, one uses Eq. (4.2):

$$q = \rho_{nf} AV(\Delta T) \tag{4.2}$$

where A is the flow area, V is the average velocity, and ΔT is the temperature difference of the fluid between the inlet and the outlet. So, an accurate $\boldsymbol{\rho_{nf}}$ value is needed to accurately determine the total heat transfer q.

4.5 Fluid friction consideration

Heat transfer fluids are circulated through pipes and heat exchanger to distribute the heat from the heat source. To transport the fluid through a system we require the pumping power to overcome the fluid friction at the wall. The Darcy friction factor f is required to determine the frictional head loss, which is given by Eq. (4.3) from White [6].

$$\frac{1}{\sqrt{f}} = -1.8\log_{10}\left[\frac{6.9}{Re_D} + \left(\frac{\frac{k}{D}}{3.7}\right)^{1.11}\right] \tag{4.3}$$

From Eq. (4.3) we notice that the friction factor f is a function of the Reynolds number Re, which in turn is dependent on the density of the nanofluid. The pressure loss Δp in a conduit of length L is found by Eq. (4.4) [6], which also depends on the nanofluid density.

$$\Delta \mathrm{P} = \frac{\mathrm{f}\, \rho_{\mathrm{nf}} L V^2}{2d} \tag{4.4}$$

From Eqs. (4.3) and (4.4) it is evident that accurate density of the nanofluid is essential in accessing the pressure loss and the subsequent pumping power.

4.6 Thermal diffusivity consideration

Thermal diffusivity α_{nf} is a measure of how fast the heat diffuses through a material. Eq. (4.5) gives the formula to find the thermal diffusivity of nanofluids using the density of nanofluids. By knowing the density of nanofluid we can accurately predict the thermal diffusivity of nanofluid.

$$\alpha_{\mathrm{nf}} = \frac{\mathrm{k_{nf}}}{\rho_{\mathrm{nf}} \mathrm{c_{p_{nf}}}} \tag{4.5}$$

Higher thermal diffusivity will be beneficial in absorbing heat faster in the furnaces used for heating buildings in cold regions.

From the previous sections, it was shown that density is needed in determining heat transfer and fluid friction, but how much does density affect them? Keeping the parameters outlined in Table 4.1 constant except for density, we can examine the effects of density on heat transfer rate, Reynolds number, Nusselt number, heat transfer coefficient, friction factor, pressure drop and pumping power (Eq. (4.1-4.4)). In Figure 4.1, the effects of changing density are shown. Examining the figure, we can see that density has a linear relationship with all the dependent parameters excluding friction factor. The increase in heat transfer rate, Reynolds number, Nusselt number, and heat transfer coefficient are nearly equal to increase in density. If the density was increased by 15% then heat transfer rate and Reynolds number would increase by 15%, while Nusselt number and heat transfer coefficient would increase by 11.8%. It was also found that friction factor is affected the least by density as shown by increasing the density by 50% the friction factor diminished by 1.2%. Pressure drop and pumping power are also shown to be fairly dependent on density, where if density were increased by 35% the pressure drop and pumping

power would also increase by 33.8%. From this analysis, we see that having accurate density measurements are vital in determining the thermal and fluid dynamic performance of a fluid.

4.7 Previous Work

Vajjha et al. [4] measured density of Al_2O_3, ZnO and Sb_2O_5: SnO_2 nanofluids with 60:40 EG/W as base fluid with different volumetric concentrations and varying temperatures between 0 ^{0}C to 50 ^{0}C. They tested these nanofluids, some up to 10% volume concentration and found that their data agreed well with the Pak and Cho Eq. (4.6) within$\pm$1%, expectable ZnO nanofluids, which showed deviation from 2 to 8%, with increase in concentration. They proposed a correlation factor as a function of ϕ to compensate this error. Cabaleiro et al. [13] performed experiments on ZnO nanoparticles dispersed in ethylene glycol and water mixture. They measured density of the nanofluid for different molar concentrations by varying pressure and temperature, which previous authors (Pak and Cho [8] and Vajjha et al. [4]) measured nanofluids under standard atmospheric pressure. Cabaleiro et al. [13] varied the pressure up to 45 MPa and temperature from 278.15 to 363.15 K. They discovered the experimental density values agreed with theoretical correlations. An average deviation of 0.35% was found in the density measurements. Pastoriza–Gallego et al. [14] studied the effects of nanoparticles size (23-27 nm and 11$\pm$3 nm) and pressure (up to 45 MPa) on CuO nanoparticles dispersed in DI water. It was found that the effect of nanoparticle size on density of nanofluid was marginal. Pastoriza–Gallego et al. [15] studied the behavior Al_2O_3 nanoparticles dispersed in DI water with varying pressures up to 25MPa, volumetric concentrations (0.5% to 2%) and nanoparticle sizes (50 nm & 20 nm). The influence of nanoparticle size on density was negligible and deviation between measured and theoretical values increased with volume concentration. Martin and Bou-Ali [16] performed experiments on fullerene – toluene nanofluids with weight fractions of 0.05, 0.1, 0.15, and 0.2 at room temperature of 25 ºC. They found the density to increase linearly with the weight fraction. Kumaresan and Velraj [17] performed experiments on Multiwalled Carbon Nanotubes (MCWNT) dispersed in 30:70 EG/W base fluid. The MWCNT had average diameter of 30-50nm, and length of 10-20 μm. The different volume fractions measured were 0.15%, 0.3% and 0.45%. They found Pak and Cho correlation Equation under predicted the density of CNT nanofluids.

The thermal performance of nanofluids was reported to depend on the temperature, concentration and the nanoparticle size of dispersed nanoparticles. Studies have shown an increase in thermal conductivity with increasing concentration [1, 18–21]. The nanoparticle size of nanofluids also showed significant impact on thermal conductivity of nanofluids. It was found that as the size of nanoparticles decreased the thermal conductivity increased [2, 12, 17–22]. From these observations it was considered important to study the effect of nanoparticle size on the density of nanofluid. Therefore our goal was to measure the density of different propylene glycol water mixture nanofluids with different nanoparticle sizes, volume concentrations, in a temperature range of 0 ^{0}C to 90 ^{0}C for a variety of nanoparticles including the CNT.

4.8 Theory

Beginning with the description given by Cheremisinoff [7], a theoretical equation for the density of a liquid containing fine solid nanoparticles can be derived from the consideration of the conservation of mass. This approach was used in early years to determine the density of the slurry containing coal powder, which contained generally microparticles. The theory can also be applied to nanofluids containing nanoparticles.

Let the mass of certain volume V_{nf} of the nanofluid be m_{nf}. Then $V_{nf} = V_{bf} + V_{np}$ and $m_{nf} = m_{bf} + m_{np}$. The density of the nanofluid is given by Eq. (4.6):

$$\rho_{nf} = \frac{m_{nf}}{V_{nf}} = \frac{m_{bf} + m_{np}}{V_{nf}} \tag{4.6}$$

In terms of the densities of the base fluid and the nanoparticles, $m_{bf} = \rho_{bf} V_{bf}$ and $m_{np} = \rho_{np} V_{np}$. Introducing these variables into Eq. (4.6), one obtains:

$$\rho_{nf} = \frac{\rho_{bf} V_{bf} + \rho_{np} V_{np}}{V_{nf}} \tag{4.7}$$

now introduce the particle volumetric concentration:

$$\frac{V_{np}}{V_{nf}} = \phi \tag{4.8}$$

Then the liquid volume fraction is

$$\frac{V_{bf}}{V_{nf}} = \frac{V_{nf} - V_{np}}{V_{nf}} = (1 - \phi) \tag{4.9}$$

Substituting Eq. (4.8 and 4.9) into Eq. (4.7), one derives:

$$\rho_{nf} = \rho_{bf}(1 - \phi) + \rho_{np}\phi \tag{4.10}$$

Pak and Cho [8] used Eq. (4.10) as the theoretical equation. They did experiments to find the density of γ-Al_2O_3 and TiO_2 nanofluids with water as base fluid with different volume concentrations at room temperature. They compared Eq. (4.10) with their measured values of density and found good agreement.

4.9 Materials and Experiments

4.9.1 Different nanoparticles

Presented in Table 4.2 below the nanofluids purchased for the experiments. The different nanoparticles used in the following experiments were Al_2O_3, ZnO, CuO, TiO_2, SiO_2, Singlewalled Carbon Nanotube (SWCNT), Multiwalled Carbon Nanotube (MWCNT) and Bamboowalled Carbon Nanotube (BWCNT). The nanofluids suspensions for the experiments were obtained from Alfa Aesar [23] and Nanostructured and Amorphous Materials Inc. [24]. The Carbon Nanotube dispersions were procured from Nanolab Research Company [25]. The nanofluid purchases from the vendor will be referred to as the mother nanofluid. The mother nanofluids were obtained as nanoparticles suspended in pure DI water at high concentrations. They were pretreated with proprietary surfactants by the manufacturer to prevent agglomeration.

4.10 Preparation of Nanofluids

First, the mother nanofluid was sonicated for 10 hours before preparation of the test samples. A Bransonic sonicator [26] with 40 kHz frequency and 185W power was used for sonication of nanoparticle suspensions. The sonication of the mother nanofluid is necessary to break up any sedimentation or agglomeration due to long term storage. After sonication of the mother nanofluid, small samples were mixed with calculated amount of 60:40 PG/W, to obtain required volume concentration ranging from 0.5% to 6%. Then the test samples were sonicated again for 5 hours to ensure an even dispersion of nanoparticles in base fluid. Using this preparation method, no

sedimentation was observed in the test samples by careful visual examination. A few of the prepared samples are shown in Figure 4.2.

4.11 Particle size image analysis

The manufacturer provided us with the average nanoparticle size (APS) of different nanofluids. To verify the APS of samples, they were subjected to the analysis in a Transmission Electronic Microscope (TEM) as an example, a test sample of 45nm APS Al_2O_3 nanofluid sample is presented in Figure 4.3. The Al_2O_3 nanoparticles appeared to be perfectly spherical in shape. Nanoparticles of different diameters ranging around 45nm were observed. The manufacturer uses an averaging technique, perhaps on an equal mass basis, to arrive at an APS. Looking at this image in Figure 4.3, it appeared that many nanoparticles were in the neighborhood of 45nm. Therefore the image analysis verified that the APS may indeed be what the manufacturer specified

4.12 Apparatus

The experiments were carried with Anton Paar DMA 4500 density measuring device [27]. An image of the measuring device is shown in Figure 4.4. This device has been used by previous authors [4, 14, 15] to measure the density of nanofluids. The apparatus can operate and maintain temperatures ranging from 0 ^{0}C to 90 ^{0}C. The apparatus has internal cooling and heating capability to maintain the sample at any temperature within 0 ^{0}C to 90 ^{0}C range.

4.12.1 Principle of measurement

The nanofluid sample is introduced into the u-shaped glass tube shown in Figure 4.4 by a 2ml syringe through the inlet port on the right hand side of the apparatus. The temperature is set to desired value between 0^{0}C and 90 ^{0}C and offer the temperature stabilizes to the set value, the U-tube is excited to vibrate at its characteristic frequency. The characteristic frequency is proportional to the density of the sample. The density of the nanofluid sample is internally calculated within the apparatus by the following equation and displayed on the screen in g/cc.

$$\rho = KA \, X \, Q^2 \, X \, f_1 - KB \, X \, f_2 \qquad (4.11)$$

where *KA* and *KB* are the apparatus constants, *Q* is the quotient of the period of oscillation of the U-tube divided by the period of oscillation of the reference oscillation and f_1 and f_2 are correction terms for temperature, viscosity and nonlinearity. The period of oscillation of the U-tube is measured by optical signals and the precise thermostatic setting of the sample temperature is achieved by platinum thermometer together with peltier elements. Because of these qualities of the apparatus, Anton Paar specified the accuracy of measurements as ± 0.00005 g/cm^3 for the density and ± 0.03 ^{0}C for temperature. A major source of error is the presence of gas bubbles in the sample within the measuring U-tube. The experimenter can set the instrument to "Filling check" mode, which automatically detects inhomogeneity and gas bubbles in the entire measuring cell and generates a warning message to eliminate faulty measurements.

4.13 Results and discussions

4.13.1 Base fluid density equation

Curve fit equations were developed for glycol base fluids using Rackett type equation using the density versus temperature data of 60:40 PG/W and 60:40 PG/W from ASHRAE The correlation for calculating the density of different fluids has been provided by Rackett [28–31]. The basic Rackett equation is shown in Eq. (4.12a).

$$\rho = A\,X\,B^{-(1-\frac{T}{T_c})^{\frac{2}{7}}} \tag{4.12}$$

where ρ is density of fluid, T_c is critical temperature of fluid, and A and B are curvefit constants.

We modified the Rackett equation for a glycol based fluid to a nondimensional form so that A and B become pure constants, presented as Eq. (4.13)

$$\frac{\rho}{\rho_0} = A\,X\,B^{-(1-\frac{T}{T_c})^{\frac{2}{7}}} \tag{4.13}$$

where ρ_0 is the density of fluid at the reference temperature $T_0 = 273$ K. The critical temperature for glycol-water mixtures was calculated using Kay's rule [32]. Another polynomial form of curve-fit equation proposed by Yaws [28] is given as Eq. (4.13). The curve-fit values for modified Rackett equation and Yaws equation for glycol base fluids are presented in Table 4.3. Equation (4.12b or 4.13) is used for calculating the density of base fluid in Pak and Cho Eq. (4.10). The

figure 4.5a compares the curve-fit equations for both fluids with ASHRAE [5] density data. A maximum deviation of 0.6% and 0.01% was observed from ASHRAE data by using Eqs. (4.12b) and (4.13), respectively for both PG/W and EG/W.

4.13.2 Benchmark testcase

A benchmark test was performed with the 60:40 PG/W base fluid using the Anton Paar density meter to verify the accuracy of the measuring instrument and the measurement procedure. The result of the experiment is provided in the graph shown in Figure. 4.5b. The experiments were carried out within a temperature range of 0 ^{0}C to 90 ^{0}C. The theoretical values for 60:40 PG/W were taken from ASHRAE [5]. The results of measurements from the density apparatus matched well with the ASHRAE values. A maximum deviation of 1.6% at 90 ^{0}C was observed between experimental and the ASHRAE values.

4.14 Density of nanofluids

The results in the following sections show the effect of the temperature on density of the propylene glycol nanofluids. The experimental results are shown for varying temperatures from 0 ^{0}C to 90 ^{0}C in 5 ^{0}C increments, for different volumetric concentration of nanofluids. All density measurements of nanofluids were conducted under atmospheric pressure. The nanoparticle density $\rho_{np}$was assumed constant in our calculations and were taken from Table 4.2, provided by the vendor, as they don't change appreciably between the range of our measurements of 0 ^{0}C to 90 ^{0}C. However, if nanofluid density was needed over a high temperature range, then nanoparticle density ρ_{np} in Eq. (4.10) must be derived from an equation as function of temperature, similar to Eqs. (4.12b, 4.13) used for base fluid.

4.14.1 Al_2O_3 nanofluid

Figure 4.6a shows experimental values of density of Al_2O_3 nanofluid with average nanoparticle size of 45nm in a temperature range 273 K to 363 K with volumetric concentrations of 1%, 2%, 3%, 4%, 5%, and 6%. The experimental density values of Al_2O_3 nanofluid agreed with the theoretical equation presented by Pak and Cho [8] Eq. (4.10). A maximum deviation of 1.19% was observed at 363 K and 3% volume concentration when compared experimental values were

compared with Eq. (4.10). As expected, the densities of nanofluids decreased with an increase in temperature and increased with an increase in nanoparticle volumetric concentration.

Figure 4.6b shows the density of Al_2O_3 nanofluid with average nanoparticle size of 20 nm and volumetric concentrations ranging from 1 to 4%. Comparing the measured density values to the Pak and Cho equation [8] Eq. (4.10), a maximum deviation of 1% was observed for the 4% volume concentration at 273K

Figure 4.6c shows the density of Al_2O_3 nanofluid with average nanoparticle size 10 nm. Different volume concentrations measured were 1%, 2% and 2.7%. The measured densities of nanofluids were compared with the theoretical equation of Pak and Cho [8]. A maximum deviation of 0.9% was observed when experimental values were compared with the theory.

4.14.2 ZnO nanofluid

Figure 4.7a shows the density measurements for ZnO with nanoparticle size of 76 nm. The ZnO nanofluid was prepared and measured with six different volumetric concentrations (1%, 2%, 3%, 4%, 5%, and 6%). The lower volumetric concentration (1%) agreed with the Pak and Cho [8] Eq. (4.10) better than the 6% concentration. The results show that as the volumetric concentration increases the experimental results show increasing deviation from theoretical values. The maximum deviation from theory was found to be 3.6% at 363K for 6% concentration, which is still reasonable. The increasing deviation may be due to a slight error in the density of nanoparticle, taken as 5600 kg/m^3 from Table 4.2 as provided by the vendor. This error will be magnified as nanoparticle concentration increases. As observed from Figure 4.7a, the Pak and Cho equation consistently over predicts the measured data. Therefore, it can be surmised that we are using a slightly higher value of the nanoparticle density ρ_{np} in Eq. (4.10).

Figure 4.7b shows the experimental density values of ZnO nanofluid with average nanoparticle size of 50 nm. The different volumetric concentrations measured were from 1 to 6%. For lower concentrations 1% and 2% the experimental values are very close to theoretical values predicted by the Pak and Cho equation. For the 6% volumetric concentration a maximum deviation of 3.6% with Eq. (4.10) was observed at 273K.

Figure 4.7c shows the experimental results of density of ZnO nanofluid with average nanoparticle size of 36 nm. Different volumetric concentrations measured were 1%, 2%, 3% and 4%. The results were compared with Eq. (4.10). There is good agreement between the experimental values and the theoretical values. A maximum deviation of 0.9% with theoretical values is observed for 4% concentration at 363 K.

4.14.3 CuO nanofluid

The density of a CuO nanofluid was measured for an average particle size of 30 nm. The density of the CuO nanoparticle is 6310 kg/m^3. The maximum concentration of the nanofluid is 5.75%.

Figure 4.13 shows the density of the CuO nanofluid measured in a temperature range of 273 K to 363 K. The particle volume concentrations measured were 1%, 2%, 3%, 4%, 5%, and 5.75%. The measured data were compared with Pak and Cho's [8] equation (4.10). A maximum error of 3.8% was found at 273 K for a 6% particle volume concentration. For lower particle concentrations, the results agree well with those of Pak and Cho's equation. It was found that as the particle volume concentration increased, the deviation also increased. Since Pak and Cho's [8] prediction falls below the measured value, it is possible that the particle density might be slightly lower than 6310 kg/m^3, the value used in our calculation.

4.14.4 TiO_2 nanofluid

The density of a TiO_2 nanofluid was measured for an average particle size of 15 nm. The density of the TiO_2 particles is 4200 kg/m^3. The maximum concentration of this nanofluid is 1.6%.

Figure 4.14 shows the density of the TiO2 nanofluid as measured in a temperature range of 273 K to 363 K. Particle volume concentrations of 0.5%, 1%, and 1.6% were measured. The results are compared with Pak and Cho's [8] equation (4.10) in Figure 4.14. The results agree with Pak and Cho's equation. A maximum error of 1.8% was found at 320 K for a particle volume concentration of 1.6%. It was found that as the particle volume concentration increased, the error also increased. We notice a consistent over prediction by Pak and Cho's equation for this nanofluid. Therefore, the true density of the nanoparticles may be slightly lower than 4200 kg/m^3.

4.14.5 SiO_2 Nanofluid

The density of a SiO_2 nanofluid was measured having an average particle size of 30 nm. The density of SiO_2 particles is 2220 kg/m^3. The maximum concentration of nanofluid prepared was 6%. Figure 4.15 shows measured densities data of the SiO_2 nanofluid with different particle volumetric concentrations of 1, 2, 3, 4, 5 and 6%. The measurements were carried out in a temperature range of 273 K to 363 K with a 5 K interval. The measured density values matched those of Pak and Cho's [8] theoretical equation. The maximum deviation between experimental data and those of the theoretical equation is 0.8% for the 3% concentration.

4.14.6 CNT nanofluids

Figure 4.11 shows the density measurements on three types of carbon nanotubes (CNT). The three different carbon nanotubes tested in our experiments were single-walled carbon nanotube (SWCNT), multi-walled carbon nanotube (MWCNT), and bamboo-walled carbon nanotube (BWCNT). The concentration of CNTs suspension was 0.3% by weight dispersed in 60:40 PG/W. The density measurements were carried out over a temperature range 273 to 363K. The density of carbon nanotube is 1300 kg/m^3 as specified by manufacturer. The densities of all three CNT suspensions were fairly close to each other as function of temperature. A maximum deviation of 2.9% was found from the Pak and Cho equation at 273K.

4.15 Effect of particle size

The effect of nanoparticle size on the density of nanofluids was studied for Al_2O_3 and ZnO nanofluids as shown in Figure 4.12. Three different nanoparticle sizes have been studied for both nanofluids. Figure 4.12a shows the variation of density of Al_2O_3 nanofluids with different nanoparticle sizes 45, 20 and 10nm for two different volume concentrations and varying temperatures. The results show that Al_2O_3 nanofluids densities are essentially same at 1 and 4% equal temperature and concentration. So the density is independent of the nanoparticle size.

Figure 4.12b shows the density data of ZnO nanofluids of three different nanoparticle sizes 76, 50 and 36 nm with varying temperatures at two volumetric concentrations of 1 and 4%. For the 1% concentration all three nanoparticle sizes yield nearly the same density values. For the 4%

volume concentration a difference of 3.6% higher value for the density of 36 nm over 76 nm was observed. This difference is similar in magnitude to the derivations we have observed for ZnO nanofluids from the theoretical equation. The three nanoparticles sizes show a consistent ($\rho_{35nm} > \rho_{50nm} > \rho_{76nm}$) trend. The 36 nm nanofluid has more nanoparticles per unit volume for the same concentration. Furthermore ZnO nanoparticles are cylindrical rod shaped, whereas Al_2O_3 particles are spherical. So the vibration of these ZnO particles in the U tube with viscous damping may be introducing non-spherical shape errors in measurements, showing difference in density, although the theoretical derivation of nanofluid density Eq. (4.10), does not show any dependence on the nanoparticle size d_{np}.

4.16 Comparison of experiments with theory

Comparisons of the density values predicted by the theoretical equation of Pak and Cho Eq. (4.10) and the experimental values for all the nanofluids tested are presented in Figure 4.13. The diagonal line in the middle of the figure represents a perfect match between the experimental and theoretical values. There are 874 data points for the density values. In Figure 4.13, all data fall within a deviation band of ± 4%.From figures 4.7 through 4.19, we have assembled the deviations of density values among our experiments and Pak and Cho's [8] equation; these results are summarized in Table 4.4.

From Figure 4.6 through 4.12, we have assembled the deviations of density values between our experiments and the Pak and Cho equation and those results are summarized in Table 4.4.

From Table 4.4 and Figure 4.13, it was found that the maximum deviation between the Pak and Cho equation and all 874 data points is -3.8% for the CuO nanofluid. Considering all 874 data points, the average deviation between measurements and the Pak and Cho equation is -0.1%. Nanofluids, being a new class of heat transfer fluids, have been the focus of significant research involving measurements of thermophysical properties. Therefore, many publications [33-45] have appeared just in the past two years for verifying and improving older correlations and also developing new correlations. We believe that the present paper fulfills that goal for the density of nanofluids.

4.17 Conclusions

The experiments were conducted to study the variation of density of nanofluids with volume concentration, temperature, nanoparticle material and nanoparticle size. First a benchmark test was performed on 60:40 PG/W by mass mixture and the results showed good agreement with a very small deviation (1.6%) with reference values taken from ASHRAE. The density of different nanofluids measured were Al_2O_3, ZnO, TiO_2, SiO_2, CuO nanoparticles and carbon nanotubes nanoparticles dispersed in 60:40 PG/W. The experiments were conducted in a temperature range of 0 ^{0}C to 90 ^{0}C. The measured density values agreed well with the theoretical equation presented by Pak and Cho Eq. (4.10). From the results it was shown the densities of nanofluids are independent of the nanoparticle size. Nanofluid densities increased with an increase in nanoparticle volumetric concentration but decreased with an increase in temperature. Based upon 874 data points, it was found that the maximum deviation between measured values and those predicted by the equation of Pak and Cho was within $\pm$4%. This deviation may be attributed to the presence of surfactants or dispersants in the nanofluids and the uncertainty in the value of the nanoparticle densities provided by the nanofluids vendor. The margin of deviation is not high. Therefore, for practical engineering calculations, the Pak and Cho equation can be adopted as an accurate formula for calculating the densities of nanofluids.

4.18 Acknowledgements

Use of the Anton Paar density meter at the Petroleum Engineering Department of the University of Alaska Fairbanks is gratefully acknowledged.

4.19 Nomenclature

ρ	Density (kg m^{-3})
Re	Reynolds number
f	Friction factor
ΔP	Pressure loss (Pa)
V	Velocity (m s^{-1})
T	Temperature (K)

ϕ	Volumetric concentration (%)
PG	Propylene Glycol
W	Water
EG	Ethylene Glycol

Subscript

bf	Base fluid
nf	Nanofluid
np	Solid particle
c	Critical temperature (K)
ρ	Density (kg m^{-3})
Re	Reynolds number
f	Friction factor

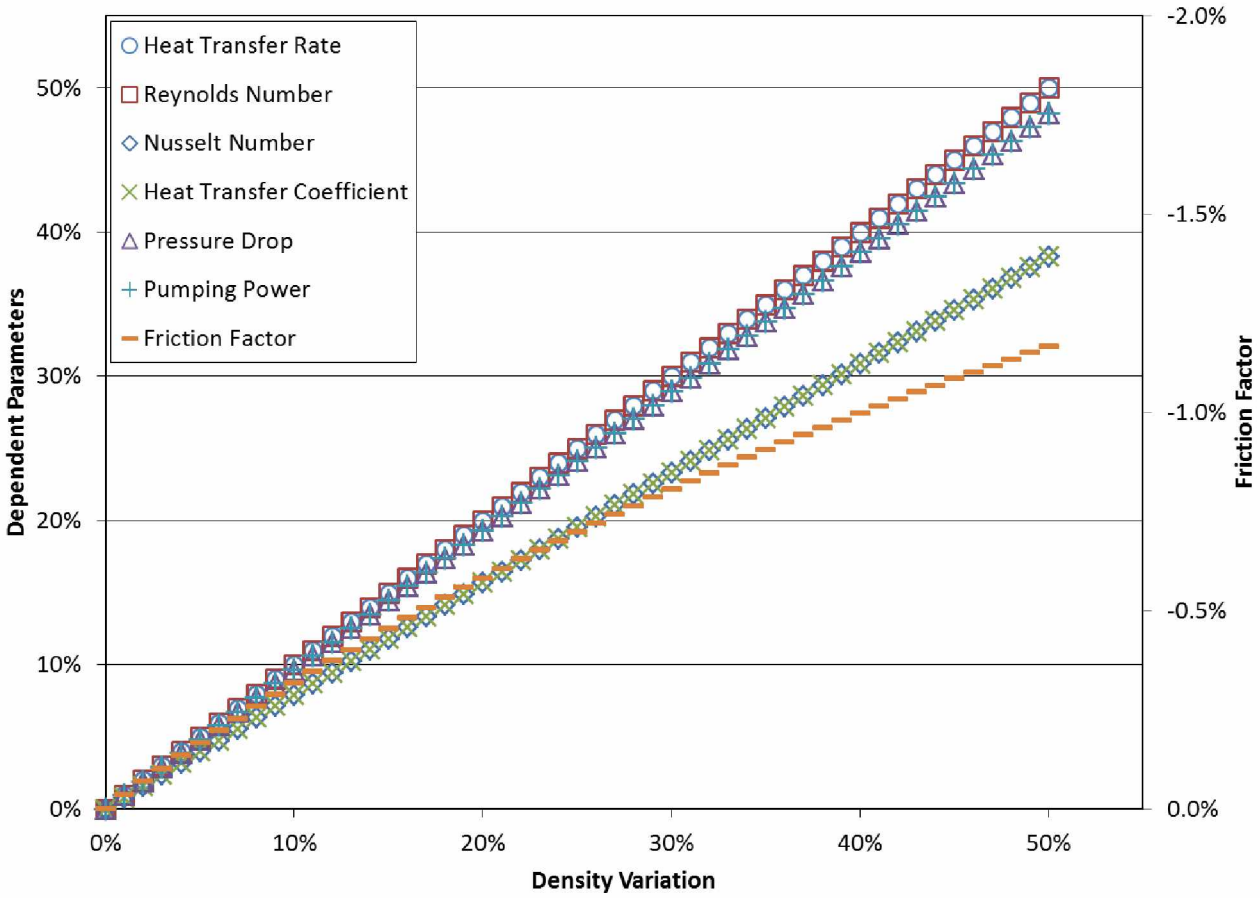

Figure 4.1. Effect of density on different parameters.

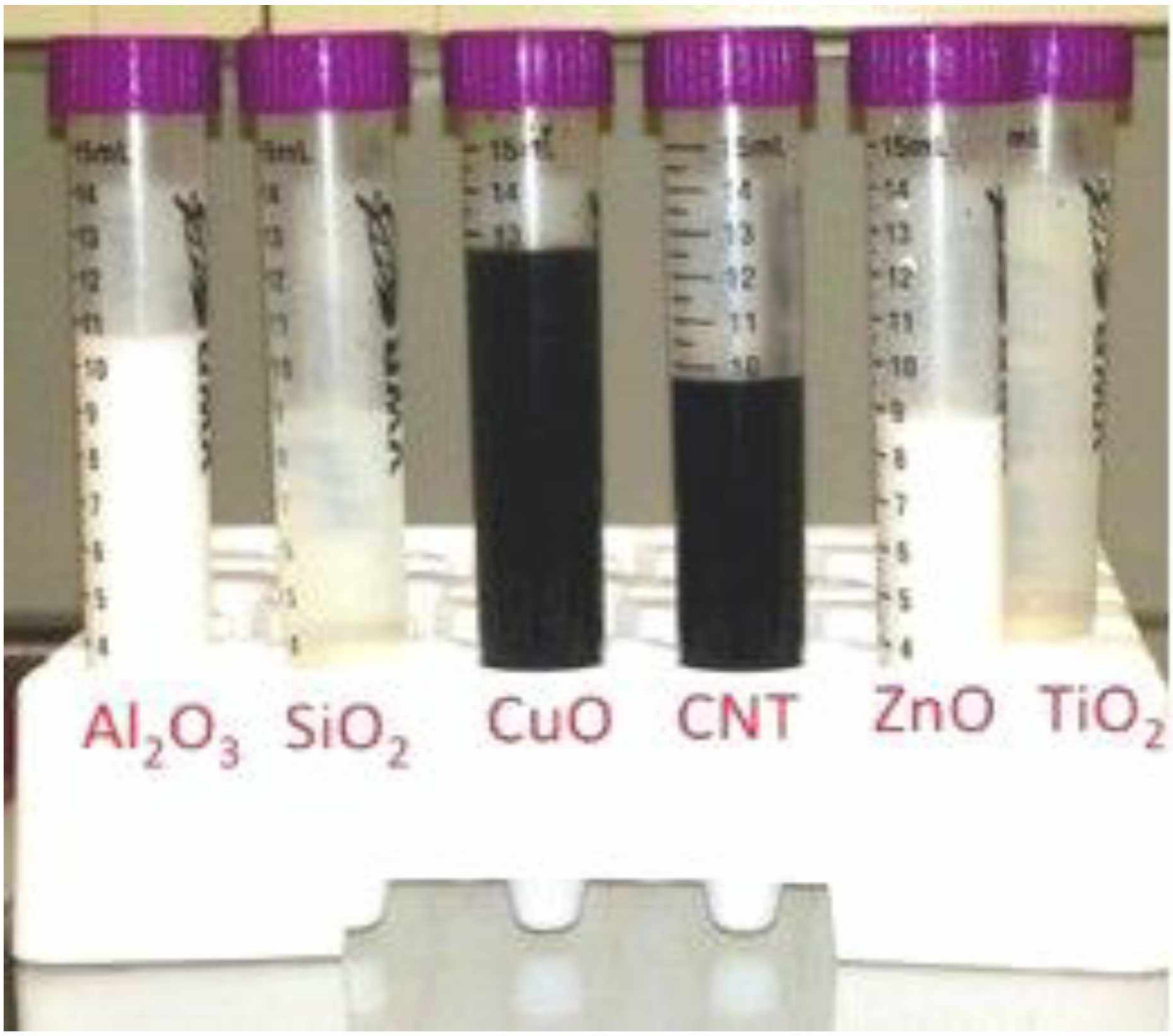

Figure 4.2. Nanofluids samples prepared for density measurements

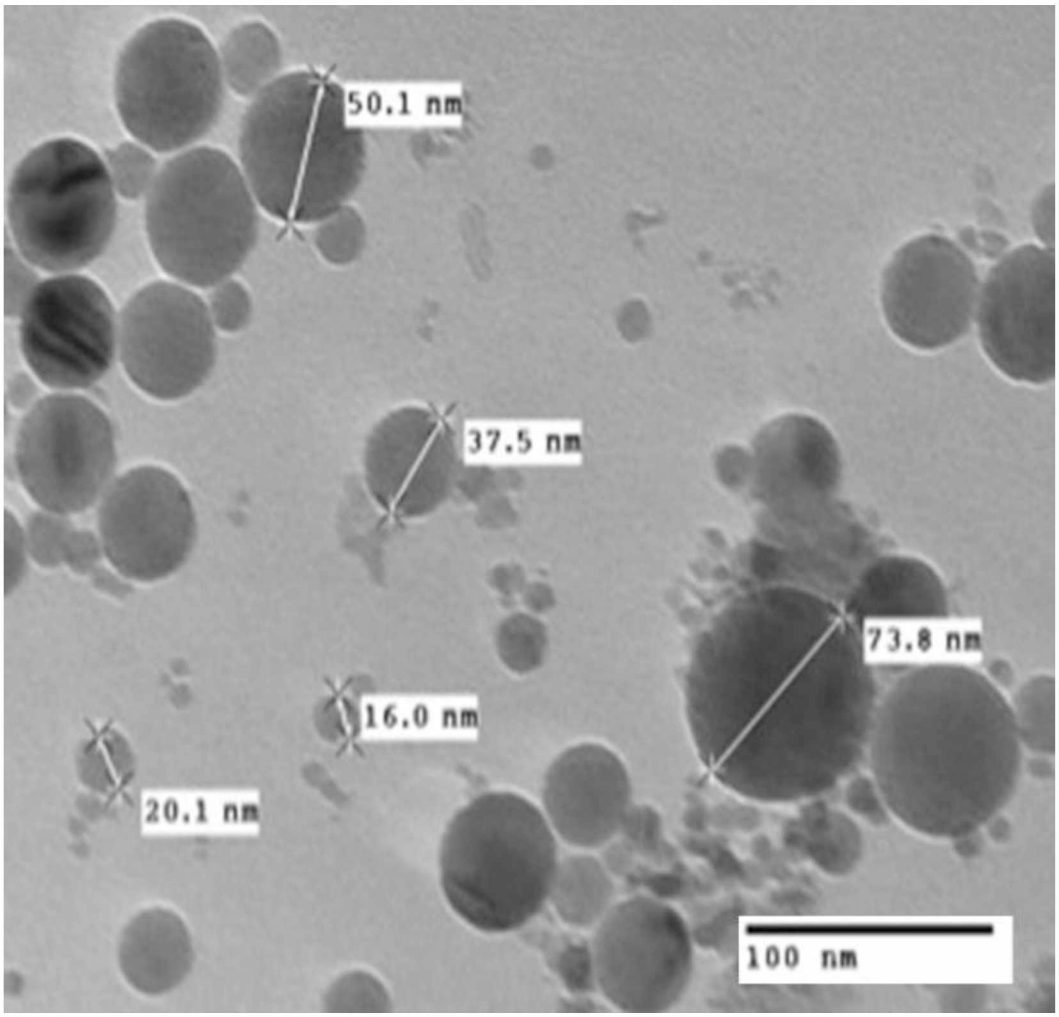

Figure 4.3. TEM images of Al_2O_3 nanoparticles with APS of 45nm.

Figure 4.4. Density measuring device Anton Paar DMA 4500

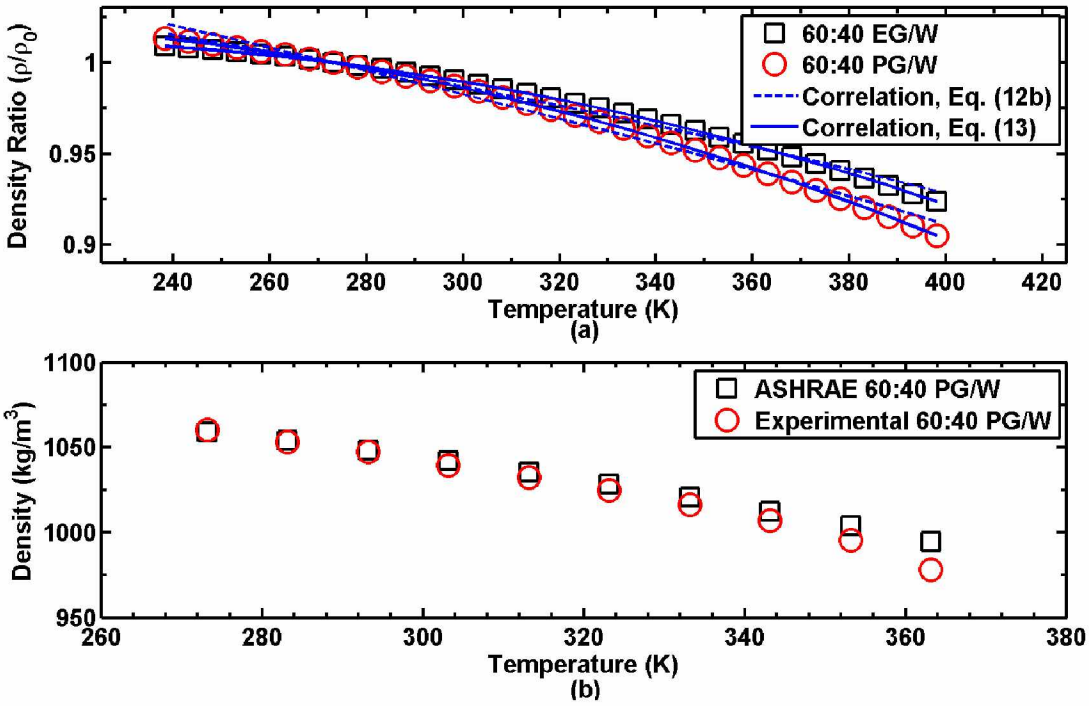

Figure 4.5. (a) Comparison of the modified Rackett and Yaws equations for PG/W and EG/W base fluids with ASHRAE data (b) Benchmark test case result for the 60:40 PG/W base fluid.

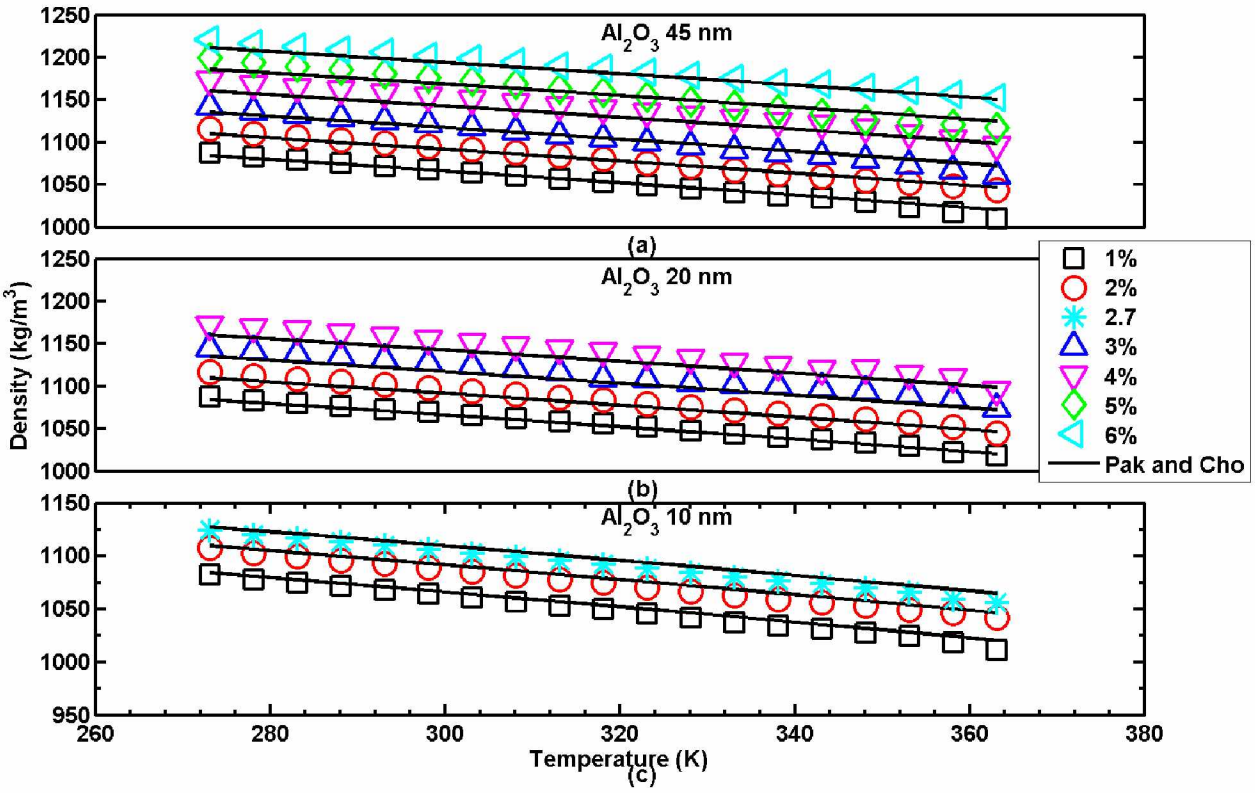

Figure 4.6. Density variation of Al_2O_3 nanofluid of APS (a) 45 nm, (b) 20 nm, (c) 10 nm with temperature and volumetric concentration.

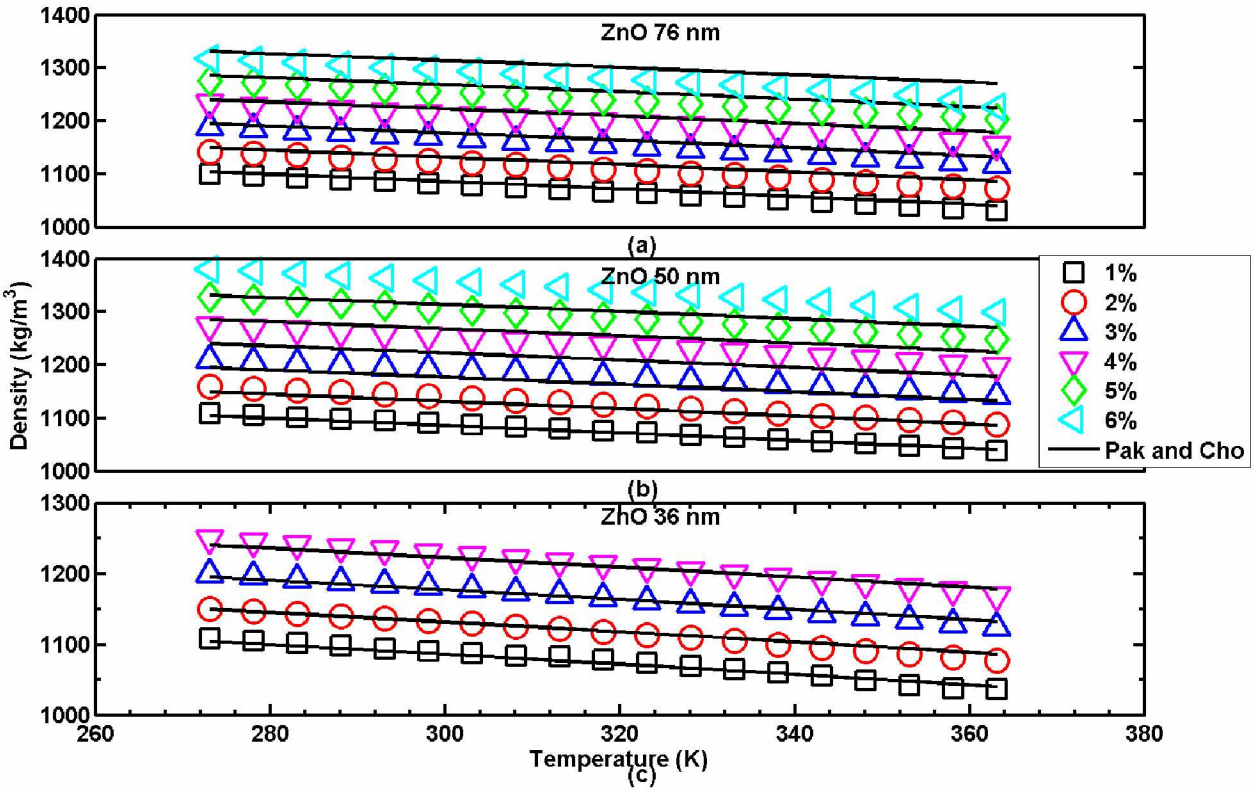

Figure 4.7. Density variation of ZnO nanofluid of APS (a) 76 nm, (b) 50 nm, (c) 36 nm with temperature and volumetric concentration.

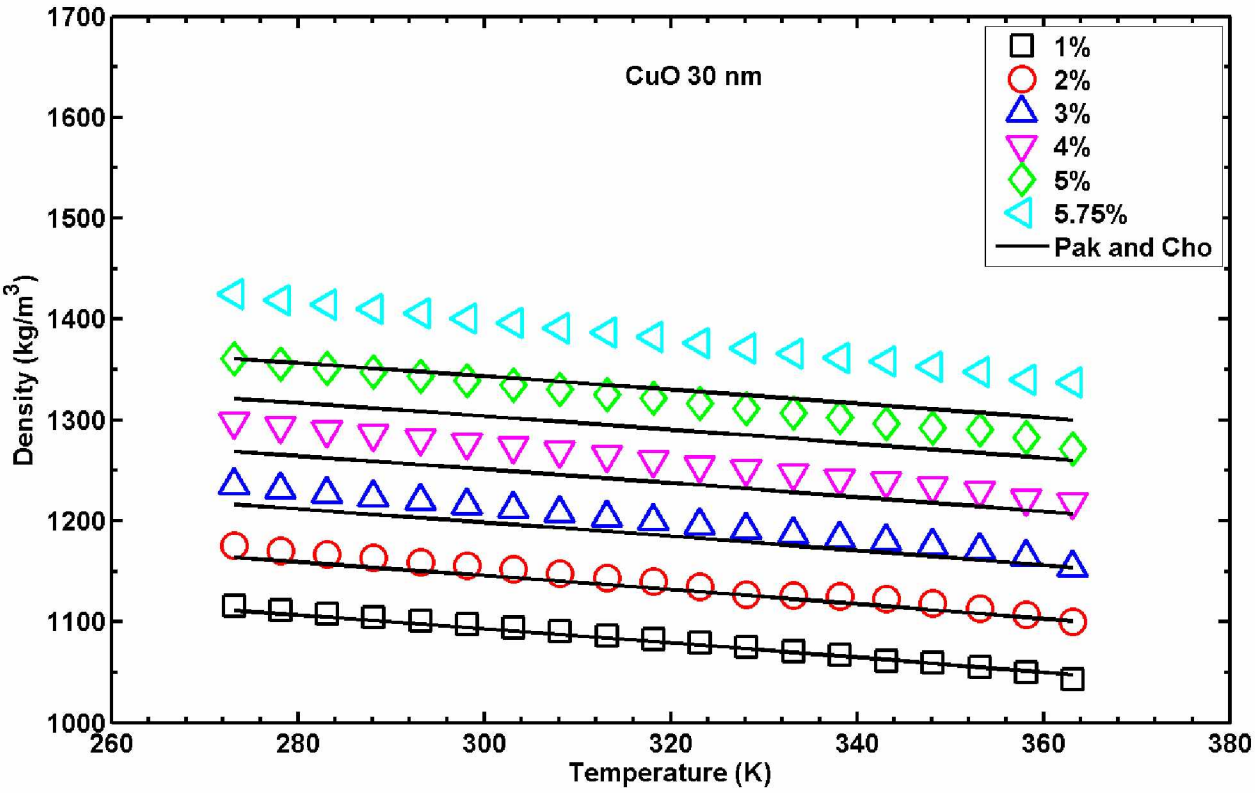

Figure 4.8. Density variation of CuO nanofluid of APS 30 nm with temperature and volumetric concentration.

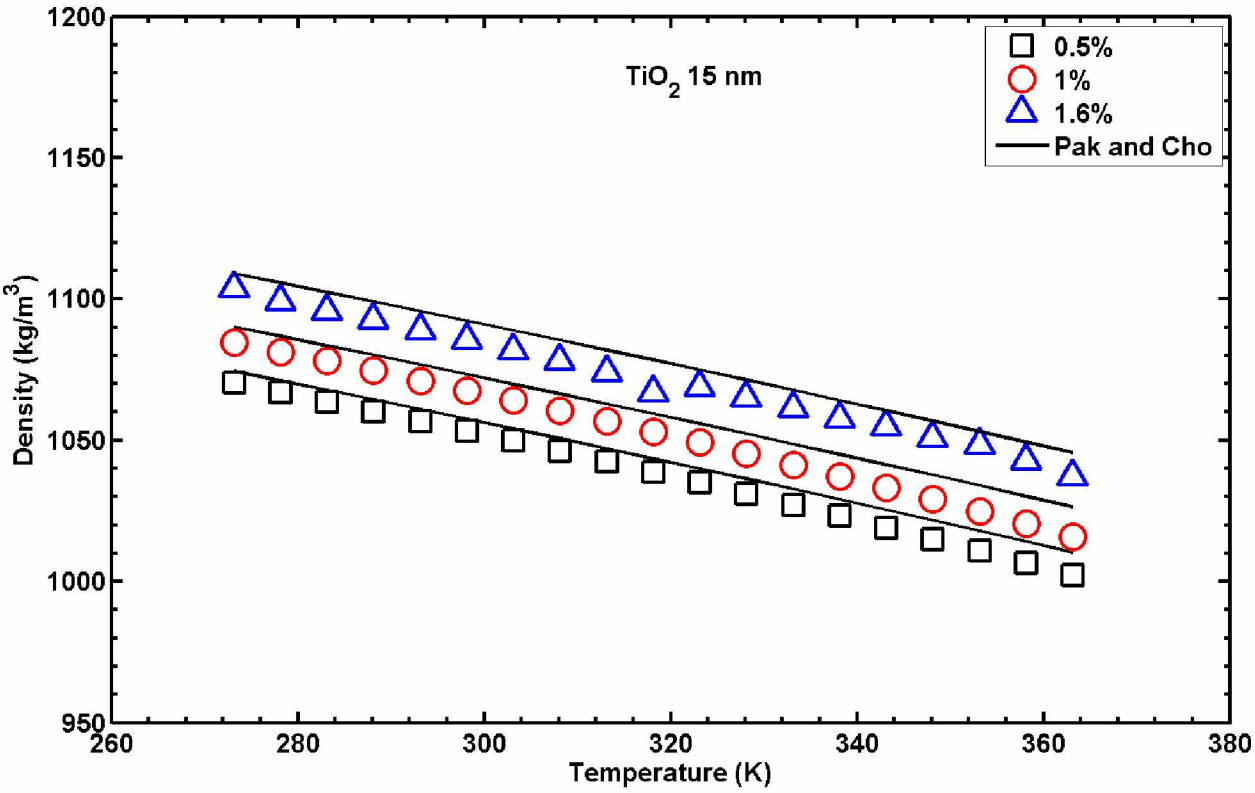

Figure 4.9. Density variation of TiO_2 nanofluid with APS 15 nm with temperature and volumetric concentration.

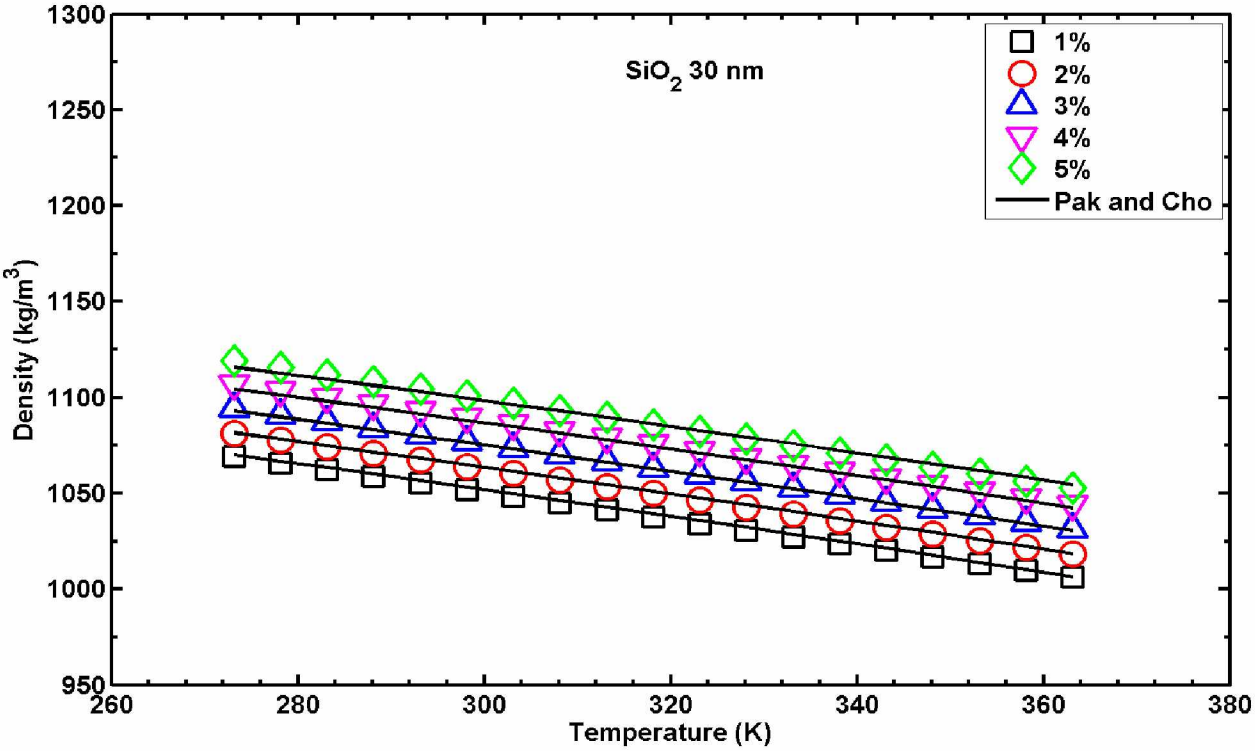

Figure 4.10. Density variation of SiO_2 nanofluids with APS 30 nm with temperature and volumetric concentration.

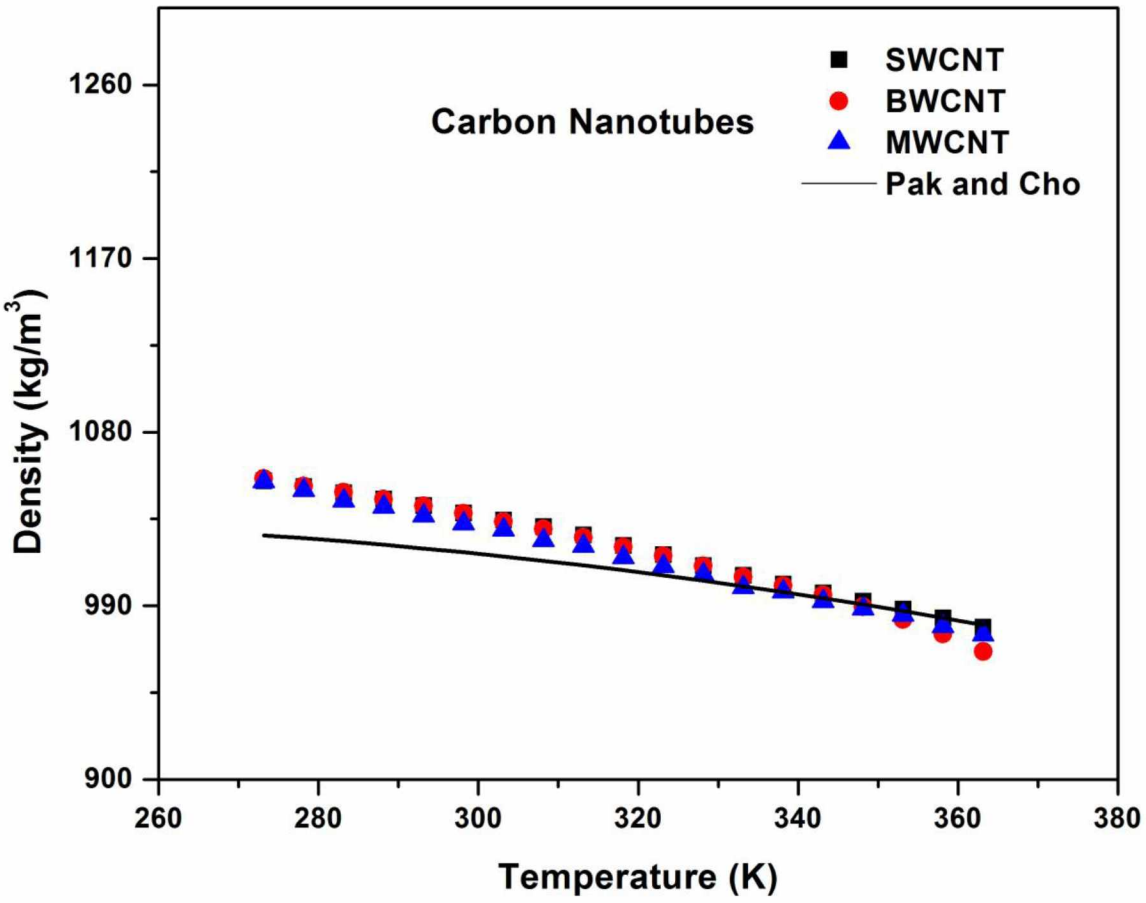

Figure 4.11. Density variation of different Carbon Nanotube nanofluids with temperature.

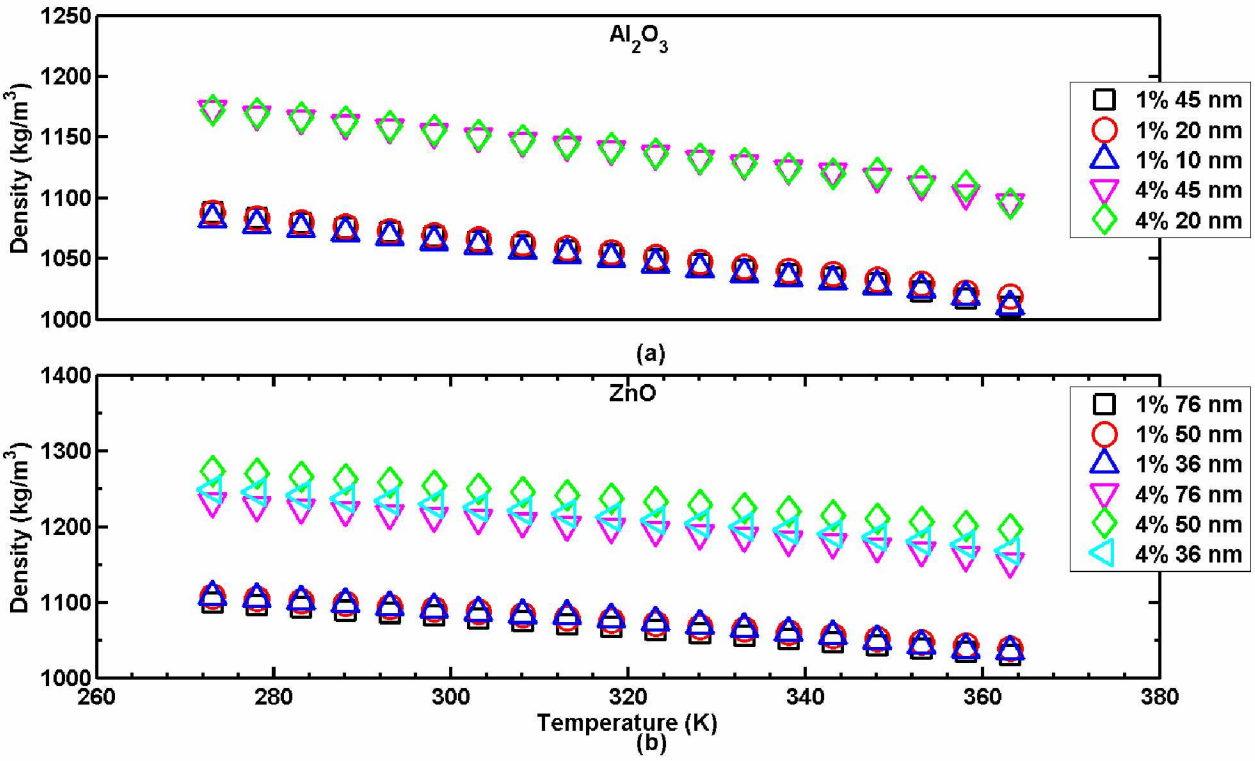

Figure 4.12 Nanoparticle size effect on density containing (a) Al_2O_3 (b) ZnO nanoparticles.

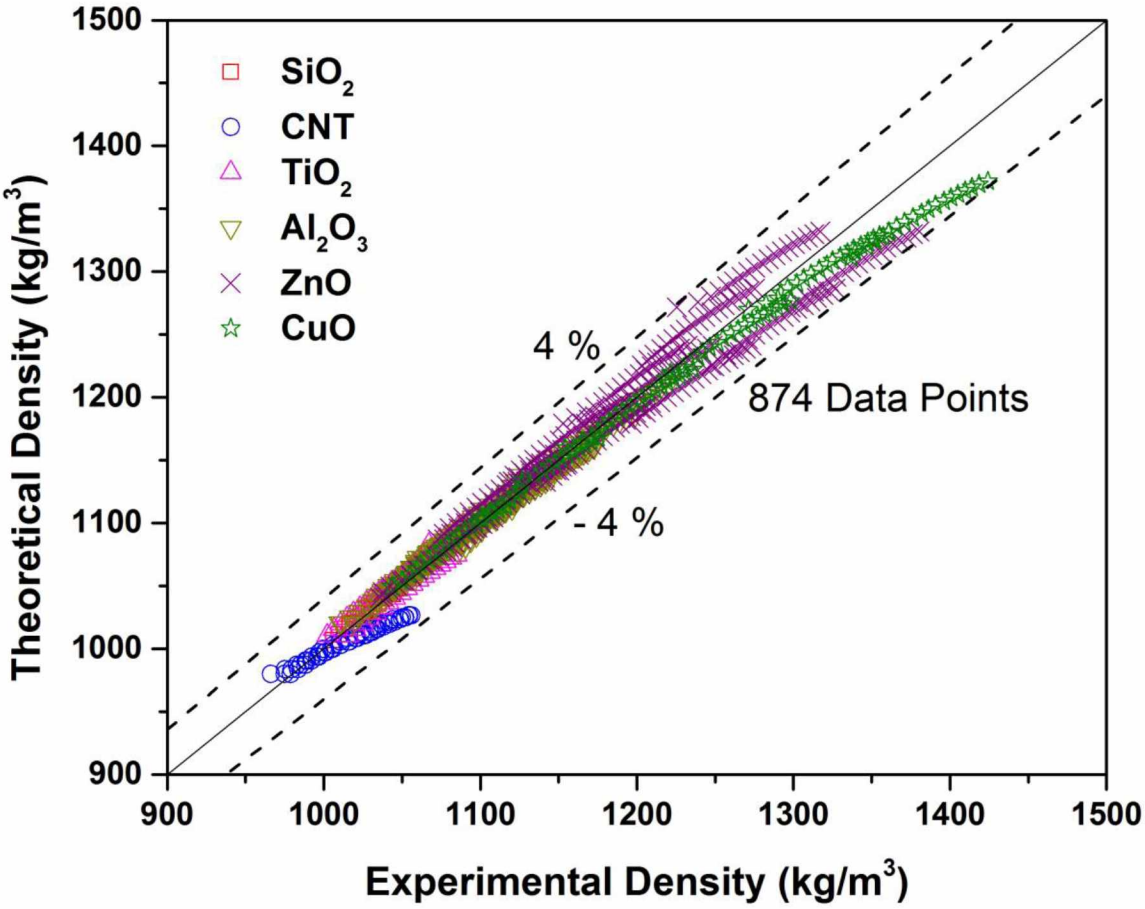

Figure 4.13 The agreement between the experimental and theoretical values of nanofluids densities within ±4%.

Table 4.1. Parameters for study of density effect on other parameters.

Parameter	Value
Average Fluid Temperature (K)	293
Fluid	Water
Density (kg/m^3)	997.92
Specific Heat (J/kg K)	4183
Viscosity (Pa s)	1.009×10^{-3}
Thermal Conductivity (W/m K)	0.598
Prandtl Number	7.056
Fluid Velocity (m/s)	0.25
Pipe Diameter (m)	0.0254
Temperature Difference (K)	10
Length of Pipe (m)	6
Pipe Roughness [62](mm)	2

Table 4.2. Material characteristics of nanofluids used in the present experiments.

Manufacturer	Material	Particle size (nm)	Particle Density (g/cc)	Mother nanofluid concentration wt % in H_2O
Alfa Aesar [23]	Al_2O_3	20	3.6	30
Alfa Aesar	Al_2O_3	45	3.6	50
Nanostructured and Amorphous Materials, Inc. [24]	Al_2O_3	10	3.6	15
Nanostructured and Amorphous Materials, Inc. [24]	SiO_2	30	2.41	25
Alfa Aesar	ZnO	76	5.6	50
Alfa Aesar	CuO	30	6.31	50
Nanostructured and Amorphous Materials Inc.	TiO_2	15	4.23	15
Nanolab Carbon nanotubes [25]	SWCNT	D 1-2nm, L 5-30 µm	1.3	3
Nanolab Carbon nanotubes	MWCNT	D 10-40nm, L 10 µm	1.3	3
Nanolab Carbon nanotubes	BWCNT	D 10-40nm, L 10 µm	1.3	3

Table 4.3. Curve fit values of modified Rackett equation for glycol base fluids.

Parameter	(60:40) EG/W	(60:40) PG/W
T_c	547.92 [K]	641.76 [K]
A	0.0453	0.17047
B	0.04174	0.15976
R^2	0.99014	0.98548

Table 4.4. Deviation in density values of different nanofluids.

Material	Particle Density (g/cc)	Particle size (nm)	Max Deviation
Al_2O_3	3.6	20	1%
		45	1.19%
		10	0.9%
SiO_2	2.41	30	0.8%
ZnO	5.6	36	0.9%
		50	3.6%
		76	3.6%
CuO	6.31	30	3.8%
TiO_2	4.23	15	1.8%
SWCNT	1.3	D 1-2nm, L 5-30 µm	2.9%
MWCNT		D 10-40nm, L 10 µm	
BWCNT		D 10-40nm, L 10 µm	

4.20 References

[1] Choi, S., and Eastman, J., 1995, "Enhancing thermal conductivity of fluids with nanoparticles," ASME Dev. Appl. Non-Newtonian Flows, **66**, pp. 99–105.

[2] Eastman, J. A., Choi, S. U. S., Li, S., Yu, W., and Thompson, L. J., 2001, "Anomalously increased effective thermal conductivities of ethylene glycol-based nanofluids containing copper nanoparticles," Appl. Phys. Lett., **78**(6), p. 718.

[3] Vajjha, R. S., and Das, D. K., 2009, "Experimental determination of thermal conductivity of three nanofluids and development of new correlations," Int. J. Heat Mass Transf., **52**(21-22), pp. 4675–4682.

[4] Vajjha, R. S., Das, D. K., and Mahagaonkar, B. M., 2009, "Density Measurement of Different Nanofluids and Their comparision With Theory," Pet. Sci. Technol., **27**, pp. 612–624.

[5] ASHRAE, 2009, "Physical Properties of Secondary Coolants (Brines)," ASHRAE Handbook, American society of Heating Refrigerator and Air Conditioning Engineers, Inc, Atlanta.

[6] White, F. M., 2006, "Viscous Fluid Flow," 3rd Edition, McGraw-Hill, New York.

[7] Cheremisinoff, N. P., 1986, Encyclopedia of Fluid Mechanics, Vol 5, Gulf Publishing, Houston, TX.

[8] Pak, B. C., and Cho, Y. I., 1998, "Hydrodynamic and heat transfer study of dispersed fluids with submicron metalic oxide particles.," Exp. Heat Transf., **11**, pp. 151–170.

[9] Bejan, A., 1993, Heat Transfer, John Wiley & Sons, Inc., New York.

[10] Huminic, G., and Huminic, A., 2012, "Application of nanofluids in heat exchangers: A review," Renew. Sustain. Energy Rev., **16**(8), pp. 5625–5638.

[11] Wang, X.-Q., and Mujumdar, A. S., 2007, "Heat transfer characteristics of nanofluids: a review," Int. J. Therm. Sci., **46**, pp. 1–19.

[12] Saidur, R., Leong, K. Y., and Mohammad, H. A., 2011, "A review on applications and challenges of nanofluids," Renew. Sustain. Energy Rev., **15**(3), pp. 1646–1668.

[13] Cabaleiro, D., Pastoriza-Gallego, M. J., Piñeiro, M. M., Legido, J. L., and Lugo, L., 2012, "Thermophysical properties of (diphenyl ether+biphenyl) mixtures for their use as heat transfer fluids," J. Chem. Thermodyn., **50**, pp. 80–88.

[14] Pastoriza-Gallego, M. J., Casanova, C., Legido, J. L., and Piñeiro, M. M., 2011, "CuO in water nanofluid: Influence of particle size and polydispersity on volumetric behaviour and viscosity," Fluid Phase Equilib., **300**(1-2), pp. 188–196.

[15] Pastoriza-Gallego, M. J., Casanova, C., Paramo, R., Barbes, B., Legido, J. L., and Pineiro, M. M., 2009, "A study on stability and thermophysical properties (density and viscosity) of Al(2)O(3) in water nanofluid," J. Appl. Phys., **106**(6).

[16] Martin, A., and Bou-Ali, M. M., 2011, "Determination of thermal diffusion coefficient of nanofluid: Fullerene–toluene," Comptes Rendus Mécanique, **339**(5), pp. 329–334.

[17] Kumaresan, V., and Velraj, R., 2012, "Experimental investigation of the thermo-physical properties of water–ethylene glycol mixture based CNT nanofluids," Thermochim. Acta, **545**, pp. 180–186.

[18] Vajjha, R. S., Das, D. K., and Kulkarni, D. P., 2010, "Development of new correlations for convective heat transfer and friction factor in turbulent regime for nanofluids," Int. J. Heat Mass Transf., **53**(21-22), pp. 4607–4618.

[19] Beck, M. P., Sun, T. F., and Teja, A. S., 2007, "The thermal conductivity of alumina nanoparticles dispersed in ethylene glycol," Fluid Phase Equilib., **260**(2), pp. 275–278.

[20] Beck, M. P., Yuan, Y. H., Warrier, P., and Teja, A. S., 2009, "The effect of particle size on the thermal conductivity of alumina nanofluids," J. Nanoparticle Res., **11**(5), pp. 1129–1136.

[21] Vajjha, R. S., and Das, D. K., 2012, "A review and analysis on influence of temperature and concentration of nanofluids on thermophysical properties, heat transfer and pumping power," Int. J. Heat Mass Transf., **55**(15-16), pp. 4063–4078.

[22] Hemalatha, J., Prabhakaran, T., and Nalini, R. P., 2011, "A comparative study on particle-fluid interactions in micro and nanofluids of aluminium oxide," Microfluid. Nanofluidics, **10**(2), pp. 263–270.

[23] Alfa Aesar (2014), www.alfaaesar.com.

[24] Nanostructured & Amorphous Materials (2014), http://www.nanoamor.com/home.

[25] Nanolab (2014). Need more

[26] Corporation, B. U., 2010, Bransonic Tabletop Ultrasonic Cleaners, Danbury, CT.

[27] Paar, A., Anton-Parr Digital Density Meter for Liquids and Gases DMA 4500, Graz, Austria.

[28] Yaws, C. L., 1999, Chemical Propeties Handbook, McGraw-Hill, New York.

[29] Hong-Yi, L., and Guojie, L., 1995, "A generalized equation of state for liquid density calculation," Fluid Phase Equilib., **108**, pp. 15–25.

[30] Valderrama, J. O., and Abu-sharkh, B. F., 1989, "Generalized Rackett-Type correlations to predict the density of saturated liquids and petroleum fractions," Fluid Phase Equilib., **51**, pp. 87–100.

[31] Vetere, A., 1992, "Again the Rackett equation," Chem. Eng. J., **49**, pp. 27–33.

[32] Moran, M., Shapiro, H., Boettner, D., and Bailey, M., 2010, Fundamentals of Engineering Thermodynamics, John Wiley & Sons, Inc., New York.

[33] Leena, M., Srinivasan, S., Prabhaharan, M., 2015, Evaluation of acoustical parameters and thermal conductivity of TiO2-ethylene glycol nanofluid using ultrasonic velocity measurements Nanotechnology Reviews, 4 (5), pp. 449-456.

[34] Hemmat Esfe, M., Karimipour, A., Yan, W.M., Akbari, M., Safaei, M.R., Dahari, M., 2015, Experimental study on thermal conductivity of ethylene glycol based nanofluids containing Al2O3 nanoparticles International Journal of Heat and Mass Transfer, 88, pp. 728-734.

[35] Xing, M., Yu, J., Wang, R., 2015, Experimental study on the thermal conductivity enhancement of water based nanofluids using different types of carbon nanotubes International Journal of Heat and Mass Transfer, 88, pp. 609-616.

[36] Buonomo, B., Manca, O., Marinelli, L., Nardini, S., 2015, Effect of temperature and sonication time on nanofluid thermal conductivity measurements by nano-flash method Applied Thermal Engineering, 91, pp.181-190.

[37] Hemmat Esfe, M., Saedodin, S., Biglari, M., Rostamian, H., 2015, Experimental investigation of thermal conductivity of CNTs-Al2O3/water: A statistical approach International Communications in Heat and Mass Transfer, 69, pp. 29-33.

[38] Hemmat Esfe, M., Rostamian, H., Afrand, M., Karimipour, A., Hassani, M., 2015, Modeling and estimation of thermal conductivity of MgO-water/EG (60:40) by artificial neural network and correlation International Communications in Heat and Mass Transfer, 68, art. no. 3249, pp. 98-103.

[39] Haghighi, E.B., Utomo, A.T., Ghanbarpour, M., Zavareh, A.I.T., Nowak, E., Khodabandeh, R., Pacek, A.W., Palm, B., 2015, Combined effect of physical properties and convective

heat transfer coefficient of nanofluids on their cooling efficiency, International Communications in Heat and Mass Transfer, 68, art. no. 3245, pp. 32-42.

[40] Bianco V., Manca O., Nardini S., Vafai K., Eds, 2015, Heat Transfer Enhancement with Nanofluids, Publisher CRC, Taylor and Francis Group.

[41] Mariano, A., Pastoriza-Gallego, M.J., Lugo, L., Mussari, L., Piñeiro, M.M., 2015, Co3O4 ethylene glycol-based nanofluids: Thermal conductivity, viscosity and high pressure density, International Journal of Heat and Mass Transfer, 85, pp. 54-60.

[42] Cabaleiro, D., Nimo, J., Pastoriza-Gallego, M.J., Piñeiro, M.M., Legido, J.L., Lugo, L., 2015, Thermal conductivity of dry anatase and rutile nano-powders and ethylene and propylene glycol-based TiO2 nanofluids, Journal of Chemical Thermodynamics, 83, pp. 67-76.

[43] Nandhakumar, R., Senthilkumar, D., 2015, Preparation and thermophysical property evaluation of al2o3-ethylene glycol and tio2-ethylene glycol nanofluids for heat transfer applications, International Journal of Applied Engineering Research, 10 (13), pp. 33226-33229.

[44] Said, Z., Saidur, R., Hepbasli, A., Rahim, N.A., 2014, New thermophysical properties of water based TiO2 nanofluid-The hysteresis phenomenon revisited, International Communications in Heat and Mass Transfer, 58, pp. 85-95.

[45] Lee, J., Han, K., Koo, J., 2014, A novel method to evaluate dispersion stability of nanofluids, International Journal of Heat and Mass Transfer, 70, pp. 421-429.

Chapter 5 Evaluation of Nanofluids in Ground Source Heat Pumps operating in Cold Climate[1]

5.1 Abstract

The coefficient of performance (COP) of cold climate ground source heat pumps (GSHP) is lower, around 2.0, compared to that of tropical climate GSHP, about 4.0. The COP of a GSHP in cold climates is limited by the circulation of heat transfer fluid in a ground heat exchanger loop at very low temperatures. This requires a greater tube length in the ground heat exchanger to absorb an adequate amount of heat. One way to increase the COP of a GSHP is by replacing the heat transfer fluid with more efficient fluid, such as a nanofluid. In this paper, a GSHP operating in central Alaska is analyzed. Analytical and numerical studies were performed on the ground heat exchanger of the GSHP. Results calculated from modeling showed good agreement with experimental data for a conventional heat transfer fluid, a methanol and water mixture, validating the models. Next, the analysis were performed using Al_2O_3 and CuO nanofluids with three different particle volumetric concentrations, 0.5, 1, and 2%. The results showed nanofluids absorbed more heat than the basefluid. The ground temperature was varied from 273 to 288K and the fluid velocity from 1 m/s to 5 m/s. The best heat absorption rate of 12% over the basefluid was observed for an Al_2O_3 nanofluid of 2% concentration at a ground temperature of 273K.

5.2 Introduction

In cold regions like Alaska, a large amount of energy is used for heating buildings. The efficiency of building heating systems can be evaluated by the coefficient of performance (COP). For example, electrical heating has a COP of 1, oil heating has a COP of 0.7, and natural gas heating has a COP of 0.85 [1]. A ground source heat pump (GSHP) has a COP of nearly 3.2 for cold temperatures [1]. The higher COP value of GSHP makes them the right choice for highly efficient

---

[1] Satti, J. R, Das, D. K., Ray, D and Lin, C., 2015, "Evaluation of nanofluids in ground source heat pumps operating in cold climates," under review by Journal of International Communications in Heat and Mass Transfer.

building heating systems for cold climates. A typical GSHP consists of the following components: pump, ground heat exchanger, condenser, and expander. A heat transfer fluid is circulated through the system to absorb heat from the ground. The heat transfer between the ground and the heat transfer fluid occurs in the ground heat exchanger (GHE) system. Presently the applications of GSHP are limited in cold climates like Alaska for the following reasons. The air temperatures in Alaska reach below 233K in winters, the ground temperatures as low as 273K [2]. The heat transfer fluid running through the system should be maintained at uniform temperatures at all times to prevent freezing. In order to improve the COP of GSHP with low freezing point fluids, a thorough analysis needed to be done on ground heat exchangers (GHEs) with different heat transfer fluids.

Recently novel heat transfer fluids have been developed, called nanofluids. Nanofluids are dispersions of nano-sized particles in a fluid [3]. Nanofluids are a new type of heat transfer fluid in which solid metallic nanoparticles (<100 nm) of very high thermal conductivity are dispersed in a fluid, which usually possesses relatively low thermal conductivity. By adding these nanoparticles, the thermal conductivity of nanofluids can be increased by nearly 10% [4]. The increase in thermal conductivity depends on the type of nanoparticle and particle concentration present in the nanofluid. Due to their high thermal conductivity, nanofluids can extract more heat from ground in shorter tube lengths. Pumping power can be decreased if a decrease in tube length is achieved. These nanofluids are the right choice as heat transfer fluids for ground source heat pumps.

In the present research project, our objective is to develop analytical and numerical models for a GHE. These models are validated by comparing the predictions with actual experimental data collected from a GSHP operating in Fairbanks, Alaska by Cold Climate Housing Research Center [1]. After validation, the model analyzes different nanofluids of varying particle volumetric concentration in ground heat exchanger systems of GSHP. We compared the results of this analysis to find the right nanofluid to improve the COP of the GSHP.

5.3 Ground source heat pumps

GSHP are an attractive alternative to conventional heating and cooling systems due to their higher efficiency. A GSHP is a type of heat pump that uses heat from the ground to heat the air inside the

building. A GSHP consists of the following components: compressor, ground heat exchanger (GHE), fluid heat exchanger, expansion valve, and air heat exchanger [5]. The components are depicted in Figure 5.1. The following parameters play a vital role in the performance of a GSHP: GHE size, depth of GHE below the surface (ground temperature), heat transfer fluid, fluid flow rate, GHE pipe size, soil type, and others [6]. In the present analysis, the performance of a GSHP is studied by replacing the traditional heat transfer fluid used at the CCHRC, methanol-water mixture, [7] with nanofluids. Thorough reviews of the different ground source heat pumps are provided by Sarbu and Sebarchievivi [8] and Omer [9].

5.4 GSHPs in arctic and subarctic regions

Ground source heat pumps are found in large numbers these days. Nearly 30% of all houses in Sweden have GSHP [8]. The number is increasing in the lower 48 states of the U.S.A. due to their higher COP. In Alaska, the use of GSHP has started recently. There are nearly 49 residential and 6 commercial units in Alaska [1]. The Cold Climate Housing Research Center (CCHRC) is performing a long-term study on GSHP in their test sites. The average COP reported for GSHP in Alaska is between 2.0 and 3.5 [1]. If we can increase the COP of the GSHP, then we can decrease the usage of energy for heating, which in turn decreases the operating costs of GSHP. Figure 5.2 compares the economic benefits of GSHP to those of electric and oil heating for five locations in Alaska. For most locations, the GSHP is shown to be economically superior.

From Figure 5.2 we can observe that GSHPs provide good economic benefits compared to electrical heating. If we can make the heat pumps run at higher efficiencies by increasing their COP, we can reduce their operating costs. If the COP of the GSHPs in Alaska exceeded or equaled that of GSHPs operated in the lower 48 states, the installation of GSHP units in Alaska would increase, which would result in economic benefits for cold climate regions such as the circumpolar nations. One way to increase the COP of GSHPs is using better heat transfer fluids. Nanofluids are new heat transfer fluids that have better heat transfer characteristics than do regular heat transfer fluids. In the present research we performed analytical and numerical studies on cold climate GSHPs with different nanofluids in ground heat exchangers (GHEs). These studies will provide guidelines and direction to perform experimental studies on GSHPs using different nanofluids to find the best performance.

The Cold Climate Housing Research Center (CCHRC) has done research on ground source heat pumps' application in Alaska. In their recent report [1], they found COP of GSHPs between 2 and 3.5 depending upon location. They showed that GSHPs are good energy savers. However, poor design of a GSHP could cause the following problems: (i) an undersized ground loop decreases the COP; (ii) smaller ground loops require higher flow rates, and thus higher pumping power to maintain the flow rates.

There have been few studies conducted on the role of heat transfer fluid in ground heat exchangers of GSHPs. In this paper we present analytical and numerical analysis using 20:80 by mass methanol and water (M/W) nanofluids on ground heat exchangers of GSHPs. The goal of this study was to evaluate the benefits of using nanofluids in comparison to the basefluid in a ground heat exchanger.

5.5 Ground heat exchanger design

The ground heat exchanger design is dependent upon many parameters, such as geological formations and material properties of pipe, liquid, and soil. A basic analytical design process is explained by Incropera and Dewitt [10]. Using the Eq's (5.1-5.7) listed below, we can calculate the GHSP pipe length required for a given amount of heat to be absorbed. The coefficient of performance of a heat exchanger can be found using Eq. (5.1):

$$COP = \frac{Q_L}{Q_H - Q_L} \tag{5.1}$$

where Q_L is heat pump capacity, Q_H is ground heat exchanger load [10] [11].

$$Q_H = m_L \times C_L \times \left(T_{L_{out}} - T_{L_{in}}\right) \tag{5.2}$$

where m_L is the mass flow rate C_L is the specific heat, T_L is the temperature of liquid. The required length of ground loop in ground heat exchanger can be found using following Eq. (5.3).

$$L = (m_L C_L R_{total})\, ln(\frac{\theta_{L_{in}}}{\theta_{L_{out}}}) \tag{5.3}$$

where L is the total length of the pipe in ground heat exchanger. R_{total} is the total thermal resistance in ground heat exchanger. $\theta_{l_{in}}$ and $\theta_{l_{out}}$ are the temperature difference between ground

temperature and fluid entering the ground heat exchanger at inlet and outlet respectively. The total thermal resistance is calculated using Eq. (5.4) [10] .

$$R_{total} = R_{conv} + R_{pipe} + R_{soil} \tag{5.4}$$

$$R_{conv} = \frac{1}{\pi D_i h_L} \ , R_{pipe} = \frac{ln\left(\frac{D_0}{D_i}\right)}{2\pi k_{pipe}} \ , R_{soil} = \frac{1}{Sk_{soil}} \ , h_L = \frac{Nu \times k_{nf}}{D_i} \tag{5.5}$$

where D_i is the inner diameter of the pipe, D_o is the outer diameter of the pipe, h_L is the convective heat transfer coefficient of the fluid, k_{pipe} is the thermal conductivity of the pipe, k_{soil} is the thermal conductivity of the soil, and S is the conduction shape factor for the pipe. From Eq. (5.5), notice that the fluid's thermal resistance can be decreased by increasing h_L, the convective heat transfer coefficient of the fluid. So, it is clear from the Nusselt number Eq. (5.5) that the increased thermal conductivity of a nanofluid, k_{nf}, would increase h_L and thus decrease the fluid thermal resistance. This results in increased heat absorption and decreased pipe length. To determine the length of the ground coil of the ground heat exchanger for the design process, the thermophysical properties of nanofluids must be accurately known.

5.5.1 Pumping power

Pumping power is devoted to pump the liquid through the ground heat exchanger. It can be calculated using Eq. (5.6) [11, 12].

$$W_p = \frac{m_L}{\eta \rho_L} \Delta P \tag{5.6}$$

where W_p is the required pumping power. m_L is the mass of the fluid circulating, η is the efficiency of the pump. ρ_L is the density of the liquid and ΔP is the pressure drop of the liquid in the heat exchanger loop. The pressure drop is given by Eq. (5.7).

$$\Delta P = \frac{4fL\rho_L V^2}{2D_h} \tag{5.7}$$

Where, f is the friction factor of pipe. V is the fluid velocity. D_h is the hydraulic diameter of pipe.

From the above two equations, if the length of the pipe decreases then pressure drop can be reduced, which helps in saving pumping power.

5.6 Ground source heat pump at CCHRC

A GSHP has been installed in CCHRC to study the long-term performance of GSHPs in cold climate environments [7]. The main purpose of this system is to supply a portion of the heat required to heat the CCHRC building. The space requires 17.6 kW of heat energy to maintain a temperature of 23°C. A portion of heat is provided by the GSHP through traditional heating systems. The heat pump at CCHRC is a liquid-to-liquid heat pump. The heat is absorbed from the ground through coils in the ground heat exchanger (GHE) by methanol water (M/W). The M/W used in the ground loop is 20% methanol and 80% water. This heat is absorbed by the refrigerant in the heat pump. The refrigerant acts as a heating liquid in the secondary loop. A brief schematic diagram of the GSHP at the CCHRC is shown in Figure 5.3.

5.7 Measurement of heat transfer fluid properties

The heat transfer fluid used in the CCHRC GSHP is a binary fluid of 20% methanol and 80% water (M/W). This fluid is selected to prevent coolant freezing due to Fairbanks' low ground temperatures. In order to do an accurate analysis, the thermal conductivity and specific heat of M/W were measured in the lab. A TCI [13] thermal analyzer measured the thermal conductivity and specific heat of the given sample at different temperatures. By using the thermal chamber, a constant temperature was maintained for the sensor to measure the properties. The measurements were taken at different temperature points to obtain the thermal conductivity and specific heat of the sample in a temperature range between -10 ^{0}C to 30 ^{0}C. The viscosity and density values were obtained from Mikhail and Kimel [14]. The reference and measured values are presented in Table 5.2.

5.8 Nanofluids

The thermal properties of a nanofluid vary depending on the concentration of nanoparticles. In this study we have considered Al_2O_3 and CuO nanofluids with three different concentrations: 0.5%, 1% and 2%. There are no thermophysical properties of methanol-water nanofluids available in the literature. The properties of the nanomaterials are presented in Table 5.3. The thermophysical properties of nanofluids can be calculated using the correlations available in the literature. Researchers [15–20] have developed these correlations for predicting the properties of nanofluids.

5.9 Viscosity

Brinkman [22] had presented a correlation for finding the viscosity of very small particles suspended in a liquid. The correlation is presented in Eq. (5.8). Using this correlation we can find the viscosity of nanofluids for different concentrations. The dependence on temperature is built in with the base fluid viscosity.

$$\mu_{nf} = \mu_{bf}\left(\frac{1}{(1-\phi)^{2.5}}\right) \tag{5.8}$$

where $\mu_{nf} and\ \mu_{bf}$ are viscosities of nanofluid and basefluid respectively and ϕ is the volumetric concentration of nanoparticles in base fluid.

5.10 Thermal conductivity

Prasher et al. [23] proposed a conduction-convection model. They considered convection as due to Brownian motion of the nanoparticles and added it to the Maxwell-Garnett conduction model. The equation they proposed was Eq. (5.9).

$$\frac{k_{nf}}{k_{bf}} = (1 + A\,Re^{m}\,Pr^{0.333}\,\phi)\left[\frac{\left(k_p(1+2\alpha)+2k_m\right)+2\phi\left(k_p(1-\alpha)-k_m\right)}{\left(k_p(1+2\alpha)+2k_m\right)-\phi\left(k_p(1-\alpha)-k_m\right)}\right] \tag{5.9}$$

where the coefficient A = 4×10^4, m=2.5 $\pm$ 15% for water-based nanofluids, m=1.6 $\pm$ 15% for ethylene glycol based nanofluids and m=1.05 $\pm$ 15% for oil-based nanofluids and α is the reciprocal of nanoparticle Biot number. The thermal boundary resistance is R_b. The k_m, $\propto$, R_b and Re can be calculated from Eq. (5.10).

$$k_m = k_{bf}\left[1+\left(\frac{1}{4}RePr\right)\right], \propto = \frac{2R_b k_m}{d_p}, \qquad and\ Re = \frac{1}{\nu}\sqrt{\frac{18KT}{\pi\rho_p d_p}} \tag{5.10}$$

where R_b of water is 0.77×10^{-8} Km^2W^{-1}.

5.11 Density

The density of the nanofluid can be calculated using a the Pak and Cho [3] correlation Eq. (5.11).

$$\rho_{nf} = (1-\phi)\rho_{bf} + \phi\rho_{np} \tag{5.11}$$

where $\rho_{nf}, \rho_{bf}, \rho_{np}$ are density of nanofluid, basefluid and solid particle respectively, and ϕ is the volumetric concentration of nanoparticles in base fluid.

5.12 Specific heat

Xuan and Roetzel [24] presented a correlation Eq. (5.12) for calculating the specific heat of nanofluids based on the conservation of energy. Using Xuan and Roeztel's correlation we can calculate the specific heat of 20:80 M/W nanofluids.

$$Cp_{nf} = \frac{\phi\rho_{np}Cp_{np} + (1-\phi)\rho_{bf}Cp_{bf}}{\rho_{nf}} \tag{5.12}$$

where $Cp_{nf}, Cp_{np}, Cp_{bf}$ are specific heats of nanofluid, solid particles and base fluid, respectively.

5.13 Analytical study

An analytical solution was obtained for the GSHP. The CCHRC GSHP ground conditions were used for the analytical solution. The model calculation of pumping power and outlet temperature from the loop matched with the values measured at CCHRC. The fluid is circulated as turbulent flow to absorb more amount of heat. From the ground. For the analysis regular heat transfer correlations were used to calculate the Nusselt number. The Nusselt number correlation used for the analysis is taken from Bejan [11].

$$Nu_d = 0.012(Re^{0.87} - 280)Pr^{0.4} \quad (1.5 \leq Pr \leq 500, 3000 \leq Re \leq 10^6) \tag{5.13}$$

where Re is the Reynolds number and Pr is the Prandtl number of the fluid.

The Darcy friction factor is necessary to calculate the pumping power required to circulate the fluid. The turbulent friction factor correlation is taken from by Bejan [11].

$$f = 0.046 * Re^{-\frac{1}{5}} \quad (2 \times 10^4 < Re < 10^6) \tag{5.14}$$

5.14 Analytical modeling with different liquids

A comparative analysis was performed with different liquids to understand their performance. The fluids studied under this analysis are water, 20:80 methanol and water (M/W), 60:40 by mass ethylene glycol and water (EG/W), 60:40 by mass propylene glycol and water (PG/W) and HFE-7000. The pipe length required to absorb 18 kW of heat calculated (CCHRC data) from ground is calculated and plotted in Figure 5.4. Similarly the necessary pumping power was also calculated to circulate different fluids in the present GSHP system and shown in Figure 5.5. The thermophysical properties for HFE 7000 was from the 3M literature [25]. For water it was taken from Bejan [11] and for glycols from ASHRAE [5].

5.14.1 Pipe length

The Figure. 5.4 shows the length of pipe required to absorb 18kW of heat from ground with different fluids with different ground temperatures. From this figure it is observed that HFE 7000 requires more length of pipe to absorb the heat compared to the other fluids. This is due to the low thermal conductivity of HFE 7000. It is a low thermal conductivity fluid but has extremely low freezing point and hence considered for application in space. Water requires least amount of piping among the different fluids among the fluids. Since water freezes at 0 °C, so it is not an ideal fluid to use in cold climate regions.

5.14.2 Pumping power

The Figure. 5.5 shows the pumping power required to circulate the fluid in the GSHP ground loop. From the graph it is observed that water requires least amount of pumping power compared to other fluids. The 60:40 PG/W requires high amount of pumping power. This is due to the high viscosity of 60:40 PG/W. The pumping power required is decreasing with increase in ground temperature. This is due to the decrease in viscosity and increase in thermal conductivity and specific heat of the fluid with temperature.

5.15 Nanofluids in GSHP

Using nanofluid thermophysical properties an analytical studies had been performed on ground loop of GSHP. Since the heat transfer fluid that is being used in CCHRC GSHP is M/W, the basefluid for our nanofluids was taken to be M/W. the nanofluid properties were calculated by using the correlations listed by Eqs (5.8-5.12). Using those properties analytical studies were conducted by changing the ground temperature to represent different months.

5.16 Ground temperatures

One of the varying parameters in the GSHP design is ground temperature because this changes from month to month during the winter. An analysis was performed to study the effect of ground temperature on heat absorption and pumping power of GSHP using nanofluids.

5.16.1 Heat absorbed

The Figure 5.6 shows the heat absorbed by different fluids as a function of different ground temperatures. The analysis was performed with M/W, Al_2O_3 and CuO nanofluids. The nanofluids were of three different concentrations; 0.5, 1 and 2%. All the fluids have same inlet temperature, volume flowrate and length. As expected, the heat absorption increases with increase in ground temperature for all the fluids. However, the nanofluids are not extracting significantly more heat from the ground, than the base fluid. At low temperatures the nanofluid properties are practically equal to that of basefluid.

5.16.2 Pumping power

The Figure 5.7 shows the pumping power variation with increase in ground temperature. The fluids that are analyzed are Al_2O_3, CuO nanofluids and M/W. It is observed that 20:80 M/W base fluid requires less pumping power than nanofluids. It is observed that 17.4% increase in pumping power for CuO 2% nanofluid compared to M/W. Nanofluids require high pumping power due to increase in viscosity and density.

Nanofluids density and viscosity are increasing at low temperatures, which resulted in high pumping power. The Figure 5.7 show, ground temperature variation between 273K and 288K has

minimal effect on pumping power variation as the properties change very little in this small temperature range.

5.17 Numerical analysis

The experimental study of the GSHP conducted by CCHRC with just the base fluid was expensive; conducting the same tests for different nanofluids would be cost prohibitive. Therefore, numerical simulations were the alternate approach. We performed these simulations to predict the performance of the ground heat exchanger (GHE). This saved expenses and long-term experimental data collection and analysis. The numerical analysis helped study the role of different parameters such as ground temperature, inlet velocity, and fluids of different properties in the performance of the GSHP.

Other researchers have performed numerical studies on GHEs. Healy and Ugursal [6] studied the effect of various parameters on GSHP performance using a computer model, G-HEADS. They improved performance of the GSHP by optimizing the parameters while designing the GSHP. Yavustruk and Spitler [26] presented a two-dimensional numerical model. They developed a water to air heat pump model. Using their model, they studied the short-term behavior of ground coupled heat exchangers. Bi and others [27] used a two-dimensional cylindrical coordinate system to model a vertical ground heat exchanger. They solved the temperature distribution in the soil and compared their numerical results with experimental data. They showed the important role played by the temperature distribution in the performance of a GSHP.

Mihalakakou and others [28] presented a model in polar coordinates. In the model, they included the moisture content of the soil around the pipe. Through their study, they proved the importance of moisture content in the soil in calculating the performance of a GSHP. The model they used was the TRANSYS simulation program. Bojic and others [29] developed a two-dimensional model in which soil has different horizontal layers with constant temperatures. They studied the heat transfer from ambient air to the ground pipes. They used steady-state energy equations to solve the problem. Demir and others [30] developed a two-dimensional model of a GSHP. They used MATLAB to perform the numerical study. They compared their result with experimental values and found a maximum error of 10% with outlet temperatures. Wu and others

[31] studied the thermal performance of a horizontal GSHP in the United Kingdom (U.K.) with both experimental and numerical methods. They performed numerical analysis using the FLUENT program, studying the effects of different parameters on the performance of a GSHP. They found larger diameter coils can extract more heat from the ground. They also found that heat extraction rate decreased with increasing coil central interval distance.

Benazaa and others [32] studied the coils in a horizontal GSHP numerically. They used an unsteady quasi-three-dimensional model simulation in their study of the influence of thermal conductivity and geometric parameters on heat exchanger efficiency. They found heat flux absorption decreases as time increases. Tube diameter played an important role in the performance of the GSHP. Fuji and others [33] studied the slinky horizontal coils in the ground heat exchanger numerically. They used the commercial finite element software FEFLOW for their analysis. They compared their numerical result with experimental values with good agreement. Congedo and others [34] studied different configurations in a horizontal GSHP in Italy. They used the CFD code FLUENT to simulate the GSHP for 1 year. They studied parameters such as soil thermal conductivity, velocity of fluid, and depth of coil below the soil surface. They found that a helical heat exchanger system provided the best performance. Sagia and others [35] performed a two-dimensional analysis on borehole thermal resistance in ground heat exchangers. They performed a steady state analysis of the problem, using the finite element software COMSOL Multiphysics for their simulations. They found borehole thermal resistance decreased as the distance between holes increased. They also found that an increase in the thermal conductivity of the ground decreased the borehole thermal resistance. Luo and others [36] numerically studied the energy absorption by a horizontal GSHP. They used the commercial finite element program FEFLOW to model the problem. They considered the effect of coil depth and diameter in energy absorption by a GSHP. They found decreased variation in fluid temperature at the outlet with increased burial depth.

5.18 Problem definition

In the present study, we performed a numerical analysis on the CCHRC's cold climate GSHP. The total length of the pipe in the ground loop of the heat exchanger in the GSHP is 1400 m. This loop is placed as a slinky coil in the ground at a depth of 2.9 m from the ground surface. The inside

diameter of the pipe is 0.75 in (1.9 cm) and its wall thickness is 0.25 in (0.635 cm). The horizontal GSHP at the CCHRC is modeled in COMSOL Multiphysics V 4.3 software [37]. A three-dimensional geometry was prepared in this software. Figure 5.8 shows the geometry used for analysis in the COMSOL software. In order to generate a successful finite element mesh around the pipe, the total slinky coil length of 1400 m was represented by six straight pipelines with U-bends. From the CCHRC's ground temperature measurements, it was determined that the soil providing the heat is a block of 280 m length, 150 m width, and 10 m height. The coil is placed 2.9 m below the surface to match the actual installation in the field. There are two domains in the model: domain 1 is the solid domain, which has solid material (soil) properties, and domain 2 is for different fluids within the pipe.

5.19 Material properties

The material properties of the soil and the pipe have been taken from the CCHRC [1,7]. These properties are shown in Table 5.5. The high density polyethylene (HDPE) pipe material is used for pipe wall materials and the values are from the CCHRC [7]. COMSOL software provides an opportunity to define the material properties as a function of temperature. Using the piecewise function in Comsol, we can define material properties at a particular temperature. We defined fluid properties separately for each fluid, since the properties are known at a particular temperature. We defined these properties in the fluid domain. Comsol interpolated the properties between the defined points. For heat transfer in the soil, the solid heat transfer module is used. For heat transfer analysis in fluids, the pipe flow module in the Comsol program is used. In the pipe flow module, both pressure and heat transfer in fluids can be modeled. Comsol solves the heat transfer in both the solid and liquid phases using a segregated solver.

5.20 Finite element mesh generation

Comsol has an inbuilt meshing program which generates the mesh in the model domain. For simplicity, we adopted the default meshing process provided by COMSOL. The default meshing process automatically changes with the physics of the domain. It has an inbuilt program to generate mesh for both solid and liquid domains separately. This automatic meshing scheme provides the common node points at solid and liquid boundaries. It also takes care of fine boundary meshing,

which is required to clearly capture the fluid dynamics and heat transfer at the pipe boundary. The program provides options for fine-tuning the meshing, like coarse mesh for larger cell sizes and fine mesh for smaller cell sizes. For our present simulations, we opted for the extremely fine-tuned mesh option. The geometry contains 45883 domain elements, 7952 boundary elements, and 759 edge elements. Figure 5.9 shows the meshing image of the geometry under computation. Figure 5.9(a) shows the mesh covering the entire domain, while Figure 5.9(b) shows the finer mesh around the pipe buried 2.9 m below the surface. Around the pipe, where the heat transfer is taking place from the soil, the finer mesh computes the heat transfer accurately. Farther away from the pipe, where temperature gradients and heat transfer in the soil are small, relatively larger elements are employed to keep the computation time reasonable.

5.21 Governing equations

A 3-dimensional steady state analysis was performed on the problem. The heat transfer between the soil and fluid was studied by using the following governing equations. For solids heat is transferred by using conduction. The heat transfer governing equation for solid was provided in Eq. (5.15).

$$\rho C_P \nabla T = \nabla \cdot (k \cdot \nabla T) + Q \tag{5.15}$$

where ρ is the density, C_P is the specific heat, k is the thermal conductivity of material, Q is the heat source.

The energy equation for the fluid flow is provided in Eq. (5.16).

$$\rho A C_P u \cdot \nabla T = \nabla \cdot Ak\nabla T + Q_{wall} + \frac{f_D \rho}{2d_h}|u|^3$$
$$Q_{wall} = hZ(T_{ext} - T) \tag{5.16}$$

where A is the cross sectional area of pipe, u is the velocity of the fluid. Q_{wall} is the heat exchange with pipe and surroundings through pipe wall, Z is the wetted perimeter of the pipe. h is the heat transfer coefficient of fluid. T_{ext} is the external temperature outside the pipe. Soil temperature becomes the T_{ext} in this case. The term $\frac{f_D \rho}{2d_h}|u|^3$ is the heat generated due to the friction in fluids. The continuity and momentum equation for fluid are provided in Eqs. (5.17) and (5.18).

$$\text{Continuity; } \nabla \cdot (A\rho u) = 0 \tag{5.17}$$

$$\text{Momentum; } 0 = -\nabla P - \frac{f_D \rho}{2d_h} u|u| + F \tag{5.18}$$

where P is the pressure of the fluid, f_D is the Darcy friction factor of the fluid, d_h is the hydraulic diameter of the fluid passage. F is the volume force of the fluid.

5.22 Boundary conditions

Solving the governing equations for the required domain necessitates defining boundary conditions from CCHRC ground temperature measurements. The temperature of the soil is nearly uniform throughout the domain and varies modestly with different months, so we assumed constant temperature boundary conditions at all faces with different values for different months. For the soil domain, a temperature is defined which represents the temperature of the ground. This temperature is changed to make repetitive runs to represent different moths of the year. At the faces of the block, a constant temperature boundary condition which has the same temperature as the soil is used. For the fluid, constant velocity and temperature are given as boundary conditions at inlet. These parameters are varied and runs are repeated to perform parametric studies. After solving for the model for given conditions, Comsol gives the results for further analysis. Comsol has a built-in post-processing tool to perform primary analysis on the obtained results. Figure 5.10 shows the results of a typical Comsol simulation for an inlet fluid temperature of 270K and outlet fluid temperature of 274.5K after performing post processing in the software.

5.23 Validation of computation

5.23.1 Outlet temperature comparison

The numerical model was validated by comparing the numerical computational results with analytical results and experimental data collected at the CCHRC. Figure 5.11 compares the outlet temperatures obtained by the Comsol model, the experiment, and analytical calculation. The experimental and Comsol model results are very close to each other. A maximum error of -0.5K was observed between the Comsol and experimental results. A maximum error of 2.32K was observed between the analytical and experimental values, possibly due to the assumption of a

single 1400 m long straight pipe built into the analytical model. These two results show that the Comsol model is predicting fairly good results compared to experimental and analytical values.

5.23.2 Heat absorption comparison

Figure 5.12 shows the comparison of the heat absorption in the ground loop from the soil for different months. A reasonable agreement between the analytical and Comsol results is observed.

5.24 Effects of different parameters

Several simulations were repeated to evaluate the effect of changing different parameters on heat absorption by the GSHP. The simulations were repeated for 0.5, 1, and 2% concentrations of Al_2O_3 and CuO nanofluids. The parameters varied were ground temperature, flow velocity, and inlet temperature of the heat transfer fluid. The effects of these parameters on GSHP performance are explained in the following sections.

5.24.1 Ground temperature variation

Ground temperature is a very important parameter which changes throughout the season and influences the heat absorbed by the ground loop. Figure 5.13 shows the effect of ground temperatures from 273K to 323K on the heat absorbed by the fluid in the ground loop of the GSHP. In Figure 5.13, we notice that as the ground temperature increases, so does the heat absorption by the fluid. From the figure, it is evident that heat absorption by the Al_2O_3 2% nanofluid is the highest. At a high ground temperature (323K), the base fluid MW absorbs the least and Al_2O_3 absorbs the most heat.

5.24.2 Heat transfer fluid velocity

The heat absorption by the fluid in the ground loop is directly related to the flow rate inside the loop: with increasing velocity, the convection heat transfer coefficient increases. We performed a flow rate parametric study inside the ground loop of the GSHP by varying the velocity from 1 to 5 m/s. The actual GSHP at the CCHRC operated at 3.7 m/s. In all cases, the fluid entering the loop was at 270K. Figures 5.14 to 5.16 show the heat absorbed by nanofluids for different flow rates at four different ground temperatures (273, 278, 283, and 288K). Figure 5.14 shows the heat absorbed

by different fluids in the ground loop at a 273K ground temperature for three different velocities, 1 to 5 m/s. From the figure, it is clear that as the flow rate increases, the heat absorption also increases. At a low flow rate of 1 m/s, we observed that nanofluids absorbed 6.5% more heat than the basefluid, M/W. At a high flow rate of 5 m/s, Al_2O_3 2% nanofluid absorbed 10% more heat than M/W. Figure 5.15 shows the heat absorbed by the fluids in the ground loop at 278K ground temperature. At a low flow rate of 1 m/s, we observed that the Al_2O_3 2% nanofluid absorbed 6% more heat than M/W. At a high flow rate of 5 m/s, Al_2O_3 2% absorbed 7.8% more heat than M/W. Figure 5.16 shows the effect of flow rate on heat absorption at 283K ground temperature. The difference in heat absorption at 1 m/s is 5.8% more for Al_2O_3 2% nanofluid. At a 5 m/s flow rate, Al_2O_3 2% absorbed 8.3% more heat than M/W. Figure 5.17 shows a similar analysis with flow rate at 288K ground temperature. At a low flow rate of 1m/s, CuO 2% nanofluid absorbed 3.7% more heat than M/W. At a high flow rate of 5 m/s, Al_2O_3 2% absorbed 7% more heat than M/W. From these results, we can say that at lower temperatures and higher flow rates, nanofluids are absorbing more heat than M/W. In this parametric study, we found that nanofluids performed better than the M/W basefluid.

5.25 Inlet fluid temperature

A parametric study was performed on the GSHP ground loop by changing the temperature at which fluid entered the ground loop. The CCHRC running conditions were used for this analysis with various pinch temperatures (T_g–T_i) ranging from 2 to 10K. Figures 5.18-5.20 show the effect of fluid inlet temperature on heat absorption at different ground temperatures. The horizontal axis in the plots gives the pinch temperature difference between the ground temperature and the fluid inlet temperature ($T_g - T_i$). Figure 5.17 shows the heat absorption by fluids for different inlet temperatures when the ground is at 273K. The nanofluids absorbed more heat than the base fluid, M/W. We found an increase of 9.3% for Al_2O_3 2% nanofluids over the base fluid for a temperature difference of 2K. Figure 5.18 shows heat absorption with varying fluid inlet temperature at a ground temperature of 278K. The nanofluids absorbed more heat than M/W. The Al_2O_3 2% nanofluid absorbed 10% more heat than M/W for a 2K temperature difference. Figure 5.19 shows the heat absorption of fluids in the ground loop for different inlet temperatures when the ground is at 283K. The Al_2O_3 2% nanofluids absorbed 10.7% more heat than M/W. Figure 5.20 shows heat absorption variation for different fluid inlet temperatures at ground temperature 288K. In this case,

an increase of 9% was observed for Al_2O_3 2% nanofluids over the base fluid, M/W. From these results, it was clear that heat absorption was increasing with increasing difference between the ground temperature and the inlet temperature. For all ground temperatures, nanofluids were absorbing more heat than M/W. This absorption increased with increasing ground temperature. Nanofluids were absorbing more heat compared to the base fluid M/W at low temperature differences.

5.25.1 Pumping power

Figure 5.21 shows the pumping power variation with different flow velocities at ground temperature of 273K for the basefluid M/W and six different nanofluids. The CCHRC heat pump ran at 3.7 m/s. The plot shows at low flow velocity the pumping power of nanofluids practically equal to that of the basefluid M/W. At high velocity of 3 m/s, 2% nanofluids require marginally more power than the basefluid. For example, there is an increase of 40W more power required for CuO 2% nanofluids, which is about 6% more than required by base fluid.

5.26 Conclusions

Analytical and numerical studies on the cold climate GSHP have been performed using nanofluids with volume concentrations ranging from 0.5 to 2%. Initially, using the analytical method, the required length of pipe to absorb 18 kW of thermal energy for the CCHRC heat pump and the pumping power required to pump the fluids in Fairbanks soil conditions were calculated. Later, using the same operating conditions of the GSHP in the CCHRC, analytical evaluations were performed by varying the ground temperature. From this analysis, it was observed that there is a marginal benefit to using nanofluids in cold climate GSHPs. Pumping power increases with nanofluids due to their increased viscosity. Ground temperature is one of the varying parameters. Secondly, a numerical study was performed using the Comsol finite element model to study the performance of nanofluids in the GSHP. We performed three parametric studies on the performance of nanofluids in the CCHRC GSHP. The results showed that with an increase in ground temperature, the nanofluids were absorbing 12% more heat than the base fluid at 273 K. In the parametric study with flow velocity variation, we found nanofluids were absorbing 10% more heat than M/W at low temperatures. In the parametric study with inlet temperature variation for a

temperature difference of 2K between ground and inlet temperatures, the 2% Al_2O_3 nanofluid absorbed 10% more heat than the base fluid. Numerical analysis showed a marginal increase in pumping power for nanofluids over the base fluid. From these results, it may be concluded that nanofluids would perform slightly better than the M/W basefluid in cold climates, with a marginal increase in pumping power.

5.27 Acknowledgement

Financial support from the Mechanical Engineering Department, University of Alaska Fairbanks is gratefully acknowledged.

5.28 Nomenclature

EG/W	60% Ethylene Glycol and 40% Water by mass
PG/W	60 % propylene Glycol and 40% Water by mass
Al_2O_3	Aluminum Oxide
CCHRC	Cold Climate Housing Research Center, Fairbanks, Alaska
COP	Coefficient of Performance
CuO	Copper Oxide
GHE	Ground Heat Exchanger
GSHP	Ground Source Heat Pump
HDPE	High Density Poly Eurethene
L	Pipe length [m]
M/W	20% methanol and 80% Water
Q	Heat absorbed [kW]
T	Temperature [K]
W	Pumping power [W]
Subscript	
bf	base fluid
g	ground
i	inlet
nf	nanofluid

np nanoparticle

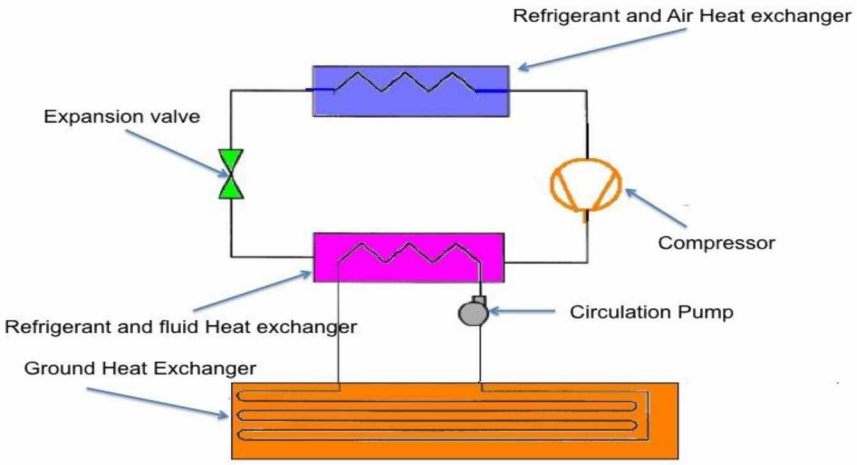

Figure 5.1. Schematic diagram of ground source heat pump

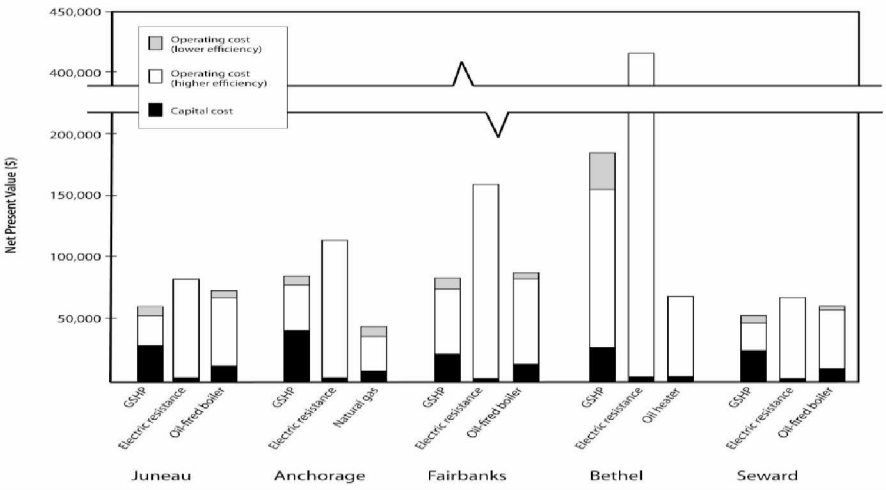

Figure 5.2. Economic assessment of GSHP in Alaska [1]

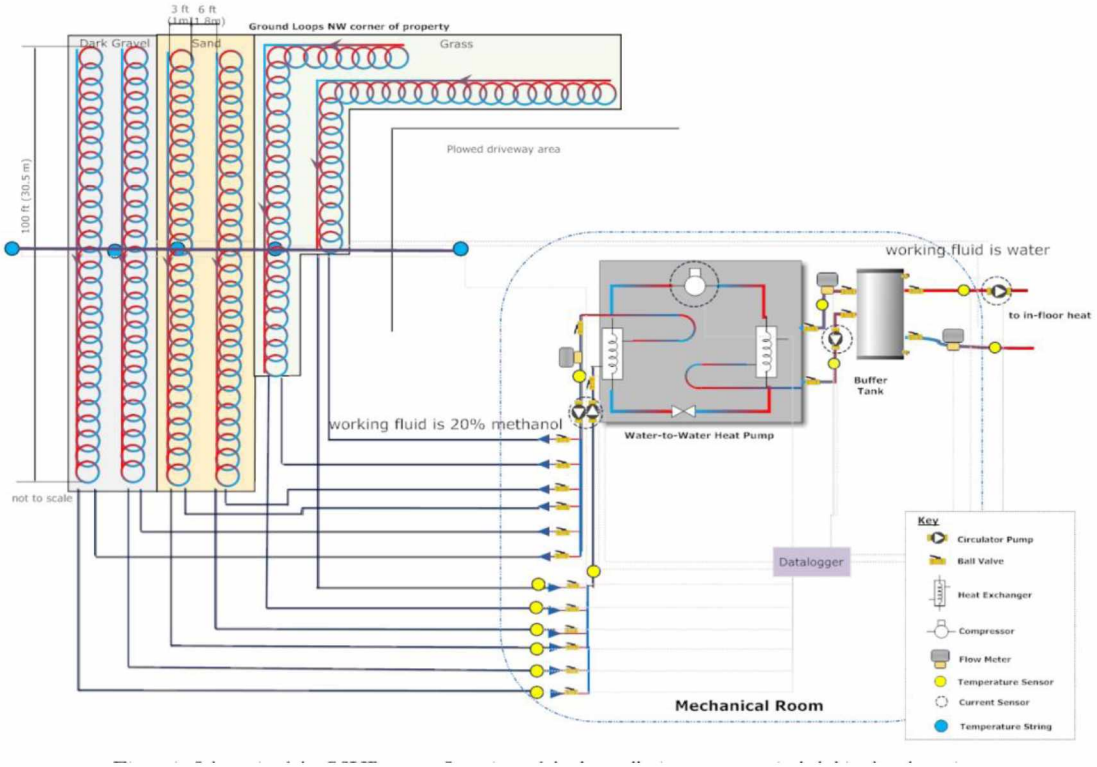

Figure 5.3. Schematic diagram of the GSHP at CCHRC in Fairbanks [7].

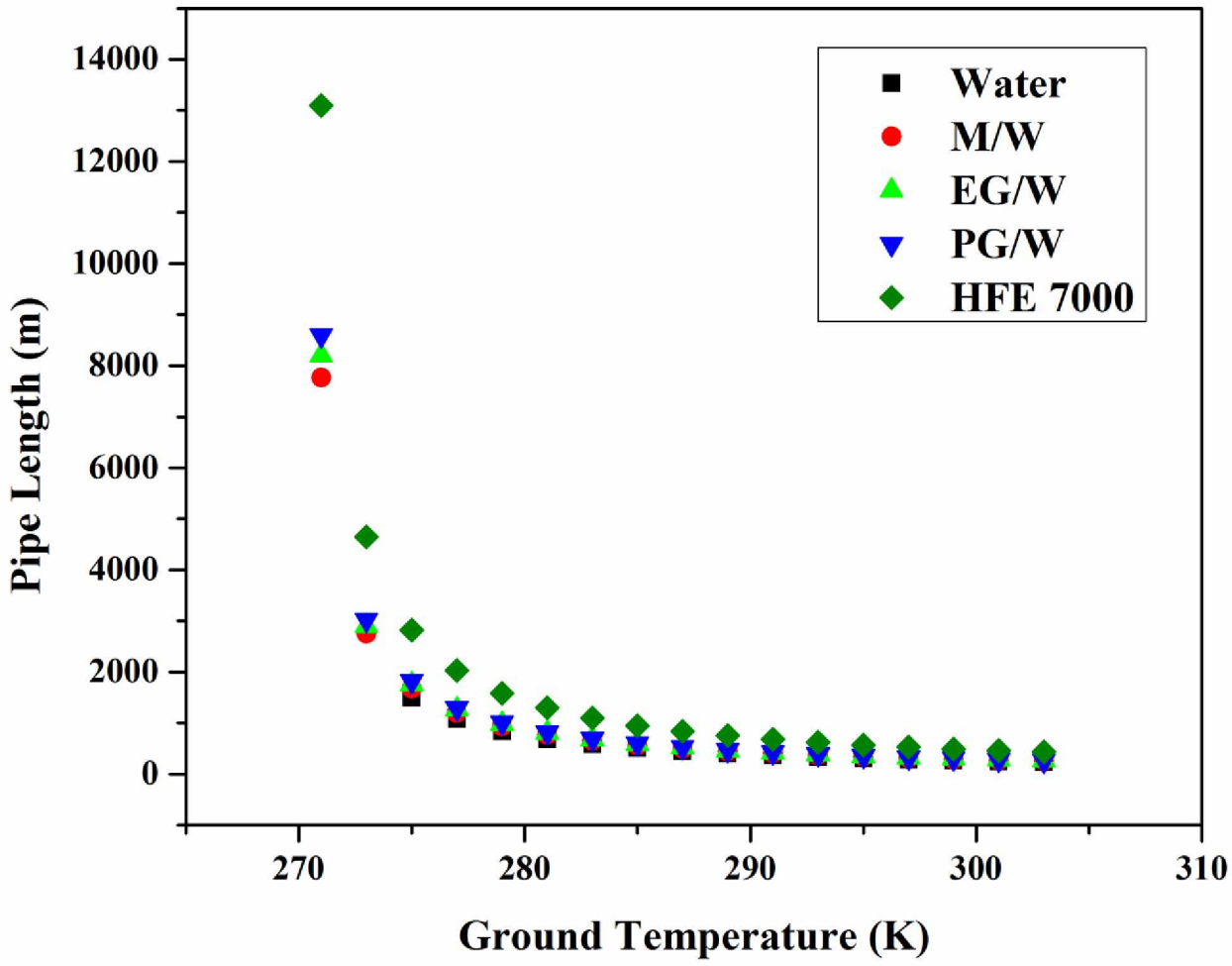

Figure 5.4. Required pipe length to absorb 18kW heat from ground with different fluids.

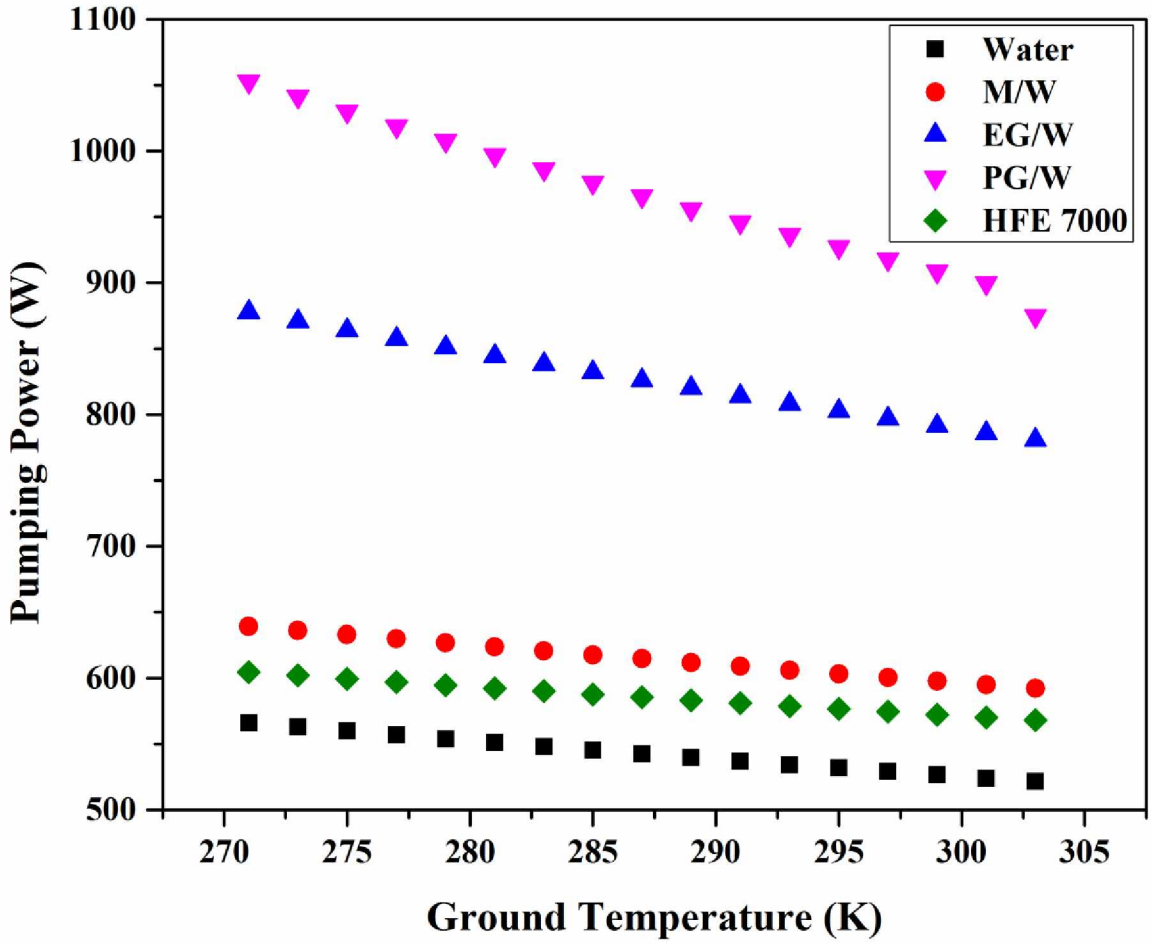

Figure 5.5. Pumping power required for different fluids for the CCHRC GSHP loop length of 1400m

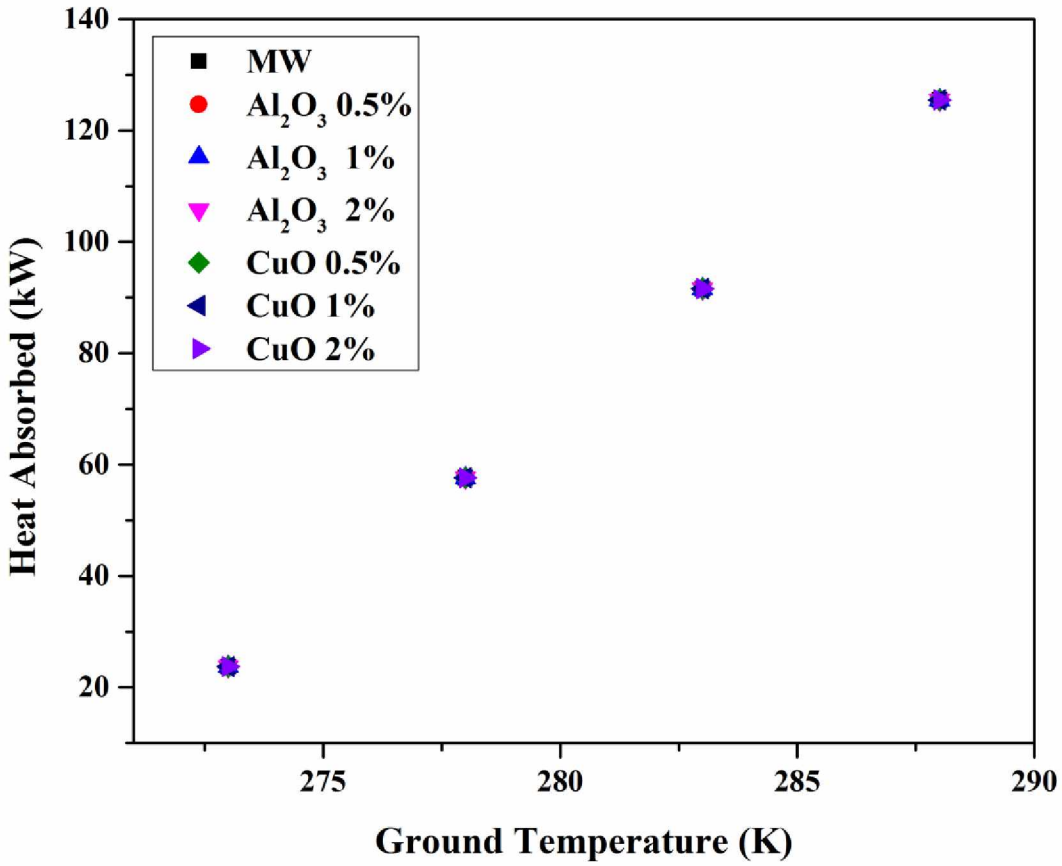

Figure 5.6. Heat absorbed by ground heat exchanger with variation in ground temperature.

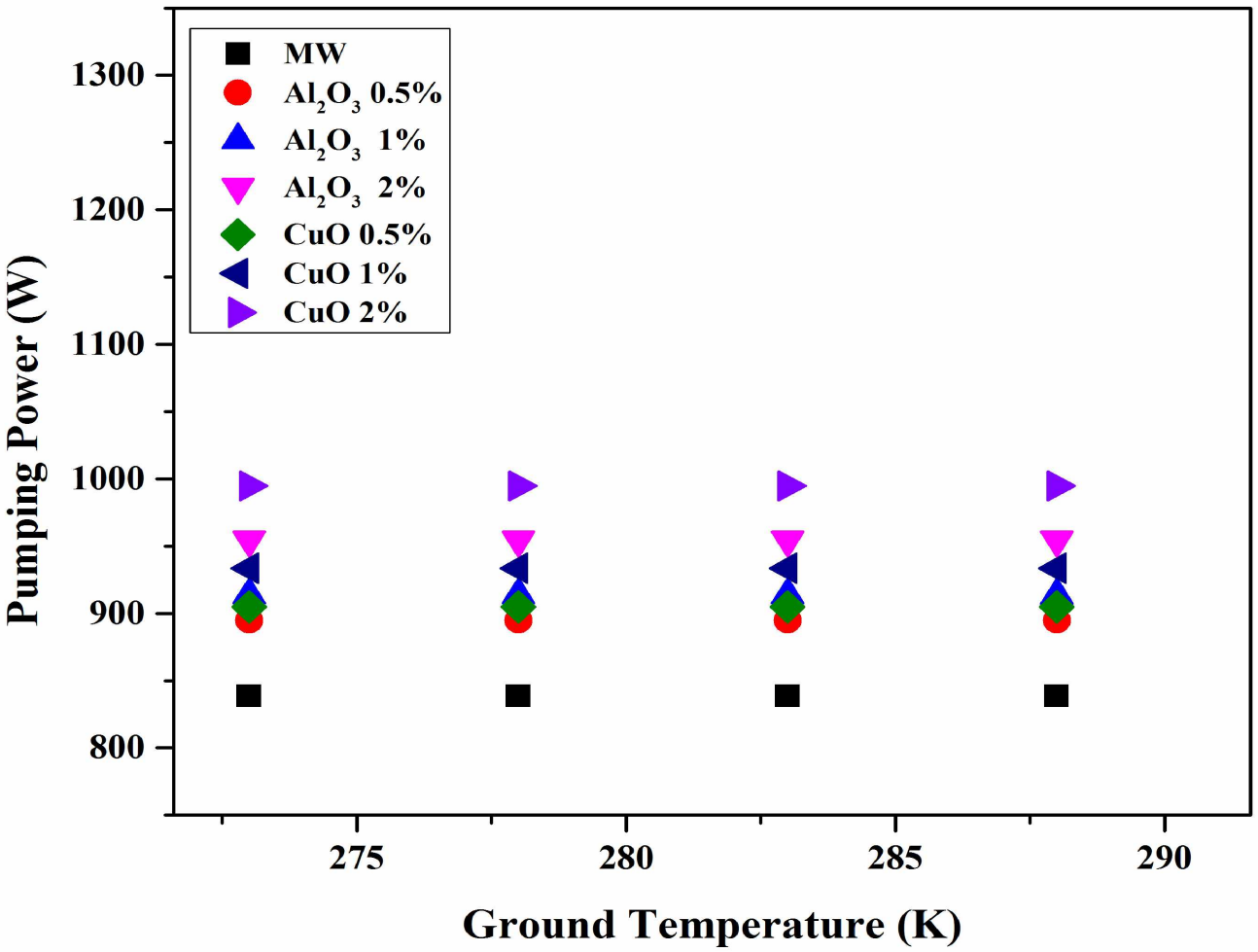

Figure 5.7. Pumping power of fluid with ground temperature.

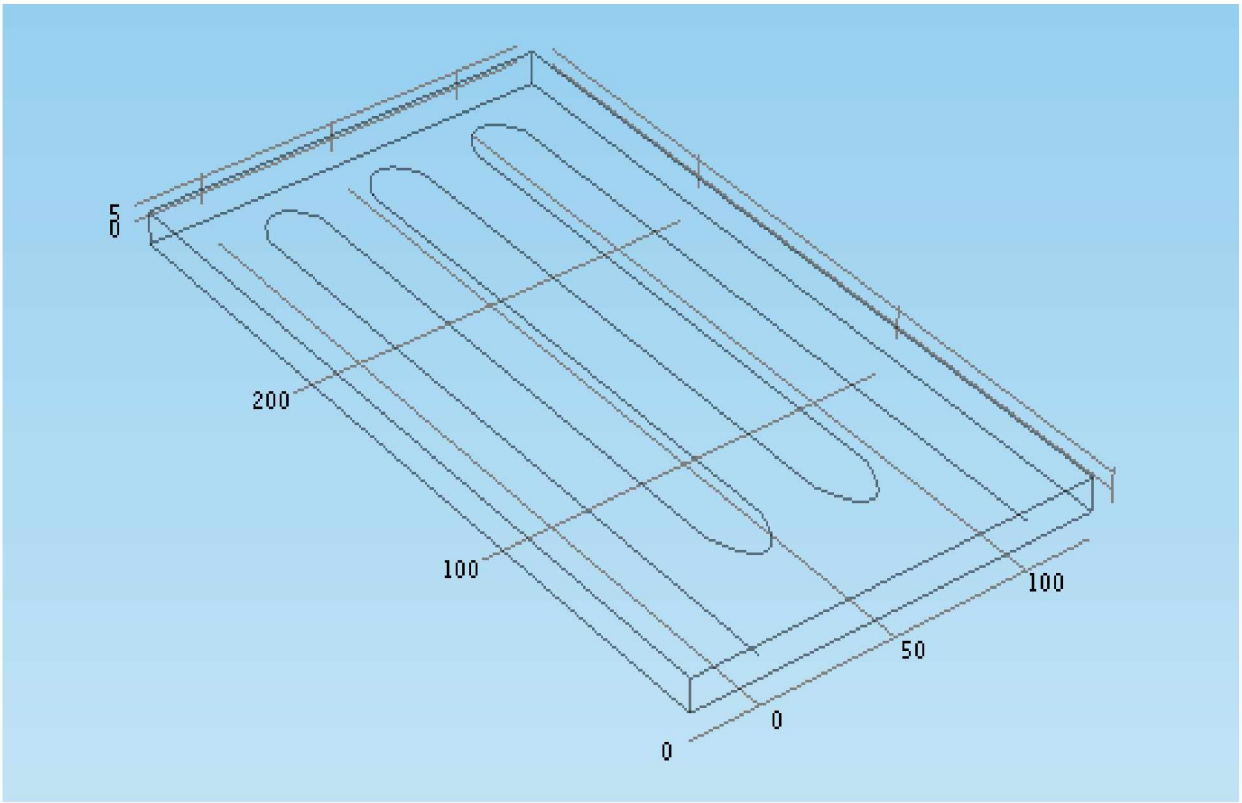

Figure 5.8. GSHP geometry design used for numerical analysis in Comsol.

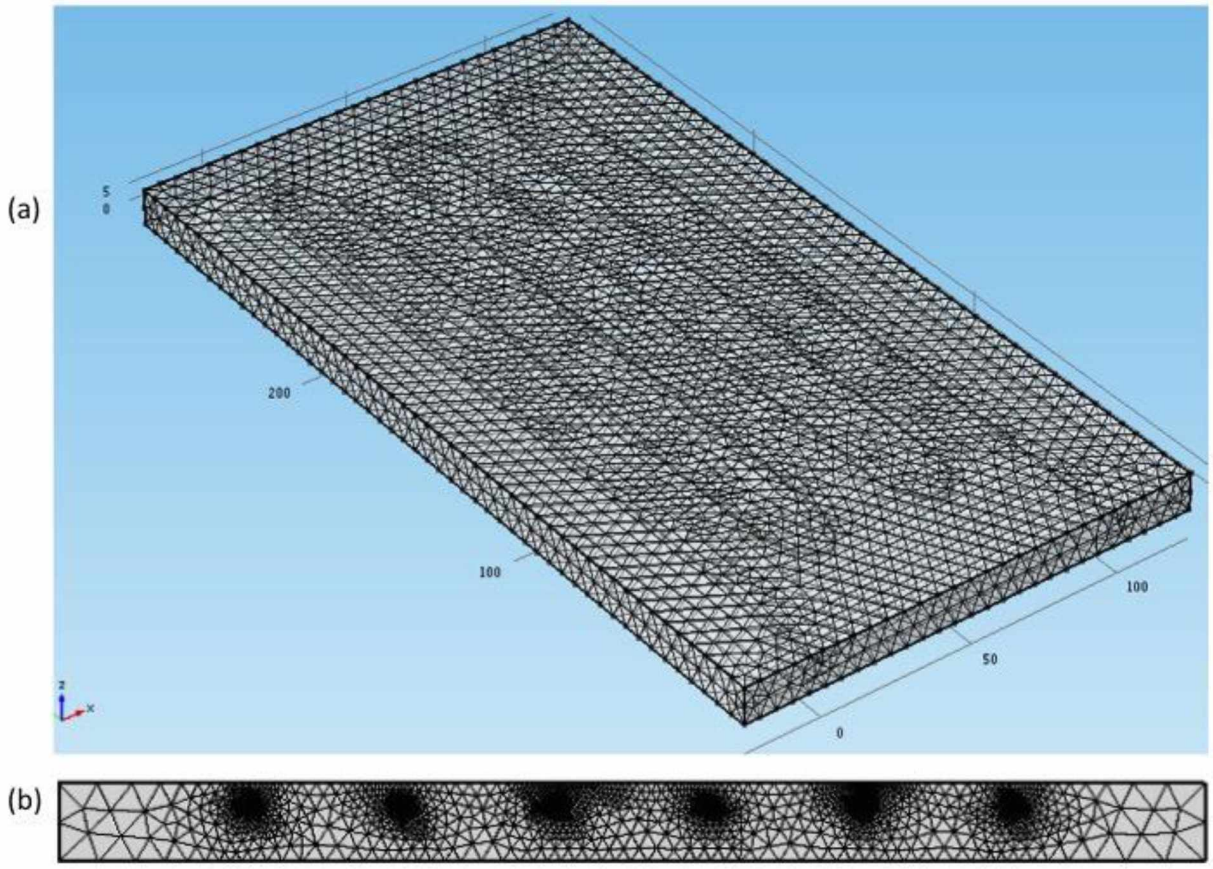

Figure 5.9. Meshing image of geometry in Comsol, (a) represents 3D view of mesh, (b) represents 2D cross-sectional view of mesh around pipes.

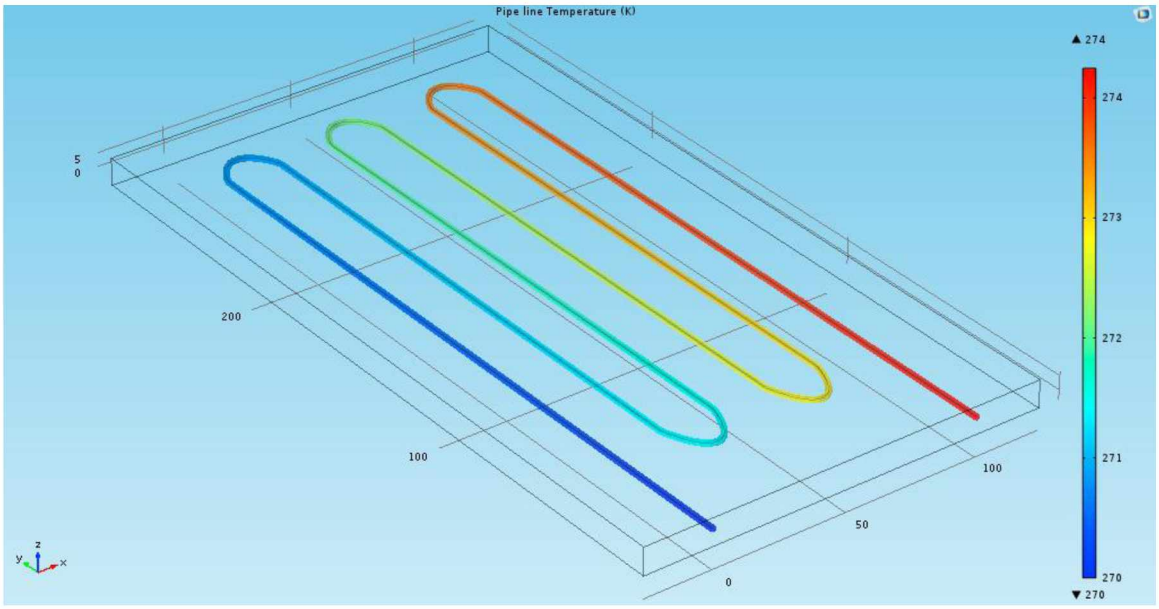

Figure 5.10. Comsol model showing results after simulation

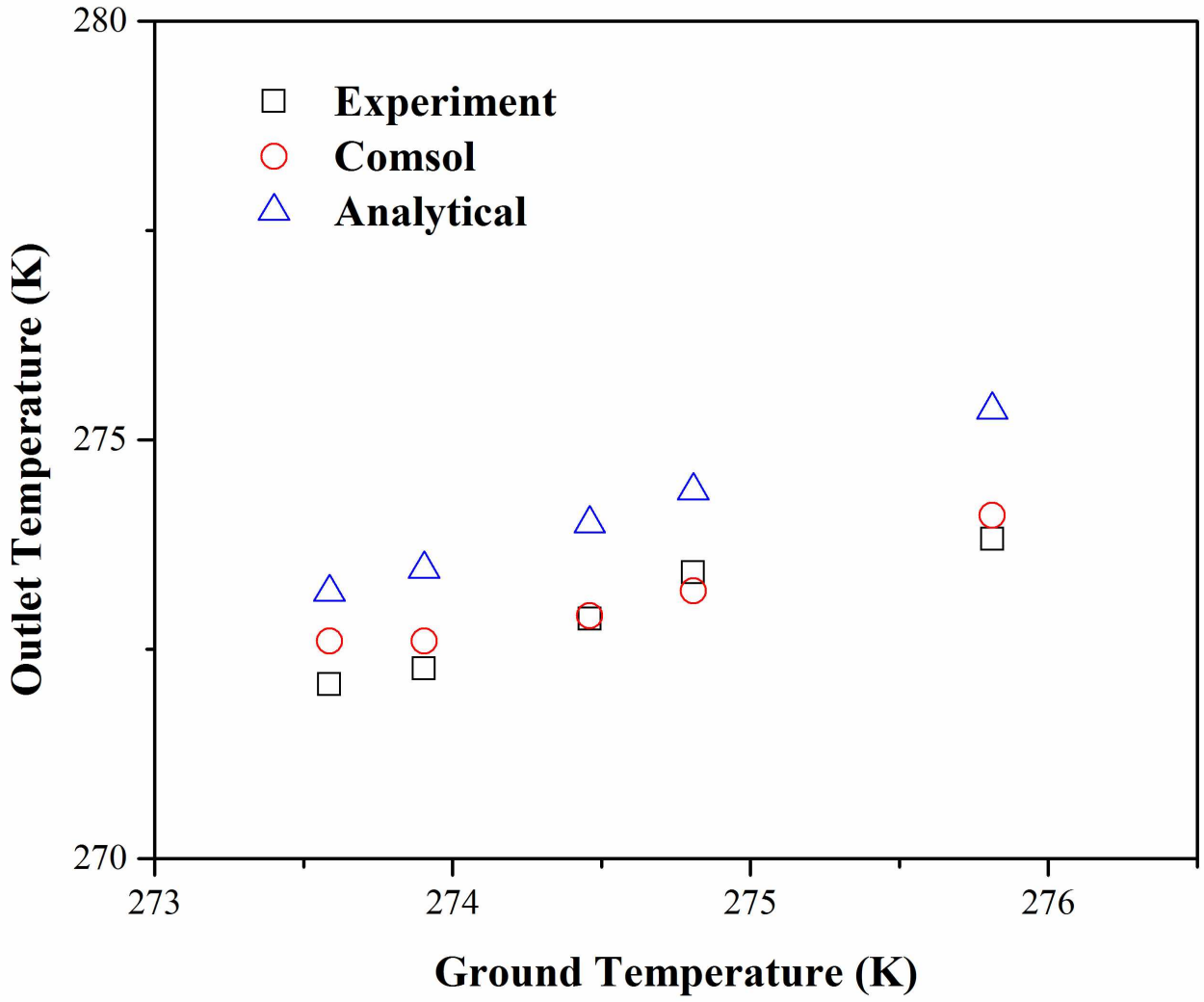

Figure 5.11. Comparison of Comsol result with experiment and analytical values.

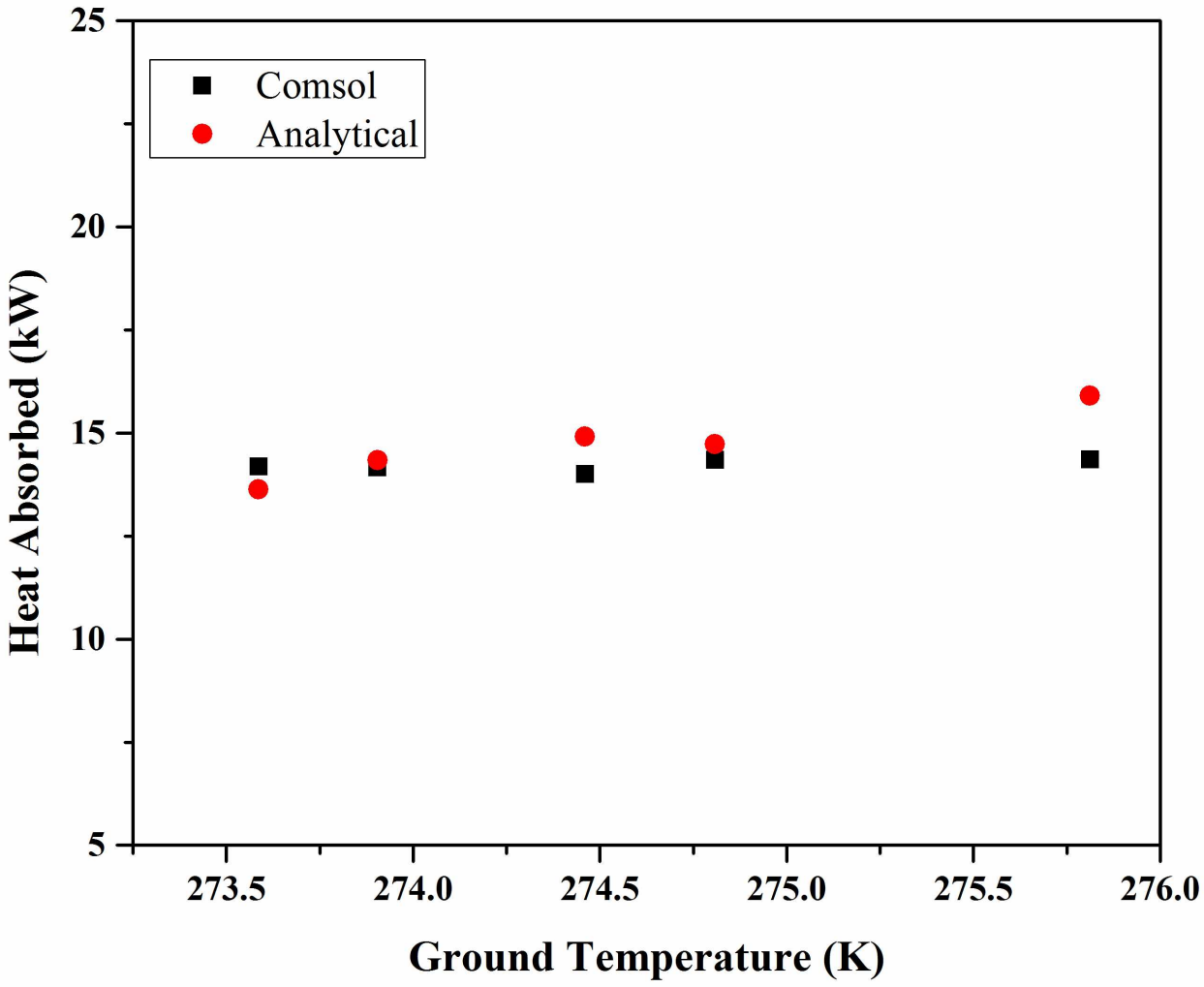

Figure 5.12. Comparison of heat absorbed by ground loop between Comsol results and analytical results.

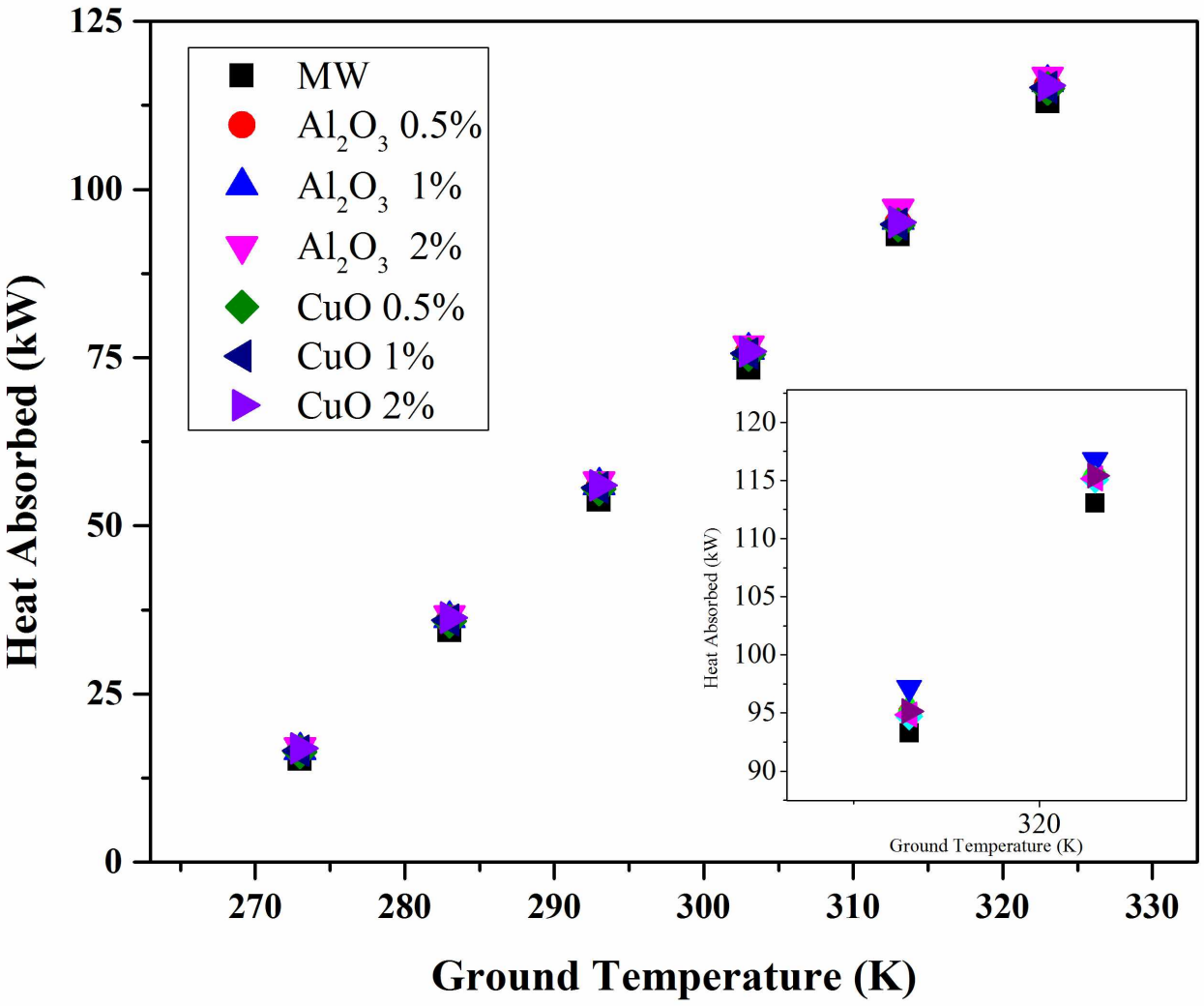

Figure 5.13. Heat absorbed by fluid in ground loop for different ground temperatures

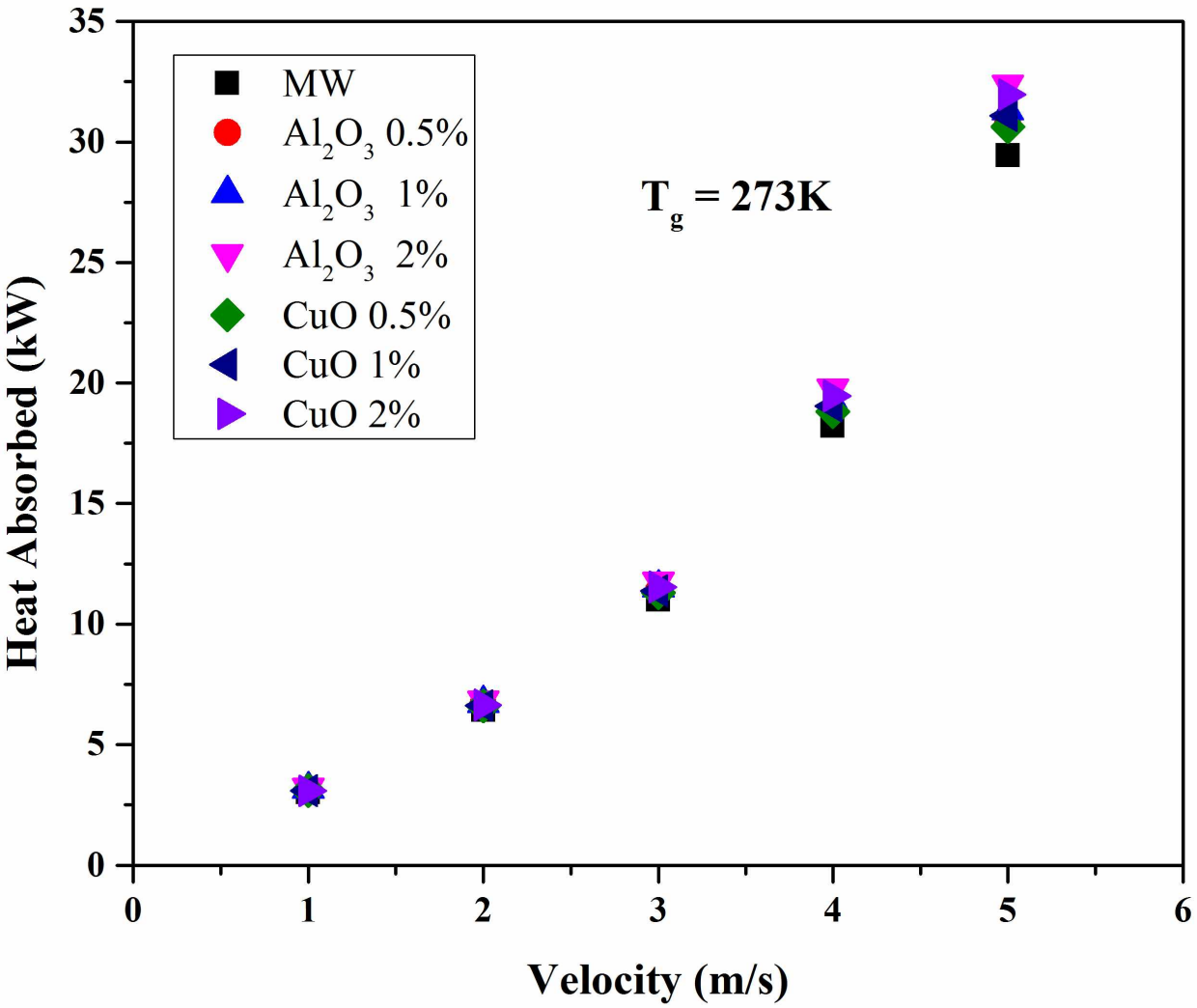

Figure 5.14. Heat absorption by fluid in ground loop for different inlet velocity at 273K-ground temperature.

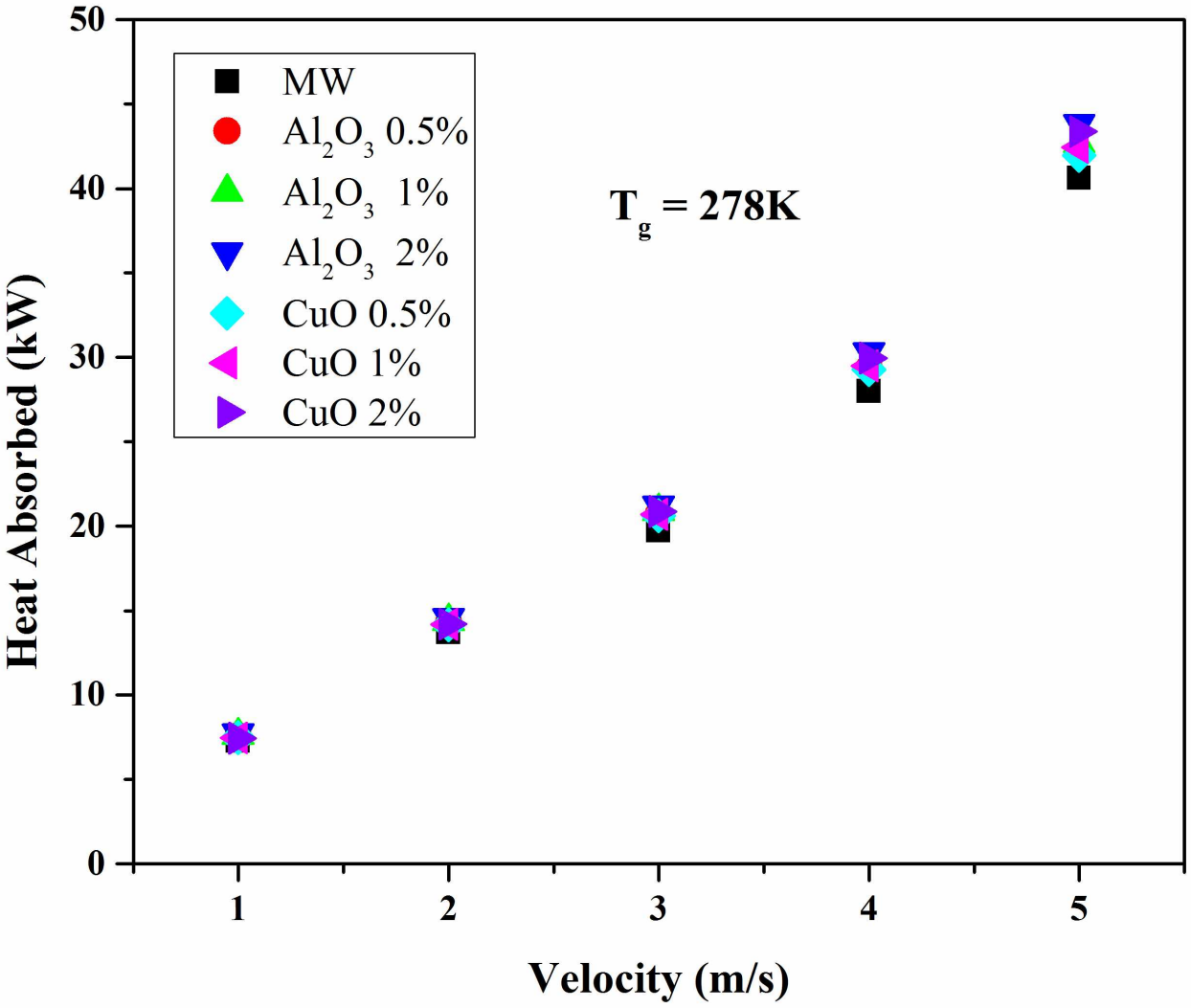

Figure 5.15. Heat absorption by fluid in ground loop for different inlet velocity at 278K-ground temperature.

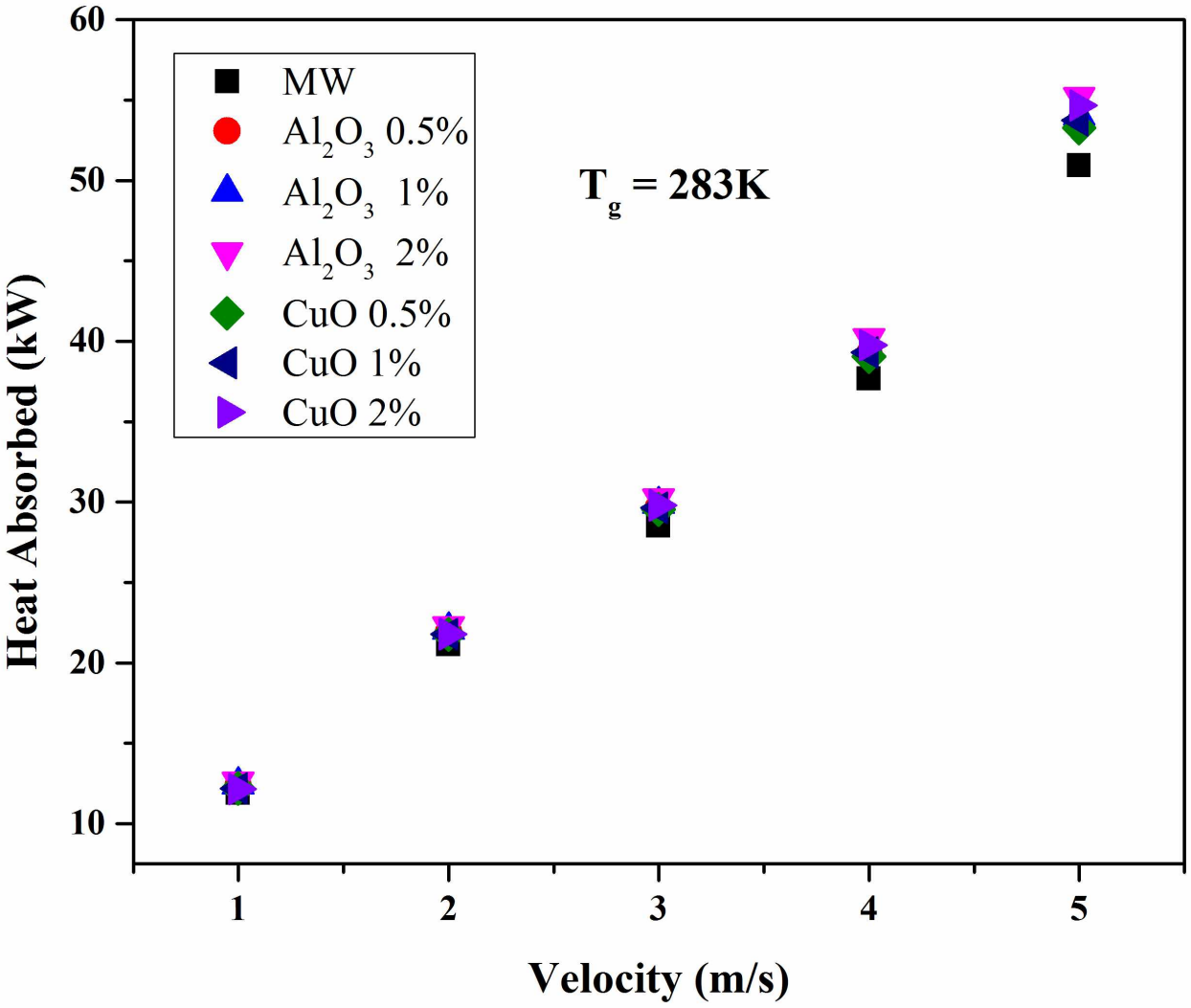

Figure 5.16. Heat absorption by fluid in ground loop for different inlet velocity at 283K-ground temperature.

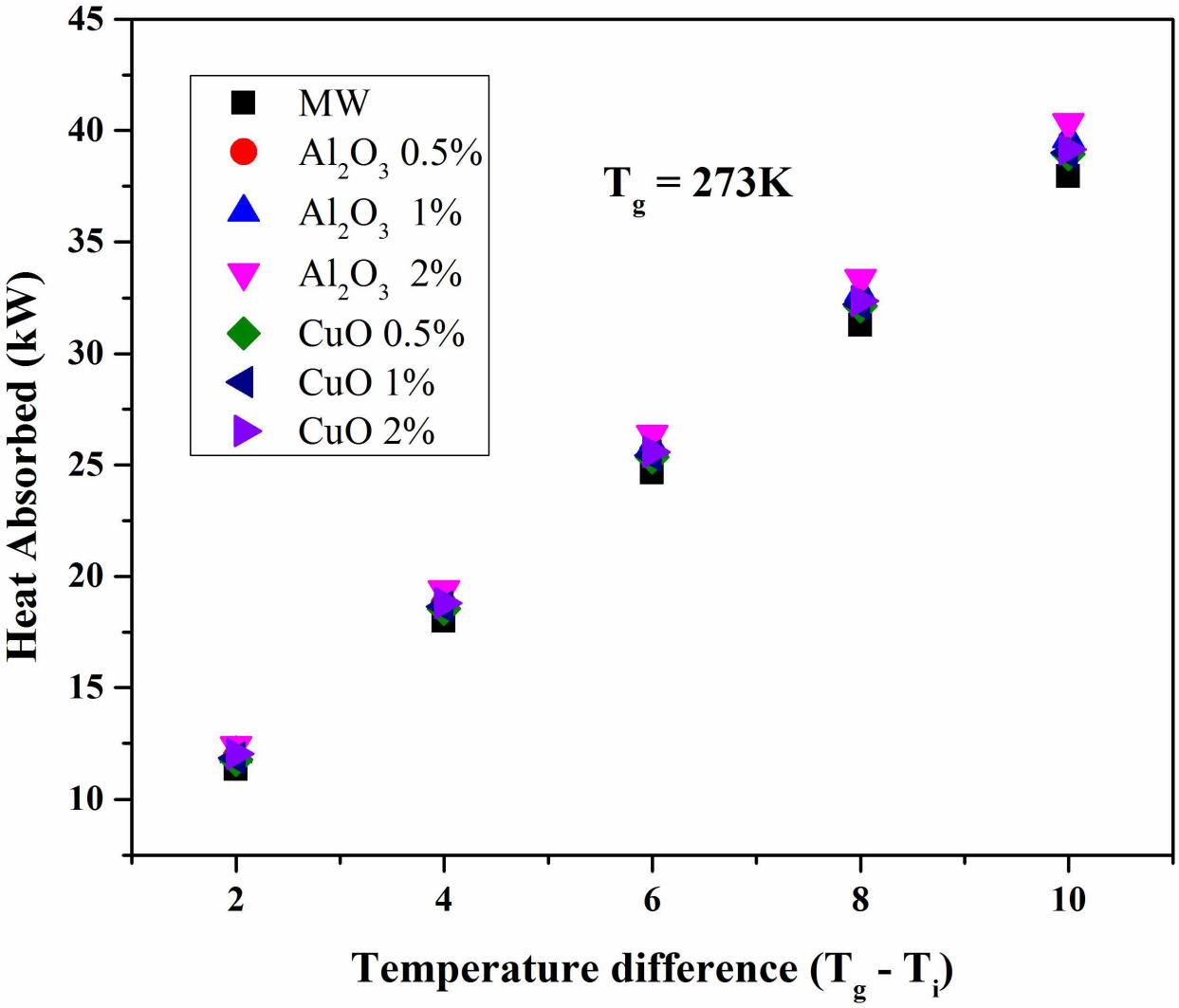

Figure 5.17. Heat absorbed by fluid in ground loop for different inlet temperatures of fluid when ground temperature is 273K.

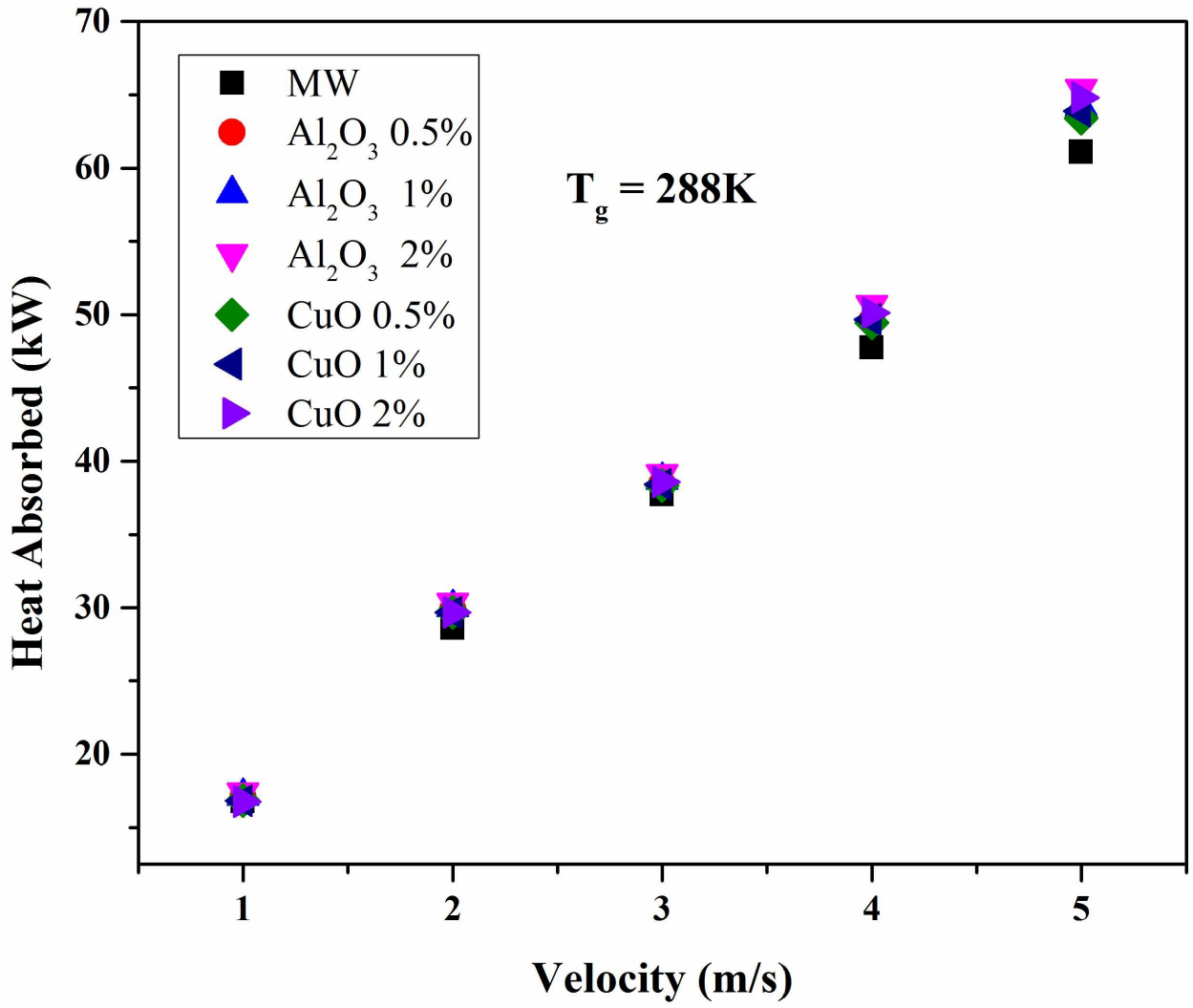

Figure 5.18. Heat absorption by fluid in ground loop for different inlet velocity at 288K-ground temperature.

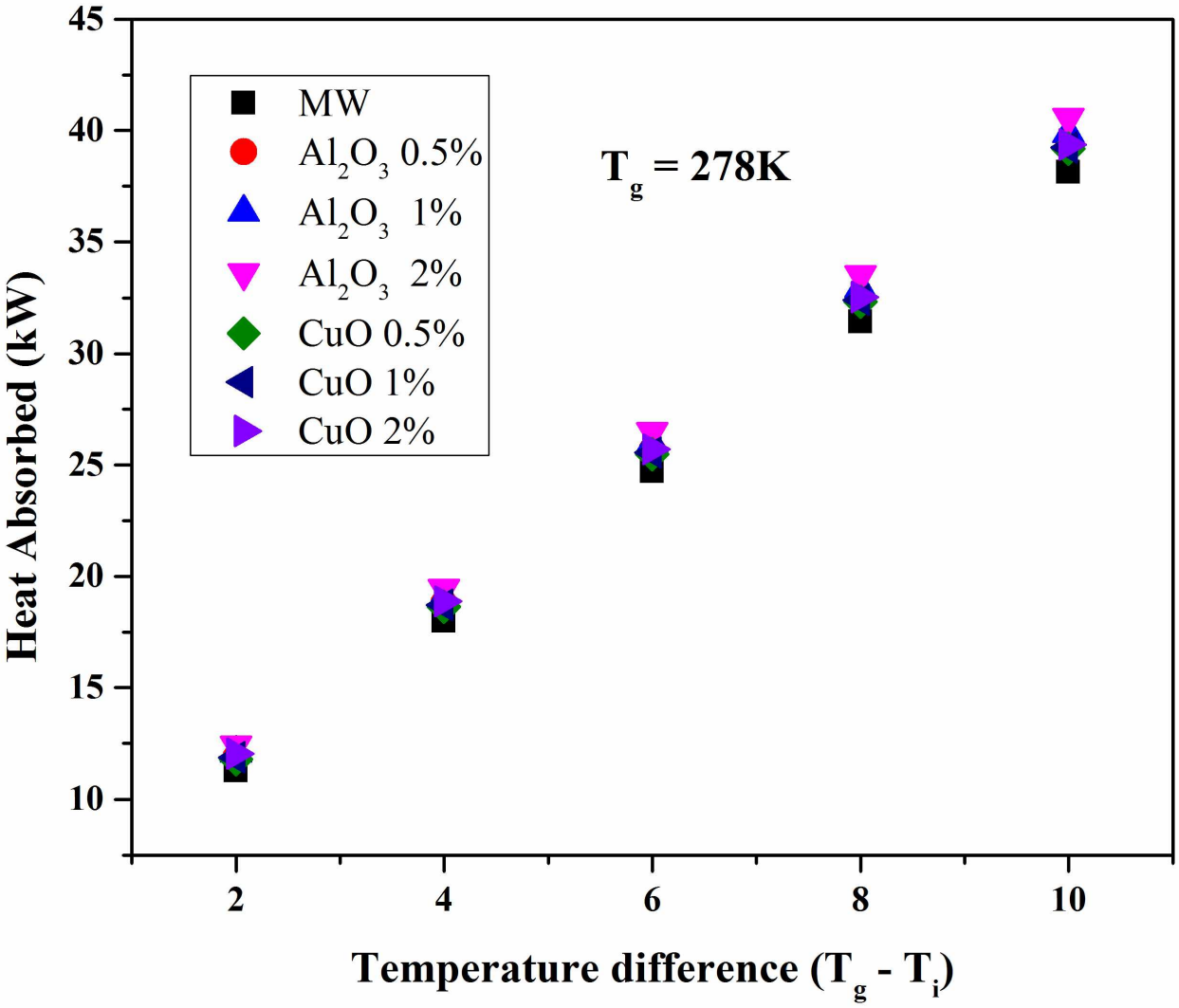

Figure 5.19. Heat absorbed by fluid in ground loop for different inlet temperatures of fluid when ground temperature is 278K.

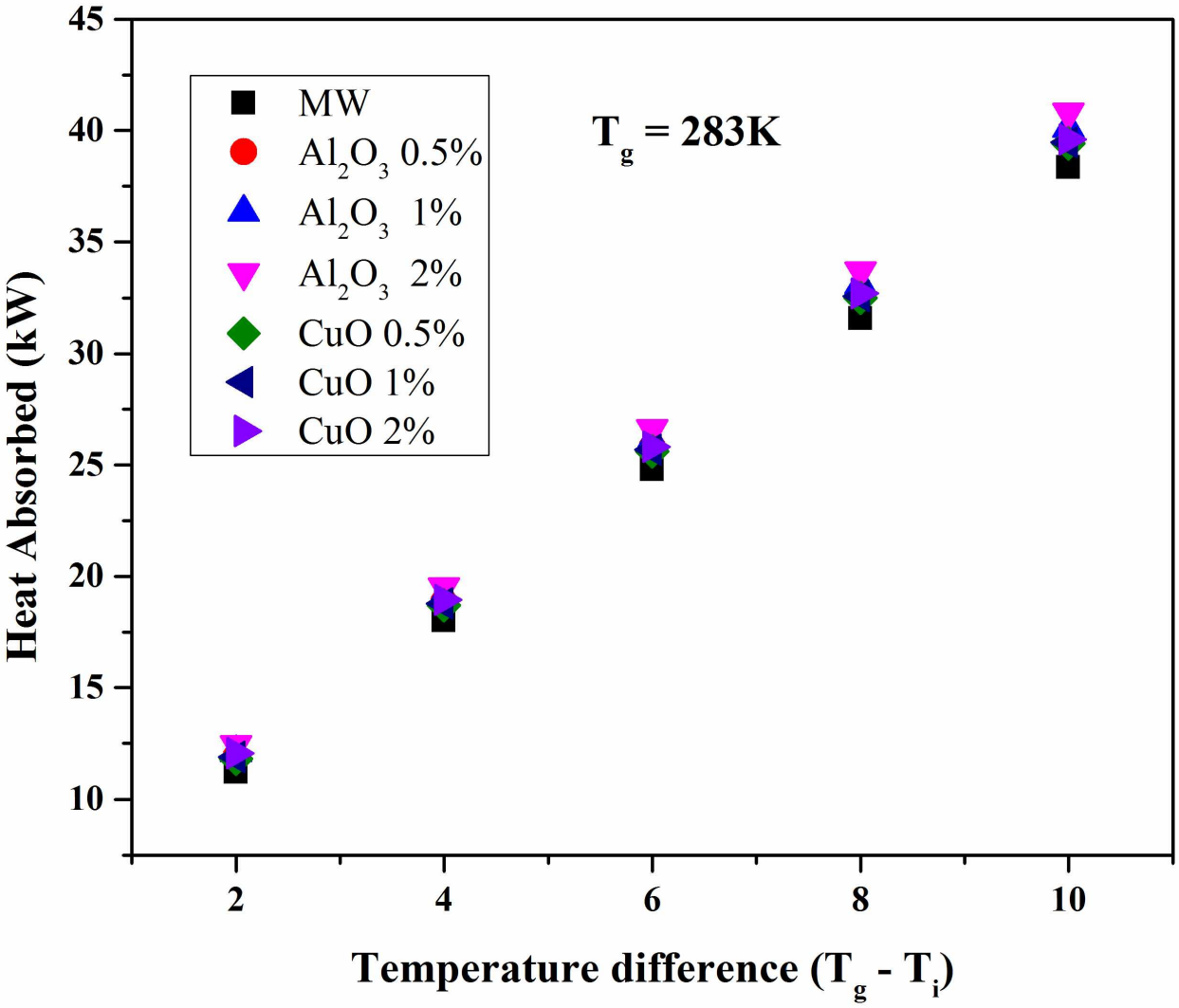

Figure 5.20. Heat absorbed by fluid in ground loop for different inlet temperatures of fluid when ground temperature is 283K.

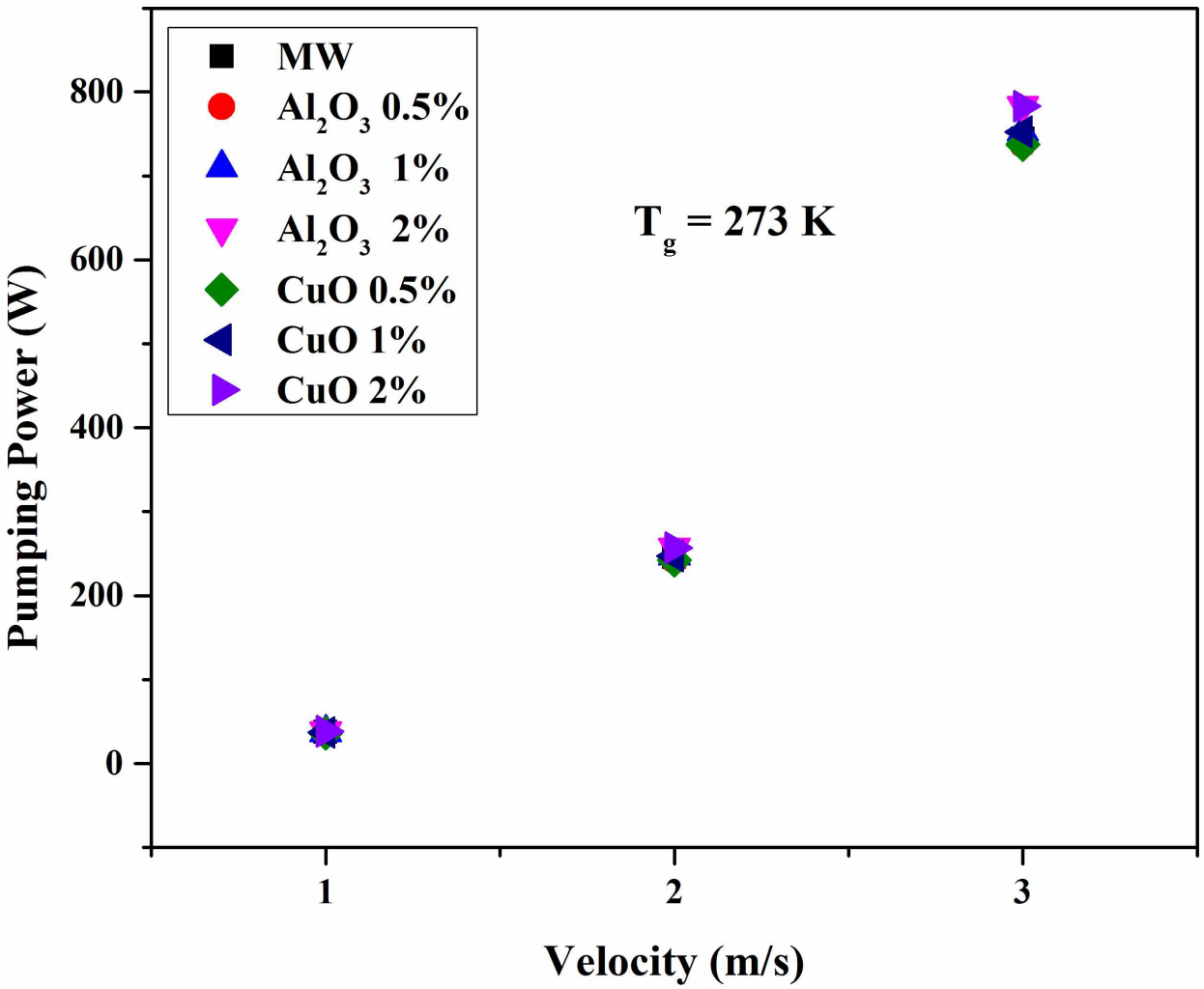

Figure 5.21. Pumping power variation with flow rate at ground temperature of 273K.

Table 5.1. Specifications of GSHP at CCHRC, Fairbanks [13].

Depth of coil below surface [m]	**2.9**
Flow rate in the loop [L/min]	62.9
Fluid outlet temperature [C]	-0.7
Fluid inlet temperature [C]	-3.5
Pipe inner diameter [inch]	0.75
Pipe outer diameter [inch]	1
Pumping power [W]	750

Table 5.2. Thermophysical properties of 20:80 M/W heat transfer fluid with temperature.

Temperature (C)	**Density (kg/m^3)**	**Specific Heat (J/kg K)**	**Thermal Conductivity (W/mK)**	**Viscosity (kg/m s)**
-10	988	3581.52	0.487	0.00292
0	986	3631.08	0.496	0.00234
10	970	3720.42	0.510	0.00187
20	965	3800.84	0.521	0.00150
30	963	3859.46	0.532	0.00120

Table 5.3. Material properties of HDPE pipe and Soil CCHRC

	HDPE Pipe	Fairbanks, Soil
Density [kg/m^3]	965	1989.49
Thermal conductivity [W/m.K]	0.51	1.42
Specific Heat [J/kg.K]	1900	1112.43

Table 5.4. Material properties of different nanoparticles.

Material	Density (kg/m^3)	Specific Heat (J/kgK)	Thermal Conductivity (W/mK)
Al_2O_3 [21]	3600	765	36
CuO [21]	6500	533	17.65

Table 5.5. Shows the properties of 20:80 M/W basefluid and nanofluids at 273K.

Material	Density [kg/m^3]	Specific Heat [J/kg K]	Viscosity [kg/ms]	Thermal Conductivity [W/m K]
M/W	970.8	3646.5	0.0023	0.4982
Al_2O_3 0.5%	983.9	3593.8	0.0023	0.5127
Al_2O_3 1%	996.4	3576.9	0.0022	0.5099
Al_2O_3 2%	1023.4153	3443.8170	0.0025	0.5096
CuO 0.5%	998.4778	3545.1967	0.0023	0.5007
CuO 1%	1026.1237	3449.3132	0.0023	0.5031
CuO 2%	1081.4153	3272.2535	0.0024	0.5080

Table 5.6. Ground temperature variation with different months in a year

Month	Ground Temperature (K)
Oct-14	275.81
Nov-14	274.81
Dec-14	274.46
Jan-15	273.9
Feb-15	273.59
Apr-15	273.41

5.29 References

[1] Alaska Center for Energy and Power and Cold Climate Housing and Research Center, 2011, Ground-Source Heat Pumps in Cold Climates, Fairbanks.

[2] Mueller, G., and Zarling, J., 1996, "Ground source heat pump monitoring," Inst. North. Eng.

[3] Pak, B. C., and Cho, Y. I., 1998, "Hydrodynamic and heat transfer study of dispersed fluids with submicron metalic oxide particles.," Exp. Heat Transf., **11**, pp. 151–170.

[4] Eastman, J. A., Choi, S. U. S., Li, S., Yu, W., and Thompson, L. J., 2001, "Anomalously increased effective thermal conductivities of ethylene glycol-based nanofluids containing copper nanoparticles," Appl. Phys. Lett., **78**(6), p. 718.

[5] ASHRAE, 2009, "Physical properties of secondary coolants (Brines)," ASHRAE Handbook, American Society of Heating Refrigerator and Air Conditioning Engineers, Inc, Atlanta.

[6] Healy, P. F., and Ugursal, V. I., 1997, "Performance And Economic Feasibility Of Ground Source Heat Pumps In Cold Climate," Int. J. Energy Res., **21**, pp. 857–870.

[7] Garber-slaght, R., Daanen, R., and Roe, A., 2014, "Ground Source Heat Pump Efficiency in Cold Climates," ASHRAE Trans.

[8] Sarbu, I., and Sebarchievici, C., 2014, "General review of ground-source heat pump systems for heating and cooling of buildings," Energy Build., **70**, pp. 441–454.

[9] Mustafa Omer, A., 2008, "Ground-source heat pumps systems and applications," Renew. Sustain. Energy Rev., **12**(2), pp. 344–371.

[10] Incropera, F. P., Dewitt, D. P., Bergman, T. L., and Lavine, A. S., 2011, Introduction To Heat Transfer, John Wiely & Sons, Inc.

[11] Bejan, A., 1993, Heat Transfer, John Wiely & Sons, Inc., New York.

[12] White, F. M., 2006, Viscous Fluid Flow, 3rd Edition, McGraw-Hill, New York.

[13] Wooden, N., 2008, Operating Procedure for the TCi: Small Volume Test Kit for Thermal Conductivity Testing, C-Therm technologies, Amherst, Nova Scotia, Canada, B4H 4S8.

[14] Mikhail, S. Z., and W.R. Kimel, 1961, "Densities and Viscosities of Methanol-Water Mixtures," J. Chem. Eng. Data, **6**(4), pp. 533–537.

[15] Kleinstreuer, C., and Feng, Y., 2011, "Experimental and theoretical studies of nanofluid thermal conductivity enhancement: a review.," Nanoscale Res. Lett., **6**(1), p. 229.

[16] Huminic, G., and Huminic, A., 2012, "Application of nanofluids in heat exchangers: A review," Renew. Sustain. Energy Rev., **16**(8), pp. 5625–5638.

[17] Murshed, S. M. S., Leong, K. C., and Yang, C., 2008, "Thermophysical and electrokinetic properties of nanofluids – A critical review," Appl. Therm. Eng., **28**(17-18), pp. 2109–2125.

[18] Das, S. K., Choi, S. U. S., and Patel, H. E., 2006, "Heat Transfer in Nanofluids—A Review," Heat Transf. Eng., **27**(10), pp. 3–19.

[19] Vajjha, R. S., and Das, D. K., 2012, "A review and analysis on influence of temperature and concentration of nanofluids on thermophysical properties, heat transfer and pumping power," Int. J. Heat Mass Transf., **55**(15-16), pp. 4063–4078.

[20] Taylor, R., Coulombe, S., Otanicar, T., Phelan, P., Gunawan, A., Lv, W., Rosengarten, G., Prasher, R., and Tyagi, H., 2013, "Small particles, big impacts: A review of the diverse applications of nanofluids," J. Appl. Phys., **113**(1), p. 011301.

[21] Lide, D., 1995, CRC Handbook of chemistry and physics, 84th edition, CRC Press, New york, USA.

[22] Brinkman, H. C., 1952, "The viscosity of a concentrated suspensions and solutions," J. Chem. Phys., **20**(4), pp. 571–581.

[23] Prasher, R., Bhattacharya, P., and Phelan, P. E., 2006, "Brownian-Motion-Based Convective-Conductive Model for the Effective Thermal Conductivity of Nanofluids," ASME J. Heat Transf., **128**(6), p. 588.

[24] Xuan, Y., and Roetzel, W., 2000, "Conceptions for heat transfer correlation of nanofluids," Int. J. Heat Mass Transf., **43**(19), pp. 3701–3707.

[25] 3M, 2010, 3M Novec 649 Engineered Fluid ™, St.Paul, MN.

[26] Yavuzturk, C., 1999, "A Short Time Step Response Factor Model for Vertical Ground Loop Heat Exchangers," ASHRAE Trans., **105**(2), pp. 475–485.

[27] Bi, Y., Chen, L., and Wu, C., 2002, "Ground heat exchanger temperature distribution analysis and experimental verification," Appl. Therm. Eng., **22**(2), pp. 183–189.

[28] Mihalakakou, G., Lewis, J. O., and Santamouris, M., 1996, "On the heating potential of buried pipes techniques - Application in Ireland," Energy Build., **24**(1), pp. 19–25.

[29] Bojic, M., Trifunovic, N., Papadakis, G., and Kyritsis, S., 1997, "Numerical simulation, technical and economic evaluation of air-to-earth heat exchanger coupled to a building," Energy, **22**(12), pp. 1151–1158.

[30] Demir, H., Koyun, A., and Temir, G., 2009, "Heat transfer of horizontal parallel pipe ground heat exchanger and experimental verification," Appl. Therm. Eng., **29**(2-3), pp. 224–233.

[31] Wu, Y., Gan, G., Verhoef, A., Vidale, P. L., and Gonzalez, R. G., 2010, "Experimental measurement and numerical simulation of horizontal-coupled slinky ground source heat exchangers," Appl. Therm. Eng., **30**(16), pp. 2574–2583.

[32] Benazza, A., Blanco, E., Aichouba, M., Río, J. L., and Laouedj, S., 2011, "Numerical Investigation of Horizontal Ground Coupled Heat Exchanger," Energy Procedia, **6**, pp. 29–35.

[33] Fujii, H., Nishi, K., Komaniwa, Y., and Chou, N., 2012, "Numerical modeling of slinky-coil horizontal ground heat exchangers," Geothermics, **41**, pp. 55–62.

[34] Congedo, P. M., Colangelo, G., and Starace, G., 2012, "CFD simulations of horizontal ground heat exchangers: A comparison among different configurations," Appl. Therm. Eng., **33-34**(1), pp. 24–32.

[35] Sagia, Z., 2012, "Borehole Resistance and Heat Conduction Around Vertical Ground Heat Exchangers," Open Chem. Eng. J., **6**(1), pp. 32–40.

[36] Luo, J., Rohn, J., Bayer, M., and Priess, A., 2013, "Modeling and experiments on energy loss in horizontal connecting pipe of vertical ground source heat pump system," Appl. Therm. Eng., **61**(2), pp. 55–64.

[37] Comsol Multiphysics (2015), http://www.comsol.com/.

Chapter 6 Overall Conclusions

The following conclusions are drawn from the preceding chapters:

6.1 Conclusions for thermal conductivity measurements of propylene glycol nanofluids and comparison with correlations

- The results showed an increase in thermal conductivity of nanofluids with increasing concentration and temperature. As the nanoparticles' diameter increased, the thermal conductivity increased.
- It was noticed that several correlations did not capture the thermal conductivity variations with temperature and concentration properly. The reason for this is that models are usually developed without considering large experimental data sets.
- The model presented by Prasher et al. proved effective. This model was refined using a broader set of experimental data, which provided a new correlation constant, m, for 60:40 PG/W based nanofluids.
- With this new value of m = 2.698, Eq. (2.8a) gives accurate predictions of thermal conductivity of different PG/W nanofluids over a wide range of concentrations, temperatures, and particle sizes. Since the nanofluids exhibit enhanced thermal conductivity with increasing temperature, it is concluded that their application in higher temperature environments will be more beneficial.

6.2 Conclusions for specific heat measurements of five different propylene glycol based nanofluids and development of a new correlation

- From a set of carefully conducted experiments, the specific heats of five different nanofluids (Al_2O_3, CuO, SiO_2, TiO_2, and ZnO nanoparticles) dispersed in a 60:40 PG/W base fluid were measured. From these data the effects of temperature (243-363 K), particle volumetric concentration (0.5 - 6%), and particle size (15 -76nm) on specific heat were studied.

- The results showed a decrease in the specific heat with increasing concentration and an increase in the specific heat with increasing temperature, which were in agreement with previously published results.
- At low concentrations (between 0.5 and 1.5%) the reduction in specific heat was small, indicating that nanofluids can be beneficial at dilute concentrations by increasing thermal conductivity and restricting the viscosity increase to a smaller value.
- The experimental results show that particle size has no significant effect on the specific heat of nanofluids. The specific heat correlations from the literature failed to predict the measured specific heat values with good agreement.
- Therefore, a new specific heat correlation was developed for five different nanoparticles dispersed in 60:40 PG/W, which predicted the specific heat values of the tested nanofluids with an average deviation of -0.094%. With additional testing in the future, this correlation can be refined to be applicable to many other nanofluids.

6.3 Conclusions for measurements of densities of propylene glycol based nanofluids and comparison with theory

- First, a benchmark test was performed on the 60:40 PG/W by mass mixture and the results showed good agreement with a very small deviation (1.6%) with reference values.
- The density was measured for different nanofluids (Al_2O_3, ZnO, TiO_2, SiO_2, CuO nanoparticles and carbon nanotubes nanoparticles dispersed in 60:40 PG/W). The experiments were conducted in a temperature range of 273 K to 363 K. The measured density values agreed well with those of the theoretical equation.
- The results showed that the density of nanofluids is independent of the particle size.
- Nanofluid densities increased with increasing particle volumetric concentration but decreased with increasing temperature.
- Based upon 874 data points, it was found that the maximum deviation between the measured values and those predicted by the equation of Pak and Cho was $\pm$4%. Therefore, equation 4.10 can be used to calculate the densities of nanofluids accurately.

6.4 Conclusions for evaluation of nanofluids ground source heat pumps operating in cold climate

- An analytical study has been performed to find the best fluid to be used in GSHPs in cold climates. The analysis measured the required length of pipe to absorb 18 kW of heat energy and the pumping power required to pump the fluids in the loop in Fairbanks soil conditions.
- An analytical study changing the flow rate in the fluid is performed. From this analysis, it is observed that there is no significant benefit to using nanofluids in cold climate GSHPs. Pumping power increases with nanofluids due to increasing viscosity. Ground temperature is one of the varying parameters.
- Three parametric studies of the performance of nanofluids in GSHPs in cold climates were conducted.
- With increasing ground temperature, the nanofluids absorb more heat than the base fluid.
- In the flow rate parametric study, we found that the nanofluids absorb more heat than M/W at low flow rates. With inlet temperature variation, nanofluids followed M/W in results.
- Numerical analysis showed an increase in pumping power for nanofluids compared to that of the base fluid. These results show that nanofluids perform slightly better than M/W in cold climates, but at the expense of increased pumping power.

6.5 Suggestions for future research

In the present research we have measured thermophysical properties of propylene glycol nanofluids and shown the application of nanofluids in a ground source heat pump. However, additional research should be done in the following areas for better understanding of nanofluids and to improve their efficiency.

- Nanofluids still need some surfactants to keep them afloat for a longer duration. Research need to be done to find a way to completely prohibit the agglomeration and sedimentation of nanoparticles.
- Nanofluid research is widely dispersed. Research should be done to find a common correlation for predicting the properties of nanofluids.

- No research has been done measuring nanofluid properties below room temperature, as we did for propylene glycol nanofluids. Experiments need to be done to study nanofluid properties at low temperatures.
- In general, the specific heat of nanofluids decreases with the addition of nanoparticles. There have been studies showing increased specific heat of salts when nanoparticles are added. If we can find a property that contributes to increase specific heat of fluids, these fluids will find good application as heat transfer fluids.
- Carbon nanotubes have higher thermal conductivity than any metal nanoparticles. Research need to be done to find the right aspect ratio to suspend them in fluid to prevent tangling of tubes. This will help in finding many applications of carbon nanotube nanofluids.
- Limited research is being done on nanofluid flow in the porous medium. In the research it was found that nanoparticles reduce the surface tension of a liquid. Decreased surface tension fluids have applications like enhanced oil recovery, decreased boiling point of liquids, and others.

Appendices

During my doctoral study in the last four years, in addition to the work presented in the chapters of this dissertation, I worked on other research projects with the members of the nanofluids group at the mechanical engineering department, UAF.

The research work was published in peer-reviewed journals. The abstracts of the papers to which I contributed and co-authored are provided in these apendices.

Appendix 1. Measurement of the thermal conductivity of silicon dioxide nanofluid and development of correlation*

Abstract

Experimental investigations were carried out for the determination of thermal conductivity of silicon dioxide (SiO2) nanoparticles dispersed in 60% ethylene glycol and 40% water by mass. Experiments conducted in a temperature range of 20 ^{0}C to 90 ^{0}C and for several particle volumetric concentrations up to 10% showed that the ratio of thermal conductivity of nanofluid to that of the base fluid increased with an increase in temperature and volumetric concentration. As an example, as much as a 20% enhancement in thermal conductivity was evidenced for a particle volumetric concentration of 10% at 87 ^{0}C Comparison of experimental results of this nonmetallic nanoparticles suspension with the well-known model developed by Hamilton and Crosser for microparticles suspensions, exhibits that this model under predicts the thermal conductivity of nanofluids. Therefore, a new correlation has been derived following recent models developed for metallic nanoparticles suspensions, which is a combination of the Hamilton–Crosser model plus a term due to the Brownian motion. This new correlation expresses the thermal conductivity of silicon dioxide nanofluid as a function of temperature, volumetric concentration and the properties of the base fluid and the nanoparticles.

---

* Sahoo, B., Das, D. K., Vajjha, R. S. and Satti, J. R. 2013, "Measurment Of The Thermal Conductivity Of Silicon Dixoide Nanofluid And Development Of Correlation," ASME Journal of Nanotechnology in Engineering and Medicine., **3**(4), pp. 041006 1-10.

Appendix 2. Measurements of the surface tension of nanofluids and development of a new correlation*

Abstract

Surface tension measurements were performed on four nanofluids containing aluminum oxide (Al_2O_3), zinc oxide (ZnO), titanium dioxide (TiO_2) and silicon dioxide (SiO_2) nanoparticles suspended in a base fluid of 60 % propylene glycol and 40 % water by mass. (60:40 PG/W). First, benchmark tests for the surface tension of water were performed, for which accurate data are available in the published literature. Measured data agreed well with the published data confirming the accuracy of the apparatus, as well as the experimental procedure. Following the benchmark tests, measurements were performed on nanofluids over a temperature range of $30\,^{o}C$ to $70\,^{o}C$ for particle volumetric concentrations ranging from 0 to 6 % and particle sizes in the range of 15 to 50 nm. From the experimental data, it was observed that the surface tension of nanofluids decreased with an increase in temperature. At a constant temperature, an increase in the particle volumetric concentration of a nanofluid caused a decrease in the surface tension. For nanofluids at fixed volumetric concentration and temperature, the surface tension was found to be lower for smaller particle sizes except the ZnO nanofluid. A statistical analysis performed on the experimental data yielded a single correlation valid for all the nanofluids tested. This surface tension correlation is a function of temperature, volumetric concentration and the size of the nanoparticles, which predicts results successfully with an average deviation of 2.6% from the measured values.

---

* Chinnam, J., Das D. K., Vajjha R. S., and Satti J. R., 2015. "Measurements of the surface tension of nanofluids and development of a new correlation", International Journal of Thermal Sciences, 98, pg-68-80.

Appendix 3. Measurements of the contact angle of nanofluids and development of a new correlation*

Abstract

Contact angle measurements were performed on deionized water, propylene glycol and mixture of 60% propylene glycol and 40% water by mass (60:40 PG/W), over a temperature range of 25 °C to 40 °C. All measurements were performed on the surface of a glass slide at the solid–fluid–air-interface. After confirming the contact angle value of water with the data of other researchers, the same procedure was applied to four nanofluids (nanoscale particles dispersed in a base fluid) containing aluminum oxide (Al_2O_3), zinc oxide (ZnO), titanium dioxide (TiO_2) and silicon dioxide (SiO_2) nanoparticles dispersed in 60:40 PG/W. For the nanofluids, the particle volumetric concentrations were varied from 0 to 6% and the average particle sizes ranged from 15 to 50 nm. From the experimental data, it was observed that the contact angles of three single phase liquids and four nanofluids were less than 90°, indicating that all these fluids were wetting to the glass surface. The contact angles of all tested fluids exhibited a continuous decrement with an increase in temperature, and a linear equation for contact angle with temperature matched the data well. For the nanofluids, an increase in the particle volumetric concentration caused a decrease in the contact angle at a constant temperature. The variation of the contact angle followed a second order polynomial relation with the volumetric concentration. For nanofluids at the same volumetric concentration and the same temperature, the contact angles were observed to be lower for larger particle sizes, except for the ZnO nanofluid. A statistical analysis performed on the experimental data yielded a correlation suitable to represent all the nanofluids tested. This contact angle correlation is a function of temperature, volumetric concentration and the size of the nanoparticles, which predicts results successfully with an average deviation of 6.3% from the measured values.

---

* Chinnam, J., Das D. K., Vajjha R. S., and Satti J. R., 2015. "Measurements of the contact angle of nanofluids and development of a new correlation", International Communications in Heat and Mass Transfer, 62, pg-1-12.